TECHNISCHE UNIVERSITÄT WIEN

PhD-Thesis

Dissertation

Toughness-enhancing additives for additive-manufactured bone replacement materials

ausgeführt zum Zwecke der Erlangung
des akademischen Grades eines Doktors der technischen Wissenschaften

unter der Leitung von
Univ. Prof. Dipl.-Ing. Dr. techn. Robert Liska
und der Betreuung von
Ass. Prof. Dipl.-Ing. Dr. techn. Stefan Baudis

E163
Institut für Angewandte Synthesechemie

eingereicht an der Technischen Universität Wien
Fakultät für Technische Chemie

von

Dipl.-Ing. Barbara Dellago, BSc.
01126632

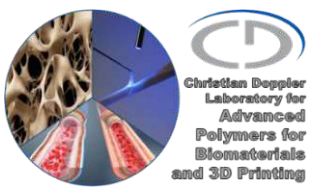

Wien, am 23.05.2023

Dipl.Ing. Barbara Dellago, BSc.

ABSTRACT

Diseases or accidents can lead to disturbed bone regeneration or loss of bone. In order to promote bone regeneration, tissue engineering is concerned with the development of materials for manufacturing artificial bone replacement materials. These can be produced by lithography-based additive manufacturing technologies. In this area, (meth)acrylates are currently the most advanced monomers. They combine favorable reactivity and mechanical properties. However, they are irritating and sometimes cytotoxic, and their degradation products (poly acids) can damage surrounding tissue. Therefore, vinyl esters (VEs) are used to circumvent these problems. Unfortunately, they lead to a decrease in reactivity, which is why thiol-ene polymerization is used to boost it. In addition, the networks are often highly brittle. This work presents two concepts to improve the material properties, especially the toughness.

On the one hand, high molecular weight polymers can be added to a vinyl ester-based thiol-ene system to improve the toughness of the final material. Therefore, different modified toughness-enhancing additives were synthesized. These additives were based on poly(ε-caprolactone), as it is already used as a biodegradable and biocompatible polymer and has been shown to be a toughness-enhancing motif. Tensile tests, DMTA measurements, and RT-FT-NIR photorheological measurements were performed to investigate the influence of toughness enhancers on the final polymer. These experiments showed increased elongation at break with no loss in tensile strength. It was also demonstrated that all T_gs were far above body temperature and that the addition of toughness enhancers did not significantly decrease reactivity.

In addition, the formation of interpenetrating polymer networks (IPNs) has been investigated. The hard network was investigated for its (thermo)mechanical properties and subsequently optimized. Furthermore, the flexible network was generated, and its influence on the hard network with increasing amounts was determined. Here, excellent results were generated as well. The glass transition temperatures were above body temperature, and the toughness of the materials could be significantly increased.

These results demonstrate the applicability of modified PCL as a toughness enhancer and IPNs as a suitable method for manufacturing bone graft substitutes.

KURZFASSUNG

Eine gestörte Knochenregeneration kann durch Krankheiten oder Unfälle hervorgerufen werden, was des Weiteren zum Verlust von Knochen führen kann. Tissue Engineering befasst sich mit der Entwicklung von Materialien, welche zur Herstellung von Implantaten für den Knochenersatz verwendet werden sollen, um die Knochenregeneration zu fördern. Diese Knochenersatzmaterialien können durch lithographiebasierte additive Fertigungsverfahren hergestellt werden. Hier sind (Meth)acrylate die derzeit am weitesten verbreiteten Monomere, da sie eine hohe Reaktivität und gute mechanische Eigenschaften aufweisen. Allerdings werden sie als reizend und teilweise zytotoxisch eingestuft, und ihre Abbauprodukte (Polysäuren) können das umliegende Gewebe schädigen. Daher werden stattdessen Vinylester (VE) verwendet, um diese Probleme zu umgehen. Leider zeigen diese eine verringerte Reaktivität, weshalb die Thiol-En-Polymerisation eingesetzt wird, um diese zu erhöhen. Darüber hinaus weisen die erhaltenen Netzwerke häufig eine hohe Sprödigkeit auf. Aus diesem Grund werden in dieser Arbeit zwei Konzepte zur Verbesserung der Materialeigenschaften, insbesondere der Zähigkeit, vorgestellt.

Die Zugabe von z.B. hochmolekularen Polymeren zu einem Thiol-En-System auf VE-basis kann die Zähigkeit des Endmaterials verbessern. Aus diesem Grund wurden verschiedene modifizierte Additive synthetisiert und ihre Auswirkungen auf das Endpolymer bestimmt. Diese Additive basierten auf Poly(ε-caprolacton), da es bereits als biologisch abbaubares und biokompatibles Polymer verwendet wird und sich in vorherigen Untersuchungen als Zähigkeitsverbesserer erwiesen hat. Um den Einfluss der Additive auf das fertige Polymer zu untersuchen, wurden Zugversuche, DMTA- und photorheologische RT-FT-NIR-Messungen durchgeführt. Diese Experimente zeigten einen Anstieg der Zähigkeit, alle T_gs lagen weit über der Körpertemperatur und diese Additive führten nicht zu einer signifikanten Verringerung der Reaktivität.

Zusätzlich wurde die Herstellung von interpenetrierenden Polymernetzwerken (IPNs) betrachtet. Hier wurde das rigide Netzwerk auf seine (thermo)mechanischen Eigenschaften untersucht und anschließend optimiert. Ebenfalls wurde der Einfluss des flexiblen Netzwerkes mit zunehmender Menge auf das rigide Netzwerk untersucht. Hierbei zeigten DMTA Messungen, dass alle T_gs weit oberhalb der Körpertemperatur lagen und die Zähigkeit der Materialien deutlich verbessert werden konnte.

Diese Ergebnisse zeigten, dass die Verwendung von modifiziertem PCL als Zähigkeitsverbesserer und auch IPNs als Herstellungsverfahren für Knochenersatzmaterialien geeignet sind.

TABLE OF CONTENTS

INTRODUCTION

1. Bone tissue engineering (BTE)

The adult human body has about 206 bones consisting of tendons, cartilage, and ligaments.[1] The stiff **skeleton** gives stability to the body and protects the vital internal organs from injury. To ensure mobility, the stiff bones are attached to several joints. Furthermore, bone is a mineral storage (calcium and phosphates) and is responsible for blood cell production.[2-4]

From a macroscopic point of view, every bone consists of an outer layer of dense cortical bone (thickness depends on functional requirement) and an inner layer of spongy bone.[5, 6] This classification is based on their density and porosity. 80 wt% of the human skeleton is compact (cortical) bone, which shows a porosity of only 3-12%. The spongy (cancellous or trabecular) bone covers 20 wt% of the bone. It has 50-90% porosity, but the chemical composition of these two types is identical.[1, 3] Bone consists of an extracellular matrix (50-70%, mainly mineralized)[7], an organic matrix (20-40%), water (5-10%), lipids (<3%), and cells. The most abundant mineral in bone is hydroxyapatite (HAp) [$Ca_{10}(PO_4)_6(OH)_2$][1, 8], which occurs as tiny crystals with a length of 20-80 nm and a thickness of 4-5 nm.[9, 10] For good mineral support, the HAp is carbonate-substituted. Besides HAp, carbonates, magnesium, and acidic phosphates without hydroxyl groups are present to make them soluble.[1] The organic matrix consists of fibrous proteins based on collagen type I (90%) and the residue of non-collagenous proteins and polysaccharides.[8]

Bone is a dynamic, mineralized, and vascularized tissue characterized by its stiffness, growth mechanisms, and ability to repair and regenerate.[4] It is estimated that 10-15% of bone in the human body is replaced by new bone each year.[11] Three main cells, osteoblasts, osteocytes, and osteoclasts, are present and responsible for the production, maintenance, and resorption of bone.[3, 6]

Osteoblasts are bone-forming cells and are essential for the formation and remodeling of the bone matrix. Collagen is formed by these cells, and they secrete calcium phosphates and -carbonates into the interstitial space of the bone. However, the minerals crystallize along the collagen fibers due to poor solubility. Mature bone cells are osteoblasts, which lose their ability to divide and are called osteocytes. Gradually, the tissue hardens, forming an exceptionally robust bone matrix. This ossification process takes several months to many years, depending on the type of bone.[6, 12] However, osteoclasts break down and resorb bone during growth and the healing phase after an injury, which leads to constant

remodeling of the bone scaffold. In the process, the pH decreases (pH ≤4), leading to mineral mobilization.[13] Erosion pits, known as "Howship's lacuna" are formed on the bone surface.[6, 12, 14-16] The bone-lining cells are modified osteoblasts that adhere to the inactive bone surface and form a protective layer.[17] These cells regulate the influx and efflux of mineral ions into and out of bones. Osteoblasts and osteoclasts are in dynamic equilibrium and preserve bone tissue.[18]

The newly formed bone is mechanically more robust and helps to maintain the strength of the bone.[6] Thus, bone remodeling can be divided into three sequential phases: resorption, reversal, and new formation. The resorption phase can be completed in about two weeks. In this phase, osteoclasts acidify the surface, dissolve the bone matrix, and form deep cavities. This phase is followed by the reversal phase, which can last up to five weeks. In this phase, the degraded surface is prepared for the following phase. The complete regeneration of the bone structure can then take up to four months.[7] The process of fracture healing is schematically depicted in Figure 1.

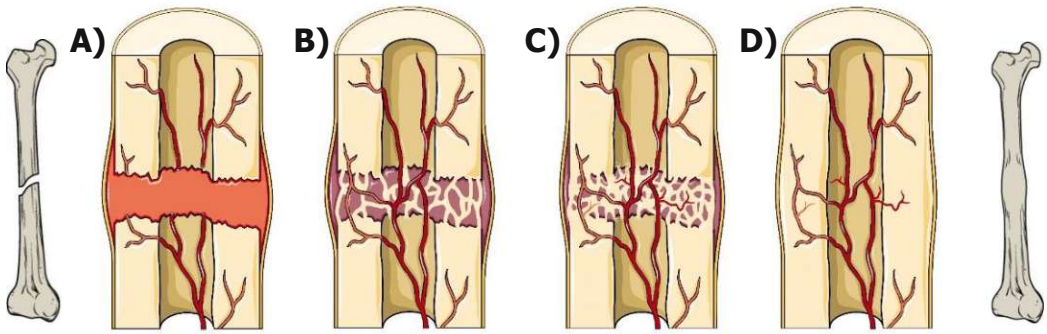

Figure 1: Process of fracture healing: A) Hematoma is formed, B) followed by a soft callus, C) formation of hard callus of spongy bone, D) healed fracture (remodeling step).[19]

Fractures may occur due to an aging population, disease, or trauma, such as accidents or sports injuries. In that case, natural bone formation can be supported. These fractures are treated by surgical reconstruction or mechanical devices. A splint, cast, or brace is sufficient depending on the break pattern, which bone fractured, and its reason.[20] Bone can regrowth to a specific size, dependent on the location of the bone loss. Spontaneous healing of defects of 6-15 cm in the femur is reported, but in the tibia, a defect of >1-2 cm is fatal and cannot be healed by the body itself.[21] Despite surgical stabilization, if a defect does not heal spontaneously and further surgical intervention is required, it is called a critical-sized defect. In this case, implants are needed to treat the loss of bone.[20]

Autografts, allografts, and various synthetic or biomimetic materials and devices are used to treat these injuries. Disadvantages of these methods include the need for additional surgical procedures or the inadequate size and shape of the bone donor. Additionally, donor site morbidity is often involved, and the recovery period after the surgical process takes a long time. For this reason, new innovative approaches are being investigated to aid in repairing and reconstructing skeletal tissue.[22] **Tissue engineering** (TE) is one such alternative that deals with solutions that avoid permanent prostheses. In this approach, an artificial tissue replacement is used, which should have the most possible similarity in structure and morphology to the natural tissue. In addition, it should be able to fulfill similar biological functions to circumvent problems such as immune rejection, pathogen transfer, or the lack of donor material. Tissue engineering can be divided into different concepts. The most used method for the regeneration of hard tissue (*e.g.*, bone) combines the application of living cells, biologically active molecules, and a temporary artificial three-dimensional (3D) porous scaffold.[23]

2. Biomaterials for bone tissue engineering

The artificial scaffolds used in bone tissue engineering (BTE) are based on different biomaterials: **ceramics**, **metals**, and **polymers/composites**.[24] Implants made from these materials must meet the human body's complex and sensitive biological system. They must show excellent biocompatibility and suitable biodegradability, as the implants only serve as a temporary scaffold while the natural bone regrows. This also means that toxic degradation products must not be formed during the degradation of the implant, thereby generating irritation or inflammation of the surrounding tissue. Furthermore, these scaffolds must provide appropriate mechanical support[25-28], with toughness being a key factor. Indeed, the artificial scaffold must prevent damage caused by compressive or tensile forces.[8]

Due to their similarity to minerals in natural bone, **ceramics** are commonly used for implants. They are made of hydroxyapatite (HAp), tricalcium-, or calcium phosphates and show good biocompatibility.[29-32] **Bioglasses** are a subclass of ceramics and were first applied as bone graft substitutes in the 1960s. They have an amorphous structure with a coating of hydroxyapatite[33, 34] and are thus capable of bone tissue binding to the implant and promoting cell growth. This combination is referred to as a bioactive material. However, poor fracture toughness and flexural strength are huge disadvantages for this

material class.[35] In comparison to the cortical bone[36] with a fracture toughness of 6-8 MPa·m$^{1/2}$, bioglasses[37, 38] lie between 0.5-1.1 MPa·m$^{1/2}$.

Implants with high fracture toughness and mechanical strength can be made of **metals**.[39] Here, magnesium (and its alloys)[24, 40], cobalt, or titan can be used, depending on the desired degradable properties of the implant.[35] They show a fracture toughness of 15-40 MPa·m$^{1/2}$ for magnesium[39] and 84-107 MPa·m$^{1/2}$ for titanium alloys[41]. Nevertheless, they must be coated with bioactive substances and can be produced only in limited geometries and complexity.[35, 42]

Polymers are another class of molecules that can be used as implant material in BTE. Depending on their origin, they are classified as *natural* or *synthetic polymers*.

The *natural polymers* include polysaccharides, *e.g.*, hyaluronic acid (large proportion in human tissues such as skin or cartilage)[43], chitosan (originates from exoskeleton of crustaceans) and alginate (brown algae)[44, 45] and proteins such as collagen (in large quantity in skin and muscle tissue), gelatin (through denaturation of collagen) and fibrin (factor of the blood clotting cascade). Several biomaterial applications are known for these polymers. For instance, they are used in drug delivery systems for antibiotics[45, 46], as wound-dressings, or in the fabrication of biodegradable hydrogels.[44, 45, 47-49] Figure 2 shows examples of natural polysaccharides.

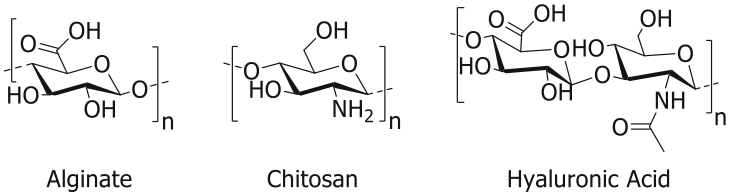

Figure 2: Chemical structure of selected polysaccharides.

In addition to natural polymers, *synthetic polymers* can be used as bases for replacement materials. Here, the major advantages are their predictable properties and the fact that they can be designed as desired. Furthermore, the risk of immunogenicity is low. They include poly(hydroxy acids) such as poly(glycolic acid) (PGA), poly(lactic acid) (PLA), and poly(ε-caprolactone) (PCL).[50-52] These synthetic polymers are depicted in Figure 3. PGA was first used as degradable sutures in the 1960s and has since been increasingly used in degradable medical implants.[44] PLA can exist in optically active D- or L-enantiomers. The mechanical properties may vary depending on whether the pure D- or L-form, or the mixture of both forms (D and L) is used. If a mixture of D- and L-form is used, amorphous

materials are obtained; otherwise crystalline. Crystallinity entails a higher modulus of elasticity, making poly(L-lactic acid), for example, applicable in load-bearing orthopedic implants.[44] PCL is a non-toxic and affordable polymer obtained by ring-opening polymerization of ε-caprolactone. It exhibits a slow rate of degradation and high permeability to many pharmaceuticals.[53, 54] For this reason, it is often used as a drug delivery system. It is also notable that it exhibits shape memory properties in thiol-ene networks, which brings the potential to biomedical applications.[55]

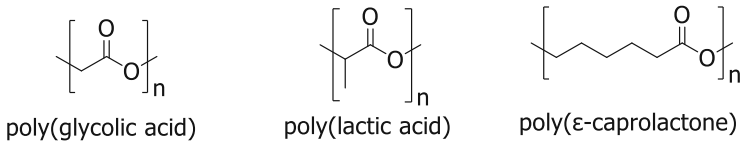

Figure 3: Chemical structures of synthetic biodegradable polymers.

A disadvantage of the polymers mentioned so far, which should not be neglected, is their degradation behavior. Implants made from these polymers suffer from bulk erosion.[56] In this case, the acidic degradation products are trapped inside, and further autocatalyze degradation occurs. However, this is not desirable because the mechanical properties of the entire scaffold decrease, and it can collapse abruptly.[57, 58] As an alternative, poly(anhydrides) and poly(carbonates) are used since here, the implants degrade according to a surface erosion mechanism.[52, 59, 60] Studies have already shown that photocrosslinkable poly(anhydrides) are suitable for the dental industry and, due to their adjustable degradation behavior, also for orthopedic applications and drug delivery systems.[51, 61, 62]

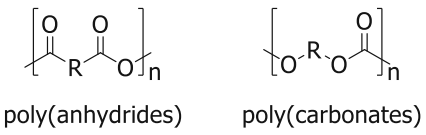

Figure 4: Chemical structure of poly(anhydride) and poly(carbonates).

Composites are also used to combine several favored properties. They consist of at least two materials; thus, specific stiffness and toughness should be achieved.[34] Mostly, they consist of a continuous phase (*e.g.*, polymer) and a filler (*e.g.*, particles or fibers) and can be categorized according to their combination of matrix and filler: *organic/organic* (*e.g.*, synthetic polymers with incorporated synthetic fibers) or *organic/inorganic* (*e.g.*, polymer with inorganic particles or fibers).[35]

These materials can be processed into materials for BTE in various ways.

3. Fabrication methods for porous artificial bone scaffolds

Human bone exhibits a hierarchical and complicated structure. This complexity must be mimicked as closely as possible by the artificial material to replace and repair damaged tissue successfully. Imaging techniques such as X-ray, magnetic resonance imaging, and computer tomography help to gain a high-resolution insight into the shapes and porosities of these bone structures. One of the challenges is the pore size. The pores should be 100-500 µm to ensure the supply of nutrients and oxygen.[63-65] In addition, degradation products must be able to be transported away, and cell adhesion and proliferation must be enabled.[66] However, mechanical support must be sufficient in addition to porosity to temporarily replace the damaged bone.[67, 68]

Various fabrication techniques are used to meet bone tissue's desired pore architecture and porosity and accomplish aspects like the infusion of growth factors, heat-labile drugs, and biological compounds to improve bone healing. These essential criteria can be met by different methods: **conventional methods**, **microspheres-based sintering** and **electrohydrodynamic techniques.**

Conventional methods include *solvent casting and particulate leaching*, for example. Here, a polymer is first dissolved in a suitable solvent, and a water-soluble porogen (*e.g.*, NaCl or sodium citrate[69]) is added.[70, 71] The mixture is poured into a mold, and the solvent is evaporated, which hardens the polymer. Then, the salt is leached out, creating a porous scaffold (see Figure 5a). High interconnectivity of pores was observed with 70 wt% of the porogen.[69] However, the shape of the pores and the interconnectivity can hardly be controlled, which limits this method.[70, 71]

In the *gas-foaming technique*, gas expansion forms bubbles in a polymer solution. The polymer solution is mixed with a gas foam component, such as water vapor, nitrogen, or carbon dioxide, until saturation.[72, 73] The pressure is then released and gas expansion occurs, forming pores (see Figure 5b). With this technique, foams with a porosity of up to 93% can be produced. However, the pores are about 100-500 µm but are hardly interconnected (only 10-30%), especially on the surface.[74-77]

If a water-based polymer solution is used, which will be frozen, this is called the *freeze-drying method* or *lyophilization*. Ice crystals are formed by freezing the aqueous phase and the polymer aggregates around them.[78] Emulsification freeze-drying can also be used. In this case, the polymer is dissolved in a water-immiscible solvent, mixed with water, and stirred continuously to form an emulsion. Afterwards, the emulsion will also be frozen.[79]

High vacuum is then used to sublimate the water or solvent, respectively, and after that, a scaffold with a small pore size and irregular porosity is formed (see Figure 5c).[80] For this reason, this method is also limited.

A polymer is dissolved in two immiscible solvents in the *thermally induced phase separation method (TIPS)*. Both phases are thermodynamically unstable at low temperatures. The solution is first heated, causing the polymer to concentrate in one phase, and then quenched by cooling down. This results in phase separation, followed by removing the solvent-rich phase by extraction, sublimation, or evaporation. Then, the polymer-rich phase hardens, forming a highly porous structure. The pores often show a size of 10-100 µm, which is unsuitable for seeding osteoblasts or bone-tissue growth.[77]

The **microsphere sintering** technique can fabricate microsphere-based scaffolds with controlled morphology.[81] First, an emulsion/solvent evaporation technique is used to fabricate a ceramic and polymer microsphere composite. Then, the green body is sintered and a porous 3D scaffold is obtained. These scaffolds show up to 40% porosity and a pore diameter of 90 µm.[37] However, their pore size and porosity and thus the mechanical property of the scaffold, can be adjusted with the temperature and sintering time.[82] Microsphere scaffolds can also be obtained by using the subcritical CO_2 sintering method. Compared to the gas foaming method, interconnective pores with higher porosity can be created here. Therefore, the CO_2 pressure has to be between 15 and 25 bar.[83]

The *electrospinning* or *electrospray technique* are **electrohydrodynamic methods**. These methods use an electrically charged fluid injected into an electric field and is shown schematical in Figure 5d. Therefore, a melt or solution of a polymer is filled into a syringe with a metallic cannula. The solution forms droplets at the needle tip because of the surface tension. Then, a high voltage is applied and the solution comes out of the syringe as a "Taylor cone".[84] The electrospinning technique results in a jet formation, whereas the electrospray method in a droplet formation.[81] Then, the fluid is deposited on a collector, and micro-/nano structures are formed. The type and concentration of the polymers can adjust the thickness and orientation of the generated fibers. These non-woven fiber scaffolds show high porosity and surface area.[85]

For this method, polymers, like polyurethanes (PU), collagen[86], or poly(ε-caprolactone) (PCL) can be used. *Natural polymers* have been thoroughly investigated as materials for biomedical applications. The major advantage of natural polymers is their high biocompatibility due to their natural origin. However, *synthetic polymers* are easily reproducible and can be produced on a large scale. Furthermore, they show a higher

uniformity of microstructure, degradation rate, and mechanical structure.[87-89] Poly(ε-caprolactone) (PCL) is one example of preferred synthetic and biocompatible polymers. It is elastic and has a low melting temperature, which makes it easy to process.[90] It also shows good degradation behavior, which can be controlled by copolymerization with other polymers or insertion of cleavable moieties.[44, 91] In addition, the mechanical properties can also be influenced by using different molecular weights.[92]

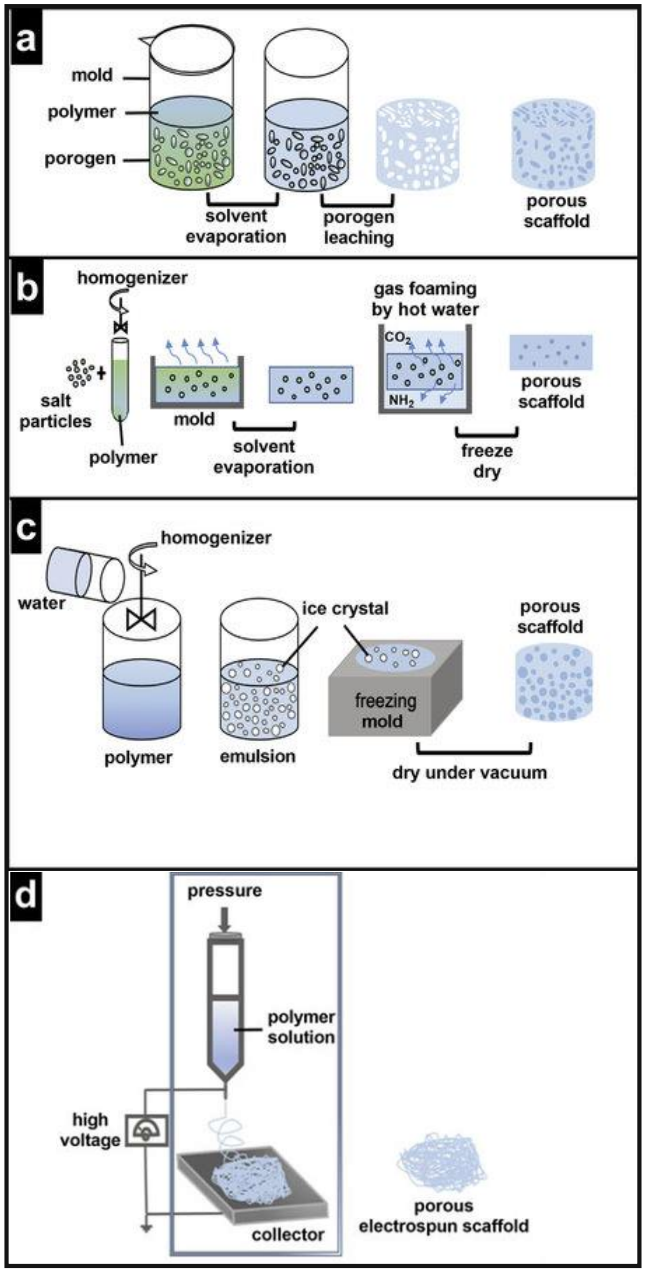

Figure 5: Schematic overview of conventional techniqzes: a) porogen leaging, b) gas foaming, c) freeze-drying and d) solution electrospinning. Adapted from N. Abbasi.[93]

The disadvantage of the methods mentioned so far is that the framework design is restricted to a certain degree. Mostly, these techniques allow only simple shapes, such as cylinders or cuboids, and are thus poorly suited for creating complex shapes, such as those found in the human skeleton. In order to then adapt these simple shapes to the desired forms, they often have to be cut or milled, which leads to the waste of materials.[66, 94-96]

4. Additive manufacturing technologies

However, these problems can be circumvented by additive manufacturing technologies (AMTs), and hence, complex and customized 3D structures for TE can be fabricated. This important technique was first introduced in the late 1980s.[97] Here, the tailor-made object is designed on the computer (CAD, computer-aided design) and sliced into several layers. Afterwards, the printing process can start, and the object is built by adding the material with a layer-by-layer technique. The principle process is depicted in Figure 6.

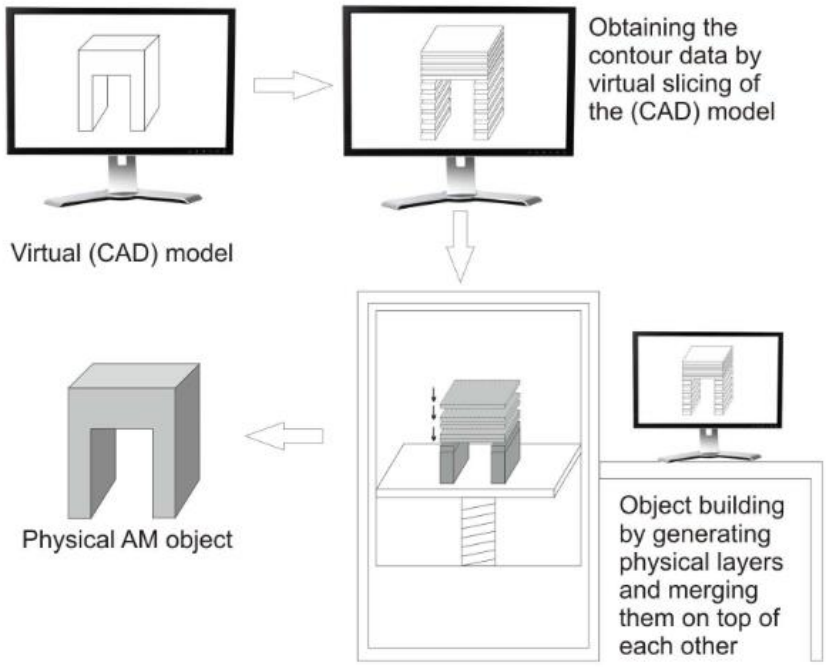

Figure 6: Principle of AMT: from CAD model to final object.[98]

This method allows very defined, interconnected pores to be fabricated without molds. A good overview of the different types of additive manufacturing technologies can be found in reviews of Leong *et al.*[99] and Hutmacher *et al.*[100]. AMT techniques can be divided into three categories, depending on their solid material forming techniques: *melt and dissolution*, *particle bonding,* and *photopolymerization of light-sensitive resins*. The last

mentioned is the most important technique for this thesis and will be further discussed in detail.

Photopolymerization in 3D printing applications is promoted due to advantages like local and temporal control of polymerization, rapid curing at low temperatures, and low heat development.[101] **Light-based AMT** can be divided into a selective deposition or selective irradiation of the photocurable resin.[97]

3D Inkjet printers work with the method of selective deposition. Here, a photosensitive resin is deposited and assembled dropwise, and then, the layer is irradiated with UV-light, which leads to a cured material. With this technique, multi-materials are possible, but the printing process needs support structures for cavities and overhanging structures. Additionally, the surface is of poor quality and unsuitable for tissue engineering.[102, 103]

3D printing techniques, which are based on selective irradiation, also called lithography-based AMTs, can be subdivided again: *two-photon polymerization* (2PP), *laser-based stereolithography* (Laser-SLA), and *digital light processing stereolithography* (DLP-SLA).

With 2PP polymerization real 3D writing is possible.[104-106] Thereby, a near-infrared (NIR) laser is used, and the photopolymerization is initiated with femtosecond pulses, with photons half the energy of conventional 3D printing methods. A suitable photoinitiator will then absorb two photons in the focal point of the laser, and the polymerization starts.[107] The photon density would be too low along the laser path for the initiation.[108] In Figure 7, the underlying absorption principle with UV-light at the surface and the 2PP polymerization is compared.

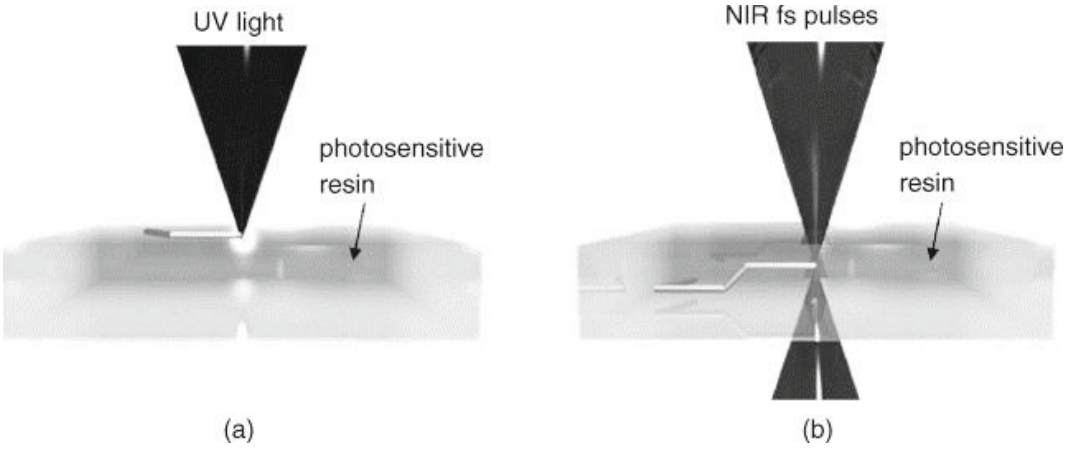

Figure 7: Comparison of a) absorption of UV light and polymerization at the surface and b) focused NIR pulses and polymerization inside of a photosensitive resin.[109]

The laser-SLA employs a UV-laser beam, which scans over the surface (xy plane) to initiate polymerization. After curing one layer, the platform will move in z-direction, and the next layer can be cured.[110] Here, two different build-ups are possible; the conventional arrangement irritates the photosensitive resin from the surface (bottom-up), or in the upside-down arrangement, the resin is irradiated through a transparent bottom window. The last mentioned avoids oxygen inhibition, and less resin is needed.[110, 111] This upside-down setup is depicted in Figure 8.

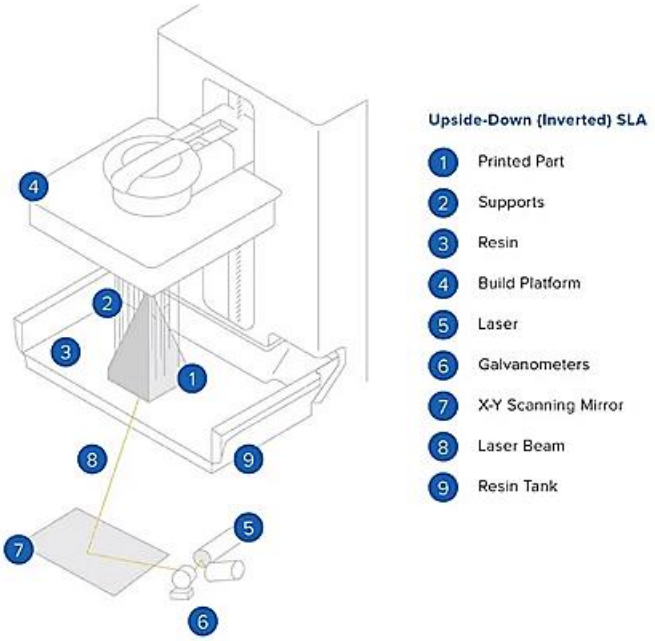

Figure 8: Schematic setup of a laser-based SLA 3D printer.[111, 112]

DLP-SLA employs a digital mirror device with a LED light source in contrast to laser-based techniques. Here, the whole cross-section of the resin is irradiated pixel-wise.[113] This setup (Figure 9, left) speeds up the process, especially when dealing with large cross-sections of a part. Additionally, a higher resolution can be achieved. Lithography-based ceramic manufacturing (LCM) is a slightly modified setup for high-viscosity resins. Here, in addition to the vat containing the resin, a wiper blade is continuously rotated, which allows the resin to be better distributed. The setup of a LCM printer is shown in Figure 9 on the right-hand side. In the LCM process, the photopolymerizable resin, which contains ceramic particles, is cured during printing, and a green body is formed. Then, the temporary green body is heated, and the organic matrix (binder) is removed. Last, a sintering process takes place to obtain the final dense ceramic parts.[114]

Figure 9: Schematic setup of a DLP-SLA 3D printer[112] and a LCM printer with a rotating blade for high-viscosity resins. Image adapted from Lithoz.[115]

Figure 10 shows the difference between Laser-SLA and DLP-SLA regarding their principle and resolution during irradiation. Laser-SLA uses a UV-laser to draw rounded lines, while DLP uses a projector screen to project layers of squared voxels. However, both can print layers with 25-300 µm thickness, allowing a good balance between detailed structures and printing speed.[112]

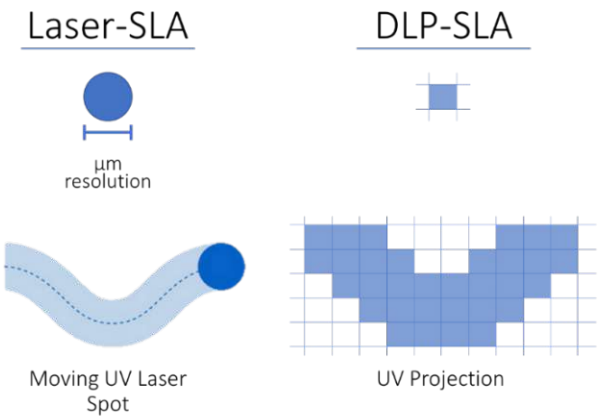

Figure 10: Principle and resolution of light-based additive manufacturing technologies (AMTs) for tissue fabrication. Laser-based stereolithography (left) and digital light processing (DLP, right), which use UV-light to initiate polymerization.[112]

5. Photopolymerization

The above-described light-based AMT techniques use photosensitive resins, where a liquid formulation is transformed into a solid material upon exposure to UV-light. This photopolymerization can occur predominantly by a radical or cationic mechanism.

A photopolymerizable system consists of three main parts: the light source of different wavelengths, a suitable monomer, and the photoinitiator (PI). Industrial designs are more complex and depend on the application; one can add mixtures of monomers, fillers, pigments, and regulating additives. However, this system must generally match requirements like low shrinkage, toughness, and color, to name a few.[116]

Understanding or being able to control the properties of the material requires an insight into the entire process from initiation to the finished polymer.

Both types of photopolymerization are described in detail in the following subchapters.

5.1. Free radical photopolymerization

Materials used for bone tissue engineering can be made, *e.g.*, from monomers polymerized *via* **free-radical polymerization**.

In the first step of free-radical polymerization, the PI is elevated upon irradiation with light in the case of photopolymerization or thermal energy to a higher energy state. Afterwards, the molecule decomposes and provides reactive compounds (radicals), which can then attack the photopolymerizable moiety (double bond) of a monomer. Due to this attack, a new radical is formed, passed to the chain end, and then can attack another monomer again. The process is repeated, and the polymer chain grows. This step is the so-called chain growth or propagation step. Upon recombination or disproportionation of two radicals, the propagation step is terminated.[117, 118] All radical photopolymerization steps can be seen in Scheme 1.

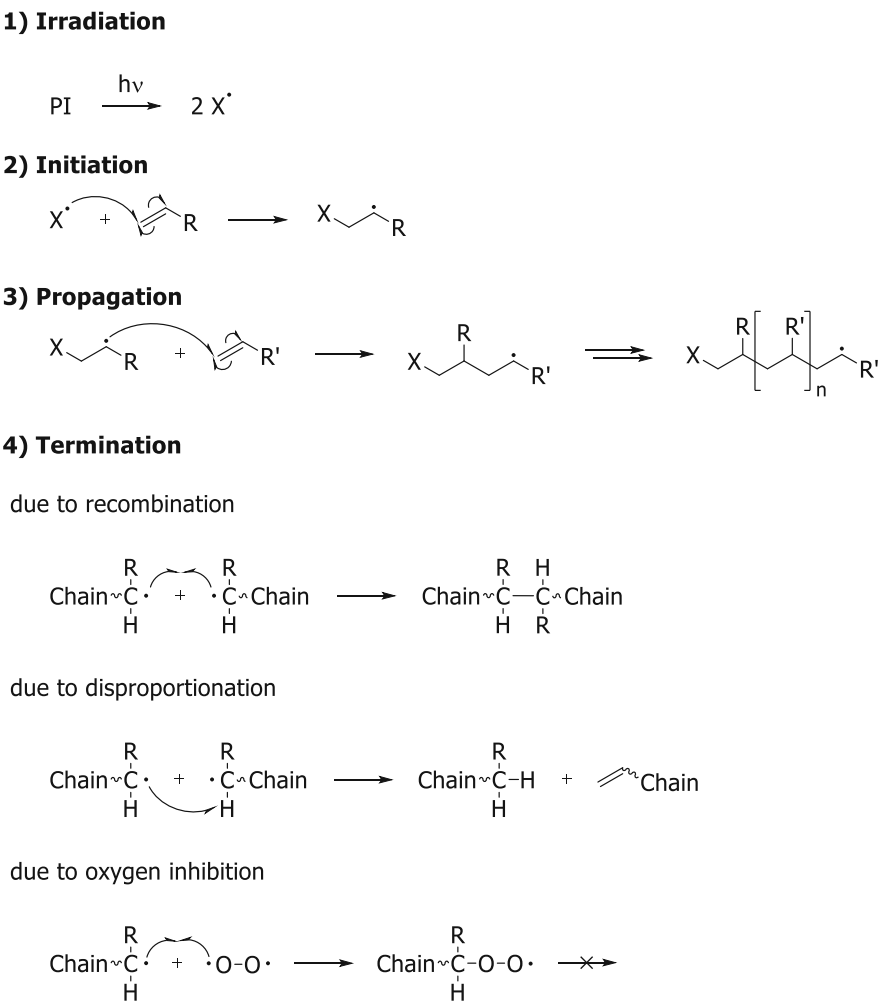

Scheme 1: Mechanism of free-radical photopolymerization: initiation, propagation, and termination steps.

Another reason for the termination of the chain growth is oxygen inhibition. Oxygen is a biradical and can recombine with an active species. However, the remaining radical cannot reinitiate a new chain. The diffusion of molecular oxygen into the monomer formulation can reach a depth of up to 60 µm, depending on the viscosity of the resin layer.[119] For this reason, an inert atmosphere is preferable for polymerization in thin layers, or expensive additives have to be used to prevent oxygen inhibition.[120, 121]

Before polymerization, most formulations are liquid at room temperature. The monomers have a low molecular weight, so the concentration of reactive double bonds is comparatively high. The choice of monomer determines the chemical and (thermo)mechanical properties. Thus, a linear polymer can be formed with monofunctional monomers or a polymer network with multifunctional ones. Some examples of low molecular weight monomers and reactive diluents are shown in Figure 11.

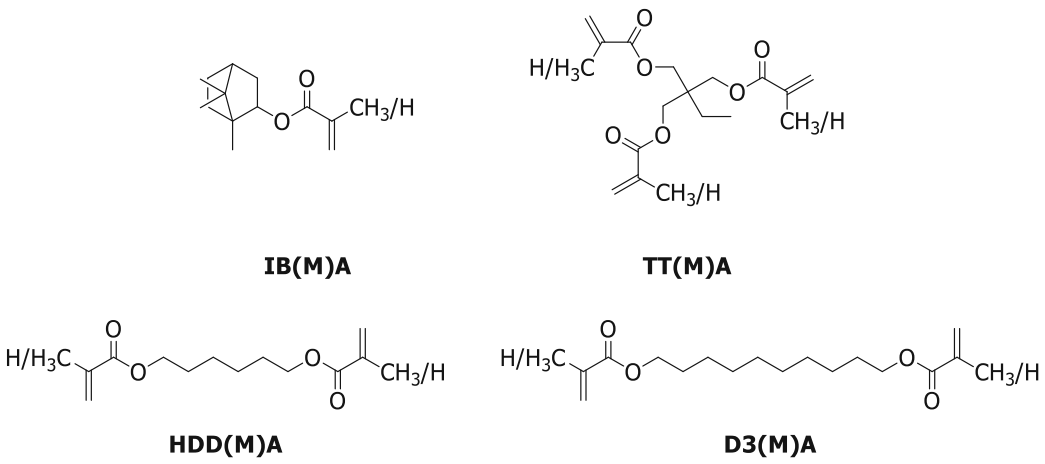

Figure 11: Chemical structures of typical monomers and reactive diluents in industry.

Usually, new covalent bonds are formed during polymerization. The liquid formulation reaches the gel point soon after initiation at low double bond conversions (DBCs), typically due to the high density of functionalities. Gradually, more covalent bonds are formed, the formulation solidifies, and immobile network domains are formed. These formations lead to shrinkage and further stresses in the material, which cannot be relieved. After that, most of the material continues to harden in the solid state, resulting in an inhomogeneous network with high internal stress (see Figure 12, left).[122] The final materials show broad glass transition temperatures and low impact resistance.[123]

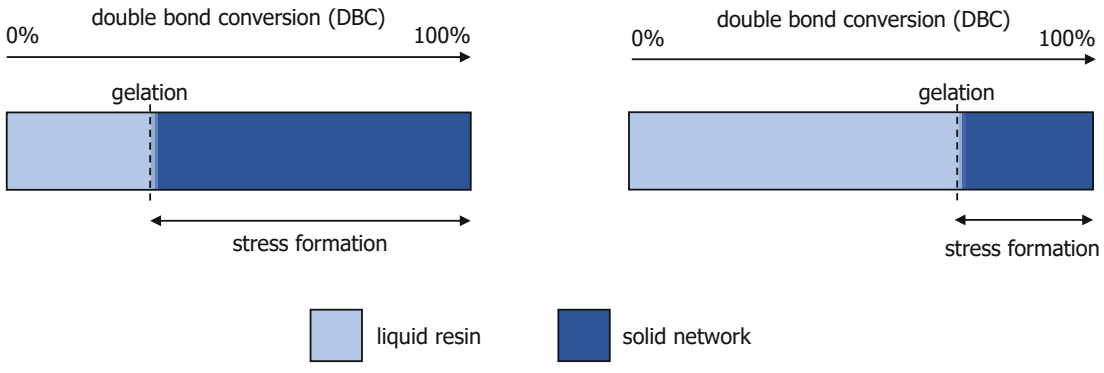

Figure 12: Formation of shrinkage stress during curing reaction for a non-regulated network (left) and a regulated network (right).

The buildup of internal stress in the material can be counteracted by tuning the monomer system. Here, the system should gel only at higher DBC and thus form a more homogeneous network. Hence, the formulation remains liquid for a longer timeframe, and significantly fewer monomers polymerize in the solid state. This process is schematically depicted in Figure 12 on the right-hand side. As a result of a more regulated/homogeneous

network, the toughness and (thermo)mechanical properties of the material can be improved.[122]

Chain transfer agents (CTAs) can promote the formation of a homogeneous network. They stop the ongoing chain growth reaction and subsequently start a new chain. This results in forming shorter chains but, at the same time, chains of approximately the same length, thus promoting the homogeneity of the entire network. The altered mechanism from the radical chain growth to a step-growth will be discussed in detail in Chapter 6.2. The regulation also results in a more defined glass transition than in a system that has been polymerized in an uncontrolled polymerization. This means the glass transition temperature decreases, but the temperature interval narrows. Furthermore, the addition of CTAs may enhance the double bond conversion because the mobility of the monomers in the formulation remains higher for a longer time due to delayed gelation.[124]

5.1.1. Photoinitiators for radical polymerization

The **photoinitiator (PI)**, which starts the photopolymerization, is a light-sensitive molecule that influences the curing speed of the resin and the final properties of the polymer. If the PI is irradiated with light, it absorbs the energy through its chromophoric groups. These chromophores contain n- or π- electrons and absorb in the UV-Vis region. Table 1 shows classic chromophores and their absorption maxima.[125] The transition from π-π^* happens at lower wavelengths than the transition from n-π^*, which the energy levels of the molecular orbitals can explain. Substances with an absorption band in the 400-800 nm range (wavelength of visible light) appear colored.[126, 127]

Table 1: Examples of chromophoric groups and their absorption maxima.[125]

Chromophoric group	λ_{max} π-π^* [nm]	λ_{max} n-π^* [nm]
C=C	170	-
C=O	166	280
C=N	190	300
N=N	-	350
C=S	-	500

Hull *et al.*[128] reported the first photocurable resin for SLA application with benzophenone as a photoinitiator.[116] Its chemical structure and absorption spectrum are shown in Figure 13. The n- and π*-orbitals of the carbonyl group barely overlap; therefore, the transition of n-π* is rare. On the contrary, the π-π* orbitals have a stronger overlapping, so the transition is more likely. The absorption spectrum depends not only on the molecule itself but also on the polarity of the solvent. Also, using the example of benzophenone, the shift due to the influence of the solvent is shown in the figure below.[129]

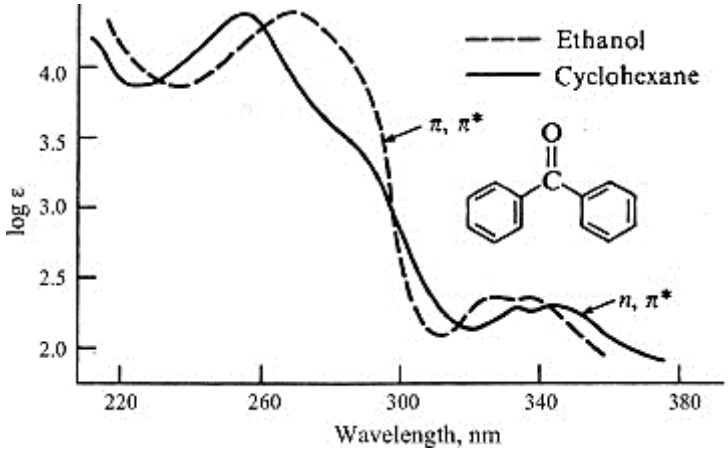

Figure 13: Benzophenone and its absorption spectrum in different solvents.[129]

Upon irradiation of the photoinitiator molecule, an electron gets excited from the ground state (S_0, electrons are paired) to a higher singlet state (S_1). In these two states, all electrons are in anti-parallel directions. Afterwards, the electron can either relax to a lower singlet state (internal conversion, IC) or reach a triplet state *via* intersystem crossing (ISC, electrons show parallel spin). Both are non-radiative processes.[130] All possible electronic transitions are shown in the Jablonsky scheme, Figure 14.[129, 131]

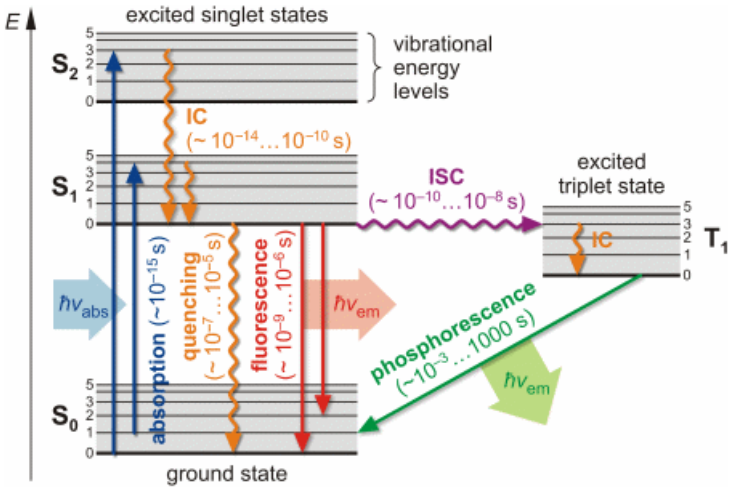

Figure 14: Jablonski diagram describing the electronic transitions of a molecule with processes of fluorescence, phosphorescence, and non-radiative transitions. IC means internal conversion and ISC intersystem crossing. Figure adapted from Steve Pawlizak (Diploma Thesis 2009).[132]

The excited singlet state is more short-lived (10^{-10}-10^{-7} s) than the triplet state (>10^{-6} s), while the last one is responsible for radical formation. Another possibility to dissipate excessive energy and relax to the ground state is the radiative deactivation (emission of photons) from the singlet state *via* fluorescence or from the triplet state *via* phosphorescence.[129, 131]

Radical PIs were classified into two types, depending on their mechanism of generating radicals from their triplet state. Norrish Type I photoinitiators contain a benzoyl chromophore to which either a tertiary carbon atom or heteroatoms (*e.g.*, phosphorus, germanium, tin, or other metals) are attached. Furthermore, molecules with diazo or peroxy moieties can be used as PI.[133] Figure 15 shows some examples of Type I PIs: Irgacure 651 (a benzyl ketal), Darocur 1173 (a hydroxyl alkyl acetophenone) and BAPO (an acylphosphine oxide).[127, 131]

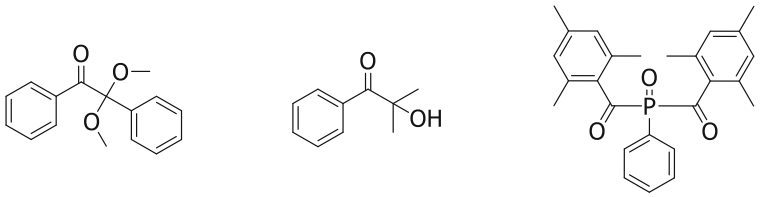

Figure 15: Chemical structures of common Norrish Type I photoinitiators.

These PIs generate radicals after a unimolecular fragmentation reaction (α-cleavage), as shown in Scheme 2 on two important photoinitiators.[127, 131] Ivocerin® is a

germanium-based and TPO-L a phosphine oxide PI, often used in dental filling and 3D printing applications.[134-136] After the homolytic cleavage of Ivocerin® into benzoyl- and germyl radicals, it shows rapid curing and an increased curing depth. These effects are based on the bathochromic shift and the higher absorption maximum of 408 nm. Therefore, it is suitable for applications in tissue engineering (short exposure, long wavelength).[135] Here, thick and highly filled systems can be cured, as longer wavelengths can penetrate deeper into the formulation.[137, 138]

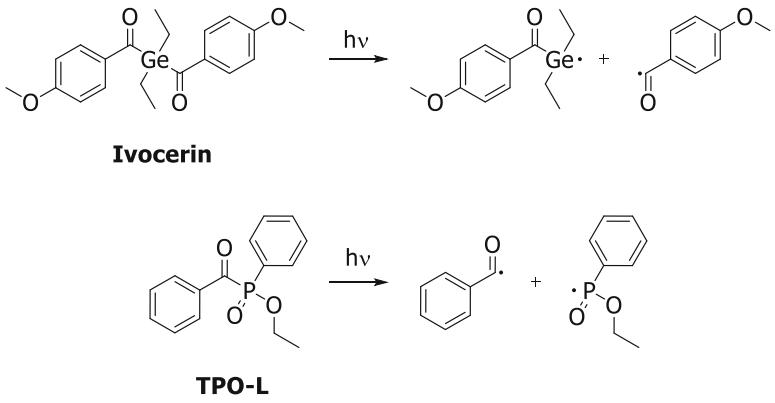

Scheme 2: Fragmentation reaction of Type I photoinitiators on the example of the germanium-based Ivocerin® and the phosphine oxide TPO-L.

Besides Type I, there are also Norrish Type II photoinitiators. This system consists of two compounds, a light-sensitive molecule and a co-initiator. Benzophenone, camphor quinones, or thioxanthones are typical Type II PIs, and amines are suitable co-initiators. With this type of PI, a bimolecular mechanism is described.[139] In the first step, an electron is transferred from the co-initiator to the chromophore, which was excited by irradiation. A proton transfer leads to the reactive co-initiator radical formation in the following step. One typical example is camphor quinone (CQ) in combination with ethyl-4-(dimethylamino)benzoate (DMAB), and their mechanism is depicted in Scheme 3.[127]

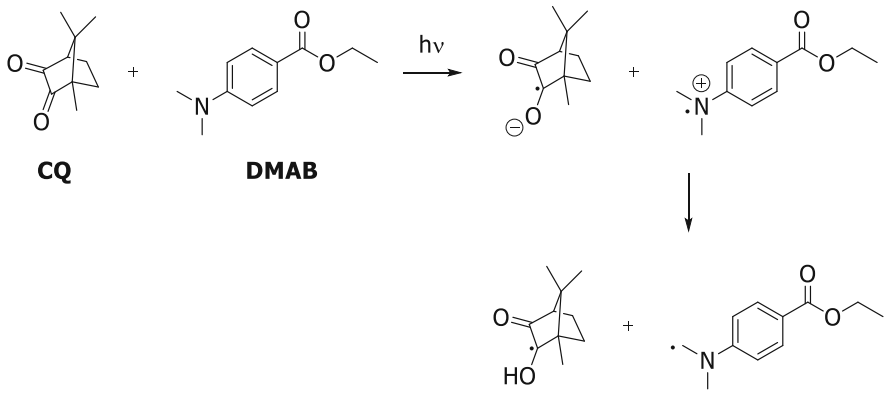

Scheme 3: Initiation mechanism of a Type II PI system on the example of CQ and DMAB.

However, they show much lower reactivity due to the bimolecular mechanism than their counterparts.[139] Nevertheless, they have an absorption window of >440 nm and show better biocompatibility. For this reason, they are often used in dental and tissue engineering applications. Unfortunately, the environment significantly impacts these PI systems, where, *e.g.*, an aqueous media, may pose a problem.[127] Here, the solvent cage effect of water may encapsulate the generated radicals and may promote recombination and prevents initiating propagation.[140]

5.1.2. Radical photopolymerizable monomers

The choice of monomer influences the reactivity and mechanical properties of the final material. Here, both the backbone (spacer) and the functional groups have an essential influence. For instance, soft polyesters, polyethers, rigid epoxy resins or polyurethanes with (meth)acrylate functionalities can be used (see Figure 16). Here, the aromatic ring structure and the additional π/π-stacking of the below-shown epoxy resin lead to hard but brittle materials. Strong (intermolecular) hydrogen bonds of, *e.g.*, urethane groups lead to (micro)phase separation and further affect the mechanical properties of the final material. Nevertheless, the resins exhibit high viscosities by adding high molecular weight monomers. For this reason, the resins are only processable after adding reactive diluents (see Figure 11).

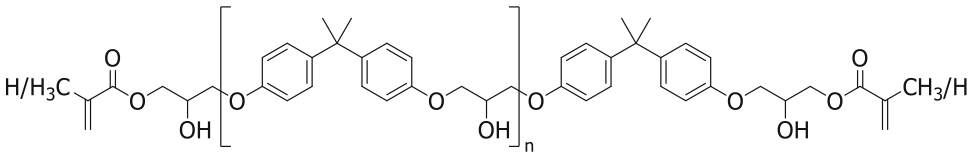

epoxy (meth)acrylate resin

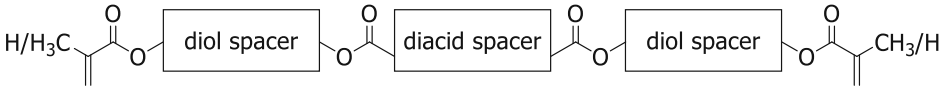

polyester (meth)acrylate resin

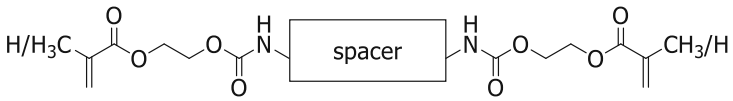

urethane (meth)acrylate resin

Figure 16: Examples of photopolymer resins with (meth)acrylate functionality.

(Meth)acrylates are favorable monomers in the dental industry as they show high reactivity. Despite their reactivity, a main issue is that they were proven to be highly cytotoxic, which is why they are avoided in BTE.[141, 142] In addition, their degradation products are high molecular weight poly(meth)acrylic acids, which cannot be removed *via* metabolic pathways and accumulate in the surrounding tissue. These acids lead to a decrease of the pH-value, followed by irritation and inflammation of the tissue. In addition, the accumulation of these acids can lead to internal degradation and consequent implant failure. This process is referred to as bulk erosion. In contrast, degradation that occurs only at the surface (surface erosion) would be desirable. The residual monomers hydrolyze to (meth)acrylic acid and these show an LD_{50} value for rats at oral intake ranging from 2260 $mg \cdot kg^{-1}$ (for methacrylic acid) to 340 $mg \cdot kg^{-1}$ (for acrylic acid).[143, 144] Comparing acrylates with methacrylates among each other, methacrylates show slightly lower cytotoxicity but also lower reactivity.

Vinyl esters (VEs), on the other hand, are considered a promising alternative to (meth)acrylates, as they exhibit significantly lower cytotoxicity.[145-150] Residual monomers can also be degraded in the body to acetaldehyde, which in turn is converted to acetic acid by acetaldehyde dehydrogenase. When the polymer is degraded, poly(vinyl alcohol) is formed, which is FDA approved.[151]

However, vinyl esters imply a low reactivity to free radical polymerization, which means that the resulting radicals are very reactive and predominantly undergo H-abstraction or homopolymerization. VEs polymerize according to the so-called chain growth mechanism, which leads to inhomogeneous materials and can weaken their properties. The chain-growth mechanism can be shifted to a step-growth mechanism using thiol-ene chemistry. When vinyl esters are combined with thiols, homopolymerization of the monomer and the thiol-ene reaction occur simultaneously.[152-155] The different reaction mechanisms of vinyl esters with and without thiols are shown in Scheme 4.

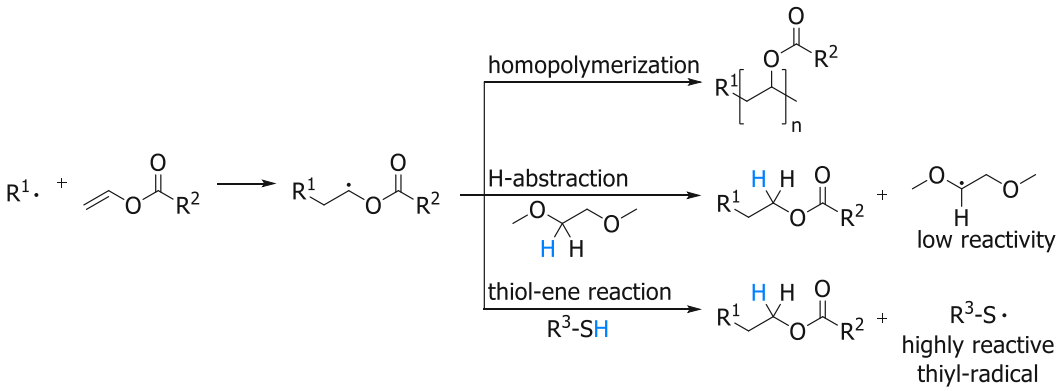

Scheme 4: Polymerization mechanism of vinyl esters and thiol-ene reaction.

Using thiol-ene reactions brings advantages such as increased reactivity, suppression of oxygen inhibition, and formation of more homogeneous networks, thus improving the material properties (*e.g.*, toughness). Thiol-ene chemistry is mainly used in dental prostheses, hydrogels, and tissue adhesives.[156, 157]

5.2. Cationic photopolymerization

Besides, free-radical polymerization, **cationic photopolymerization** can be used to generate scaffolds for bone replacement materials. Like free-radical photopolymerization, a liquid resin is converted into a solid material by exposure to light. However, in the cationic mechanism, other monomers and photoinitiators are used.

Initiation of cationic photopolymerization, a photoacid must first be generated (see Scheme 5). In this process, the photoinitiator (*e.g.*, an iodonium salt) is irradiated with a UV-source, which leads to an excitation into the singlet state. This state is energetically unstable and leads to a homolytic or heterolytic fragmentation into various radical and cationic species. In the next step, these species react with the monomer, solvent, or other protogenic components that generate the photoacid (HX), which initiates the polymerization reaction.[158]

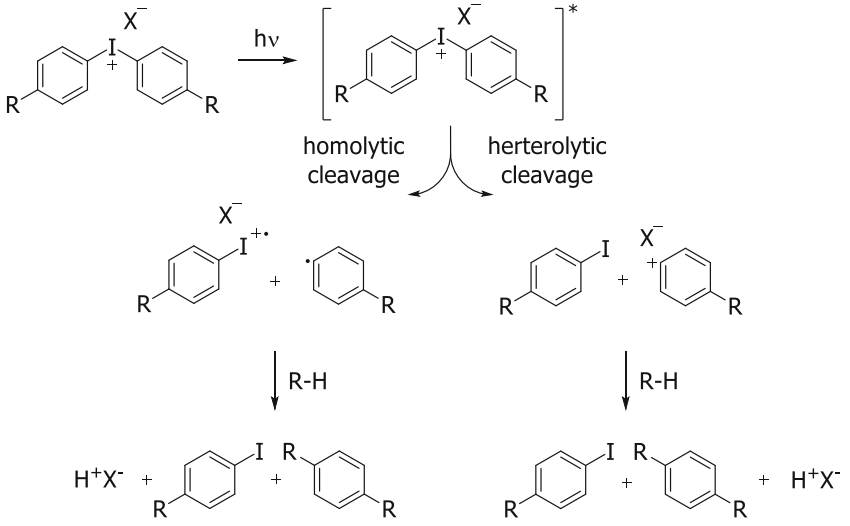

Scheme 5: Mechanism to generate the photoacid HX from the photoinitiator upon irradiation.[158]

After the formation of the photoacid, the photopolymerization reaction can start. This process will be described using oxetane as monomers and is shown in Scheme 6.

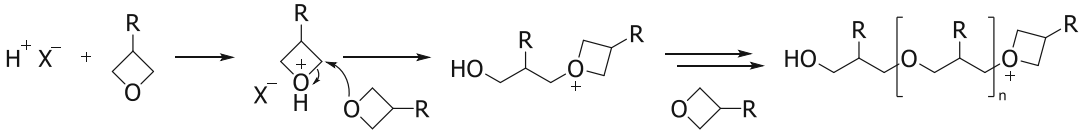

Scheme 6: Mechanism of cationic photopolymerization of an oxetane monomer.

In the initiation step, the photoacid (Brønsted or Lewis acid) provides a proton or carbocation, which can rapidly add to the monomer. The formed secondary oxonium species attacks the cyclic ether monomer *via* nucleophilic ring-opening (S_N2-reaction), generating a tertiary oxonium species. Last, the cyclic ether monomer attacks the tertiary oxonium ion, and thus, chain growth occurs.[159] During this, the positive charge is transferred from the chain end to the electron-donating group of the same molecule. A termination step only appears if a negatively charged ion, *e.g.*, of the photoinitiator or an impurity, recombines with the growing polymer chain.[160-162]

5.2.1. Photoacid generators

Crivello et al. presented in the 1970s diaryliodonium- and triarylsulfonium salts as cationic photoinitiators. These two classes show high efficiency, stability, and solubility in almost every cationic monomer.[163, 164]

These photoinitiators are also called photoacid generators (PAGs) for forming an acid, which initiates the polymerization reaction.[163, 164] The cation of the PI functions as a

chromophore and defines the PAG's quantum yield, absorption wavelength, and thermal stability. In contrast, the anion determines the acid strength generated during the decomposition of the PAGs and the propagation rate.[165] It is evident that the anions are highly fluorinated (Figure 17), which causes a low nucleophilicity of the counterions. Therefore, the ion dissociation is higher, resulting in a higher reactivity and acid strength. The nucleophilicity of the below-shown anions decreases from left to right.[125]

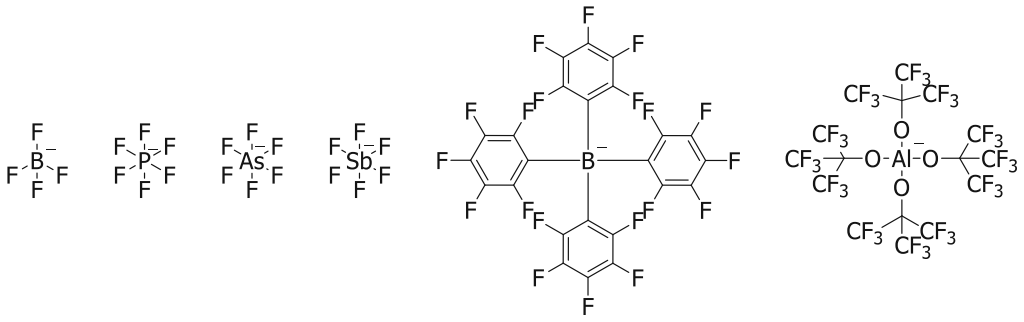

Figure 17: Typically used anions for photoacid generators (PAGs).

Examples of some PAGs, are the borate-based triarylsulfonium salt Irgacure® 290 (IC290), the antimonate-based triarylsulfonium salt (Cyracure uvi 6976, S-Sb), and the iodonium aluminate (I-Al) and are depicted in Figure 18. Diaryliodonium salts show a maximum absorption wavelength λ_{max} of 227 nm and have a slightly higher photoreactivity than sulfonium salts. Anyway, triarylsulfonium salts show an improved λ_{max} with about 300 nm and exhibit excellent thermal stability in comparison to diaryliodonium-based PAGs.[97, 164, 166]

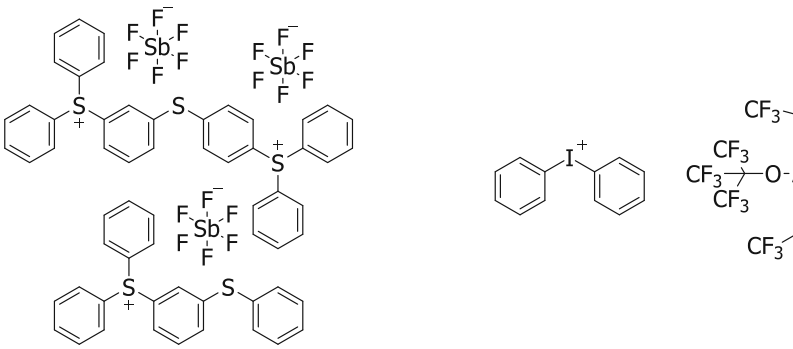

S-Sb **I-Al**

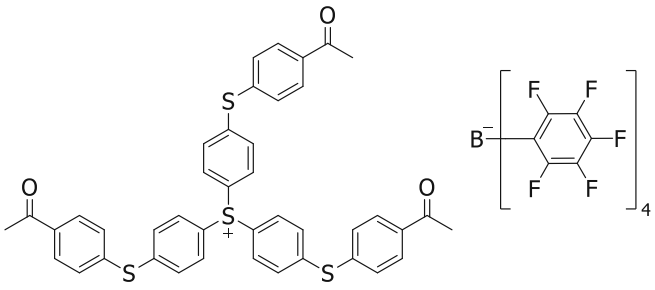

IC290

Figure 18: Chemical structures of cationic photoinitiators IC290, S-Sb, and I-Al.

5.2.2. Cationic photopolymerizable monomers

In cationic photopolymerization, **epoxides** are currently the most common monomer class. They show low shrinkage (2-3%)[161] during the polymerization, excellent mechanical properties, and good thermal and chemical resistance.[167] BADGE, an aromatic bisphenol-A glycidyl ether, is the most widely used epoxy monomer in industry. Unfortunately, the starting materials, bisphenol-A and epichlorohydrin, show elevated health risks. An excellent alternative to BADGE is the cycloaliphatic epoxide CE. It shows lower viscosity, good electrical properties, and better resistance against weather influence.[168, 169] These industry-suitable difunctional monomers are depicted below in Figure 19. They find applications in coatings, adhesives, or printing inks.[161] Monofunctional monomers like phenyl glycidyl ether (PGE) function as a reactive diluent to lower the viscosity of the resin or as a promoter for better adhesion.[161]

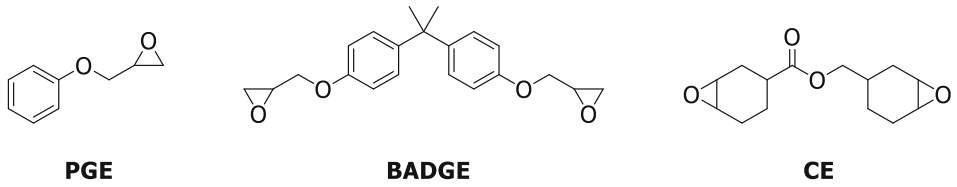

Figure 19: Industrial important epoxide monomers PGE (phenyl glycidyl ether), BADGE (bisphenol-A glycidyl ether), and CE (3,4-epoxycyclohexylmethyl-3,4-epoxycyclohexylcarboxylate).

Other important monomers for cationic photopolymerization are four-membered cyclic ethers, the so-called **oxetanes**. Oxetanes with substituents in their 3,3-position polymerize faster and are thus used more frequently than 2,4-substituted ones.[170, 171] Examples of difunctional oxetanes are 3,3'-[oxybis(methylene)]bis[(3-ethyl)oxetane] (**DOX**) and 1,4-bis(((3-ethyloxetane-3-yl)methoxy)methyl) benzene (**XDO**), which are depicted in Figure 20. This monomer class is also used in coatings, printing inks, or adhesives due to their similar structure to epoxides.

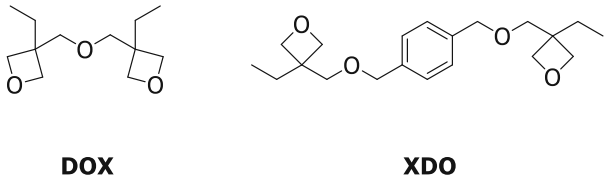

Figure 20: Structures of the difunctional oxetanes **DOX** and **XDO**.

Oxetanes are great alternatives to monomers with epoxy functionalities, showing lower toxicity. Furthermore, they show less shrinkage during polymerization.[172, 173]

Various advantages compared to free radical photopolymerization are provided by cationic photopolymerization. The most crucial one is that there is no inhibition due to oxygen. Further, low shrinkage during network formation is observed upon ring-opening polymerization. Moreover, the polymerization may continue after the light source has been removed and the cationic polymerization has been initiated. This process is also called "dark reaction". Here, no termination reactions happen, and relatively long-lived protonic acid-initiating species are present.

In contrast, bases and basic components such as urethanes, amines, or thiols may inhibit the reaction, which is an enormous drawback.[97, 164] Hydroxyl-containing molecules, like water or alcohol, may act as so-called chain transfer agents (CTAs), even in small amounts. Here, these molecules transfer the active center away from the growing chain. This mechanism will be discussed in detail in subchapter 6.2.

6. Strategies for photopolymer toughening

Uncontrolled photopolymerization of small molecules with, *e.g.*, (meth)acrylic functionalities leads to inhomogeneous networks, which have a high cross-link density and yield in hard but also brittle materials.[124, 174] Thus, these materials cannot be used without improvement in dental applications or as materials for additive manufacturing technology.

One fundamental property is the toughness of photopolymers. Toughness is described as the ability to absorb energy, *e.g.*, in the form of abrupt impact (impact resistance) or while being pulled apart (tensile toughness) without breaking. Nevertheless, increasing toughness frequently decreases hardness and stiffness.[124, 175] High strength, stiff, and hard polymeric materials show limited toughness due to their low elastic behavior. However, high strength, stiffness, and toughness are often desired for one material for engineering applications. Toughness can be determined by, *e.g.*, tensile testing.

During tensile tests, the load is applied and raised steadily until the failure of the specimen, and a stress-strain curve is recorded. Exemplary curves for brittle, tough, and elastomeric materials are shown in Figure 21.[124]

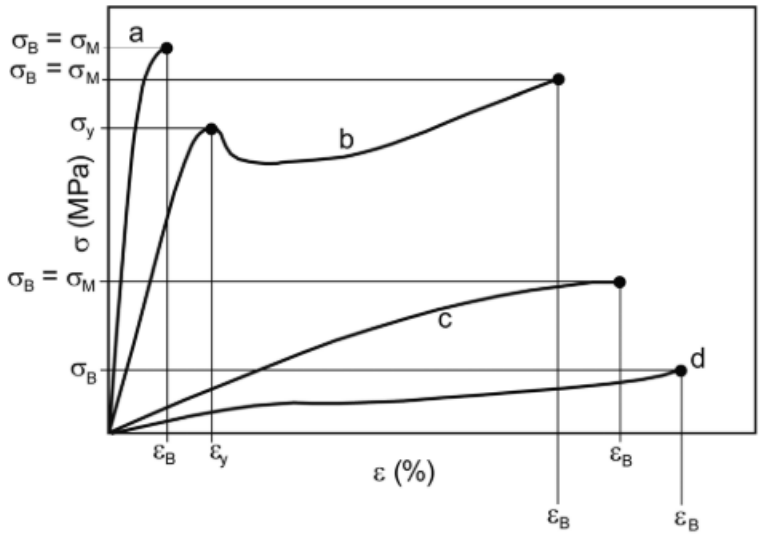

Figure 21: Exemplary stress-strain curve for brittle (a), tough materials with a yield point (b), tough materials without yield point (c), and elastomers (d). Figure adapted from Ligon-Auer.[124]

Photopolymers, *e.g.*, acrylates, are rather brittle and show a stress-strain curve corresponding to a) in Figure 21. Curves b) and c) describe tough materials with or without a yield point. If elastomeric materials are measured, they show a curve as depicted in d). The deformation energy U_T is related to the toughness of the material and is defined as

the area under this curve. If high values for U_T are determined, a good resistance against crack growth is given.[124]

Several opportunities are known to improve this essential material property. First, organic and inorganic fillers were added to the resin. Due to the interaction of the polymers and the surface of the particles, the mechanical properties, like hardness, stiffness, heat distortion temperature, and toughness, were improved.[124, 176, 177] Copolymerization of **high molecular weight additives** showed a positive affection, especially on the toughness.[35, 178] Moreover, adding **chain transfer agents** to the formulation leads to regulating the polymer network, which also results in a tougher material.[124, 179] Another technique is the generation of **interpenetrating polymer networks**, where two or more networks are interlaced but not covalently bonded.[124, 178]

6.1. High molecular weight additives

One method to change the final material's mechanical properties is adding high molecular weight molecules to the monomer solution. The physical interaction alone reduces the crosslink density and leads to the dissipation of the loaded stress, which in turn reduces brittleness and consequently increases toughness. Preliminary studies showed that covalent incorporation into the polymer network further increases the toughness of the material.[35, 146] Examples of high molecular weight additives are polyesters, -ethers, or -urethanes, which can be functionalized with photopolymerizable end-groups. Thus, by adding these molecules to a photocurable resin, thermoplastic-like materials are formed after curing. The enhanced toughness is obtained by an internal strengthening mechanism in which the long polymer chains interlace and orient themselves in the stretching direction.[180] One drawback is the relatively high viscosity of these resins, making them sometimes less suitable for traditional stereolithography. However, this problem can be circumvented by using hot lithography.[181]

6.2. Chain transfer agents

Thiols, which act as H-donors, are probably the best-known type of chain transfer agent (CTA). When thiols are used as CTAs, the radical of a growing polymer chain abstracts a hydrogen atom from the thiol, and the chain is terminated. The resulting highly reactive thiyl-radical then initiates the growth of another chain. However, to ensure this, the

hydrogen of the thiol must be easily abstractable. Here, the chain-growth polymerization can change to a step-growth mechanism or a mixture of both, depending on the electron density of the monomer. Electron-rich monomers with norbornene- or allyl functionalities tend to polymerize in a step-growth way.[153]

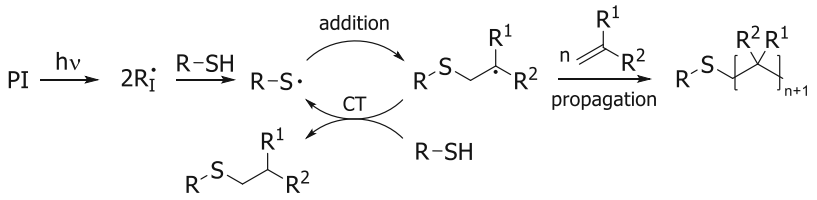

Figure 22: Mechanism of radical photopolymerization with thiols as chain transfer (CT) agents. Ongoing chain-growth is terminated by H-abstraction from thiol; formed thiyl radical initiates a new chain.[153]

More distributed and shorter chains are generated, whereas the homogeneity of the polymer network gets improved. Hence, the material's toughness gets enhanced and the shrinkage stress during the polymerization decreases. Another advantage of thiol-ene chemistry is reduced oxygen inhibition.[153]

Besides thiols, alcohols and water can act as CTAs for formulations containing epoxides or oxetanes (cationic polymerization). Cationic polymerization generally shows an activated chain end mechanism (ACE). The contrary mechanism, in this case, is the active monomer mechanism (AM). The last-mentioned mechanism occurs when alcohols are present during the cationic polymerization of, *e.g.*, epoxides. The AM-mechanism is depicted in Figure 23.

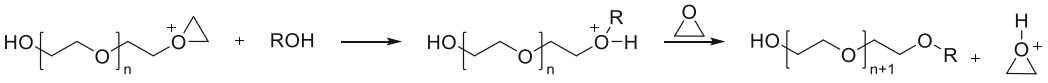

Figure 23: Activated monomer mechanism (AM) on the example of an epoxide.[182]

During the polymerization, the alcohol attacks the growing ionic chain, generating a protonated ether. A present epoxy monomer can then deprotonate the latter species, resulting in a termination reaction of the growing chain. The proton is transferred to the epoxy monomer, and a new chain can be initiated. Therefore, polymers with alkoxy end groups, which are derived from the used alcohol, are generated.[162, 183] Finally, this changes the polymerization rate and regulates the network structure.[172]

Water can also function as CTA and accelerate the cationic polymerization rate. However, the polymerization can be inhibited under high humidity conditions for vinyl ether- and epoxide-containing resins. The inhibition can be explained as follows: Low water concentration within the resin increases the rate and conversion, but a high humidity

means that the water concentration at the specimen's surface is highly-localized. Therefore, low molecular weight polymers are generated due to excessive chain transfer.[183]

6.3. Interpenetrating polymer networks

The classic concept uses different monomers with the same photopolymerizable functionality (*e.g.*, (meth)acrylates). However, they consist of either soft or hard segments, and therefore, the mechanical properties can be adjusted. After photopolymerization, they form one random network.[124]

A different way of polymer toughening is the creation of interpenetrating polymer networks (IPNs). This approach will generate at least two separate but interlaced networks and form one photopolymer. One network, for instance, consists of hard and rigid segments and should provide stiffness and modulus to the material. The other network is made from soft and flexible monomers, providing toughness and the ability for plastic deformation.[184]

Depending on the network structure and polymerization technique, three different types of IPNs can be defined. A *sequential* IPN is present if a monomer is swollen into an existing polymer network and cured afterwards. However, it could also be that two monomers with different orthogonal photoreactive groups (*e.g.*, cationic and radical) are present, and they were cured sequentially. A *simultaneous* IPN is stated if two networks are formed at the same time but do not interfere with the other. Polymerization of a monomer, while another polymer is present, is related to a *semi*-IPN type.[184, 185] The difference between a semi-IPN and an IPN is depicted schematically in Figure 24.

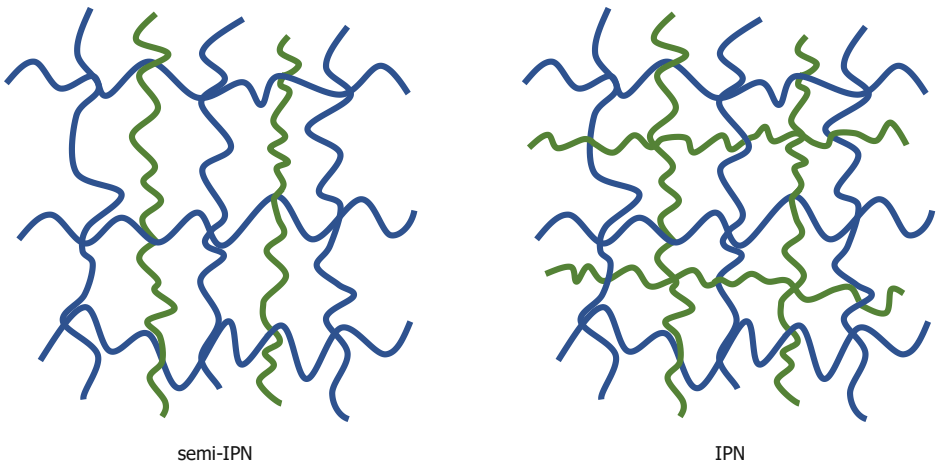

Figure 24: Schematic representation of an IPN and a semi-IPN.[184]

Disadvantages like oxygen inhibition[120, 121] or shrinkage stress[122] for radical polymerization and low conversions or humidity sensitivity for cationic polymerization[167] can be overcome using the orthogonal polymerization technique. The solvent effect explains the low oxygen inhibition for the radical system, whereas the cationic monomers profit from the air humidity, leading to accelerated polymerization. For this reason, IPNs are often used for impact resistance materials or in coatings and biomedical applications.[186]

OBJECTIVE

Lithography-based additive manufacturing technology has become increasingly prominent recently, especially in bone tissue engineering (BTE). Here, patient-specific porous implants can be generated with high resolution. (Meth)acrylates are currently the state-of-the-art monomers for digital light processing stereolithography (DLP-SLA). They combine favorable reactivity and mechanical properties and find applications in BTE (*e.g.*, as bone cement)[187] or in dental restoratives.[50] However, they show high irritancy or cytotoxicity, and their degradation products (poly acids) can harm the surrounding tissue. Therefore, vinyl esters (VEs) are used instead to circumvent this problem. Unfortunately, the obtained networks lacked sufficient toughness for bone graft substitutes (especially for screwed implants). In addition, substituting (meth)acrylates with VEs leads to decreased reactivity due to poor resonance stabilization of the formed radicals of VEs. The generated radicals are highly reactive, which leads to side reactions (hydrogen abstraction) instead of the preferred addition to monomers. For these reasons, a mixture of vinyl esters with thiols was used to boost the reactivity and improve the mechanical properties (impact resistance) through thiol-ene moderated network formation.[145] Radicals, which are formed during the initiation step, preferably react with the thiol, which is very susceptible to hydrogen abstraction. A highly reactive thiyl radical is generated, and this can propagate polymerization. Due to that, it could be expected that the initiation of low reactive radicals (from hydrogen abstraction reactions) can be achieved. However, the toughness of such materials is still insufficient. There are two different concepts, which should be evaluated within this thesis to further improve the toughness.

I.) The addition of high molecular weight (MW) polymers is hypothesized to further improve this property of the final material. Therefore, it is the aim to synthesize and investigate different toughness-enhancing additives. These additives should be based on the polyester poly(ε-caprolactone) (PCL), which is already applied as a biodegradable and biocompatible polymer. Furthermore, its toughness-enhancing ability was proven in previous studies.[35, 146] The described polymer should be used as a diol so that it can be easily end-capped with vinyl- /allyl carbonate and norbornene functionalities. Their impact on the chemical and (thermo)mechanical properties, especially on the toughness, of the final polymer, should be determined. Additionally, the influence of different molecular weights of the polymers should be investigated. Further toughness improvement could arise by broadening the polydispersity index (PDI) by mixing different MWs of the polymers.

Furthermore, the impact of two different thiols, one flexible and one rigid, on the final properties should be determined.

Finally, the best-performing system should be 3D printed, and the influence of varying sterilization methods on the (thermo)mechanical properties should be studied.

II.) Another way to improve the toughness of the final material is the formation of interpenetrating polymer networks (IPNs), which is the second goal of this thesis. Here, two different curing mechanisms (radical and cationic) will form two different networks, which are interlaced, but not covalently bonded. One network should contain flexible segments, and the other one hard segments.

The flexible system should contain the above-mentioned high molecular weight additives, in combination with thiols. In contrast, the hard matrix should be made of polyethers, which derive from oxetanes. Therefore, the synthesis of new multifunctional oxetanes as cationic monomers will be in focus. Moreover, they will be combined with hydroxyl-terminated chain transfer agents, which should be also synthesized. However, both compounds should contain esters as degradable moieties.

The combination of both networks is hypothesized to improve the mechanical properties of the final polymer system. For this reason, IPN materials should be generated and fully characterized. Therefore, their photoreactivity and (thermo)mechanical properties will be investigated.

GENERAL PART

A. Toughness enhancers for 3D-printed photopolymers

1. State of the art

1.1. Photopolymers for tough bone replacement materials

The fabrication of medical devices, surgical guides, or patient-specific artificial bone scaffolds *via* additive manufacturing technologies has become increasingly important over the past few decades. Light-based AM techniques have the advantage of showing excellent resolutions, and the mechanical and functional properties can be influenced by adapting the resin. Here, parameters such as biocompatibility, viscosity, reactivity, mechanical properties, and degradation behavior play specific roles.[188] The mechanical properties, such as tensile strength and modulus of elasticity, of the artificial scaffold must be matched to the surrounding tissue to ensure good load transfer and tissue integration. Photopolymer networks are often highly cross-linked, resulting in brittle scaffolds. For this reason, when selecting the resin, consideration must be given to ensure that sufficient ultimate toughness is provided.[35, 146, 189]

(Meth)acrylates were already introduced in the 1960s by Sir John Charnley for bone cements[187] or found application in dental restoratives.[50] Due to their high reactivity and stiffness, they are state-of-the-art monomers for DLP-SLA.[107] Acrylates show high reactivity but also undergo Michael addition reactions with thiols and amines present in, *e.g.*, proteins within the human body. Therefore, materials from these monomers cause irritation and sometimes toxicity in the surrounding tissue. Methacrylates show less cytotoxicity compared to acrylates but also a lower reactivity.[147, 190]

For this reason, (meth)acrylates were replaced by vinyl ester- (VE) and vinyl carbonate-based monomers for biomaterials because they show good biocompatibility and degradation behavior but do not undergo Michael addition.[145, 147, 149, 190] The final degradation product through hydrolyzation of these poly(vinyl esters) and poly(vinyl carbonates) is poly(vinyl alcohol) (PVA). PVA is a non-toxic product, FDA-approved and is already used in biomedical applications.[191]

The formation of scaffolds with insoluble 3D polymer networks requires multifunctional monomers. For instance, divinyl adipate (DVA) is a difunctional vinyl ester. It is already used in formulations for additive manufacturing to fabricate bone replacement scaffolds,

which were also tested *in vivo*.[191] However, DVA is the only commercially available multifunctional monomer.

Unfortunately, during the curing process, the photopolymers show high volumetric shrinkage, rendering the final materials too brittle for intended applications, especially for screwed implants.[189, 191]

1.2. Toughness-enhancing strategies for photopolymers

The high toughness of the final material is essential, especially when used as a bone replacement material. Here, the implant must not crack or fail when it is, for example, screwed or when external forces are applied.

The mechanical performance of glassy (meth)acrylate or epoxy networks, especially the tensile or fracture toughness and impact strength, can be improved by a variety of methods. Researchers are trying to translate known toughening strategies from epoxy-based systems to acrylate-networks to reduce brittleness and enhance the toughness. However, there is no significant change in polarity during radical photopolymerization, impeding the polymerization-induced phase separation. Last is a well-known technique to efficiently increase the toughness in thermosetting epoxy systems.[192-194] In radical systems, on the one hand, modifications of the chemistry in (meth)acrylated glassy networks can be made, or toughness-enhancing additives can be used to enhance the mechanical properties.

1.2.1. Changes in the photopolymerization mechanism

The photopolymerization of multifunctional acrylates leads to rapid gelation and further to inhomogeneous photopolymer networks, which show high brittleness and low toughness. A regulated network homogeneity is proposed to enhance toughness, which can be induced by changing the mechanism from a chain growth to a step-growth mechanism using **chain transfer agents** (CTAs).

For instance, *thiol-ene chemistry* can be used, where thiols act as CTAs, which can regulate the polymerization kinetic and, therefore, tailor the mechanical properties of the final polymer.[195] Thiols are hydrogen donors, and after initiation, the generated thiyl radical reacts with an unsaturated double bond in an anti-Markovnikov manner. In combination with electron-rich alkenes (vinyl ether, allyl ether, or norbornenes), thiols react *via* an ideal step growth mechanism. Here, a delayed gelation results in a moderated network

formation.[152, 153, 196, 197] The storage modulus decreases, and the glass transition temperature range is narrowed down.[145] Furthermore, the shrinkage stress during the polymerization will be reduced while the fracture toughness increases.[145, 198]

For example, specimens showed an improvement in fracture toughness after adding a urethane tetra allyl ether monomer with PETMP as thiol to a bisGMA/TEGDMA compared to the system containing merely methacrylate monomer.[197] Here, the mechanism from chain growth (homopolymerization of (meth)acrylates) was changed to a mixed chain growth/step growth-like manner. Sycks and his research group published an article using thiol-ene chemistry and simultaneously incorporated a spiroacetal moiety into the polymer backbone using 3,9-divinyl-2,4,8,10-tetraoxaspiro[5.5]undecane. As a result of this, a tough semi-crystalline photopolymer was formed. Variation of the crosslink density led to a tuneable crystallinity and microstructure and further to controllable (thermo)mechanical properties.[199, 200]

Besides thiol-ene chemistry, also *thiol-yne* polymerization is possible. This concept was first described in the 1930s and has been taken up in the field of photopolymerization in recent years.[195, 201] Thiols and monomers with carbon-carbon triple bonds should ideally be converted in a 2:1 ratio. First, a vinyl sulfide will be generated, and then, in a second reaction with another thiol, the thioether bridge will be formed. These highly crosslinked and homogeneous networks exhibit unique thermomechanical properties, such as higher toughness than thiol-ene systems and (meth)acrylate photopolymers.[201-204]

Unfortunately, the incorporation of thioether bridges into the polymer network due to thiol-ene/yne chemistry can reduce the hardness and storage modulus.[59, 145]

Moreover, *addition fragmentation chain transfer (AFCT)* reagents can be used. Here, the propagating radical will attack the AFCT, and a leaving group will form again a reactive radical after cleavage, which can undergo further propagation. For instance, *e.g.*, allyl sulfones, β-allyl sulfides, or vinyl sulfone esters can be used.[122, 205-208] The combination of allyl sulfides and (meth)acrylate-based monomers is presented by Bowman *et al.*[209] and Sato *et al.*.[210] Their research groups showed that the shrinkage stress induced by photopolymerization was significantly reduced for the acrylate system.[209] However, the AFCT reagent was not ideal for the methacrylate system, and here, a reduction in shrinkage stress was only achieved in combination with thiol-ene chemistry.[210] Our research group also investigated AFCTs reagents (β-allyl sulfones) in a methacrylate-based resin. With this system, the shrinkage stress was decreased, while the

conversion and the toughness were improved.[122, 209] Furthermore, our research group synthesized a heterotelechelic hybrid oligomer. This oligomer is based on poly(propylene oxide) with one methacrylic- and one AFCT end group. This study showed successful toughening by regulating the network structure due to the AFCT mechanism while acting simultaneously as a reactive diluent for highly viscous resins.[211] A particular case of AFCT is the *reversible-addition fragmentation chain transfer (RAFT)*. As RAFT agents, dithioesters and trithiocarbonates can be used.[212]

Moreover, there are also other approaches that use photo-"click" reactions to improve ductility and toughness. For example, *copper-catalyzed azide-alkyne cycloaddition (CuAAC)*.[213-215] Light-induced CuAAC uses Cu(II), which is simultaneously reduced to Cu(I) using photochemical reactions. The advantage is that air-sensitive Cu(I) is formed in situ.[216] As a product of the CuAAC reaction, triazole-based networks are generated, which showed excellent mechanical properties due to multiple deformation-recovery cycles. The research group of Song *et al.* suggests that the generated triazoles can improve tensile strength despite a highly cross-linked structure and a glassy network state. However, this is only possible if there are sufficient freely rotatable links between the network junctions.[217, 218]

1.2.2. Additives for photopolymer toughening

Another approach to generate tough materials is the use of additives.

One method in epoxide-based resins is the addition of **inorganic nanoparticles**, such as silica,[219-221] Al_2O_3[222], and $CaCO_3$,[223, 224] to enhance the toughness of photocurable polymers. Due to strong interactions, it is assumed that polymer chains attached to the nanoparticles behave differently than polymer chains within the polymer matrix. Because of the large surface area of the nanoparticles, many polymer chains are attached to the nanoparticles even at low filler loadings and thus occupy the largest part of the polymer matrix. This can lead to new material properties.[177] For example, high adhesion between particles and matrix can prevent separation under loading, which leads to an increase in modulus and strength.[124] However, the exact mechanism has not been fully clarified, but numerous studies show that particle size, morphology, and filler-matrix interaction affect toughness behavior.[225, 226] Unfortunately, this effect was not observed in tested acrylate-based networks. Here, the nanoparticles only led to improved stiffness and

hardness. In general, the strategies for polymer toughening of epoxy resins can not be easily transferred to radical photopolymerized networks.[124]

In the work of Maalihan *et al.*, surfactant-modified chitosan **particles** were added to a poly(methacrylate) (PMA) matrix to increase the toughness of the composite. For this purpose, chitosan was modified by ionic complexation with the anionic surfactant sodium dodecyl sulfate. This composite material was 3D printed and investigated for its mechanical properties. It was recognized that the use of the modified chitosan particles resulted in a 184% increased toughness than the pure PMA.[227]

Another method is the addition of **natural** or **synthetic rubbers**. Here, phase separation has been identified as an important parameter for rubber toughness, which means that both particle size and the interface between rubber and matrix must be regulated. This can be done either by using *liquid rubbers* with low molecular weight or preformed *core/shell-particles (CSPs)*.[228] As *liquid rubber*, hydroxy-terminated polyether, *e.g.*, poly(epichlorohydrin) or vinyl-terminated poly(butadiene-acrylonitrile) can be used. During curing, a separated rubber-rich phase will be formed within the brittle one. This formation leads to improved fracture toughness.[229] *CSPs* are solid, preformed with an elastomeric core and a thin layer of a glassy shell. The glassy shell suppresses the agglomeration of the particles, and hence, the size and shape of the particles can be regulated. For example, the core of a CSP can consists of styrene/butadiene and has a PMMA-shell. Added to a bisphenol-A-diglycidyl ether (BADGE)-based resin, it can increase the fracture toughness.[116, 228, 230, 231] Another publication describes core/shell organic-inorganic hybrid polymer nanoparticles (Si-ASA HPNs) with a silicone-modified butyl acrylate copolymer (PBA) core and a styrene-acrylonitrile copolymer (SAN) shell to improve the toughness of poly(methyl methacrylate) (PMMA). These studies showed that the addition of silicone-modified poly(acrylonitrile-styrene-acrylate) (Si-ASA) to PMMA improved the impact strength and elongation at break. Especially materials with 5 wt% silicone showed the best results.[232]

Salminen *et al.* published an article in which networks based on butyl acrylate could be improved by adding **dynamic crosslinkers**. These dynamic crosslinkers consist on a cationic and an anionic molecule, where both also have a double bond as a polymerizable group. The ion pairs form dynamic crosslinks, which can break and reform upon deformation. Breaking the weak ionic bonds allows the energy to dissipate, preserving the stronger covalent network.[233-235] Formation of covalent bonds by reaction of the double bond is used for dimensional stability of materials. This study investigated dynamic

crosslinkers, such as tributyl (4-vinylbenzyl) ammonium sulfopropyl acrylate and trihexyl (4-vinylbenzyl) ammonium sulfopropyl acrylate. The covalent bonds led to a reduction in elasticity but had little effect on strength. However, the dynamic bonds led to a significant increase in elasticity.[236]

Another method is the addition of **prepolymer blends**, *e.g.*, linear/block polymers[237-239] or elastomers.[240] Some degree of heterogeneity in the polymer network can lead to suppressed crack propagation and increased toughness. Such heterogeneous materials, which consist of two different phases, can be formed when partially compatible polymers are mixed at high temperatures,[241] by self-assembly of block copolymers,[242] or by polymerization-induced phase separation (PIPS).[243]

For example, Szczepanski and Stansbury studied various methacrylate polymers, *e.g.*, PMMA and PEMA in TEGDMA, and their behavior upon UV irradiation. It was recognized that phase separation results in prolonged self-acceleration and, thus, higher monomer conversions than in homogeneous monomer systems.[244, 245]

Furthermore, blending with high-molecular-weight molecules reduces the network density, and introduced stress can be easier dissipated. This effect can be evoked by physical interaction alone. However, it can be further promoted if these molecules are chemically incorporated into the network.[146]

Some examples of high molecular-weight polymer blends are shown in Figure 25.

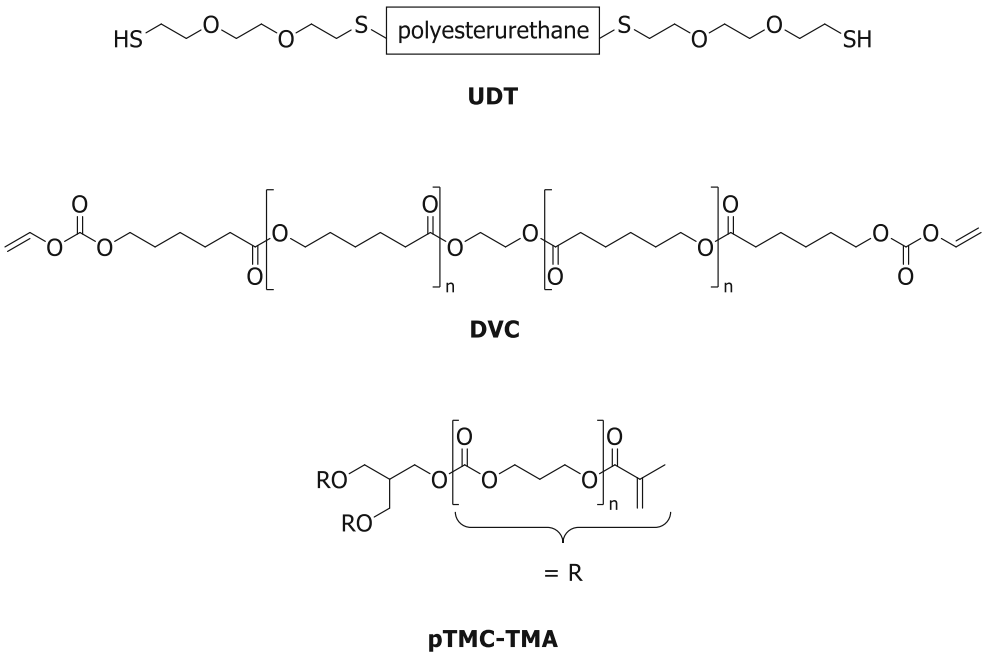

Figure 25: Examples of high molecular weight polymer blends: polyesterurethane dithiol (UDT)[146], polyester (DVC)[146] and poly(trimethylene carbonate) with methacrylate endgroups (pTMC-TMA)[246].

2. Synthesis

2.1. Synthesis of PCL-based toughness enhancers

Vinyl ester-based (VE) formulations are well-examined for additive manufacturing technology in tissue engineering. They show excellent biocompatibility and degradation behavior. However, highly crosslinked networks made from VEs have poor mechanical properties because they are rather brittle. For this reason, the blending of these resins with high molecular weight PCL was investigated in our research group. Previous studies showed that the covalent incorporation into the final polymer network led to improved (thermo)mechanical properties, especially high glass transition temperatures (T_gs) and high tensile toughness (U_T).[35, 146]

In this work, high molecular weight PCLs are chemically modified with photocurable end groups and investigated. Photopolymerizable end groups are, for instance, vinyl carbonates (VC), allyl carbonates (AC) and norbornenes (NB). However, synthesizing vinyl carbonates (VCs) as end group modification from hydroxyl-terminated PCL and vinyl chloroformate entails high costs and, thus, is inconvenient. Consequently, toughness enhancers with alternative photopolymerizable moieties based on PCL are demanded (Figure 26). In this study, the effect of varying end groups on the photochemical and

(thermo)mechanical properties of the final materials is determined and compared to already established VCs. Therefore, key indices like the reactivity, double bond conversion, gel point and modulus, tensile strength, elongation at break and glass transition temperature are investigated. Allyl carbonates (ACs) were of interest because they exhibit no homopolymerization (in contrast to VCs) and are inexpensive in their synthesis. The norbornene functionality (NB) should be preferred during the copolymerization of thiols with vinyl esters, which may lead to domain-formation.[157] Therefore, an increase in mechanical properties, like toughness, is hypothesized.

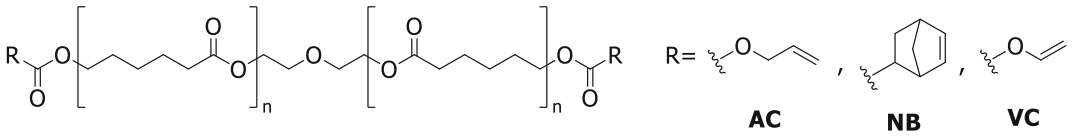

Figure 26: PCL-based toughness enhancers with investigated end-group modifications.

As mentioned before, the used PCL has hydroxyl functionalities and can be end-capped with AC, NB, or VC. The obtained modified PCLs were tagged with the code **YxkPCL**: Y indicates the functionality and xk is the molecular weight (MW) in kDa. All three modifications of PCL were synthesized and investigated. However, only the AC modifications will be discussed in detail; the results of VC and NB as end group modifications can be found in the enclosed appendix. Furthermore, the molecular weight was varied (10kDa and 45kDa) and their influence on the mechanical properties was investigated.

2.1.1. Synthesis of allyl carbonate-modified PCL (ACxkPCL)

The hydroxyl-terminated PCL is commercially available and was used as received for the synthesis of the allyl carbonate-modified PCL (**ACxkPCL**). In a one-step synthesis, the diol can be converted with an excess of allyl chloroformate to obtain the desired product. The synthesis was performed similarly to Orman *et al.*.[35]

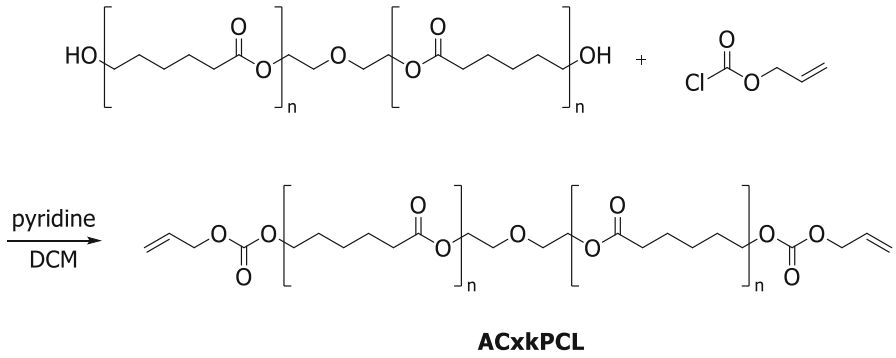

ACxkPCL

Scheme 7: One-step synthesis of allyl carbonate modified PCL (**ACxkPCL**).

Therefore, the hydroxyl-terminated PCL diol (1 eq) was dissolved in dry DCM under an argon atmosphere. Then, dry pyridine (4 eq. for 10kDa|12 eq. for 45kDa) was added as an acid scavenger. Afterwards, dropwise, allyl chloroformate (4 eq.|12 eq) was added. The amount of allyl chloroformate was adjusted from 4 to 12 eq. for the 45kDa PCL due to insufficient conversion. For purification, the product was precipitated as a white powder. **AC10kPCL** showed a conversion of 96% and **AC45kPCL** of 92%, which was determined with ^{31}P-NMR. This procedure is described in detail in the following subchapter.

2.1.2. Hydroxyl value via ^{31}P-NMR spectroscopy of (un)functionalized PCLs

PCLs with hydroxyl end groups in different molecular weights were used as starting materials. After functionalization with photopolymerizable moieties, no OH groups should be left. A typical way to determine the OH number is the titration method. However, this method requires a large amount of samples for reproducible values. Furthermore, the viscosity increases with increasing MW, and the solubility is inadequate. Alternatively, quantitative ^{31}P-NMR spectroscopy can be used. Here, the sample amount is in the mg-range, which is the major advantage of this method.[247]

2-Chloro-4,4,5,5-tetramethyl-1,3,2-dioxaphospholane (TMDP) functions as a phosphorylation reagent and cyclohexanol as an internal standard (IS). TMDP reacts with the hydroxyl groups, releasing hydrochloric acid, which is quenched with added pyridine. The reaction scheme is shown below (Scheme 8). Now, the converted phosphorous atom can be determined *via* ^{31}P-NMR spectroscopy. The internal standard makes it possible to quantify the hydroxyl values.

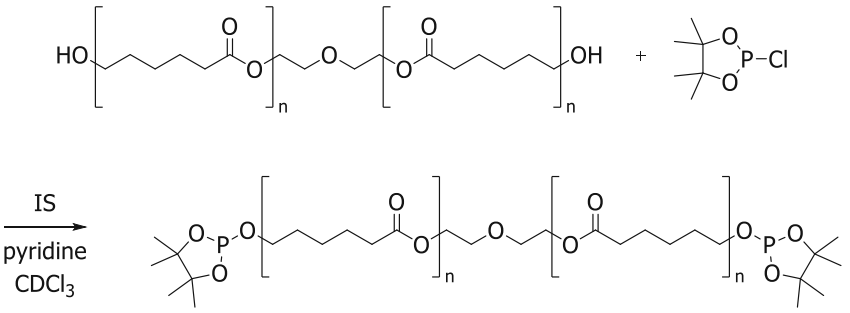

Scheme 8: Phosphorylation of aliphatic OH groups of PCL diol with TMDP agent for quantification of hydroxyl value *via* ^{31}P-NMR spectroscopy.

First, the sample was dissolved in dry deuterated chloroform, to which dry pyridine and cyclohexanol are added. After dissolving, TMDP was diluted in dry $CDCl_3$ in another vial and added to the first solution. The combined solution was mixed entirely and transferred to an NMR tube. Since TMDP is sensitive to moisture, all steps were done in an argon atmosphere. The spectrum was measured immediately, but latest within 12 h. To determine the conversion of the reaction, the ^{31}P-NMR spectra were processed in the following way: The signal-to-noise ratio was corrected, and then a Fourier transformation was performed. The phase was adjusted, and the signal at 132.2 ppm was set as the reference signal. Then the baseline was manually corrected in the range 150-142.5 ppm. The integral corresponding to the internal standard (144.7-145.2 ppm) was set to 1. After that, the aliphatic hydroxyl groups (147.1 ppm) could be determined.

$$OH\ \left[\frac{mmol}{mg}\right] = \left[\frac{c_{standard} \cdot V_{standard} \cdot I_{funct.gr.}}{M_{standard} \cdot I_{standard} \cdot m_{sample} \cdot x_{funct.gr.}}\right] \quad \textbf{(1)}$$

$c_{standard}$: cyclohexanol concentration as internal standard (IS) [~40 mg/mL]
$V_{standard}$: volume of IS [µL]
$I_{funct.gr.}$: integral of corresponding functional group in the defined integration area
$M_{standard}$: MW of IS [100.158 g/mol]
$I_{standard}$: integral of IS: 1 [-]
m_{sample}: sample amount [~30 mg]
$x_{funct.gr.}$: number of functional groups per monomer [-]

First, the aliphatic OH value of the starting material must be determined to calculate the conversion of a reaction. Subsequently, the product is characterized and both OH numbers are compared. In the best case, no hydroxyl groups are left after functionalization.

For the products **AC10kPCL** and **AC45kPCL**, a conversion of 96% and 92% was achieved.

The conversions for the other PCL modification can be found in the experimental part, respectively, in the appendix.

2.2. Selection and synthesis of thiols used as CTA

Due to low cytotoxicity, vinyl esters (VE) are used monomers for 3D printed biomedical devices, *e.g.*, as bone graft substitutes. However, these monomers show low photoreactivity. Additionally, the fabricated materials lack high toughness, which is unfavorable for bone graft substitutes. Thiols can be used to boost photoreactivity and reduce brittleness.[145, 190]

The first investigated thiol (**Thiol 1**) is the commercially available 1,1,1-trimethylolpropane-tris(3-mercaptopropionate). In a previous study by Orman *et al.*,[35, 146] specimens containing **Thiol 1** showed promising results regarding the chemical and (thermo)mechanical properties. However, it is very flexible and has three ester groups, which may cleave under acidic conditions. Therefore, the alternative thiol 1,3,5-tris(3-mercaptopropyl)-1,3,5-triazine-2,4,6-trione (**Thiol 2**) without ester groups was synthesized. In contrast, **Thiol 2** has no cleavable moieties and has a more rigid core than **Thiol 1**. Therefore, it is hypothesized that the mechanical properties will be further enhanced. The chemical structures of the investigated thiols are depicted in Figure 27.

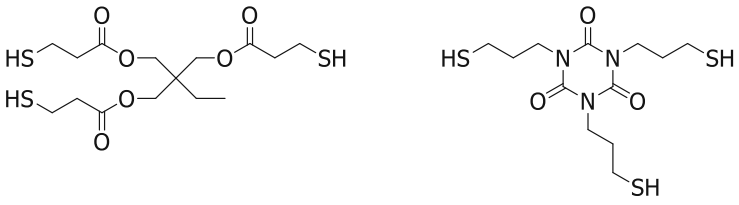

Figure 27: Chemical structures of the used thiols: 1,1,1-trimethylolpropane-tris(3-mercaptopropionate) (**Thiol 1**) and the synthesized 1,3,5-tris(3-mercaptopropyl)-1,3,5-triazine-2,4,6-trione (**Thiol 2**).

1,3,5-Tris(3-mercaptopropyl)-1,3,5-triazine-2,4,6-trione (**Thiol 2**) was synthesized in a two-step procedure according to Reinet *et al.*.[248, 249] Therefore, triallyl isocyanurate was converted with thioacetic acid by radical thiol-ene click reaction and then hydrolyzed (Scheme 9).[248, 249] This considerably more rigid trithiol was of interest to further improve the photochemical and (thermo)mechanical properties.

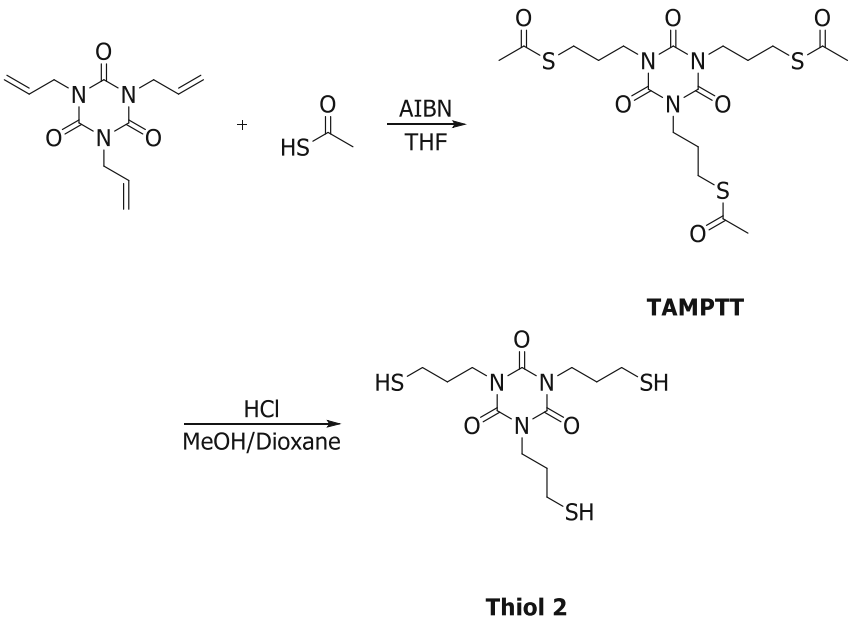

Scheme 9 Synthesis of 1,3,5-tris(3-mercaptopropyl)-1,3,5-triazine-2,4,6-trione (**Thiol 2**) with tris[3-(acetylthio)propyl]isocyanurate (**TAMPTT**) as intermediate.

In the first step, the intermediate product tris[3-(acetylthio)propyl]isocyanurate (**TAMPTT**) was synthesized. Therefore, a suspension of 1,3,5-triallyl-1,3,5-triazine-2,4,6-trione (1 eq.), thioacetic acid (3.6 eq.), and AIBN (0.15 eq.) was purged with argon to remove all traces of oxygen for a proper radical addition reaction. Afterwards, the solvent was removed, and the crude product was recrystallized to obtain **TAMPTT** with a 72% calculated yield as a white solid.

The synthesis of the intermediate **TAMPTT** was followed by hydrolyzation to obtain **Thiol 2**.

Therefore, **TAMPTT** (1 eq.) was dissolved in a mixture of MeOH and dioxane and, afterwards, conc. HCl (3.2 eq.) was added. **Thiol 2** was isolated as colorless oil in a 93% calculated yield and used without further purification.

3. Characterization of PCL based toughness enhancers

3.1. Investigation of the chemical properties

3.1.1. Formulation preparation of functionalized PCLs

Two reference formulations were prepared; one with the commercially available **Thiol 1** and one with the synthesized rigid **Thiol 2**. Therefore, the difunctional vinyl ester divinyl adipate (DVA) was mixed with the thiols in a (molar) double bond (db) ratio of

15 db%. In preliminary studies, the thiol content was varied and showed that a ratio of 1:1 led to too soft materials. At 15db%, the best ratio between reactivity and final mechanical properties was found.[35] Here, the thiol was entirely consumed by thiol-ene reaction first, and the residual double bonds react subsequently by homopolymerization.[145]

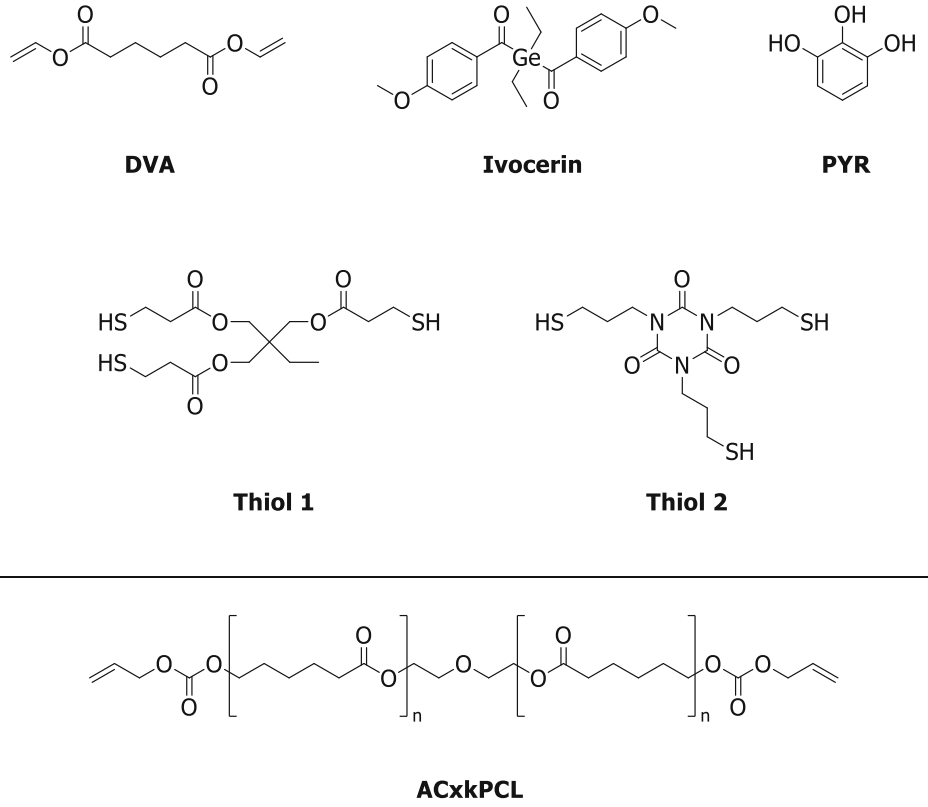

Figure 28: Structures of the components used in the references (top, **Ref. Thiol 1** and **Ref. Thiol 2**) and the investigated additives (bottom); divinyl adipate (DVA) as vinyl ester monomer, 1,1,1-trimethylolpropane-tris(3-mercaptopropionate (**Thiol 1**) and 1,3,5-tris(3-mercaptopropyl)-1,3,5-triazine-2,4,6-trione (**Thiol 2**) as network regulator, bis(4-methoxybenzoyl) diethylgermanium (Ivocerin®) as photoinitiator, pyrogallol (PYR) as a stabilizer and **ACxkPCL** as additives.[189]

Divinyl adipate (DVA), 15db% of thiol (**Thiol 1** or **Thiol 2**) referenced to the sum of double bonds (here only DVA), 0.5wt% Ivocerin® as photoinitiator and 0.02wt% pyrogallol as inhibitor were mixed. These compositions were defined as reference systems (**Ref. Thiol 1** or **Ref. Thiol 2**). Then, 5-25wt% toughness enhancers (**ACxkPCL**) were added to the reference system. However, the thiol amount was adjusted (sum of DB from DVA and toughness enhancers) and calculated using equation 2. However, this equation can only be used if all monomers have the same number of functionalities. All substances,

which were used, are depicted in Figure 28. The formulations were heated up to ensure the melting of the PCL component and mixed until complete homogeneity was assured.

$$n_{thiol} = \frac{n_{\sum ene}}{100} \cdot \frac{x}{s} \cdot d \qquad \textbf{(2)}$$

n_{thiol}: amount of thiol in the formulation [mol]

$n_{\Sigma ene}$: amount of monomers in the formulation, referenced to the sum of DVA and toughness enhancers [mol]

x: db% of thiol

s: number of SH-groups per thiol molecule [-]

d: number of reactive double bonds per monomer molecule [-]

3.1.2. RT-FT-NIR-photorheology

The photochemical influence of allyl carbonate-modified toughness enhancers on the VE-based formulations should be investigated. Therefore, RT-FT-NIR photorheology measurements were conducted to determine important *in situ* parameters: time to reach the gel point (t_{gel}, onset of the normal force F_N), double bond conversion at the gel point, and the end of the measurement (DBC_{gel} and DBC_{final}), the time to reach 95% of DBC_{final} (t_{95}) and the shrinkage stress (F_N).[250] These key indices are essential to evaluate the applicability of formulations for the 3D printing process *via* DLP-SLA (digital light processing stereolithography). t_{gel} provide information about the reactivity and the minimum irradiation time, thus, a small t_{gel} value is crucial. DBC_{gel} and DBC_{final} define chemical conversion during polymerization. For the DBC, high conversions are desired. In contrast, t_{95} should be as small as possible since this value determines the printing speed. A printed layer must have sufficient stability (*e.g.*, conversion) to deposit the next layer in the z-direction. The shrinkage stress, determined with the normal force, should also be low.[250] The calculated DBCs describe the overall system since the recorded signals in the spectra cannot be separated between vinyl esters and those of the toughness enhancers. In Figure 29 t_{gel}, DBC_{gel}, DBC_{final} and t_{95} are depicted. Here, the values of the references and the trend of formulations with an increasing amount of toughness enhancer are shown. The numerical data can be found in the experimental part (Table 3 and Table 4).

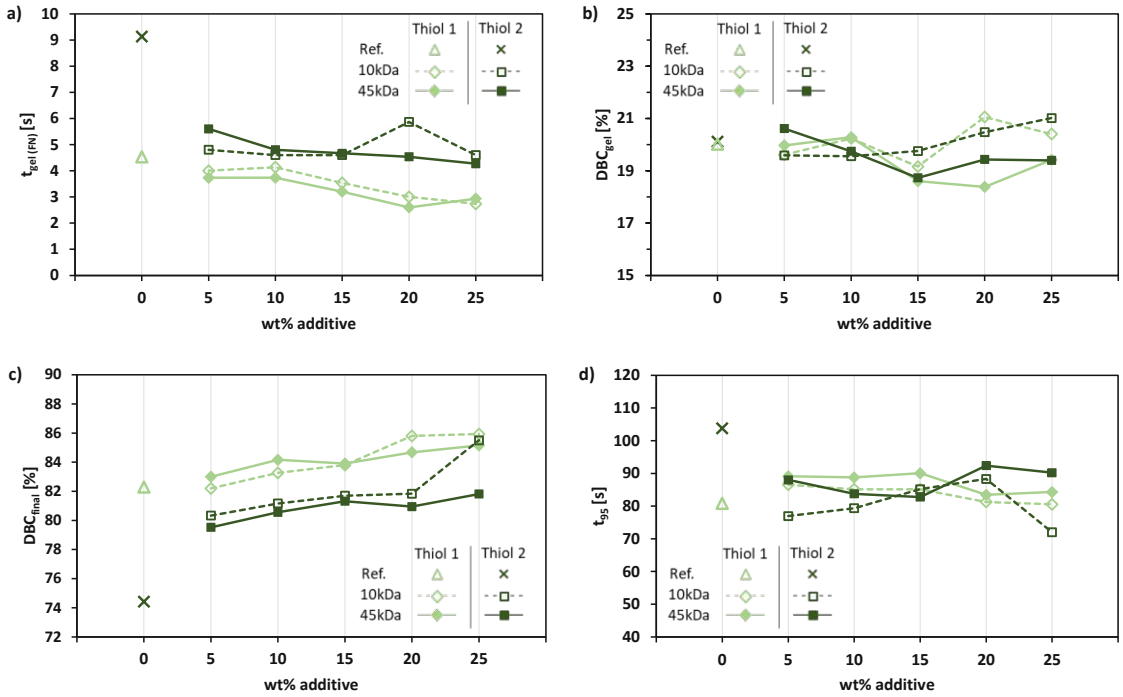

Figure 29: Photorheological measurements results of formulations containing DVA, 15 db% thiol, 0.5 wt% Ivocerin and 0.02 wt% PYR at room temperature (25 °C). **Ref. Thiol 1** (without additive): light green triangle; containing additional 5-25 wt% **ACxkPCL** (diamonds) or **Ref. Thiol 2** (without additive): dark green cross; containing additional 5-25 wt% **ACxkPCL** (squares). Empty symbols with dashed lines indicate **AC10kPCL** and full symbols with solid lines indicate **AC45kPCL**. The straight lines are only for better visibility. a) Obtained values for the gel point (t_{gel}); b) obtained values for the double bond conversion at t_{gel} (DBC_{gel}); c) obtained values for the final double bond conversion (DBC_{final}) and d) obtained values for the time to reach 95% of the final DBC (t_{95}).[189]

First, the formulations with the commercial and flexible thiol will be considered. The reference **Ref. Thiol 1** (without any toughness enhancer) needed 4.5 s (±0.5 s) to reach the time until gelation t_{gel}. Adding toughness enhancer led to a decrease in time (4.0 s (±0.8 s) to 2.7 s (±0.4 s)) with an increasing amount of **AC10kPCL**. A similar trend was observed for formulations containing the higher molecular weight additive **AC45kPCL**. In contrast to **Thiol 1**, the reference system with the rigid thiol **Ref. Thiol 2** was significantly slower. Without any toughness enhancer, t_{gel} was reached at 9.1 s (±0.3 s). After adding 5wt% of the toughness enhancers, the time dropped drastically. For formulations containing **AC10kPCL** t_{gel} decreased to 4.8 s (±0.2 s) and **AC45kPCL** to 5.6 s (±0.0 s), respectively. With higher amounts of **AC10kPCL**, t_{gel} was reduced to 4.6 s (±0.2 s for 25 wt%). The double bond conversion at the gel point was slightly increased with an increasing amount of **AC10kPCL**. This effect was observed for both thiols. Formulations containing the higher molecular weight were found to have a slight decrease. This

observation can be explained by the faster gelation of the formulation, that the polymer network has a shorter time for gelation. Formulations that contain **Thiol 2** and the higher MW PCL exhibited higher viscosity, which may pronounce this trend. Here, an increased autoacceleration may occur; the suppressed termination means longer chains, resulting in a shorter gelation time.[244] However, DBC_{gel} is for all formulations between 19-21% (±<1.2%). DBC_{final} was enhanced due to the addition of a toughness enhancer. Adding 25wt% of **ACxkPCL** to formulations containing **Thiol 1** DBC_{final} increased to ~86% (±<1.0%), whereas the reference **Ref. Thiol 1** only reached 82% (±0.2%). The addition of **ACxkPCL** to formulations containing **Thiol 2** also led to an increased DBC_{final}. However, the differences between the reference (DBC_{final} = 74% (±0.2%)) and the other formulations (80-86% (±<0.2%) for **AC10kPCL** and 80-82% (±<0.3%) for **AC45kPCL**) are more significant. In general, only a slight difference could be observed if the molecular weights were compared. One exception is the formulation containing **Thiol 2** and 25wt% **AC10kPCL**. Here, the value is higher than with the 45kDa toughness enhancer. Due to the addition of toughness enhancers, t_{95} increased, which was mainly observed in formulations with the flexible **Thiol 1**. The reference showed a time of 81 s (±4.0 s), then it was delayed to 81-89 s (±<3.7s). At higher concentrations, the viscosity increased, and the trend was counteracted. The increased viscosity led to insufficient diffusion of the monomers and therefore, the polymerization rate was decreased.[244] The additives lowered the values for formulations containing the rigid **Thiol 2**. Here, the reference showed a time to reach 95% of the final DBC of (104 s ± 5.8 s) and after the addition values between 72-88 s (±<4.3 s). Regardless of which thiol was used, all formulations are promising for stereolithography. They show short gelation times (small values for t_{gel}) and good photoreactivity (high DBC values). As mentioned above, t_{95} determines the printing speed, so this value is also essential.[35] During the measurements, the gap size was kept constant. A negative force (normal force) acts on the stamp and this can be used as an indicator for the shrinkage stress in the material.[250] During polymerization, the shrinkage stress must be monitored, as this can lead to problems in the layer-wise printing process. If residual stresses occur, creep distortions can arise long after the finished printing process. Furthermore, shrinkage may cause cracking and delamination of the layers in the building part.[251] During the measurements, a F_N of about -11 N was observed for both references. All formulations containing **ACxkPCL** showed similar but slightly lower values (-9 N) than the references. However, typically used systems containing, *e.g.*, (meth)acrylates as photocurable groups show substantially higher values (-27 N).[205, 252]

3.2. Investigation of (thermo)mechanical properties

3.2.1. Sample preparation of functionalized PCLs

The freshly prepared formulations were kept at 50 °C until use (max. 2 h) to avoid unintended recrystallization and to decrease the viscosity for easier handling. The formulations were transferred into silicon molds for tensile- and DMTA specimens and possible bubbles were removed. Then, the specimens were cured in a PrograPrint Cure[253] from Ivoclar with λ = 460 nm and an intensity of 274 mW/cm^2. The exposure time was 10 minutes on each side. Before the measurements, the samples were ground and polished with sandpaper in multiple steps to ensure uniform geometries and to remove artifacts from the surface.

3.2.2. DMTA

Information about the chemical properties, *e.g.*, network cross-linking, was obtained with the RT-FT-NIR-photorheology measurements. However, the change in network architecture affects the thermomechanical properties of the final material. In this section, the influence of toughness-enhancers (**AC10kPCL** and **AC45kPCL**) and varying thiols (**Thiol 1** and **Thiol 2**) will be characterized *via* dynamic mechanical thermal analysis (DMTA). The glass transition temperature (T_g) and the storage modulus G' are essential parameters. T_g is the temperature where a reversible transition from a hard state into a viscous or rubbery state occurs. This temperature is described as the maximum dissipation factor (tanδ). A classic behavior for brittle materials is a wide temperature range for T_g, which characterizes a nonregulated polymer network.[244] The storage modulus at the rubber plateau G'_R provides information about the crosslink density of the final polymer. Here, high values correspond to a high network density.[205, 254] A known fact is that toughness-enhancing additives lead to a drop in the storage modulus. For this reason, the storage moduli at room- and body temperature ($G'_{25\,°C}$ and $G'_{37\,°C}$) are also characteristic values. DMTA measurements were performed from -100 °C to 200 °C with a heating rate of 2 °C·min^{-1} and in torsion mode. T_g and $G'_{37\,°C}$ will be discussed in detail, but the values for G'_R and $G'_{25\,°C}$ can be found in the experimental part (Table 5 and Table 6).

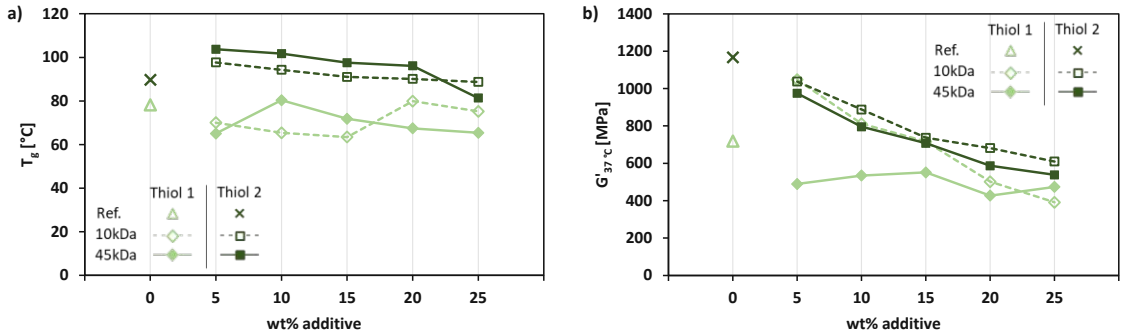

Figure 30: Results of DMTA measurements of formulations containing DVA, 15 db% thiol, 0.5 wt% Ivocerin and 0.02 wt% PYR. **Ref. Thiol 1** (without additive): light green triangle; containing additional 5-25 wt% **ACxkPCL** (diamonds) or **Ref. Thiol 2** (without additive): dark green cross; containing additional 5-25 wt% **ACxkPCL** (squares). Empty symbols with dashed lines indicate **AC10kPCL** and full symbols with solid lines indicate **AC45kPCL**. The straight lines are only for a better visibility. a) Obtained values for the glass transition temperature (T_g); b) obtained values for the storage modulus at body temperature ($G'_{37\,°C}$).[189]

The reference with the flexible thiol (**Ref. Thiol 1**) and without any toughness-enhancing additive showed a glass transition temperature (T_g) of 78 °C. After adding toughness enhancers with a MW of 10kDa, the T_gs dropped to 75-63 °C, except for the formulation of 20wt%. This formulation showed the highest T_g with ~80 °C. Decreasing values between 65-80 °C were found for formulations containing an increasing amount of **AC45kPCL**, whereas the highest T_g was found for 10 wt%. In contrast to **Thiol 1**, formulations containing the more rigid **Thiol 2** showed higher values. **Ref. Thiol 2** showed a T_g of 90 °C, but the addition of **ACxkPCL** led to raised T_gs. 98 °C – 89 °C were reached for **AC10kPCL** and T_gs ranging from 104 °C to 81 °C for formulations containing **AC45kPCL**, whereas only 25 wt% was below the reference. However, generally, a trend of decreasing T_gs with an increasing amount of additive was found. All specimens exceed a glass transition temperature above the human body temperature (37 °C). T_g ≥37 °C is an essential threshold value for evaluating their suitability as bone graft substitutes; otherwise, they may become soft and deform in the body. Exemplary curves for selected specimens of the loss factor, which is representative of T_g, are depicted in Figure 31a.

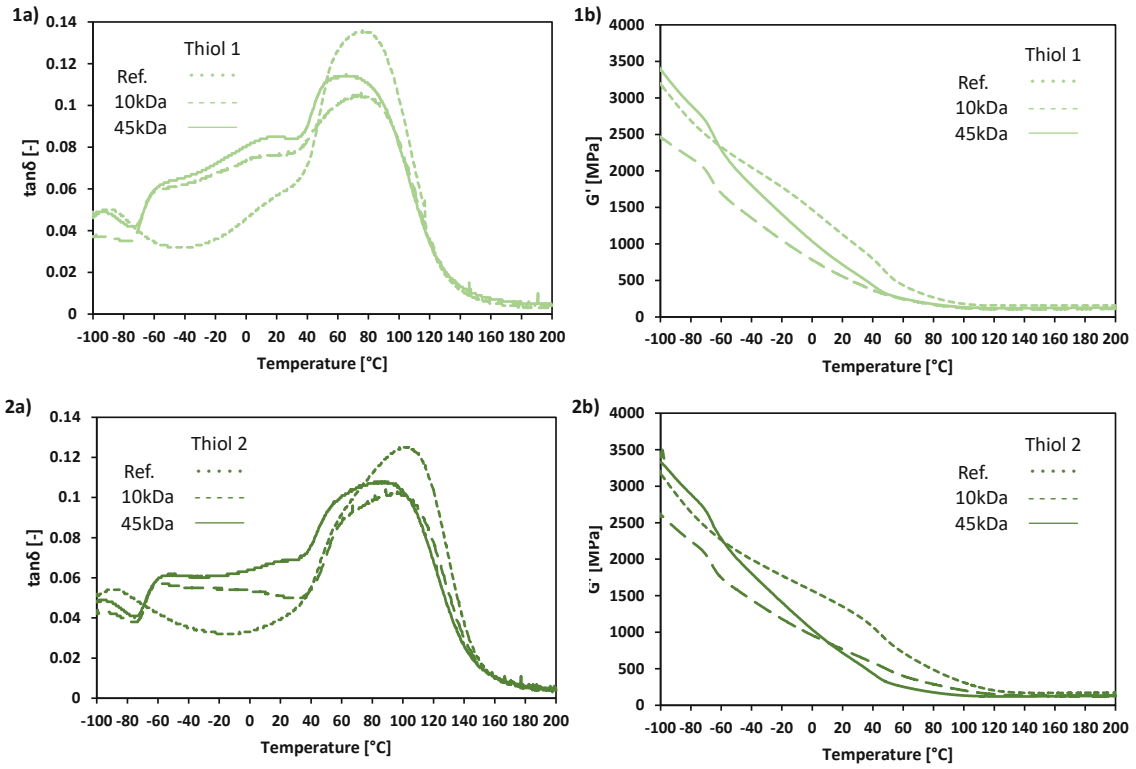

Figure 31: a) Loss factor (tanδ) and b) storage modulus (G') for formulations containing DVA, 15 db% thiol, 0.5 wt% Ivocerin and 0.02 wt% PYR. **1) Ref. Thiol 1** (without additive): light green dotted line; containing additional 25 wt% **ACxkPCL** (light green) or **2) Ref. Thiol 2** (without additive): dark green dotted line; containing additional 25 wt% **ACxkPCL** (dark green). Dashed lines indicate **AC10kPCL** and solid lines indicate **AC45kPCL**.

Considering the storage moduli at body temperature $G'_{37\,°C}$, a trend of decreasing values with an increasing amount of toughness enhancers can be observed. **Ref. Thiol 1** showed a modulus of < 720 MPa, and **Ref. Thiol 2** of <1170 MPa. All formulations showed values below the references, except formulations containing 5 and 10wt% **AC10kPCL** and **Thiol 1** showed higher values than the reference (1050 and 810 MPa). For bones, the literature describes storage moduli between 3 and 9 Gpa depending on the measurement frequency and water content.[28] Exemplary curves for selected specimens of the storage modulus are shown Figure 31b.

In literature, similar trends were found for PCL-based polymer blends[255] and vinyl carbonate-modified PCL toughness enhancers.[146] They described an improved network homogeneity for a low amount of high MW reactive macromers and, thus, enhanced (thermo)mechanical properties. However, DMTA measurements confirmed that adding **ACxkPCL** led to a beneficial combination of lowered network density and raised T_g.

3.2.3. Tensile tests

Brittle materials are obtained if multifunctional monomers polymerize to a highly crosslinked polymer network.[145, 190] Tougher but softer networks are received if the networks are more regulated and widened.[146] After adding PCL-based additives, an opacity of the manufactured materials is often recognizable. The opacity appears due to phase separation, which improves impact strength by efficiently dissipating the propagating cracking forces between the two phases.[124] Tensile tests were done, and the tensile toughness was calculated to determine the impact of the additives. Ye *et al.* showed that phase separation enhances the tensile toughness.[256]

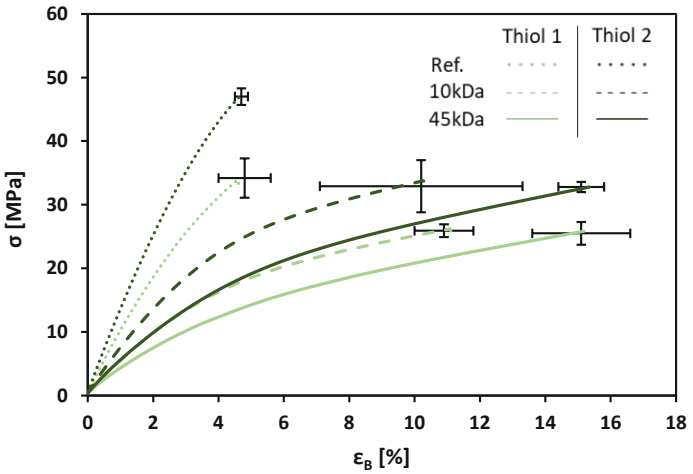

Figure 32: Tensile test curves for formulations containing DVA, 15 db% thiol, 0.5 wt% Ivocerin and 0.02 wt% PYR. **Ref. Thiol 1** (without additive): light green dotted line; containing additional 25 wt% **ACxkPCL** (light green) or **Ref. Thiol 2** (without additive): dark green dotted line; containing additional 25 wt% **ACxkPCL** (dark green). Dashed lines indicate **AC10kPCL** and solid lines indicate **AC45kPCL**.[189]

These experiments were performed at room temperature on a universal testing machine with a 1 kN load sensor and a traverse speed of 5 mm·min^{-1}. The stress-strain curves give information about the strength and plasticity of the specimens. Five replicates were measured for reproducibility. Figure 32 shows exemplary stress-strain curves for the two reference systems and specimens containing 25 wt% of **ACxkPCL**. The selected curves correspond most closely to the average values. The inserted error bars correspond to the average values of the maximum tensile strength (σ_M) and elongation at break (ε_B) with standard deviation. Figure 33 shows only the trend (average values) of the tensile strength and elongation at break for greater clarity. The exact values and the standard deviation can be found in the experimental section (Table 7 and Table 8).

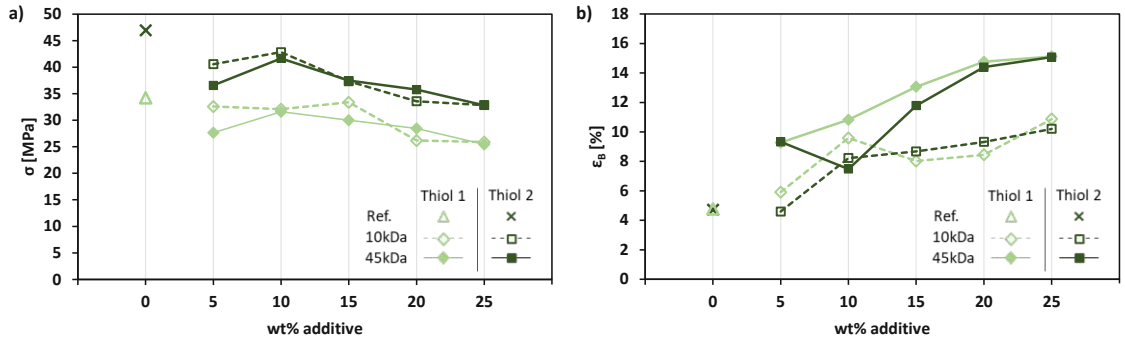

Figure 33: Results of tensile test measurements of formulations containing DVA, 15 db% thiol, 0.5 wt% Ivocerin and 0.02 wt% PYR at room temperature. **Ref. Thiol 1** (without additive): light green triangle; containing additional 5-25 wt% **ACxkPCL** (diamonds) or **Ref. Thiol 2** (without additive): dark green cross; containing additional 5-25 wt% **ACxkPCL** (squares). Empty symbols with dashed lines indicate **AC10kPCL** and full symbols with solid lines indicate **AC45kPCL**. The straight lines are only for better visibility. A) Obtained values for the tensile strength σ; b) obtained values for the elongation at break ε_B.[189]

Formulations containing **Thiol 1** and the low molecular weight additive **AC10kPCL** hardly influenced the tensile strength (σ), but the elongation at break (ε_B) increased. In particular, ε_B could be doubled to 10% by comparing the formulations containing 25 wt% and the reference. A steady decrease of σ was observed due to the addition of **AC45kPCL**. The values of the high MW and the small MW formulations matched for higher amounts of the additive. However, the elongation at break increased up to 15%. Often the tensile strength is influenced by a severe loss due to the addition of toughness modifiers, but the elongation at break values increased.[124] Nevertheless, this trend was already recognizable in previous studies.[146]

Specimens containing the more rigid **Thiol 2** showed a decrease in σ after adding **ACxkPCL** compared to the references. Despite that, ε doubled (for additives with 10kDa) to tripled (for additives with 45kDa) values with an increasing amount of additive. The tensile strength lies between 47 Mpa (Ref. without additive) and 36 Mpa. These findings are close to cortical bone, where values between 50 Mpa and 151 Mpa were reported.[257]

To further characterize the specimens, the tensile toughness U_T should be determined. Therefore, U_T was calculated from the area under the stress-strain curve of the tensile tests and should be used primarily for comparisons within a study.[257] Toughness is defined as the amount of energy the material can absorb in the form of deformation before the initiated stress leads to a crack in the material[258].

Formulations, which contain **Thiol 1** and the low MW additive **AC10kPCL**, showed that the addition led to a slight increase in tensile toughness U_T (ranging from 1.5 $MJ \cdot m^{-3}$ to

2.1 MJ·m^{-3}) compared to the reference (1.0 MJ·m^{-3}). Noteworthy is the formulation with 10 wt%, which showed the highest tensile toughness. An increase in U_T is also observable for formulations containing **AC45kPCL**. Here, with 20 wt%, the tensile toughness was almost tripled (2.8 MJ·m^{-3}) compared to the reference formulation (**Ref. Thiol 1** 1.0 MJ·m^{-3}). All formulations containing **Thiol 2** showed higher U_T than the ones with **Thiol 1**. After adding the toughness-enhancing additives, higher values (up to 2.4 MJ·m^{-3} for 10kDa) were found than the reference (1.3 MJ·m^{-3}). One exception was the formulation containing 5wt% **AC10kPCL**. **AC45kPCL** led to more than tripled values for U_T (3.5 MJ·m^{-3} for 20 wt%) compared to formulations without additives. The trend of the tensile toughness is depicted in Figure 34 and the exact values for all formulations can be found in the experimental section (Table 7 and Table 8).

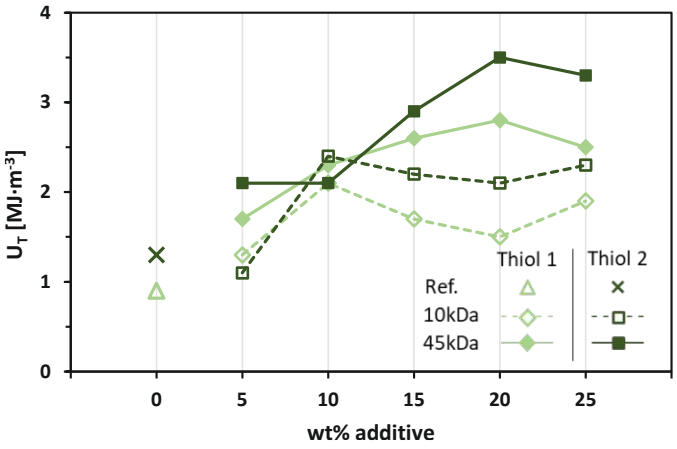

Figure 34: Calculated tensile toughness U_T of formulations containing DVA, 15 db% thiol, 0.5 wt% Ivocerin and 0.02 wt% PYR at room temperature. **Ref. Thiol 1** (without additive): light green triangle; containing additional 5-25 wt% **ACxkPCL** (diamonds) or **Ref. Thiol 2** (without additive): dark green cross; containing additional 5-25 wt% **ACxkPCL** (squares). Empty symbols with dashed lines indicate **AC10kPCL** and full symbols with solid lines indicate **AC45kPCL**. The straight lines are only for better visibility.[189]

Besides tensile tests, 3-point bending tests from selected materials (references, 5 and 25wt% of **ACxkPCL**) were performed to corroborate the results of the tensile tests further. As expected, these results show the same trend and are provided in the Appendix (Figure 68 and Table 31).

4. Influence of sterilization methods on (thermo)mechanical properties

It is mandatory to deactivate bacteria, viruses, and fungi of medical devices before they can be used *in vivo*. Otherwise, inflammations, infections, and implant failure can be caused. Heat (dry or moist), chemicals (ethylene oxide (EO), ozone, hydrogen peroxide, peracetic acid), or radiation (gamma radiation) are standard sterilization techniques to ensure sterile samples.[259] However, the characteristics of the material can be affected depending on the sterilization method. For example, heat as a procedure is unsuitable for the above-characterized samples, as they show glass transition temperatures of ≤100°C. Hydrogen peroxide, for example, may lead to oxidation or peracetic acid to degradation of the materials. For these reasons, sterilization with ethylene oxide and gamma radiation was chosen. Additionally, these techniques are used by KLS Martin in collaboration with DMB Apparatebau GmbH (SteriVIT for ethylene oxide) and BBF Sterilisationsservice GmbH (for gamma radiation).[259]

DMTA and tensile test specimens of formulations containing **Thiol 2** and 25wt% of **AC45kPCL** were characterized after sterilization and compared to freshly prepared specimens to find a suitable method and dose. In sum, three batches were investigated.

First, ethylene oxide (6% EO, 94% CO_2) was used. Here, the samples were packed in gas-permeable packages and the chamber was evacuated and heated to 55 °C. Then, the EO was injected and the sterilizer conditions were held for 2 h. However, EO is a toxic and explosive gas; therefore, further aeration is needed to remove residual EO.[259, 260]

The second method was γ-radiation according to DIN EN ISO 11137,[261] applying two different doses. The samples were packed into an aluminum box and placed near the ^{60}Co-radiation source during this process. The highest applied dose was 30.5 kGy. Nevertheless, high energy may break bonds and thus increase stress and brittleness in the material. For this reason, the lowest possible dose of 18 kGy was also investigated.[259, 260]

DMTA experiments were conducted and the curves are depicted in Figure 35, whereas the exact values are listed in the experimental part in Table 9.

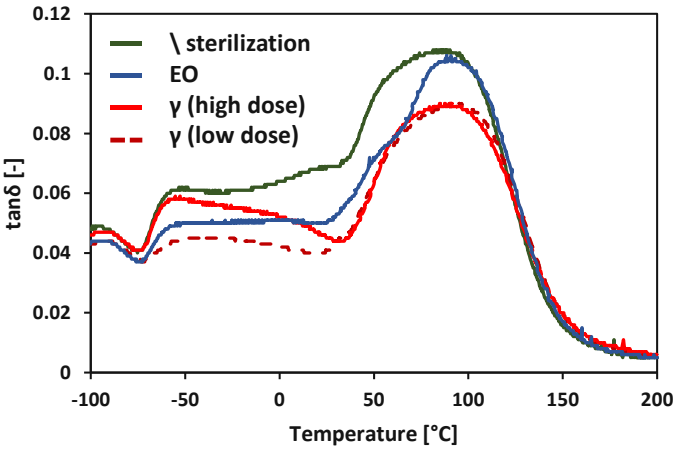

Figure 35: Effect of sterilization methods on DMTA measurements for formulations containing DVA, 15 db% **Thiol 2**, 0.5 wt% Ivocerin and 0.02 wt% PYR and 25wt% **AC45kPCL**. The solid green line depicts the specimens without sterilization, solid blue ethylene oxide, solid light-red line γ-sterilization with high dosage and dashed dark-red γ-sterilization with low dosage.

In these experiments, hardly any influence can be detected for the γ-irradiated samples. In the case of the sample sterilized with EO, a slight shoulder can be seen at approx. 50 °C. This shoulder may again indicate the recrystallized domains of PCL.

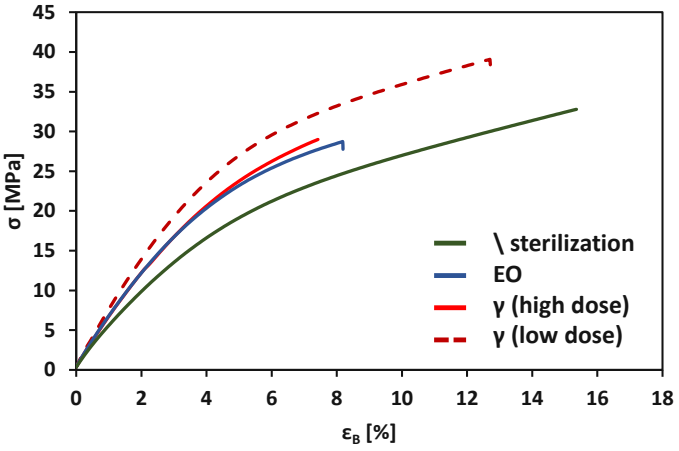

Figure 36: Effect of sterilization methods on tensile test experiments for formulations containing DVA, 15 db% **Thiol 2**, 0.5 wt% Ivocerin and 0.02 wt% PYR and 25wt% **AC45kPCL**. The solid green line depicts the specimens without sterilization, solid blue ethylene oxide, solid light-red line γ-sterilization with high dosage and dashed dark-red γ-sterilization with low dosage.

In addition, tensile test experiments were done and exemplary curves are shown in Figure 36.

Specimens, which were treated with EO or a high dosage of γ-radiation, decreased their tensile strength (~32 MPa) and their elongation of break was significantly lower (~8%)

compared to untreated specimens (σ = 33 MPa and ε_B = 15%). γ-radiated specimens with a low dosage show similar values as the untreated specimens. The increased modulus of all sterilized samples can be explained by further crosslinking during the sterilization or because of crystallization. All values can be found in the experimental part in Table 10.

Consideration of the tensile toughness U_T, untreated specimens show the highest U_T of 3.3 $MJ \cdot m^{-3}$, followed by specimens treated with the low dosage γ-radiation with 2.8 $MJ \cdot m^{-3}$. EO (2.1 $MJ \cdot m^{-3}$) and a high dosage of γ-sterilization (1.8 $MJ \cdot m^{-3}$) led to a significant decrease in U_T. The evident deterioration of EO-sterilized samples is surprising since EO is compatible with most polymers. However, during this sterilization method, the samples were heated up to 50 °C, which is close to the melting point of PCL. Thus, recrystallization of PCL after cooling down is possible, and the formed grain boundaries may be the source of fracture.

To sum up the results from both analyses, EO can be excluded as a sterilization method because it deteriorates the mechanical properties. Moreover, ethylene oxide is a toxic and carcinogenic gas, and often residues remain in the material.[262] In addition, irradiation with a high dose of gamma radiation also resulted in reduced values in the tensile tests, so this method is also excluded. For this reason, γ-radiation with a low dosage is an acceptable sterilization method for these materials.

5. 3D Fabrication of medical device

As a proof-of-concept, a 3D printing process will be done. However, viscosity measurements must be performed first because the threshold for DLP-SLA, especially lithography-based ceramic manufacturing (LCM), is ≤100 Pa·s.[263] In Figure 37, the viscosity of the reference systems (without additives) and formulations with increasing toughness enhancers is depicted.

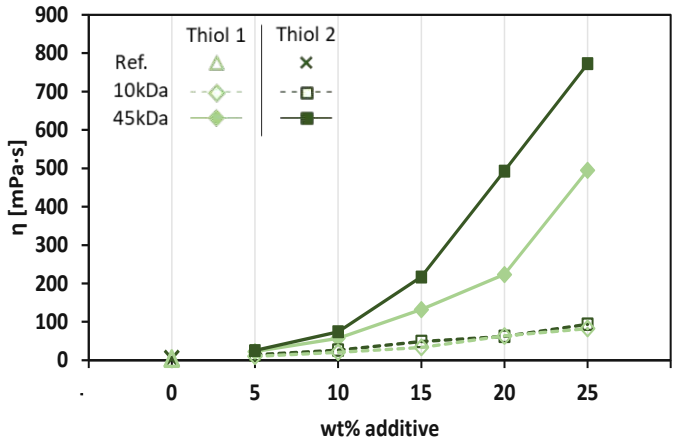

Figure 37: Rheological measurement results of formulations containing DVA, 15 db% thiol, 0.5 wt% Ivocerin and 0.02 wt% PYR. **Ref. Thiol 1** (without additive): light green triangle; containing additional 5-25 wt% **ACxkPCL** (light green diamonds) or **Ref. Thiol 2** (without additive): dark green cross; containing additional 5-25 wt% **ACxkPCL** (dark green squares). Empty symbols with dashed lines indicate **AC10kPCL** and full symbols with solid lines indicate **AC45kPCL**. The straight lines are only for better visibility. [189]

It can be seen that the viscosity rises with an increasing amount of additive. Looking at **AC10kPCL**, it can be recognized that there is no significant difference in viscosity between the various thiols. Formulations with higher MW and rigid **Thiol 2** show significantly higher values than those with low MW additives. However, even these are far below the threshold. The exact values can be found in the experimental part (Table 11 and Table 12).

The formulation with the highest amount of the high MW toughness enhancer and the rigid thiol should be printed as proof of concept and to test the limit of the investigated formulations. However, light penetration tests were done to find the best combination of the light absorber Quinoline Yellow (QY) and Ivocerin® as the photoinitiator. QY prevents overpolymerization due to excessive and scattered light, which simultaneously leads to a loss in reactivity. Therefore, the photoinitiator concentration was slightly increased to counteract this disadvantage. Thus, the printed formulation contained DVA as a main monomer, **Thiol 2** (15db% regarding DVA and **AC45kPCL**), 25wt% **AC45kPCL**, 0.02wt% pyrogallol as an inhibitor, 0.75wt% Ivocerin® and 0.06wt% QY. This formulation showed a viscosity of ~780 mPa·s and, thus, is suitable for printing.

Light penetration tests were done to find the optimum adjustments for light intensity and light dose for the printing process. After finding the best parameters for the printing process using DLP-SLA, surgical screws were printed. These screws were built at 38 °C with a light intensity of 71.3 mW·cm^{-2} and a light dose of 500 mJ·cm^{-2} for the first 5

layers. Afterwards, the light dose was decreased to 400 mJ·cm^{-2}. The layer thickness was 25 µm and an exposure time of ~5.6 s was used. The printed screws and a microscopic image of one, can be seen in Figure 38.

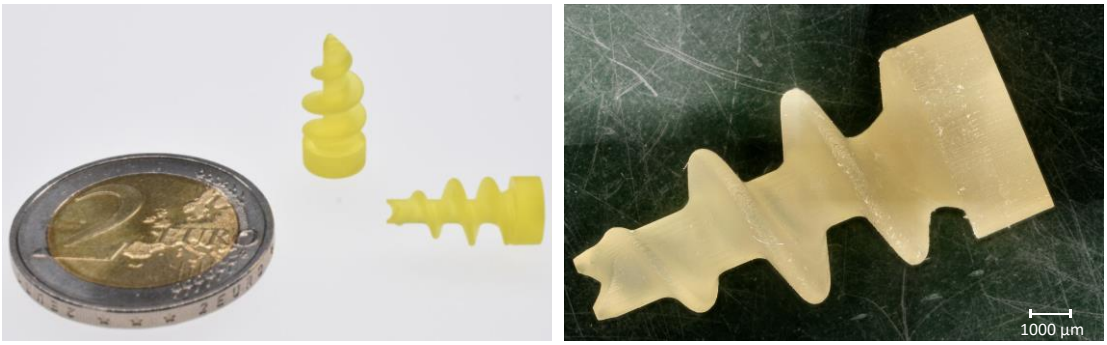

Figure 38: Microscopic image (right) of surgical screws of the formulation containing DVA, 15 db% **Thiol 2**, 25 wt% **AC45kPCL**, 0.75 wt% Ivocerin, 0.02 wt% PYR and 0.06 wt% QY printed by digital light processing.

Shrinkage during the printing process is a common problem, which may lead to cracks and delamination and, at long last, to defective parts.[251] In order to study the dimensional accuracy of the printed parts was studied by overlaying the original .stl file with a 3D scan of the printed screw. The picture shows a color code according to shrinkage or expansion (Figure 39); negative values (blue) indicate shrinkage.

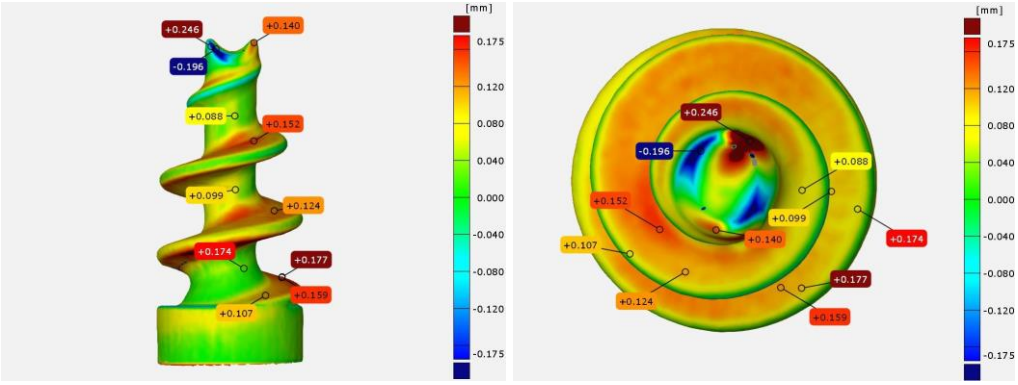

Figure 39: Overlays of the stl file and scan of a printed screw to observe the shrinkage during the printing process (positive values indicate a negative change in dimension).

It can be observed that the screw after printing is 100 to 200 µm smaller than the CAD screw. However, no cracks or delamination of the printed parts is noticeable.

6. Conclusion

In this work, PCL-based toughness enhancers in two varying molecular weights (10kDa and 45kDa) and different end-group modifications were successfully synthesized. Allyl carbonate- (AC), vinyl carbonate- (VC), and norbornene- (NB) functionalities were investigated. Moreover, the influence of two different thiols, the commercially available **Thiol 1** and the synthesized rigid **Thiol 2**, was envisioned. The impact on the photochemical *via* RT-FT-NIR-photorheology and (thermo)mechanical properties *via* DMTA and tensile tests was investigated for the reference systems (without additive) and for formulations containing the thiols and increasing amount of toughness enhancers. However, the varying photopolymerizable moieties show no significant differences in their properties compared to vinyl carbonates. For this reason, only **ACxkPCL** was discussed and VC- and NB- modifications can be found in the appendix.

The addition of **ACxkPCL** led to a decrease in t_{gel} and an increase in the DBC_{final}, which are essential parameters for the printability of bone implants. Moreover, the shrinkage stress was significantly decreased compared to commonly used (meth)acrylates monomers. Both toughness enhancers (10kDa and 45kDa) showed T_gs above the human body temperature when added to photopolymer precursor formulations, which is crucial for bone replacement implants. The only disadvantage was the decrease in storage modulus. However, this is an already known side issue due to the addition of toughness of high molecular weight additives. For example, nano-hydroxy apatite has been frequently used as filler and may further enhance polymer-based bone grafts' mechanical properties.[264]

Calculation of tensile toughness (U_T), defined as the area of the curves, proved that the addition of toughness enhancers led to tripled values. Moreover, a 3D printing of surgical screws *via* DLP-SLA was successful without cracks or delamination of the printed part. Low shrinkage was exhibited by overlaying a 3D scan of the manufactured screw and the original .stl file. This proved that formulations containing high concentrations of toughness enhancers are feasible for printing bone implants. Lastly, specimens were sterilized with two different methods (ethylene oxide (EO) and γ-radiation). Moreover, γ-radiation was applied in low and high dosages. Their (thermo)mechanical properties were determined and showed that the low dosage of γ-radiation did not influence the properties and, therefore, is a suitable sterilization method.

In sum, the concept of incorporating high molecular weight toughness enhancers into vinyl ester-based thiol-ene formulations showed an enhancement of the material's toughness. This was reached due to the dissipation of external stress in the different phases (phase separation). Nevertheless, the limits of these systems were demonstrated.

B. Interpenetrating polymer networks

1. State of the art

IUPAC Compendium of Chemical Terminology defines the term IPN (Interpenetrating Polymer Network) as follows: They are polymers consisting of at least two networks that are at least partially intertwined at the molecular level but are not covalently bonded to each other. In addition, they cannot be separated except when chemical bonds are broken.[265, 266] They are incompatible polymer networks in which one network is synthesized and/or crosslinked in the presence of another.[267, 268]

Depending on the network structure and polymerization technique, three types of IPNs can be defined: *sequential IPN*, *semi* IPN or *simultaneous* IPN.

Sequential IPN: one polymer network is generated first and the second one is formed afterwards. There are two possible techniques. On the one hand, a polymer network can be created first; then, the second component is soaked into the existing polymer network and cured. On the other hand, both components can be present simultaneously and cured sequentially. In this case, the networks can be polymerized based on different orthogonal photoreactive groups, *e.g.*, cationic and radical, or one network can be cured photochemically and the other thermally.

Semi-IPN: one polymer network is formed and another polymer is present in a linear form.

Simultaneous IPN: both components are present and polymerized simultaneously but do not interfere with the other.[184, 185, 269]

Another way to classify IPNs is based on their curing mechanism.

1.1. Thermal radical or cationic polymerization and/or polycondensation

Aylsworth submitted a patent for a phenol-formaldehyde resin in 1914. This resin was cured with rubber and sulfur, resulting in higher tensile strength and elongation of the material.[268] However, the term interpenetrating polymer networks (IPN) was founded later in the 1960s by Millar.[270] He used copolymer beads of divinylbenzene and polystyrene and soaked them in a mixture of divinylbenzene and styrene monomers, and as a thermal initiator, he used azobisisobutyronitrile (AIBN). After soaking, the impregnated beads were thermally polymerized to form a second network, which was partially bound to the first network. The network was then sulfonated to produce an ion exchange material.[270] Frisch,

Sperling, Klempner, and Shibayama studied the thermodynamics of phase separation and the effects on the mechanical behavior of IPN materials.[265, 271, 272]

Frisch *et al.* published their work about interpenetrating elastomeric networks. These networks were prepared by polymerization in an emulsion. Thereby, a polyether-based poly(urethane-urea) network was mixed with a linear poly(butadiene-acrylonitrile). They found that the maximum tensile strength of the IPNs was significantly higher than that of the pure polymers. The elongation was close to the one of poly(urethane-urea), even with a very high percentage of poly(butadiene-acrylonitrile). The only exception was the reference made to 100% poly(butadiene-acrylonitrile), which exhibited very low elongation.[271]

Sperling also described a sequential method to generate IPNs. In 1972, he cured butadiene and then swelled it with a mixture of styrene and small amounts of triethyleneglycoldimethacrylate (TEGDMA). Then the monomer mixture was cured by photopolymerization to finally obtain an IPN. These networks exhibited significantly higher impact strengths when compared to commercial graft copolymers, block copolymers, and high-impact polystyrene (HIPS).[273] Sperling attempted to create simultaneous interpenetrating networks (SINs) in addition to sequential networks. In SINs, two independent reactions must take place, which must not interfere with each other. For this reason, he used a mixture of bisphenol-A-diglycidyl ether with triethylamine and ethyl acrylate with small amounts of diethylene glycol dimethacrylate. In addition, he added a photoinitiator and irradiated the resin while simultaneously heating it. This combination created a network that had increased strength.[274]

The research group of Kim was also involved in the production of SINs. A polyurethane (PU) prepolymer was first prepared from poly(ε-caprolactone) glycol and diphenylmethane diisocyanate. Subsequently, a mixture of 1,4-butanediol and trimethylolpropane and styrene, and divinylbenzene was added. Dibenzoyl peroxide was also added as an initiator and cured at 80 °C. This resulted in a phase-separated SIN material with increased tensile strength.[275]

1.2. Photochemical polymerization

The replacement of thermal polymerization leads to several advantages. For example, curing at room temperature and without solvents became possible and it is less expensive in energy and cost. Furthermore, thermal polymerization often leads to phase separation

due to the miscibility of the polymers and the time that is necessary to form the final material.[276]

Photochemical curing resulted in more homogeneous materials with better properties due to the elimination of the phase separation.[276]

In 1982, Sperling created a sequential IPN for the first time, cured only by photopolymerization. He used n-butyl acrylate with divinylbenzene or acrylic anhydride as a crosslinker, 1-dodecanethiol as a transfer reagent and benzoin as a photoinitiator. After the first curing, this network was soaked with a mixture of styrene, crosslinker and photoinitiator and then cured again by light irradiation. This resulted in both homo- and IPN networks. These could then be swollen with an ammonium hydroxide solution, resulting in the degradation of the acrylic acid hydride networks. However, the divinylbenzene networks remained. The degraded network could now be dissolved, resulting in a porous scaffold. The different morphologies were then examined by scanning electron microscopy (SEM).[266]

Using triethanolamine as a PU crosslinker and the polymerization of aryl acid into the PS backbone resulted in ionic interactions, which led to increased tensile strength and, in some cases, increased modulus and glass transition temperature. This modification of a PS/PU-SIN was investigated by Hsieh.[277]

In the early 1990s, the first IPN-based hydrogel was published by Ilmain *et al.*. This hydrogel was based on poly(acrylamide) and poly(acrylic acid). Large volume transitions were induced by hydrogen bonding between the networks.[278] In the following years, more and more publications appeared. For example, an IPN based on poly(vinyl alcohol) and poly(acrylic acid) was presented by Gudeman and Peppas. These exhibited significant swelling differences with minor pH changes.[279]

Another model of IPNs is a semi-IPN. Here, a monomer is polymerized while another polymer is already present.[184, 185] A thermoreactive semi-IPN was presented by Zhang *et al.*, which was based on poly(vinyl alcohol) and poly(N-isopropyl acrylamide).[280]

Decker and Decker published a vinyl ether and acrylate monomer system in 1997. These were supposed to be polymerized *via* two different polymerization mechanisms; one by radical polymerization and the other by cationic polymerization. However, some copolymerization occurred here, so the principle of IPNs with two separate networks was not given.[281] Decker reported an IPN system using the same principle but based on acrylate and epoxide monomers a few years later. He also conducted a reactivity study on

bisphenol-A-diacrylate and a difunctional biscycloaliphatic epoxide. In addition, he studied the influence of atmospheric oxygen, the addition of light stabilizers, and the dark reaction typical for cationic polymerization. He also discovered that the conversion of epoxides was favored by thermal post-treatment at 80 °C after photopolymerization.[282, 283]

Sangermano's research group is also working on the formation of IPNs. They used bis(1-ethyl(3-oxetane-yl))methyl ether, cyclohexene oxide, divinyl ether, and polyethylene glycol diacrylate. As a cationic photoinitiator, they used triphenyl sulfonium hexafluoroantimonate. Within this study, they found that the epoxy groups significantly increased the reaction rate of the oxetane groups. Likewise, this was evident in the addition of vinyl ethers. They explained this effect by radicals generated by the cleavage of the cationic photoinitiator, thereby promoting acrylate polymerization.[284] In other papers, they investigated the effects on the thermomechanical properties of IPNs. They used photopolymerized acrylic-epoxy hybrid films of hexanediol diacrylate and 3,4-epoxycyclohexyl methyl 3',4'-epoxycyclohexyl carboxylate. They recognized that the glass transition (tanδ) occupied a wide temperature range. This suggests good damping characteristics of the material. Furthermore, they found less shrinkage during polymerization than for pure hexanediol diacrylate systems and better adhesion properties.[285]

The temperature dependence of the polymerization rate of epoxy/methacrylate IPNs was studied by Bunel *et al.*. They used a dimethacrylate polyether in combination with bisphenol-A and bis-(3,4-epoxycyclohexyl)adipate as the resin. Through these experiments, they realized that increased temperature increases the polymerization kinetics of oxiranes but reduces it for dimethacrylates. For this reason, the polymerization temperature is crucial for the final properties of the IPN.[276]

James Crivello demonstrated another essential finding. He showed that oxetane polymerization could be accelerated by using epoxides. Crivello used an oxetane/(meth)acrylate mixture for the studies. He also realized that the formation of an IPN is faster than the homopolymerization of the monomers. The formed IPNs were transparent, colorless, and hard. For IPNs where the cured radical network was above 50 wt%, he could detect inhibition by atmospheric oxygen.[286]

Guymon *et al.* also worked with oxetane/acrylate systems and investigated the appearance of phase separations as a function of irradiance. In this case, the oxetane groups were used for the hard network and the acrylate groups for the soft network. Triarylsulfonium

hexafluoroantimonate salts were used as both radical and cationic photoinitiators. The two monomer systems were mixed in different ratios and irradiated with intensities ranging from 10 to 1500 mW cm^{-2}. Only minor differences were observed if the amount of acrylate monomer was low. However, above 30 wt% acrylate content, noticeable phase separation could be observed. In addition, if the irradiation intensity was increased, the phase separation decreased again or was even wholly suppressed. If strong phase separation occurred, brittle materials were obtained. However, high toughness and elongation at break were observed when phase separation was suppressed.[287]

Formation of IPNs *via* 3D printing

In the early 2000s, the production of IPNs also became popular *via* 3D printing. For example, IPN hydrogels made from alginate and f-GelMA (fish gelatin with methacrylate groups) were successfully produced. This study showed that IPNs exhibited different properties compared to the individual networks, for example, in their swelling ratios, degradation, and cell behavior. Therefore, they postulated a potential application in the field of tissue engineering.[288] However, hydrogels made from GelMA with silk sericin are also known. Here, the monomers in an aqueous solution with a photoinitiator are applied in layers through thin nozzles. These solutions are called bio-inks. Each layer was then irradiated with UV light to cure it. These hydrogels exhibited increased strength compared to plain networks.[288, 289]

Huang *et al.* introduced a cycloaliphatic silicone/epoxy resin and printed it using stereolithography.[290] They also printed so-called 4D hybrid materials. Here, the 3D constructs have an additional shape memory effect.[291]

Hoekstra *et al.* fabricated IPNs orthogonally by photopolymerization. For this, they used an oxetane/acrylate system. Here, it was possible to control the phase separation and produce so-called liquid crystal IPNs.[292] Often, IPNs are printed and then thermally post-cured to produce improved final properties.

IPNs for 3D printing have also been studied in our research group. Reactivity studies were first performed to find the best monomers. Monomers included glycidyl ether, oxetane ether, glycidyl ester, and oxetane ester. It was found that at room temperature, only the oxetane ether showed excellent reactivity. For this reason, the curing of the networks had to happen sometimes at elevated temperatures (50-120 °C). Nevertheless, the influence of different PI systems, curing temperatures and light intensities were also investigated.

In further work, the influence of chain transfer agents in the cationic system was investigated.[293, 294]

All these examples show that IPNs have played an essential role for decades in combining and improving the properties of two different materials. However, only in the last decade have lithography-based techniques become increasingly attractive. There are still many opportunities to generate novel 3D structured IPN materials.

2. Influence of radical system on cationic photopolymerization

Incorporating high molecular weight toughness enhancers into vinyl ester-based thiol-ene formulations led to an increase of tensile toughness, which is preferable for bone replacement materials, but soon their limit was reached. Therefore, interpenetrating polymer networks (IPNs) should be generated. IPNs are two different polymer networks that are not covalently bonded but interwoven and can not be separated without breaking chemical bonds. Usually, they consist of one rigid and one flexible polymer network. They are of interest as they combine the properties of both polymer networks and the mechanical properties of the final material, *e.g.*, tensile toughness, can exceed those of the individual polymer networks.[276]

In this work, a wavelength-selective sequential IPN should be created. Here, the soft and hard segments possess two different functional groups and are polymerized sequentially with two different light sources and curing mechanisms. First, the radical group will polymerize, and the second segment's polymerization with the cationic moiety will be slightly delayed. Therefore, the formulation will be first irradiated with a wavelength of 405 nm and afterwards with 365 nm. The process is visualized in Figure 40.

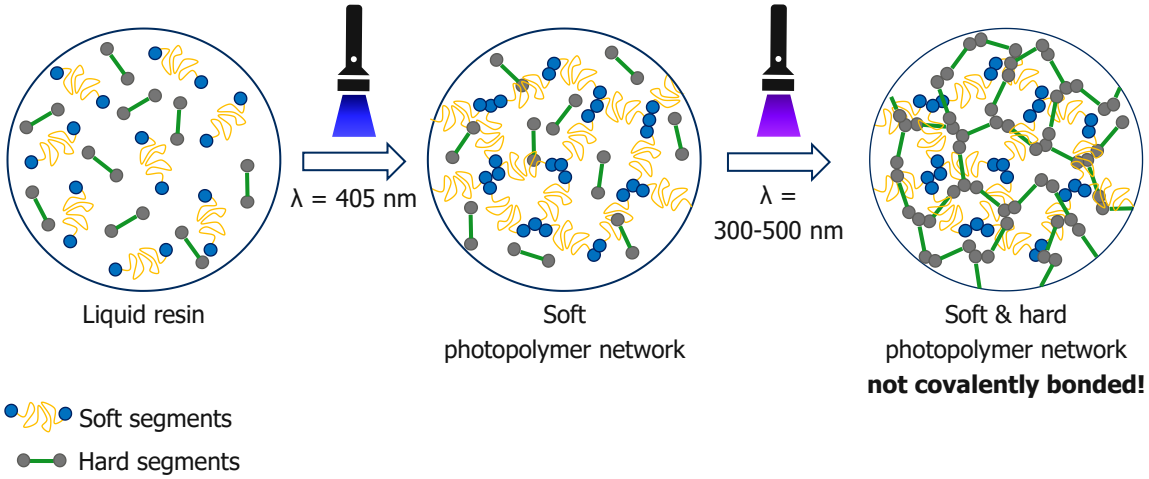

Figure 40: Formation of an interpenetrating polymer network due to photopolymerization at different times.

As a soft polymer network, the high molecular weight poly(ε-caprolactone) (PCL) should be used. This polymer is s already well studied and its excellent properties are well known. The formation of a network is possible if PCL is end-capped with photopolymerizable groups. Here, the monomer should be polymerized in a step-wise mechanism. In addition, thiols should be used as chain transfer agents (CTAs) since this leads to a more homogeneous network formation. This system should be formed *via* a radical mechanism. The syntheses of these monomers are described in Chapter A.2.1 or Appendix A.1.

The hard segments, in contrast, should consist of polyethers derived from oxetane moieties. Oxetanes are thermally stable and show less shrinkage than epoxide monomers.[172, 173] Here, different oxetane monomers with varying rigidity should be synthesized and investigated. In addition, hydroxyl-containing compounds should be synthesized and act as CTAs. The hard network should be formed *via* a cationic mechanism.

2.1. Inhibition study of cationic polymerization due to thiol-ene chemistry

Cationic photopolymerization is considered very vulnerable to alkaline traces and impurities, which can suppress the initiation or propagation of the cationic mechanism. Using a thiol-ene system in combination with a cationic system may lead to the reaction of thiols with protonated epoxides to form sulfides. These sulfides can now act as nucleophiles and react with terminal oxonium. Alkylsulfonium salts can be formed in the subsequent process, but they are not reactive under UV-Vis irradiation. However, they can

act as thermal initiators and start the homopolymerization of epoxide-functionalized monomers.[295]

For this reason, a study should be made if thiols, which are used for the soft network, will inhibit the second cationic curing step. Therefore, norbornene functionalized polycaprolactone (**NB10kPCL**) should be used and polymerized *via* thiol-ene chemistry. Norbornene functionalities were chosen as they show the highest reactivity in thiol-ene chemistry.[296] This monomer has a molecular weight of 10kDa; therefore, the thiol concentration is relatively low even if the thiol is used in equimolar ratio to the norbornene functionality. As thiol the commercially available difunctional 2,2'-[1,2-ethanediylbis(oxy)]bis-ethanethiol (DOD) should be used, and as radical photoinitiator, the phosphine oxide TPO-L. The cationic system will contain monomers with oxetane functionalities. For this study, the dioxetanes 3,3'-[oxybis(methylene)]bis[(3-ethyl)oxetane] (**DOX**) and 1,4-bis(((3-ethyloxetane-3-yl)methoxy)methyl) benzene (**XDO**) were used. The borate-based triarylsulfonium salt Irgacure® 290 (IC290) was added as a cationic photoinitiator. All compounds for the radical and cationic systems are depicted in Figure 41.

radical system:

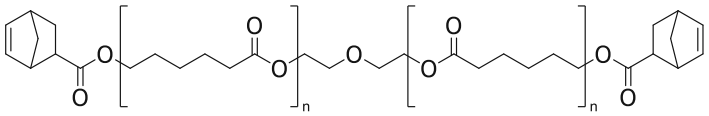

NB10kPCL

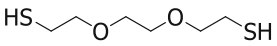

DOD

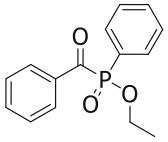

TPO-L

cationic system:

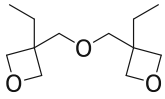

DOX

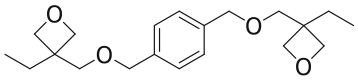

XDO

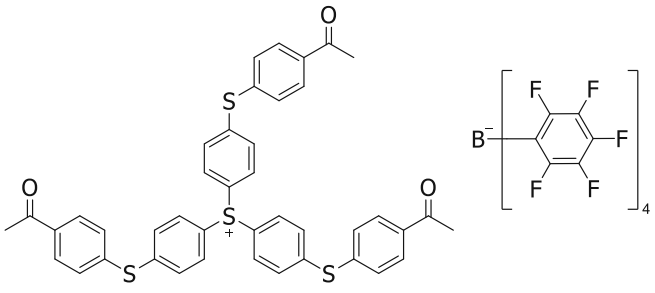

IC290

Figure 41: Compounds for the radical and cationic system to determine the photoreactivity of oxetanes *via* photo-DSC.

The influence of low-concentrated DOD on the cationic polymerization should be determined with three different formulations of each cationic monomer (**DOX** and **XDO**).

First, a formulation only containing oxetane and the cationic PI was prepared (Form. 1). Then, one formulation (Form. 2) contained additionally the thiol DOD. DOD is added in an amount (equimolar ratio to norbornene (NB) functionalities), which would be necessary for the thiol-ene reaction if the norbornene functionalized PCL would be present. Last, a formulation, which contains the oxetane monomer, DOD, **NB10kPCL** (10wt%) and the

cationic and radical PI (see Table 1, Form. 3) was prepared. The cationic and radical photoinitiators and the thiol were always added as additional mmol or mol% to the monomers.

Table 2: Formulations to determine the photoreactivity of oxetanes *via* photo-DSC.

Formulation	Dioxetane [wt%]	IC290 [mol%]	DOD* [mmol]	NB10kPCL [wt%]	TPO-L [mol%]
Form. 1	100	0.5	-	-	-
Form. 2	100	0.5	0.04	-	-
Form. 3	90	0.5	0.04	10	0.5

*equimolar to NB-functionalities

Figure 42 shows the results of the photo-DSC measurements of the different formulations for the two dioxetanes (**DOX** in grey and **XDO** in red). In general, it can be shown that **DOX** was more reactive than **XDO**, which was expected. A closer look at the heat deflection (ΔH) showed a slight decrease due to the addition of the thiol **DOD**. The impact on **XDO** as a monomer is higher compared to **DOX**. Nevertheless, ΔH slightly increased again after adding the monomer for radical polymerization (**NB10kPCL**). In sum, the reaction rate was slowed down due to the addition of thiol and radical monomer, but the polymerization heat could be matched again.

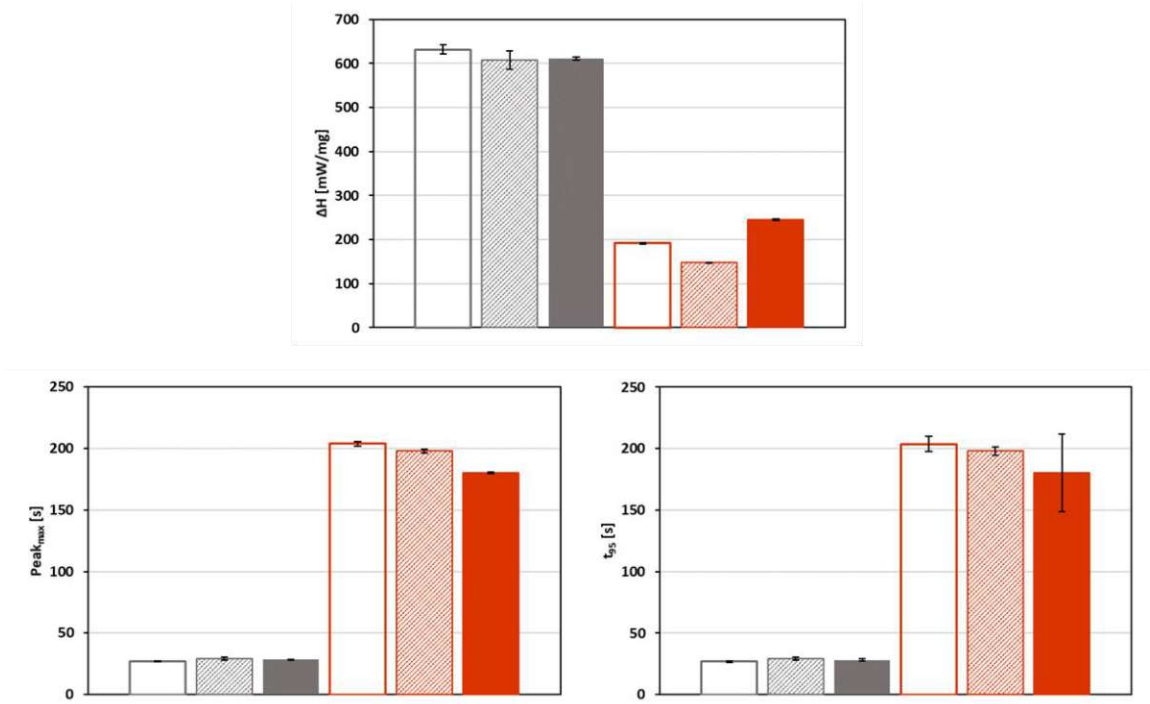

Figure 42: Results of Photo-DSC measurements for formulations containing **DOX** (grey) and **XDO** (red). Formulations only containing the cationic polymerizable monomer and cationic PI (Form. 1, unfilled □), formulations containing additional thiol (Form. 2, dashed ▨) and formulations with thiol, radically photopolymerizable monomer and radical PI (Form. 3, bulk ■).

In sum, adding a thiol-ene system hardly influenced the cationic photopolymerization. Therefore, the formation of an IPN should be possible.

2.2. Investigation of thermomechanical properties of an IPN *via* DMTA

However, in order to investigate the mechanical properties of the formed IPNs, the difunctional thiol was changed to the trifunctional thiol 1,1,1-trimethylolpropane-tris(3-mercaptopropionate) (**Thiol 1**) to generate a cross-linked network. The commercially available oxetane **DOX** was used for the first trials to prepare DMTA specimens. Formulations containing **DOX** and the PI IC290 (0.5mol%) were overpolymerized (losing their shape due to expansion, dark brown discoloration, and cracks) during photopolymerization in the UV-oven. Hence, the cationic PI was reconsidered. The combination of Cyracure uvi 6976 (S-Sb, 1wt%) and TPO-L (1wt%) showed promising results in previous work.[294] For this reason, the cationic initiator system was changed to the antimonate-based (S-Sb) photoacid generator. The replaced thiol and cationic PI can be seen in Figure 43.

trifunctional thiol:

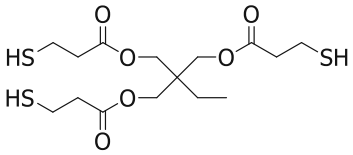

Thiol 1

cationic photoinitiator:

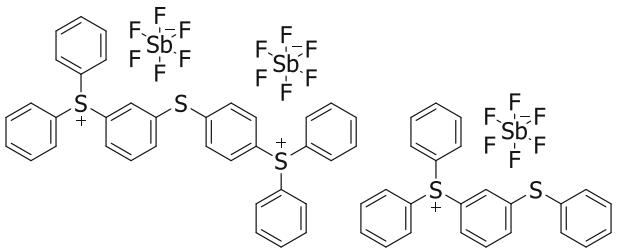

S-Sb

Figure 43: Chemical structures of the trifunctional thiol (**Thiol 1**) to generate a radical crosslinked polymer network and the antimonate-based cationic photoinitiator.

Specimens were cured in a PrograPrint Cure[253] from Ivoclar® with a wavelength of 405 nm and an intensity of 274 mW·cm^{-2} for free radical photopolymerization. After an exposure time of 10 minutes, the samples were rotated and cured on the other side for 10 minutes. Then, the cationic photopolymerization was done in the UV oven at 50% intensity with a broadband lamp. Again, both surfaces were cured for 10 minutes. Before the measurements, the samples were ground and polished with sandpaper in multiple steps to ensure uniform geometries and to remove artifacts from the surface.

For the initial evaluation of the final properties of the IPN, the thermomechanical properties (glass transition temperature (T_g) and storage modulus (G')) were determined *via* DMTA measurements. Because, if the T_g would drop far below the body temperature due to the addition of the PCL-based toughness enhancer, another radical or cationic system would have to be found. For this experiment varying specimens were prepared. As a reference, one specimen containing only the cationic system (**DOX** and 1wt% S-Sb, **Ref. DOX**) was cured in the UV-oven. Afterwards, 10wt% **NB10kPCL**, **Thiol 1** (equimolar to **NB10kPCL**), and 1wt% TPO-L were added to the reference system. This formulation was cured with the above-described procedure and is called **IPN** and the following discussion.

The results of the glass transition temperature T_g and storage modulus G' were depicted in Figure 44.

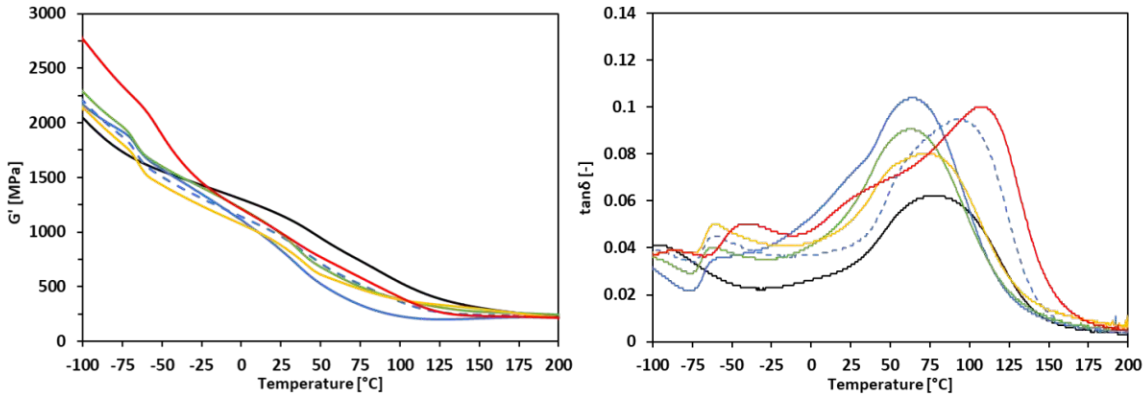

Figure 44: Storage modulus (G', left) and loss factor (tanδ, right) over temperature for **Ref. DOX** (—), IPN (—), IPN 2ndcycle (- - -), IPN_pc90 °C (—), IPN_pc120 °C (—), IPN_pc180 °C (—).

The reference system in black (**Ref. DOX**) showed a glass transition temperature T_g of 71 °C and a storage modulus at body temperature G'_{37} of 1066 MPa. After adding the thiol-ene system (IPN, solid blue line), the T_g and G'_{37} decreased to 62 °C and 680 MPa, respectively. Nevertheless, the reference and the IPN specimens showed inhomogeneous polymer networks due to uncontrolled photopolymerization.[122] This can result in internal stress, broad glass transition temperatures and low impact resistance at high temperatures.[123] Hydroxyl-containing molecules can be used as chain transfer agents to avoid these drawbacks.

The influence of the thermal post-curing for this system was not known, and therefore, a second cycle (-100 to 200 °C) was conducted (IPN 2nd cycle, blue dotted line). As a result, the glass transition temperature was shifted again to 90 °C; hence, a suitable post-curing temperature (pcX°C) should be investigated. The specimens were post-cured and now tagged with IPN_pcX°C, whereas X indicates the temperature at which the sample was thermally post-cured for 12 h. The different specimens were stored at 90 °C, 120 °C or 180 °C for 12 h each and were measured afterwards. IPN_pc90°C showed no significant influence on T_g compared to the not post-cured sample (IPN), but post-curing at 120°C showed an increase of ~5°C compared to IPN. The process at 180 °C showed the most decisive influence on the T_g, which could be increased to 103 °C. However, post-curing the specimens at 180°C is too harsh. Because post-curing at 120 °C only improved by 5 °C in T_g, it was decided that thermal post-curing would not be implemented because it is highly time-consuming. Furthermore, the T_g of the IPN (62 °C) is still far above the body temperature, which is necessary for the application as bone replacement material.

3. Synthesis of multifunctional and degradable oxetane monomers

The choice of monomers and additives for both networks of the IPN determines the properties. Beside good mechanical properties, *e.g.*, high toughness, suitable biodegradability must also be considered. If these materials are to be applied in biomedical applications, *e.g.*, as bone replacement implants, they are only a temporary scaffold until the bone has re-grown. Due to that, both networks of IPNs must have groups that can be degraded under hydrolytic conditions.

Unfortunately, commercially available oxetanes are only difunctional and contain no cleavable moieties. For this reason, new, at least trifunctional monomers with ester as degradable groups should be synthesized. Previous studies showed that oxetane esters, as depicted in Figure 45 on the left-hand side, need curing temperatures above 150 °C and have low polymerization rates. Hence, they are not suitable for 3D printing applications.[293] For this reason, an ethylene glycol spacer should be inserted between the ester groups and the oxetane moiety (see Figure 45, right-hand side) to overcome this problem.

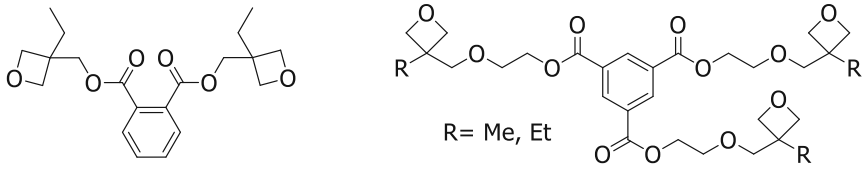

Figure 45: Chemical structure of difunctional oxetane ester (left) and trifunctional oxetane monomer with ethylene glycol spacer and esters as cleavable groups (right).

There are two commercially available compounds to introduce an oxetane group into a molecule: 3-chloromethyl-3-methyloxacyclobutane (MOCl) and 3-ethyl-3-hydroxymethyl oxetane (EOM). Both are depicted in Figure 46.

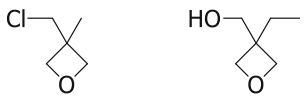

Figure 46: Chemical structure of 3-chloromethyl-3-methyloxacyclobutane (MOCl) and 3-ethyl-3-hydroxymethyloxetane (EOM).

The first idea was to insert the oxetane functionality into the molecule when the ester group and ethylene glycol spacer are already present. For this purpose, a model reaction with the commercially available bis(2-hydroxyethyl)terephthalate (BHET) and MOCl should be used (see Scheme 10). Unfortunately, the synthesis will need harsh conditions, and the ester will presumably cleave.

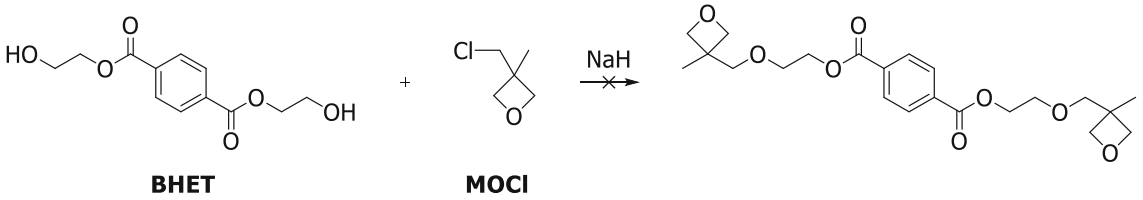

Scheme 10: Synthesis of difunctional degradable monomer with oxetane functionalities.

Nevertheless, a small-scale synthesis was done with NaH, but as expected, the ester cleaved, and the product could not be isolated.

For this reason, the desired trifunctional monomer cannot be synthesized *via* this synthetic route.

In literature,[297] a synthesis is presented, where an oxetane-containing molecule is modified with a good leaving group to further etherify it with ethylene glycol. Then, this molecule can be converted with a carbonyl chloride to synthesize, *e.g.,* the trifunctional oxetane monomer 1,3,5-tris[(3-ethyl-3-oxetanyl)methoxyethyl]-1,3,5-benzenetricarboxylate (**TOx**, Scheme 11).

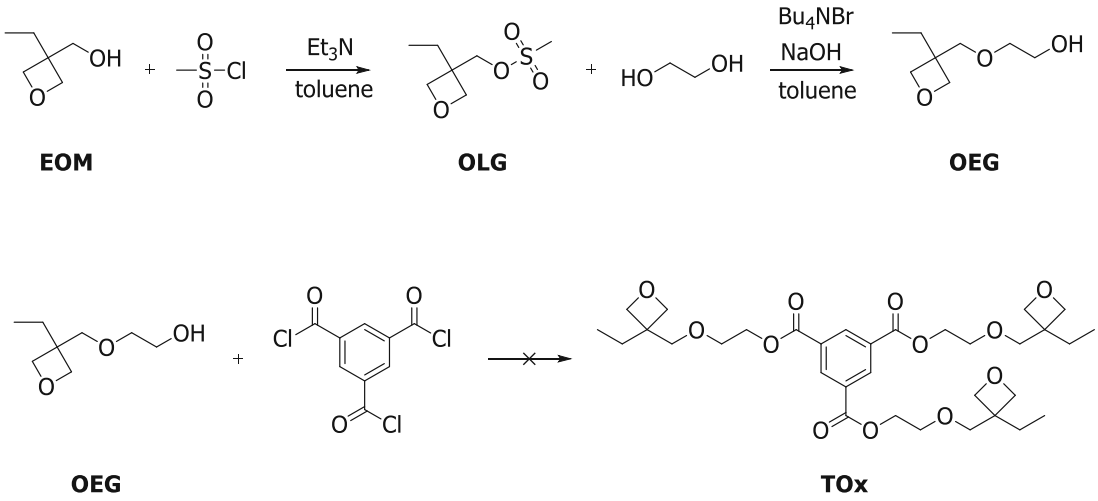

Scheme 11: Three-step synthesis of trifunctional oxetane monomer **TOx**.

In the first step, 3-ethyl-3-methanesulfonyloxymethyloxetane (**OLG**) was synthesized. Therefore, 3-ethyl-3-hydroxymethyloxetane (EOM, 1 eq.) was diluted with triethylamine (1.2 eq.) in toluene and then, methane sulfonyl chloride (MsCl, 1.2 eq.) was added

dropwise. The organic phase was evaporated and the product **OLG** was isolated with an 81% calculated yield as a yellow oil. It was used without further purification for the next step.

In the following step, 3-ethyl-3-(4-hydroxyethyl)oxymethyloxetane (**OEG**) was synthesized. Therefore, ethylene glycol (2.1 eq.) was dissolved in toluene and then, sodium hydroxide pellets (1.16 eq.) and tetrabutylammonium bromide (0.03 eq.) were added. Afterwards, the before-synthesized **OLG** was added dropwise, the two phases were stirred vigorously and the pH was set to ~9 with diluted acetic acid. The phases were separated, the organic phase was removed and the crude product was obtained in 36% calculated yield.

In literature, the crude product was purified by distillation (19 mbar, 157-159 °C), but with this method, no pure product was obtained, only mixed fractions of **OLG** and **OEG**. Purification by Kugelrohr distillation also did not yield a pure product.

Due to insufficient purity, poor yields, and the fact that mixed products (1-3 fold substituted) would be formed in the subsequent step, this synthesis was neglected. For the following experiments, commercially available bifunctional monomers such as **DOX**, **XDO** and **S160** (see Figure 47) must be used.

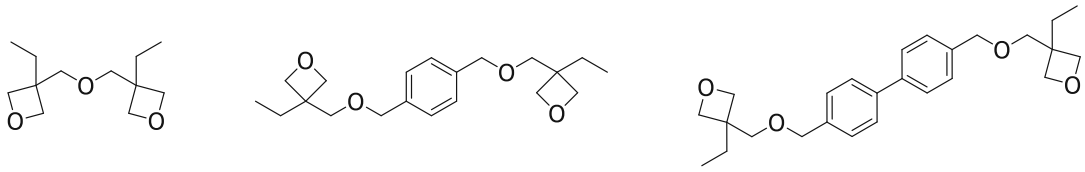

DOX **XDO** **S160**

Figure 47: Chemical structure of commercially available bifunctional monomers.

Unfortunately, these contain no cleavable moieties and therefore, the strategy of multifunctional molecules for crosslinked networks with esters as cleavable moieties has to be allocated to chain transfer agents.

4. Influence of a chain transfer agent on the cationic photopolymerization of oxetanes

Uncontrolled photopolymerization leads to an inhomogeneous network formation.[122] This can result in internal stress, broad glass transition temperatures and low impact

resistance.[123] These effects were observed in the first DMTA measurements (Figure 44, Chapter 2.2) of **DOX**. Chain transfer agents (CTAs) can overcome these problems. These molecules transfer the active center of a growing chain to another chain and promote a more homogeneous polymer network. This further improves the material's toughness and (thermo)mechanical properties.[122, 172] As CTAs in cationic polymerization hydroxyl-containing molecules like water or alcohols can be used.

The strategy of multifunctional molecules for crosslinked networks with esters as cleavable moieties was allocated to the chain transfer agents because the synthesis of such oxetane monomers (Chapter 3) was unsuccessful. The two planned chain transfer agents 1,3,5-tris(2-hydroxyethyl)-1,3,5-benzenetricarboxylate (**THEB**) and 3,4-dihydroxy-cyclohexanecarboxylic acid (**CEOH**) are depicted in Figure 48.

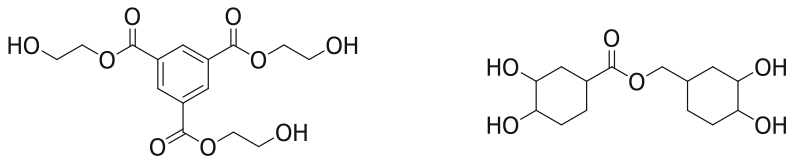

THEB **CEOH**

Figure 48: Chemical structures of multifunctional degradable chain transfer agents.

Using chain transfer agents is intended to promote a step growth reaction. For this reason, a photo-DSC study was performed, followed by an evaluation of the conversion *via* ^{1}H-NMR. The aim is to determine whether the alcohol (CTA) reacts with the oxetane or most oxetane monomers homopolymerize. For this purpose, first, a monofunctional oxetane was synthesized.

4.1. Synthesis of 3-[benzyloxy(methyl)]-3-ethyloxetane (BOX)

The monofunctional oxetane 3-[benzyloxy(methyl)]-3-ethyloxetane (**BOX**) was synthesized in a one-step synthesis according to Kury *et al.*[293] and is depicted in Scheme 12.

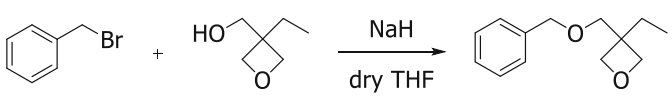

EOM **BOX**

Scheme 12: Synthesis of monofunctional 3-[benzyloxy(methyl)]-3-ethyloxetane (**BOX**).

Therefore, 3-ethyl-3-oxetanemethanol (EOM, 1.1 eq.) was diluted and NaH (1.5 eq.) was added portion-wise to the pre-cooled solution. Then, benzyl bromide (1.0 eq.) was added

dropwise. The organic phase was removed, and the residual oil was purified by column chromatography and **BOX** was isolated as colorless oil in a 52% calculated yield.

4.2. Study of adduct formation of BOX with chain transfer agents

^{1}H-NMR measurements followed photo-DSC experiments to evaluate the conversions of **BOX** and two varying alcohols as CTAs; 1-hexanol and 1,2-cyclohexanediol (**CHD**), respectively. 1-Hexanol was chosen, as it has a primary alcohol as in **THEB**, and **CHD** because it has two secondary alcohols in ortho-position as in **CEOH**.

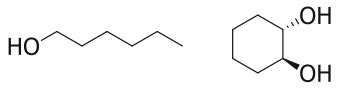

1-hexanol **CHD**

Figure 49: Chemical structures of 1-hexanol and 1,2-cyclohexanediol (**CHD**).

One formulation only containing **BOX** and 1wt% S-Sb as cationic photoinitiator was prepared. Then, two formulations containing **BOX**, S-Sb, and the CTAs in an equimolar ratio (referred to the functional groups) were mixed. Photo-DSC measurements were conducted at room temperature with a broadband lamp with a wavelength of 300-500 nm and 60 mW·cm^{-2} light intensity. The samples were irradiated for 300 s twice. After the irradiation, the samples were quenched in $CDCl_3$ with pyridine to stop the dark reaction of the oxetane. Then, a ^{1}H-NMR was measured immediately to determine the conversion.

Figure 50 shows the NMR spectra of **BOX** before (black) and after (red) irradiation. **BOX** showed a complete conversion *via* homopolymerization.

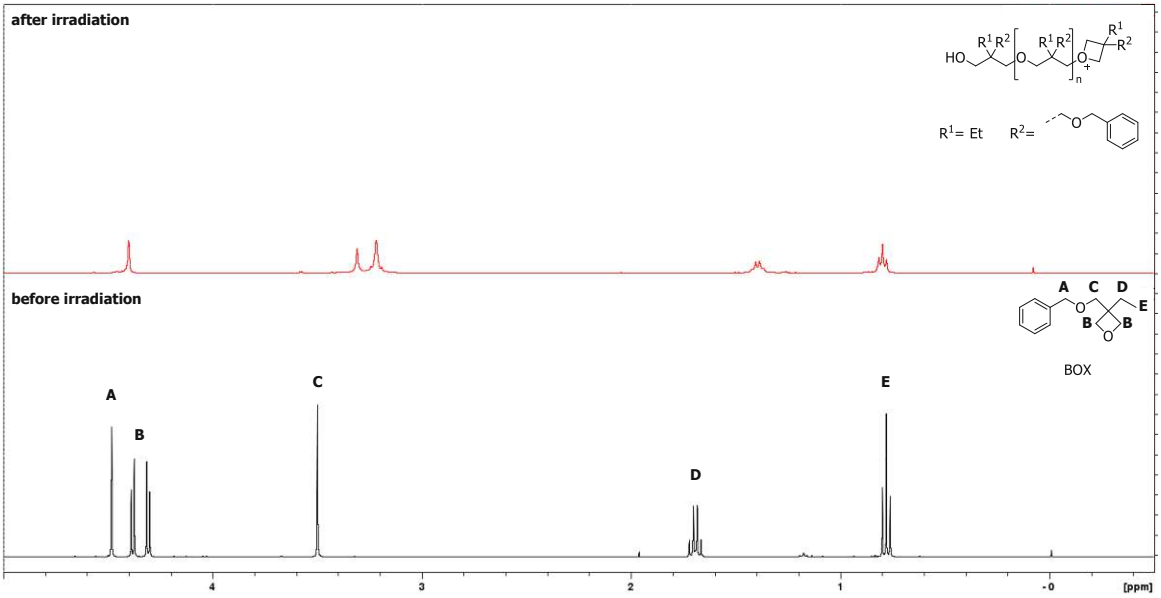

Figure 50: Section of ^{1}H-NMR spectra in $CDCl_3$ + pyridine of **BOX** before (bottom) and after irradiation (homopolymerization, top).

However, with this setup, formulations containing the CTAs were irradiated, but neither a reaction between oxetane and alcohol nor homopolymerization of the oxetane was observable. Therefore, the light intensity was increased to 200 mW·cm^{-2} and the polymerization temperature was set to 100 °C. Now, polymerization heat ΔH was detectable by photo-DSC.

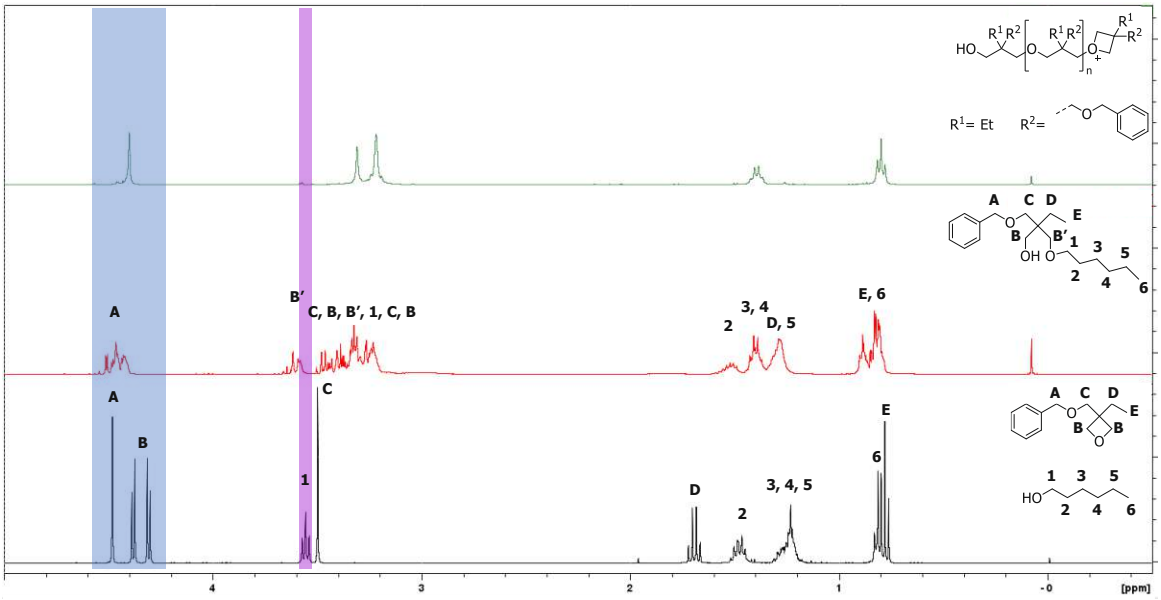

Figure 51: Section of ^{1}H-NMR spectra in $CDCl_3$ + pyridine of **BOX** + 1-hexanol before (bottom) and after irradiation (middle). For better comparison, the ^{1}H-NMR spectrum in $CDCl_3$ + pyridine of **BOX** Is shown on the top (homopolymerization).

Figure 51 shows the ^{1}H-NMR spectra of the formulations containing the formulation of **BOX** and 1-hexanol before (black) and after (red) irradiation and additionally compared to the homopolymerized **BOX** (green). The blue highlighting shows distinctive signals of the CH_2-group (A) next to the aromatic ring and the two CH_2-groups (B) of the oxetane group. After the homopolymerization of **BOX**, the signals of B are shifted from 4.4 ppm to 3.2 ppm. Signal A (4.5 ppm) only slightly shifts to 4.4 ppm. However, here the signal is always a singlet. If **BOX** and 1-hexanol are irradiated and an adduct formation happens, signal A shows a strong splitting of the signal. The purple highlighting shows the CH_2-group (1) next to the OH-group of 1-hexanol. After irradiation, this triplet (1) at 3.6 ppm was no longer observable. For this reason, an adduct formation of **BOX** and 1-hexanol and no homopolymerization is suggested.

The spectra of **BOX** and **CHD** are depicted in Figure 52. Again, the spectrum of the unirradiated sample is shown in black, the irradiated one in red, and the homopolymerized sample of **BOX** in green.

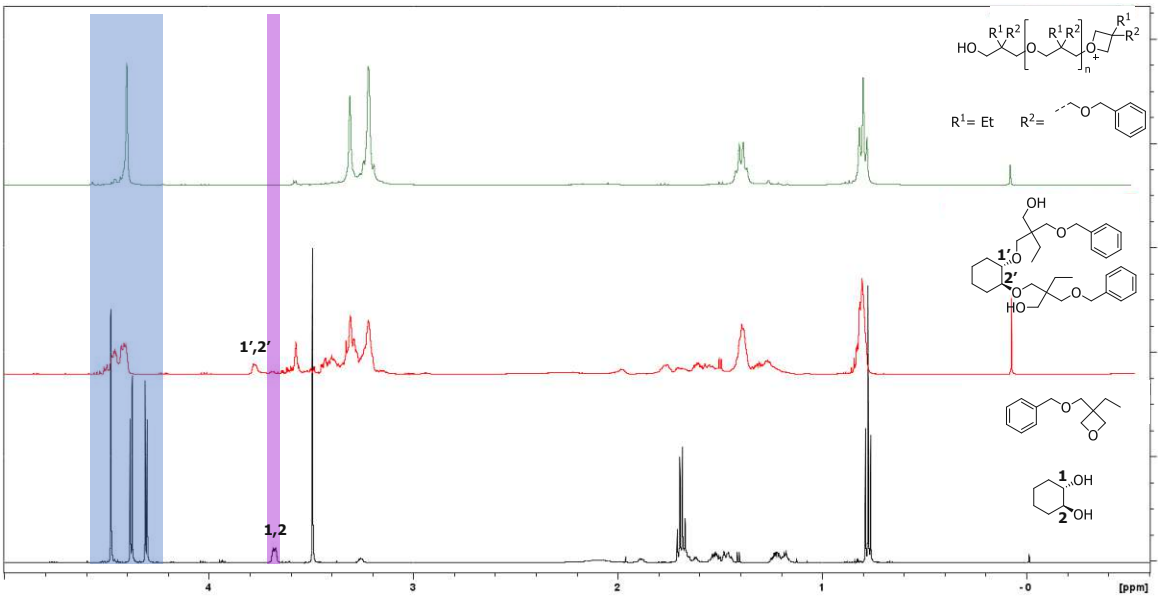

Figure 52: Section of ^{1}H-NMR spectra in $CDCl_3$ + pyridine of **BOX** + **CHD** before (bottom) and after irradiation (middle). For better comparison, the ^{1}H-NMR spectrum in $CDCl_3$ + pyridine of **CHD** Is shown on the top (homopolymerization).

The distinctive signals of the CH_2-group (A) next to the aromatic ring and the two CH_2-groups (B) of the oxetane group are again highlighted in blue. However, for better clarity, no labels are shown. The purple highlighting shows the CH-groups (1 and 2) next to the OH-groups of 1,2-cyclohexanediol (**CHD**) at 3.65 ppm. If **CHD** reacts with **BOX**, this signal is shifted to 3.8 ppm. After irradiation, a small residue (≤12%) of the CH-groups

(1, 2) is still detectable at 3.65 ppm. However, the major amount of **CHD** reacts with the oxetane monomer to form an adduct.

5. Synthesis of multifunctional degradable chain transfer agents

The experiment described above demonstrated that alcohols react with oxetanes as chain transfer agents and that there are only negligible amounts of homopolymerization of oxetanes.

For this reason, multifunctional alcohols are now to be synthesized in order to generate a crosslinked polymer network. Furthermore, hydrolytically cleavable groups are to be included so that a degradable network is finally created. The degradability of the networks is essential for their use as bone replacement material.

5.1. Synthesis of 1,3,5-tris(2-hydroxyethyl)-1,3,5-benzene tricarboxylate (THEB)

Four attempts were necessary to synthesize **THEB** successfully.

The first attempt to synthesize **THEB** was a one-step synthesis similar to the literature.[298] The reaction scheme is shown in Scheme 13. A carboxylic acid can be converted with alcohol to form an ester in a process called Fischer esterification. As an acid catalyst, concentrated sulfuric acid was used and the equilibrium should be shifted to the side of the product by removal of the water by azeotropic distillation.

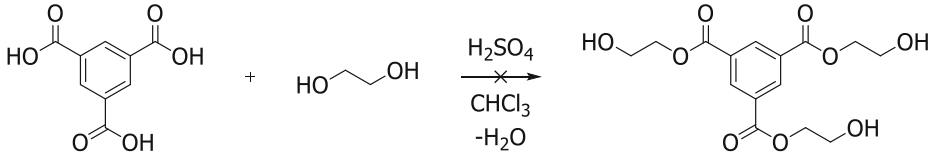

THEB

Scheme 13: One-step synthesis of 1,3,5-tris(2-hydroxyethyl)-1,3,5-benzenetricarboxylate (**THEB**) starting with 1,3,5-benzenetricarboxylic acid and ethylene glycol.

Here, 1,3,5-benzenetricarboxylic acid (1 eq.) was mixed with an excess of ethylene glycol (6 eq.) in chloroform and as a catalyst, conc. H_2SO_4 (3 drops) was used. A Dean-Stark apparatus removed the formed water during the procedure. The reaction mixture was heated to reflux and stirred for three days. ^{1}H-NMR spectroscopy showed that a mixture

of side-products (varying substitution and oligomerization) was formed. Therefore, the product was rejected, and another synthetic route was suggested.

Noordzij *et al.*[299] described a one-step synthesis, where 1,3,5-benzenetricarbonyl trichloride was used as starting material instead of the carboxylic acid (Scheme 14).

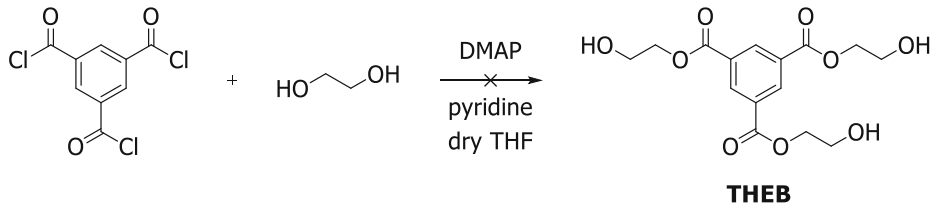

Scheme 14: One-step synthesis of 1,3,5-tris(2-hydroxyethyl)-1,3,5-benzenetricarboxylate (**THEB**) starting with 1,3,5-benzenetricarbonyl trichloride and ethylene glycol.

Therefore, a solution of ethylene glycol (4.5 eq.), pyridine (3.5 eq.) and cat. DMAP in dry THF was stirred in an ice bath. The reaction was performed in anhydrous conditions. Afterwards, 1,3,5-benzenetricarbonyl trichloride (1 eq.) was added dropwise and stirred for 16 h at room temperature. The solvent was removed, and the residual solid was dissolved in chloroform again. Then, the organic phase was extracted with 0.01 M HCl and deion. water and the solvent was removed *in vacuo*. ^{1}H-NMR spectroscopy showed that the product was oligomerized and therefore, the product was rejected.

Due to the reason that one-step syntheses of **THEB** did not lead to the desired pure product, another synthetic route was used. Wang *et al.*[300] described a two-step synthesis. First, the intermediate trimethyl benzene-1,3,5-tricarboxylate (Scheme 15) should be synthesized and in the second step, transesterification should lead to the desired product.

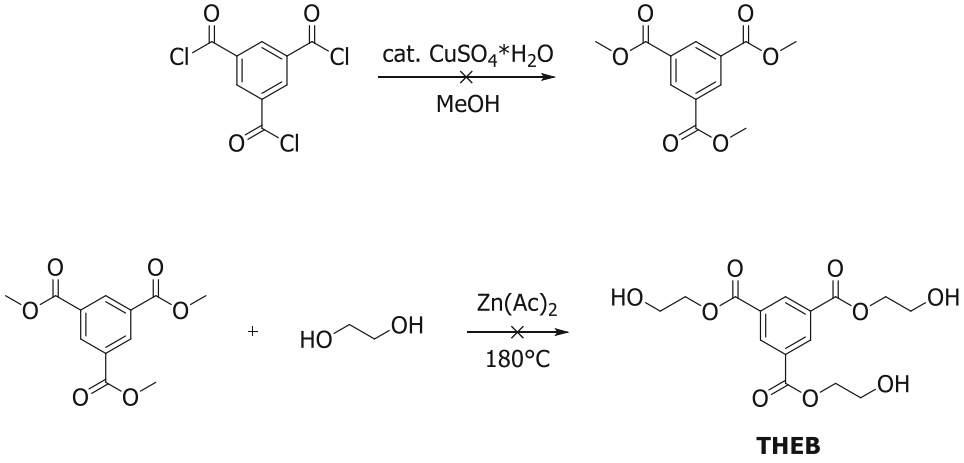

Scheme 15: Two-step synthesis of 1,3,5-tris(2-hydroxyethyl)-1,3,5-benzenetricarboxylate (**THEB**) starting with 1,3,5-benzenetricarbonyl trichloride.

Therefore, 1,3,5-benzenetricarbonyl trichloride (1 eq.) was dissolved in methanol and $CuSO_4 \cdot 5\ H_20$ (0.01 eq.) was used as a catalyst. The reaction mixture was stirred at reflux for 18 h. The conversion was followed by ^{1}H-NMR spectroscopy. Here, the formation of three products (one- to three-esterified) could be detected. However, after another 48 h still, no complete conversion could be achieved and therefore, the second step was not performed.

Azumaya *et al.*[301] described another synthetic route (Scheme 16), which should suppress an oligomerization during the synthesis of **THEB**. Therefore, the acid chloride will be esterified with one-side-protected ethylene glycol. Afterwards, the protecting group will be cleaved off, leading to the trifunctional hydroxyl-terminated chain transfer agent **THEB**.

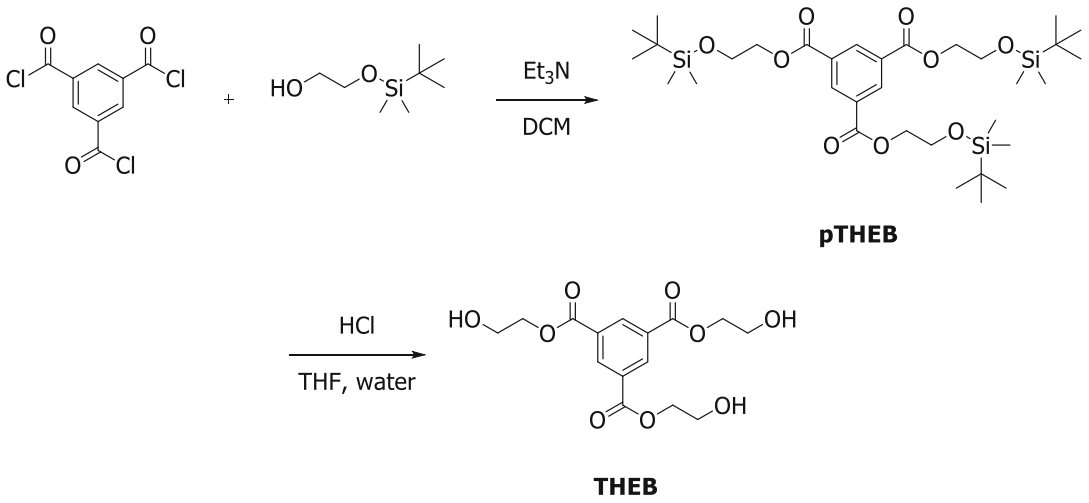

Scheme 16: Two-step synthesis of 1,3,5-tris(2-hydroxyethyl)-1,3,5-benzenetricarboxylate (**THEB**): starting with 1,3,5-benzenetricarbonyl trichloride and a one-side protected ethylene glycol to synthesize a protected intermediate (**pTHEB**), followed by hydrolyzation to obtain **THEB**.

In the first step, 1,3,5-tris[2-[[(1,1-dimethylethyl)dimethylsilyl]oxy]ethyl]ester-1,3,5-benzenetricarboxylic acid (**pTHEB**) was synthesized in a dry argon atmosphere. Therefore, 2-(tert-butyldimethylsilyloxy)ethanol (3.6 eq.) and triethylamine as an acid scavenger (3.6 eq.) were mixed and a solution of 1,3,5-benzenetricarbonyl trichloride (1 eq.) in dry DCM was added dropwise. The conversion was followed by TLC. The crude product was purified by column chromatography and **pTHEB** was isolated as a white powder with a 24% calculated yield.

The second step of the synthesis of **THEB** is the hydrolyzation of the protected intermediate **pTHEB**. Therefore, **pTHEB** (1 eq.) was dissolved in THF and 0.5 mL 6 M HCl was added. The product precipitated as a white solid, which was washed for purification. **THEB** was isolated as a white powder with an 81% calculated yield.

5.2. Synthesis of (3,4-dihydroxycyclohexyl)methyl 3,4-dihydroxy cyclohexane carboxylate (CEOH)

The second synthesized chain transfer agent is the tetrafunctional (3,4-dihydroxycyclohexyl)methyl 3,4-dihydroxycyclohexanecarboxylate (**CEOH**). **CEOH** was synthesized in a one-step synthesis by a ring-opening of the difunctional epoxide 3,4-epoxycyclohexylmethyl 3,4-epoxycyclohexanecarboxylate (CE). The reaction was done according to Ratcliffe *et al.*, see Scheme 17.[302]

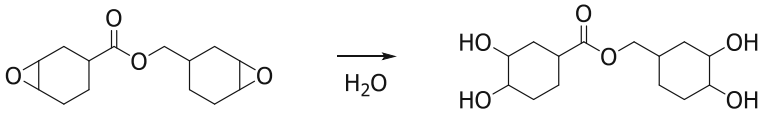

CE **CEOH**

Scheme 17: One-step synthesis of (3,4-dihydroxycyclohexyl)methyl 3,4-dihydroxycyclohexanecarboxylate (**CEOH**).

Therefore, 3,4-epoxycyclohexylmethyl 3,4-epoxycyclohexanecarboxylate (CE) was mixed with water and stirred for 16 h at 80 °C. However, too hot or too long reaction time will lead to cleavage of the ester. The water was removed and the viscous colorless product was recrystallized to obtain **CEOH** in 82% calculated yield as a white powder.

6. Selection of cationic photocurable system

In the previous section, the adduct formation of chain transfer agents with oxetane-containing molecules was investigated by a ^{1}H-NMR study. After that, one trifunctional (**THEB**) and one tetrafunctional (**CEOH**) chain transfer agents were successfully synthesized.

Now, the effect of these CTAs on the (thermo)mechanical properties of varying oxetane monomers should be investigated by DMTA and tensile test measurements.

6.1. Formulation preparation of the cationic photocurable formulation

Formulations with only the varying monomers and the cationic photoinitiator (1wt% S-Sb) were prepared. In addition, formulations with the chain transfer agents in a 1:1 molar ratio (referred to the functionalities) were mixed. The three different monomers 3,3'-[oxybis(methylene)]bis[(3-ethyl)oxetane] (**DOX**), 1,4-bis(((3-ethyloxetane-3-yl)methoxy)methyl) benzene (**XDO**) and 4,4'-bis[(3-ethyloxetan-3-yl)methoxymethyl]-

1,1'-biphenyl (**S160**) are shown on the top and the two CTAs 1,3,5-tris(2-hydroxyethyl)-1,3,5-benzenetricarboxylate (**THEB**) and (3,4-dihydroxycyclohexyl)methyl 3,4-dihydroxycyclohexane carboxylate (**CEOH**) on the bottom of Figure 53.

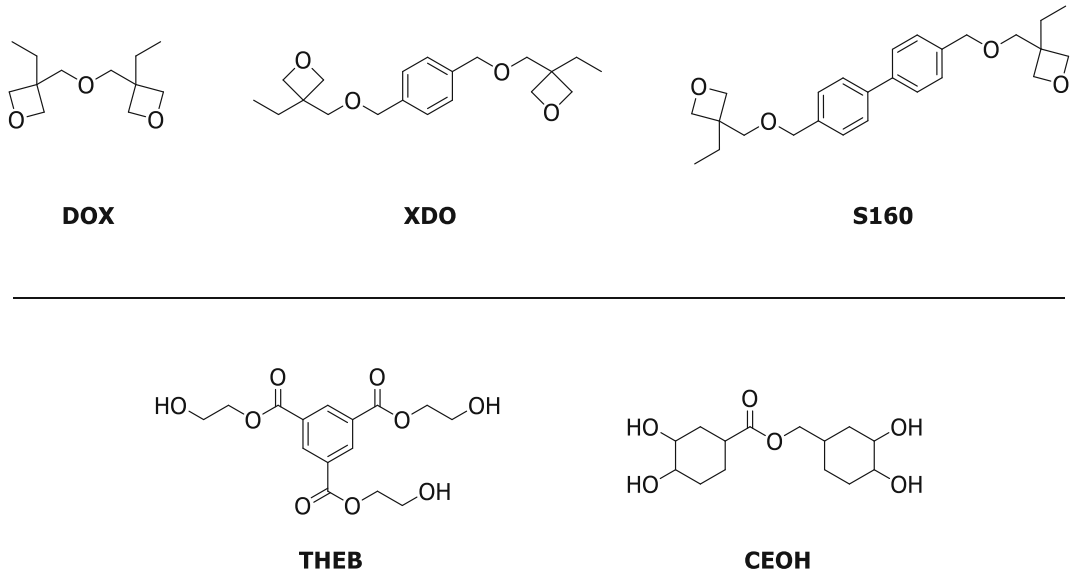

Figure 53: Chemical structures of the commercially available oxetane monomers **DOX**, **XDO** and **S160** (top) and the synthesized CTAs **THEB** and **CEOH** (bottom).

The formulations only containing the monomers and S-Sb remained liquid at room temperature. In contrast, the formulations containing additional CTAs were heated up to 120 °C to ensure melting of the CTAs in the monomer and mixed until complete homogeneity was assured.

6.2. Sample preparation of the cationic photocurable system for (thermo)mechanical testing

The freshly prepared formulations were kept at 120 °C temperature until use to avoid unintended recrystallization and to decrease the viscosity for easier handling. The formulations were transferred with a hot glass pipette into pre-heated silicon molds (120 °C) for DMTA- and tensile specimens. However, **THEB** recrystallizes immediately during the transfer. Consequently, these formulations could not be transferred to the molds, and their homogeneity was not ensured. For this reason, formulations containing the monomers alone and formulations that additionally contain **CEOH** as CTA were discussed in the further chapters.

Possible bubbles were removed, and the specimens were cured in a hot mold at 120 °C with λ = 365 nm and an intensity of 630 mW/cm^2. The exposure time was 5 minutes on each side. Before the measurements, the samples were ground and polished with sandpaper in multiple steps to ensure uniform geometries and to remove artifacts from the surface.

6.3. Investigation of thermomechanical properties *via* DMTA

In order to investigate the thermomechanical properties, DMTA measurements were conducted. These experiments should provide information about the glass transition temperature (T_g), where a reversible transition from a hard state into a viscous or rubbery state occurs. This temperature is determined by the maximum of the loss factor (tanδ). A classic behavior for brittle materials is a wide temperature range for T_g, which characterizes a nonregulated polymer network.[244] The second important parameter is the storage modulus G'. G' at the rubber plateau (G'_R) provides information about the crosslink density of the final polymer. Here, high values correspond to a high network density.[205, 254] DMTA measurements were performed from -100 °C to 200 °C with a heating rate of 2 °C·min^{-1} and in torsion mode.

It is expected that the use of CTAs changes the network architecture and therefore affects the thermomechanical properties of the final material. Compared to the homopolymerized monomers, formulations containing CTAs will decrease in T_gs and create more homogeneous networks. Here, the OH groups are involved in the active monomer (AM) mechanism, which affects the chain transfer reaction. This leads to a decrease in the crosslink density and the mobility of the polymer network is increased.[303]

Figure 54 shows the tanδ and G' curves of the DMTA measurements for formulations containing the three varying monomers and formulations containing the CTA **CEOH** additionally. The exact values can be found in the experimental part (Table 15).

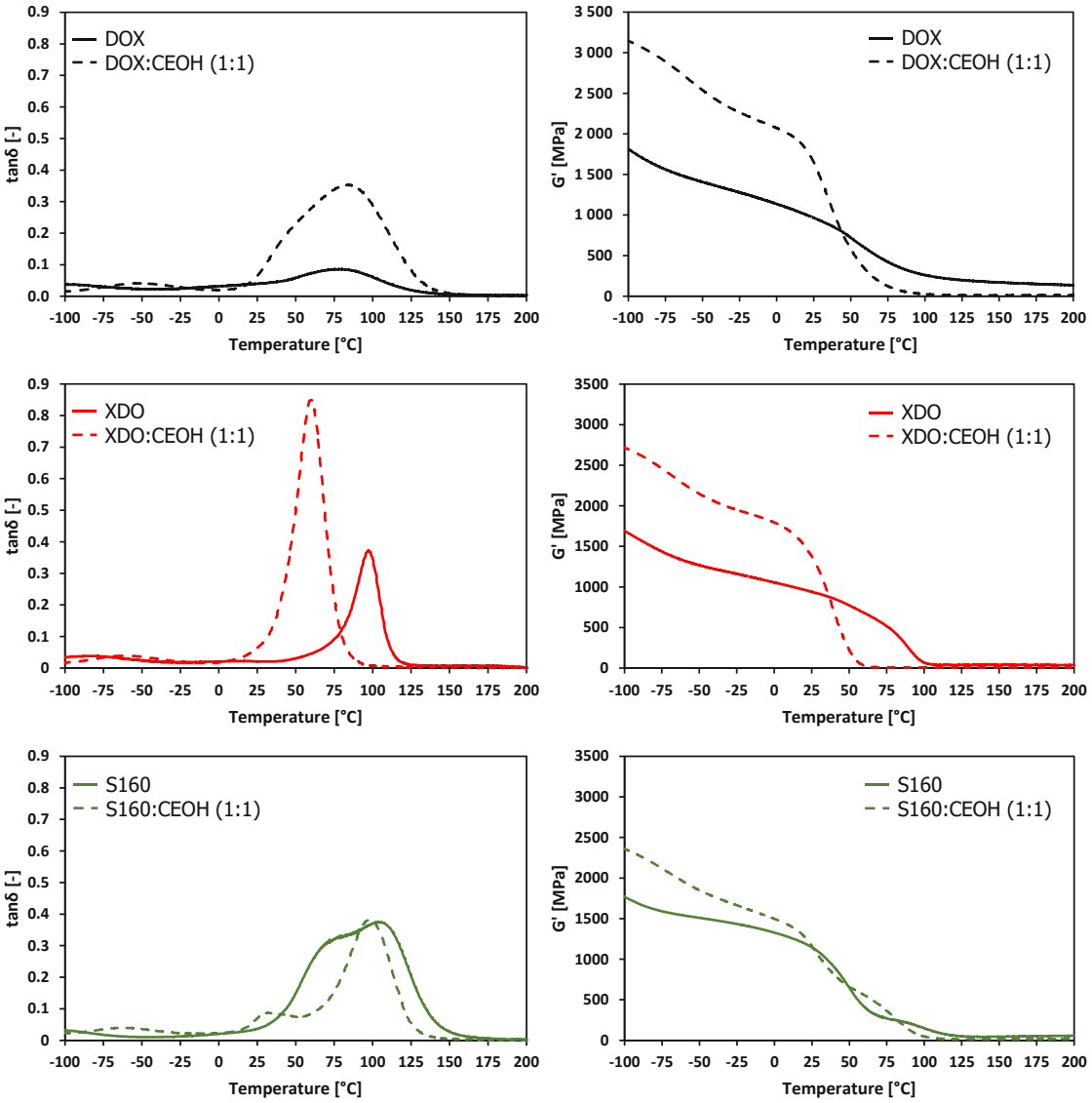

Figure 54: Curves of the loss factor (tanδ) and storage modulus (G') of DMTA measurements of formulations containing the monomers **DOX** (solid black), **XDO** (solid red) and **S160** (solid green) and 1wt% S-Sb. Formulations that contain additional **CEOH** as CTA are shown in dashed lines; the color is according to their monomers.

Considering formulations containing **DOX** as a monomer show that formulations without CTA have a glass transition temperature T_g of 77 °C, but the temperature range is very broad. This corresponds to an inhomogeneous network. Furthermore, the storage modulus G' decreases slightly over the measured temperature range. After adding the CTA, the T_g increased to 82 °C, which was unexpected. However, the temperature range of the glass transition is again broad. The curve of G' shows a significantly steeper decrease, meaning the network became more homogenous.

Formulations containing only **XDO** and the ones containing additional **CEOH** show narrow glass transition temperatures. Here, T_g dropped from 97 °C to 61 °C. However, the curve of G' is significantly steeper for formulations containing **CEOH**.

If formulations containing **S160** as a monomer are now considered, an additional shoulder (71 °C) occurs during the glass transition (max. of tanδ 104 °C). After adding **CEOH**, the peak became narrower and T_g dropped to 97 °C. However, a second peak at 30 °C is now clearly visible. This indicates a non-homogeneous polymer network, which is also shown by the curves of the storage modulus.

However, all specimens showed glass transition temperatures above 37 °C, which is essential for applications in the human body.

6.4. Investigation of mechanical properties *via* tensile tests

Besides DMTA measurements, tensile tests should be performed. The addition of CTAs is expected to result in slightly softer but tougher materials. Such materials are received if the networks are more regulated and widened.[146] These experiments were performed on a universal testing machine with a 1 kN load sensor and a traverse speed of 5 mm·min^{-1} at room temperature. The stress-strain curves give information about the strength and plasticity of the specimens. Five replicates were measured for reproducibility. Figure 55 shows exemplary stress-strain curves for the varying monomers and in combination with **CEOH** as CTA. The exact values can be found in the experimental section (Table 16).

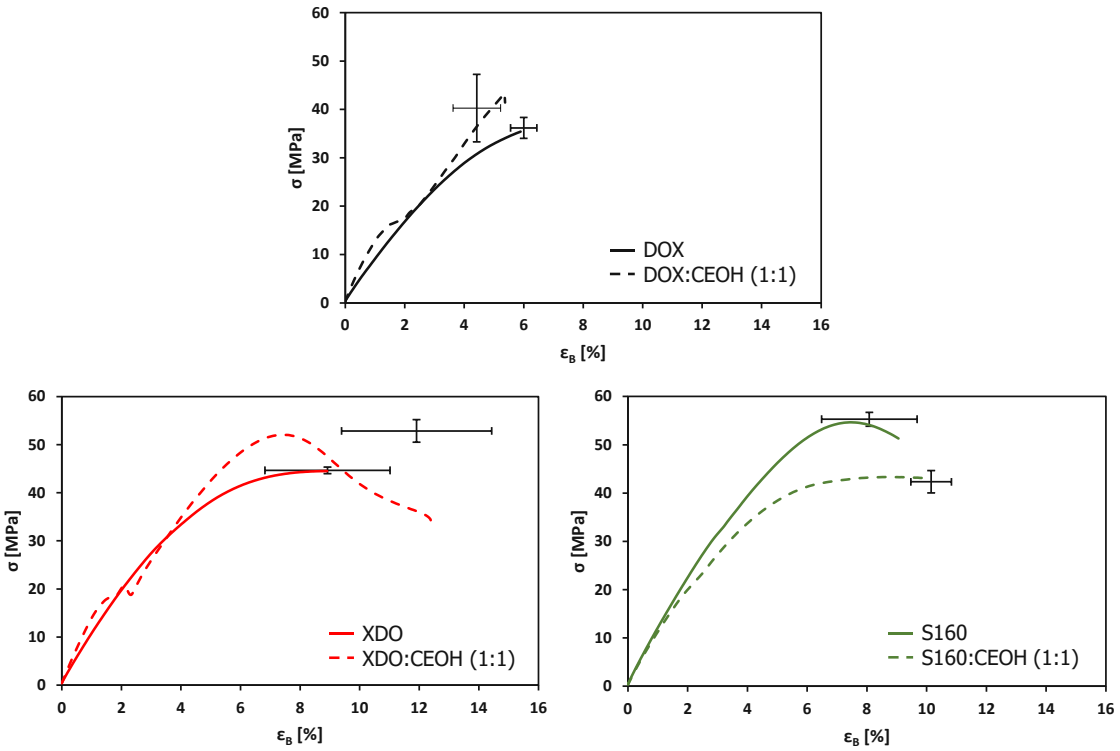

Figure 55: Stress-strain plot of formulations containing the monomers **DOX** (solid black), **XDO** (solid red) and **S160** (solid green) and 1wt% S-Sb. Formulations that contain additional **CEOH** as CTA are shown in dashed lines; the color is according to their monomers. The inserted error bars correspond to the average values of the maximum tensile strength (σ_M) and elongation at break (ε_B) with standard deviation.

Besides the elongation at break (ε_B) and tensile strength (σ), the tensile toughness (U_T) should be used primarily for comparisons within this study. U_T is defined as the amount of energy the material can absorb in the form of deformation before the initiated stress leads to a crack in the material.[258] Therefore, U_T was calculated from the area under the stress-strain curve of the tensile tests.[257]

The stress-strain curves with **DOX** as a monomer show hardly any change after adding the CTA. Here, 36-40 MPa tensile strength and 4-6% elongation at break were achieved. Comparing U_T from both specimens, it remains the same at ~1 MJ·m^{-3}. Formulations containing **XDO** show a significant increase in ε_B (from 8 to 12%) and strength (from 44 to 53 MPa). Thus, the tensile toughness increased from 2 to 4 MJ·m^{-3}. Again, formulations containing **S160** showed an increase in elongation at break (from 8 to 10%) and a loss in σ (from 55 to 42 MPa) due to the addition of **CEOH**. However, U_T was consistent with ~3 MJ·m^{-3} for these specimens.

7. Formation of interpenetrating polymer networks: screening of the radical system

The preliminary studies showed that **XDO**, especially in combination with the chain transfer agent **CEOH** led to improved (thermo)mechanical properties. For this reason, the limiting conditions of the cationic system should now be combined with the radical system to generate interpenetrating polymer networks (IPNs): 1) only **XDO** and, therefore, homopolymerization of the oxetane and 2) **XDO** containing additionally **CEOH** (equimolar ratio, referred to their functionality) and therefore, an adduct formation of oxetane and alcohol.

The combination of cationic and radical networks should yield tough materials.

7.1. Formulation preparation of IPNs

Two reference formulations were prepared; one with only **XDO** (**Ref. XDO**) and one with **XDO** and **CEOH** in equimolar ratio, referred to the functionalities (**Ref. XDO:CEOH**). As a cationic photoinitiator 1wt% S-Sb was added.

The previous Chapter A showed that higher MWs (45kDa compared to 10kDa) showed better (thermo)mechanical properties. However, the functionality (norbornene (NB), vinyl carbonate (VC) and allyl carbonate (AC)) of the modified PCL showed no significant influence on the system. For this reason, the AC-modified PCL with a molecular weight of 45kDa (**AC45kPCL**) was chosen as the radical monomer. Here, only a one-step synthesis is necessary, compared to the NB-functionalized PCL, and it is less expensive than the synthesis of the VC-modified PCL. In addition, the PCL-based monomer should be combined with a thiol. Therefore, the trifunctional thiol 1,3,5-tris(3-mercaptopropyl)-1,3,5-triazine-2,4,6-trione (**Thiol 2**) should be used. Again, formulations from the previous chapter showed better performance compared to **Thiol 1**. The thiol is used in an equimolar ratio to the monomer, referred to the functionalities. As a radical photoinitiator 1 wt% TPO-L was used.

The monomers and chain transfer agents of both systems are depicted in Figure 56. The radical system was added 5-25wt% to the cationic system. Both photoinitiators are always referred to the entire formulation (cationic and radical system), as they would otherwise be too diluted.

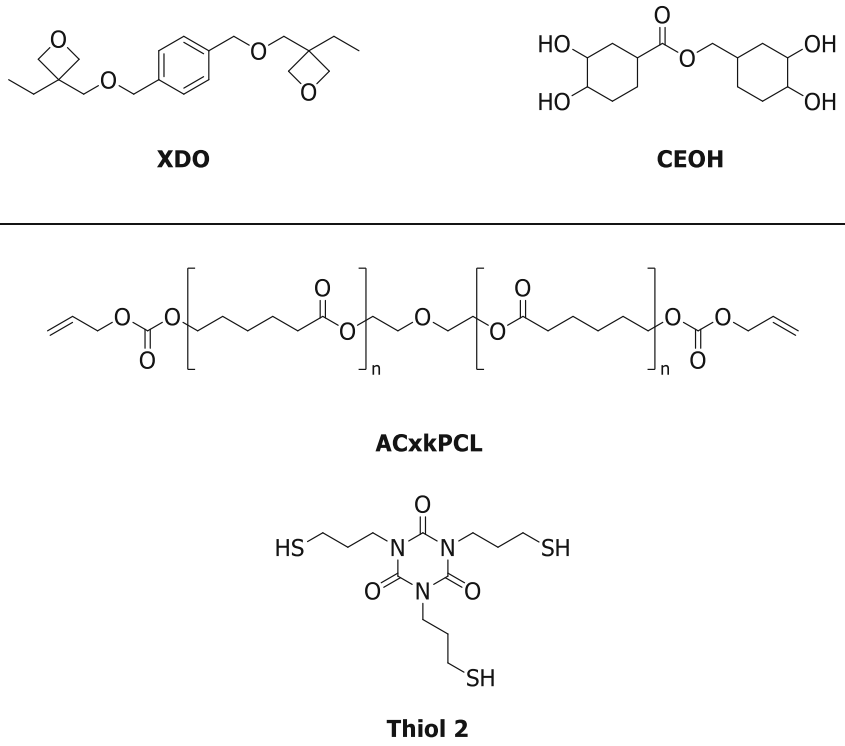

Figure 56: Chemical structures of the cationic system **XDO** and **CEOH** (top) and the radical system **AC45kPCL** and **Thiol 2** (bottom).

The formulations were heated up to 120 °C to ensure the melting of the CTAs and the PCL-based monomer and mixed until complete homogeneity was assured.

7.2. Sample preparation of IPNs for (thermo)mechanical testing

The freshly prepared formulations were kept at 120 °C for a maximum of 20 min to avoid unintended recrystallization and to decrease the viscosity for easier handling. A preliminary NMR study using **BOX** and **Hex** showed that the formulation could be stored stably at 120 °C for at least one hour. However, the formulation is not stable for 24h at this elevated temperature. The formulations were transferred with a hot glass pipette into pre-heated silicon molds (120 °C) for DMTA- and tensile specimens.

Possible bubbles were removed, and the specimens were cured in the hot mold at 120 °C. First, they were irradiated with λ = 405 nm and an intensity of 36 mW·cm^{-2}, followed by irradiation with λ = 365 nm and an intensity of 630 mW·cm^{-2}. The exposure time was 5 minutes for each wavelength. Then, the mold was cooled down, and the specimens were turned and returned to the hot mold. Afterwards, the specimens were irradiated again with both wavelengths. Before the measurements, the samples were ground and polished

with sandpaper in multiple steps to ensure uniform geometries and to remove artifacts from the surface.

7.3. Investigation of thermomechanical properties of IPNs *via* DMTA

In this chapter, the thermomechanical properties of the IPNs should be determined and compared to the reference systems. Again, the glass transition temperature (T_g) and the storage modulus are essential parameters, especially at the body temperature ($G'_{37°C}$).

Figure 57 shows exemplary DMTA curves for the two reference systems (**XDO** and **XDO:CEOH**) and specimens containing additional 25 wt% of **AC45kPCL**. Figure 58 shows only the trend of the glass transition temperature and storage modulus at body temperature for greater clarity. The exact values can be found in the experimental section (Table 17).

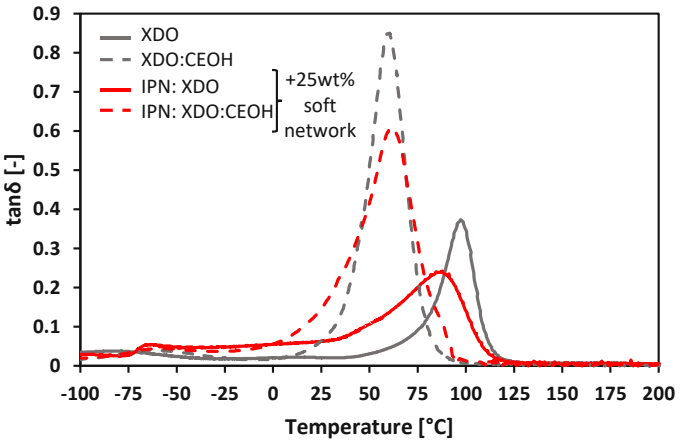

Figure 57: Exemplaric DMTA curves for the two reference systems (**XDO** and **XDO:CEOH**) and specimens containing additional 25 wt% of **AC45kPCL** (IPN).

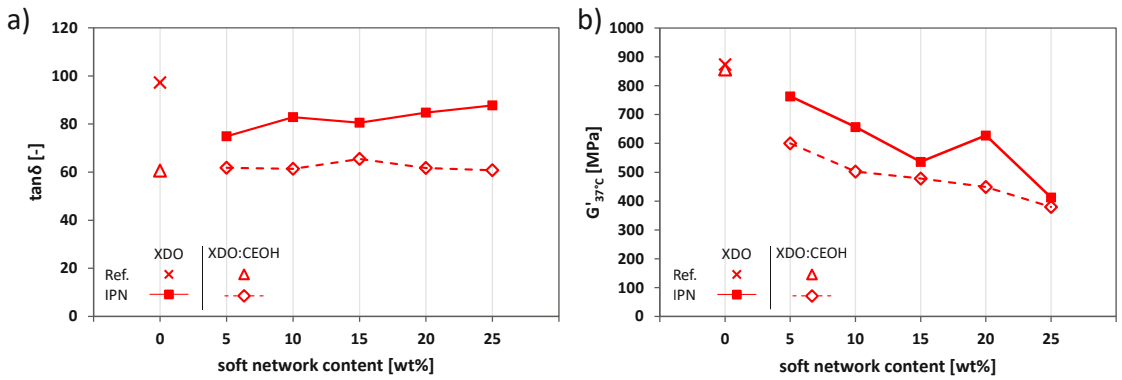

Figure 58: Results of DMTA measurements of formulations containing only **XDO** (**Ref. XDO**): cross; and containing additional 5-25 wt% **AC45kPCL** as a radical system (squares ≡ IPN) or **XDO** with **CEOH** as chain transfer agent (**Ref. XDO:CEOH**): triangle; and containing additional 5-25 wt% **AC45kPCL** as a radical system (diamonds ≡ IPN). Full symbols with solid lines indicate the cationic system (**XDO**) and empty symbols with dashed lines indicate the cationic system (**XDO:CEOH**). The straight lines are only for better visibility. a) Obtained values for the glass transition temperature (T_g); b) obtained values for the storage modulus at body temperature ($G'_{37\,°C}$).

The reference with only **XDO** (**Ref. XDO**) and without the radical system showed a glass transition temperature (T_g) of 97 °C. After adding the radical system and therefore, forming an IPN led to a drop of the T_g to 75 °C. However, with an increasing amount of the radical system, the glass transition temperature increased to 89 °C. All specimens containing **CEOH** showed hardly any influence on the T_g. The reference (**Ref. XDO:CEOH**) showed a T_g of 61 °C. After adding the radical system, the temperature range between 61 and 65 °C. However, the threshold of $T_g \geq 37$ °C, necessary for bone graft substitutes, was significantly exceeded.

Considering the storage moduli at body temperature $G'_{37\,°C,}$ a decreasing trend with an increasing amount of toughness enhancers can be observed for all specimens. **Ref. XDO** and **Ref. XDO:CEOH** showed both a modulus of ~870 MPa. After forming an IPN, the storage modulus decreased significantly. However, specimens containing only the oxetane monomer showed slightly higher values (760-412 MPa) than those containing the CTA (600-380 MPa). All exact values are listed in the experimental section in Table 17.

Nevertheless, DMTA measurements confirmed that the formation of IPNs led to a favorable combination of lowered network density and rising or at least steady T_g.

7.4. Investigation of mechanical properties of IPNs *via* tensile tests

Besides the thermomechanical properties, the tensile strength (σ) and elongation at break (ε_B) should be determined. The addition of the soft radical network is expected to reduce the tensile strength but increase the elongation at break, which should result in tougher materials. The toughness of the materials will be determined by the tensile toughness (U_T), which is calculated by the area under the stress-strain curve.

Figure 59 shows exemplary stress-strain curves for the two reference systems (**XDO** and **XDO:CEOH**) and specimens containing additional 25 wt% of **AC45kPCL**.The selected curves correspond most closely to the average values. The inserted error bars correspond to the average values of the maximum tensile strength (σ_M) and elongation at break (ε_B) with standard deviation. Figure 60 shows only the trend (average values) of the tensile strength and elongation at break for greater clarity. The exact values and the standard deviation can be found in the experimental section (Table 18).

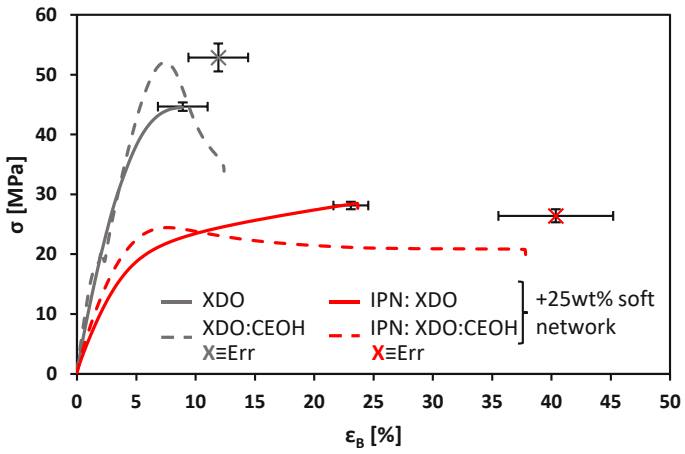

Figure 59: Exemplary stress-strain curves for the two reference systems (**XDO** and **XDO:CEOH**) and specimens containing additional 25 wt% of **AC45kPCL** (IPN). The inserted error bars correspond to the average values of the maximum tensile strength (σ_M) and elongation at break (ε_B) with standard deviation.

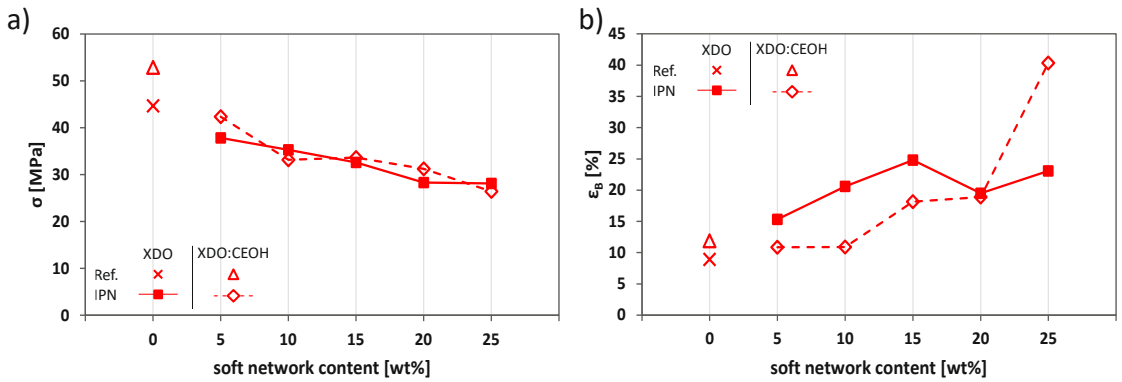

Figure 60: Results of tensile tests of formulations containing only **XDO** (**Ref. XDO**): cross; and containing additional 5-25 wt% **AC45kPCL** as a radical system (squares ≡ IPN) or **XDO** with **CEOH** as chain transfer agent (**Ref. XDO:CEOH**): triangle; and containing additional 5-25 wt% **AC45kPCL** as a radical system (diamonds ≡ IPN). Full symbols with solid lines indicate the cationic system (**XDO**) and empty symbols with dashed lines indicate the cationic system (**XDO:CEOH**). The straight lines are only for better visibility. a) Obtained values for the tensile strength σ; b) obtained values for the elongation at break ε_B.

The reference **Ref. XDO** showed a tensile strength of 45 MPa and after adding the radical system, the values dropped with an increasing amount (38-28 MPa). As expected, the elongation at break increased due to the formation of an IPN. Here, the values range from 9% (for reference) up to 25%. The maximum of ε_B was reached for the IPN with 15wt% of the soft network. The reference containing the chain transfer agent **CEOH** (**Ref. XDO:CEOH**) showed a slightly higher value with 53 MPa than the other reference. However, after adding the radical system, a decrease is noticeable again with an increasing amount. A slight but steady increase of ε_B was observed due to adding the radical system (up to 20wt%) to the cationic system **XDO:CEOH**, ranging from 12-19%. However, adding 25wt% of the soft network led to a fourfold value of the elongation at break (40%) compared to the reference.

For better comparison, the tensile toughness U_T was also determined.

Formulations containing **XDO** and the soft network showed that the addition increased the tensile toughness U_T (ranging from 4.8 $MJ \cdot m^{-3}$ to 6.5 $MJ \cdot m^{-3}$) compared to the reference (2.8 $MJ \cdot m^{-3}$). The highest value was observed for the specimen with 15wt% soft network content. U_T for **Ref. XDO:CEOH** was calculated with 3.9 $MJ \cdot m^{-3}$ and after addition of the soft network, the values ranged between 2.7 $MJ \cdot m^{-3}$ and 8.9 $MJ \cdot m^{-3}$. The formulation with 25wt% of the soft network is noteworthy because this specimen showed the highest tensile toughness overall. Here, U_T was more than doubled compared to the

reference. The exact values for all formulations can be found in the experimental section (Table 18).

8. Conclusion

This chapter investigated the formation of IPNs and these should be made from an oxetane and a thiol-ene network.

Therefore, photo-DSC experiments were determined to investigate the influence of thiols on the cationic system. This study showed that the low concentration of thiols did not inhibit the cationic photopolymerization. Further, preliminary DMTA measurements of the first IPNs showed that these materials have high T_gs but are non-regulated.

A future application of the created IPNs is the use as bone replacement implants. Hence, crosslinked polymer networks must be formed, which are also degradable over a suitable time frame. For this reason, the synthesis of multifunctional and degradable oxetane monomers was attempted. Unfortunately, no monomers could be achieved.

Hence, this strategy was allocated to chain transfer agents (CTAs). Further, chain transfer agents should also lead to more homogenous polymer networks. ^{1}H-NMR studies showed that alcohols as CTA react with oxetanes in an adduct formation. Therefore, the synthesis of multifunctional and degradable CTA was planned. The synthesis of degradable CTAs; one trifunctional (**THEB**) and one tetrafunctional (**CEOH**), was successful. DMTA and tensile test measurements investigated their influence on three commercially available oxetane monomers. These experiments showed that using CTAs requires high curing temperatures of ≥120°C (limit of hot lithography).

The most promising monomer (**XDO**) was then combined with **AC45kPCL** and **Thiol 2** (radical system) to create IPNs. The (thermo)mechanical properties of the IPNs were investigated by DMTA measurements and tensile tests. Here, glass transition temperatures of ≥61 °C were achieved, which is a crucial parameter for application in the human body. Further, the tensile toughness U_T was calculated. Here, values ranging between 2.7 and 8.9 MJ·m^{-3} were reached, which indicates promising materials.

SUMMARY

People have an increasingly higher life expectancy due to better medical care. However, this also increases age-related diseases, such as infections and tumors, which often relate to the joints and bones. However, trauma and fractures due to accidents can also lead to health problems. Due to these reasons, bone regeneration can be disturbed or even wholly prevented, especially if the damaged tissue exceeds a critical size. For this reason, tissue engineering (TE) is concerned with, for example, the development of new materials suitable for artificial bone scaffolds. These three-dimensional scaffolds should serve as supporting structures and thus assist the healing process and the treatment of these diseases. These materials must have essential properties such as biomimetics, patient specificity, biocompatibility, degradability, and suitable mechanical properties.

These scaffolds can be fabricated by lithography-based additive manufacturing technologies (L-AMT). It has been shown that the resulting structural size and surface topology positively affect the bone regeneration process. However, (meth)acrylate photopolymers are often used in the industry for L-AMT resins. These have the disadvantages of being cytotoxic, exhibiting undesirable degradation behavior, and can lead to inflammation in the tissue. In recent years, new monomer systems, including those in our research group, have been developed, which exhibit significantly lower cytotoxicity than (meth)acrylates. These monomer systems include vinyl esters, vinyl carbamates, and vinyl carbonates. However, such resins show high shrinkage during polymerization, and the final resins are usually brittle and exhibit low strength, making them unsuitable as bone graft substitutes.

The aim of this work was to improve the (thermo)mechanical properties of materials that will be used for bone replacement. Two strategies were pursued for this purpose:

I.) **Addition of high molecular weight photopolymerizable additives** to an established vinyl ester-thiol system

II.) **Formation of interpenetrating polymer networks (IPNs)**

In the **first chapter**, PCL-based toughness enhancers were added to an established vinyl ester-thiol system. Vinyl carbonate (VC)-modified PCLs have already been investigated in a previous study by our research group. However, synthesizing VC-functionalized PCLs entails high costs and, thus, is inconvenient. Therefore, photopolymerizable groups like allyl carbonates (AC) and norbornenes (NB) as alternative

functionalities were investigated and compared to VCs. Allyl carbonates (ACs) were of interest because they exhibit no homopolymerization (in contrast to VCs) and are inexpensive in their synthesis. The norbornene functionality (NB) should be preferred during the copolymerization of thiols with vinyl esters, which may lead to domain-formation and therefore, enhanced (thermo)mechanical properties were hypothesized.[157] The effect of varying end groups on parameters like the reactivity, double bond conversion, gel point and modulus, tensile strength, elongation at break and glass transition temperature were investigated. A good comparison between the materials can be made with the tensile toughness, which can be calculated from the stress-strain curves. PCL and its influence were studied in two molecular weights (10kDa and 45kDa). Moreover, the influence of two different thiols, the commercially available **Thiol 1** and the synthesized rigid **Thiol 2**, was examined.

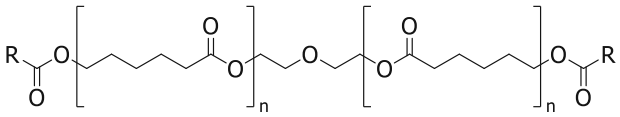

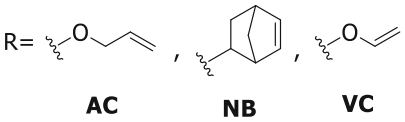

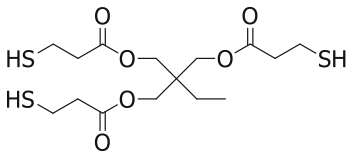

Thiol 1

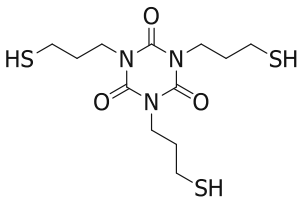

Thiol 2

However, no significant difference could be detected between the photopolymerizable groups, neither photochemically nor in the (thermo)mechanical properties.

In general, the addition of toughness enhancers reduced the t_{gel} of photopolymerizable precursor formulations and increased the final double bond conversion. These are essential parameters for the printability of the materials. All specimens showed glass transition temperatures well above body temperature, which is crucial for the applicability as bone replacement material. Considering the tensile toughness of the materials, this could be tripled compared to references without additives.

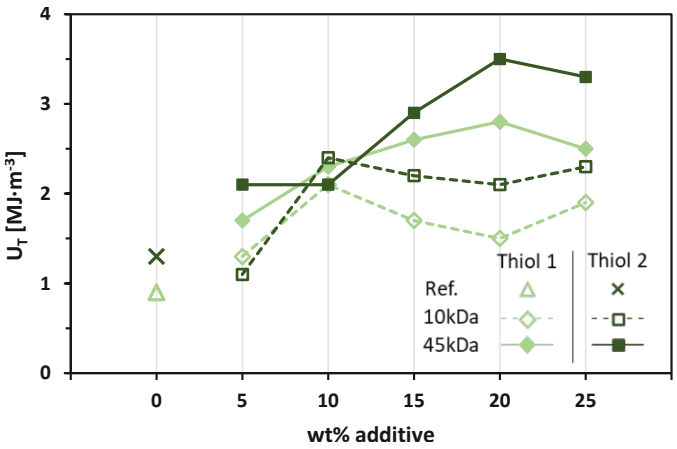

The system with the highest addition of toughness enhancer and the rigid **Thiol 2** was printed as a proof-of-concept. No cracks or delaminatons were detected in the final construct and it was shown that shrinkage during polymerization is very low. Finally, the influence of different sterilization methods on the (thermo)mechanical properties was investigated, and a low dose of γ-radiation was found to be the most suitable.

However, the concept of incorporation of high molecular weight toughness enhancers into vinyl ester-based thiol-ene formulations showed an enhancement of the material's toughness but is limited.

The **second chapter** will prepare so-called interpenetrating polymer networks (IPNs). IPNs consist of at least two networks that are intertwined but not covalently bonded to each other. This means that they can only be separated if chemical bonds are broken. In this work, sequential IPNs will be prepared. This means that both systems for the two networks are present but only cured sequentially.

The flexible network should consist of high molecular weight polymers in combination with thiols. For this reason, a PCL-based polymer was again chosen. The other network should be the hard matrix. For this purpose, small oxetane monomers were chosen to be polymerized *via* the cationic mechanism.

Since the addition of thiols could inhibit the cationic polymerization, the influence of these was studied by measuring the photoreactivity. Here it was proven that thiols in low concentrations, which are required for high molecular weight molecules, do not inhibit the cationic polymerization.

However, the first thermomechanical measurements showed that the formed IPNs consist of very inhomogeneous networks. For this reason, alcohols should be used as chain transfer agents. Furthermore, the cationic system formed in the first experiments was not degradable, so the synthesis of new degradable multifunctional monomers was planned. However, it was found that esters as degradable groups are difficult to insert into an oxetane monomer. For this reason, the concept was transferred to CTAs. Two CTAs (**THEB** and **CEOH**) were successfully synthesized.

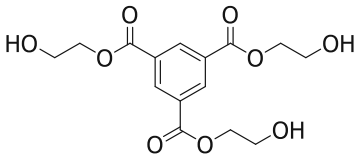

THEB

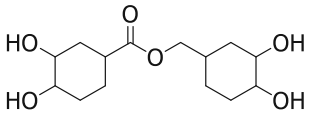

CEOH

^{1}H NMR spectroscopy experiments showed that alcohols undergo adduct reactions with oxetanes and oxetanes hardly homopolymerize. For this reason, it was hypothesized that the polymerization of difunctional monomers with multifunctional alcohols should result in a homogeneous polymer network.

This hypothesis was proven with DMTA measurements. Three commercially available monomers were tested (**DOX**, **XDO**, **S160**).

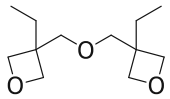

DOX

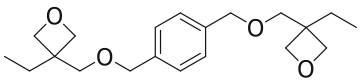

XDO

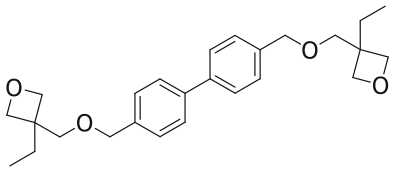

S160

However, DMTA measurements could only be performed with **CEOH** as CTA and only at high temperatures (>120 °C) since **THEB** was not dissolved in the monomers. Tensile tests were also performed. The best monomer was selected based on high glass transition temperature, homogeneous network, and high tensile toughness. **XDO** was found to be the best monomer and was therefore used for the formation of IPNs.

For the preparation of IPNs, the radical system (**AC45kPCL** with **Thiol 2**) was added in increasing weight percent to the cationic system.

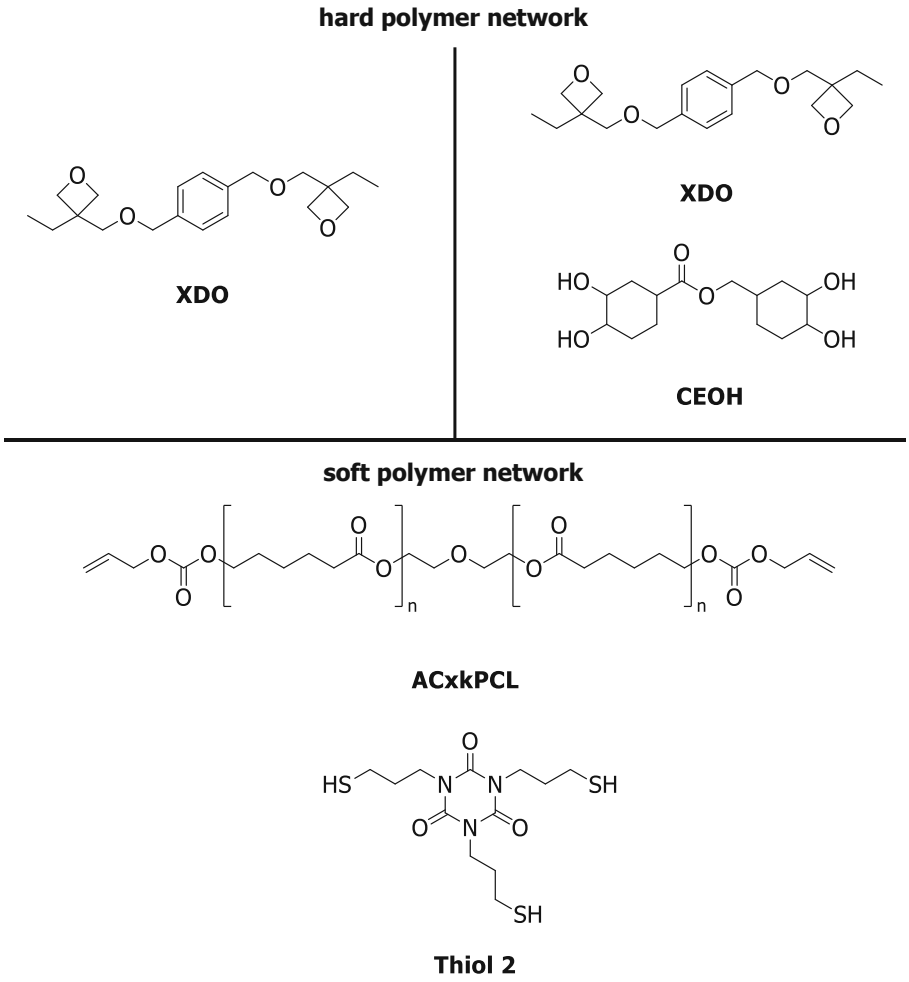

Again, all materials were tested for their (thermo)mechanical properties. Each material exhibited a glass transition temperature far above body temperature and the tensile toughness could be tripled for the system **XDO:CEOH** with 25 wt% of the soft network.

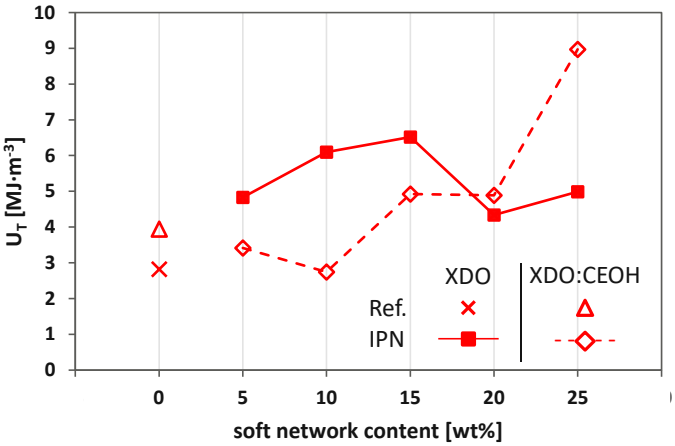

Comparing the tensile toughness of the vinyl ester-based thiol-ene systems with the IPNs, it can be shown that significantly higher values were achieved by producing IPNs. However, the toughness of both concepts is in the same order of magnitude of cortical

bone with 2-12 MJ·m^{-3}.[3] Therefore, both concepts are suitable for bone replacement materials.

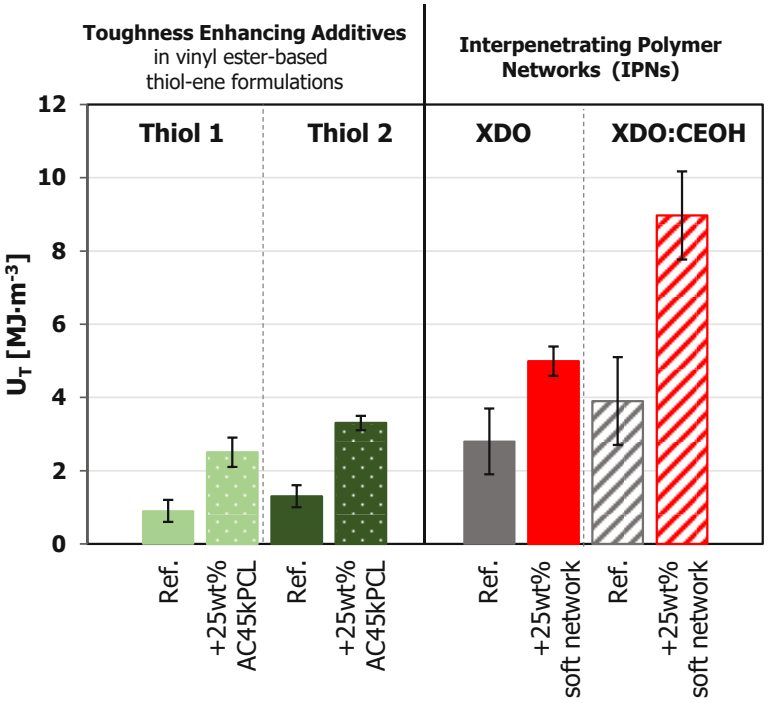

EXPERIMENTAL PART

A. Toughness enhancers for 3D-printed photopolymers

2. Synthesis

2.1. Synthesis of PCL based toughness enhancers

2.1.1. Synthesis of allyl carbonate modified PCL (ACxkPCL):

The allyl carbonate-modified PCL (**ACxkPCL**) synthesis was performed similarly to Orman *et al.*.[35] Therefore, the commercially available hydroxyl-terminated PCL was converted with an excess of allyl chloroformate to obtain the product.

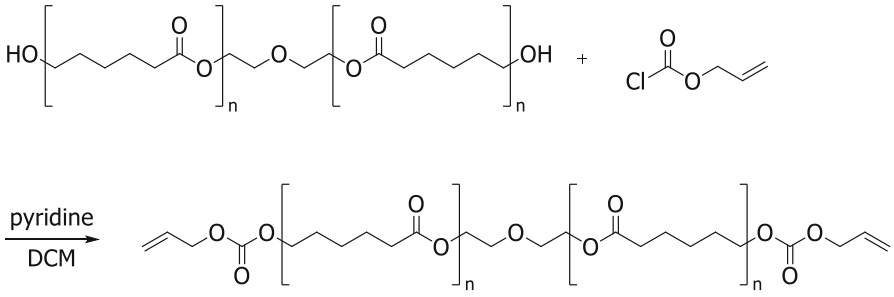

ACxkPCL

Compound	eq.	n [mmol]	m [g]	V [mL]
PCL diol (10kDa|45kDa)	1	5|1	50|50	-
dry Pyridine	4|12	20|13	-	1.6|1.1
Allyl chloroformate	4|12	20|13	-	1.8|1.5
dry DCM				200|400

The hydroxyl-terminated PCL diol and dry pyridine were dissolved in 200 | 400 mL of dry dichloromethane under an argon atmosphere and cooled to -5 °C. Allyl chloroformate was added dropwise to the stirred solution within 10 min. The reaction was kept at 0 °C for 30 min and stirred for another 24 h at room temperature. The reaction mixture was quenched with 5 mL deionized water and extracted with 3 x 500 mL 1N HCl, then two times with 500 mL sat. $NaHCO_3$ solution and last with 500 mL water once. Afterwards, the crude product was purified by doubled reprecipitation in cold MeOH (1200 mL). The purified product was filtered and dried

at 40 °C in vacuum. The products could be obtained quantitatively as a white powder. The product **AC10kPCL** showed a conversion of 96% and **AC45kPCL** of 92%.

^{1}H NMR (600 MHz, $CDCl_3$, δ): 5.92 (ddt, J = 17.3, 10.4, 5.8 Hz, 2H, -C<u>H</u>=CH_2), 5.35 (dt, J = 17.2, 1.5 Hz, 4H, -CH=C<u>H</u>$_2$), 4.60 (dt, J = 5.8, 1.4 Hz, 4H, -C<u>H</u>$_2$-CH=CH_2), 4.17 (t, J = 6.7 Hz, 4H, -O-C<u>H</u>$_2$-CH_2-O-), 4.05 (t, J = 6.7 Hz, ~300 or 1800H, -CO-O-C<u>H</u>$_2$-CH_2-CH_2-CH_2-CH_2-CO-O-), 3.62 (m, 4H, -O-CH_2-C<u>H</u>$_2$-O-), 2.28 (t, J = 7.5 Hz, ~300 or 1800H, -CO-O-CH_2-CH_2-CH_2-CH_2-C<u>H</u>$_2$-CO-O-), 1.63 (ddt, J = 13.8, 11.6, 7.2 Hz, ~600 or 3600H, -CO-O-CH_2-C<u>H</u>$_2$-CH_2-C<u>H</u>$_2$-CH_2-CO-O-), 1.41 – 1.33 (m, ~300 or 1800H, -CO-O-CH_2-CH_2-C<u>H</u>$_2$-CH_2-CH_2-CO-O-) ppm; GPC (THF): $\overline{M_w}$ = 14 or 44 kDa. DS calculated from ^{31}P(IG)-NMR = 96% or 92%.

2.1.2. Hydroxyl value via 31P-NMR spectroscopy of (un)functionalized PCLs

The OH number of the unfunctionalized PCL diols and the products were calculated to determine the conversion of the functionalized PCL diols. The samples were measured by quantitative ^{31}P-NMR spectroscopy.[247] Cyclohexanol was used as an internal standard (IS) and chromium(III)acetylacetonate ($Cr(acac)_3$) as a relaxation reagent. As the phosphorous agent 2-chloro-4,4,5,5-tetramethyl-1,3,2-dioxaphospholane (TMDP) is moisture sensitive, the used solvents must be anhydrous. Two solutions were prepared, mixed and measured immediately afterwards. Therefore, approx. 30 mg of the sample was dissolved in 200 µL $CDCl_3$ and 100 µL pyridine. 100 µL of a prepared IS/$Cr(acac)_3$ mixture in pyridine (c_{IS} = ~40 mg/mL, $c_{Cr(acac)3}$ = ~5 mg/mL) was added and the compounds were mixed with a Vortex until a complete homogenization. The second solution is a mixture of 300 µL $CDCl_3$ and 100 µL of the phosphorous agent TMDP. The latter solution was added to the first prepared solution, containing the sample and after a short mixing time, the ^{31}P-NMR was measured. The spectra were recorded using a 600 MHz spectrometer. Samples with a molecular weight of 10 kDa were recorded with 128 scans, whereas samples with 45 kDa were with 256 scans.

2.2. Selection and synthesis of thiols as CTA

2.2.1. Synthesis of 1,3,5-tris(3-mercaptopropyl)-1,3,5-triazine-2,4,6-trione (Thiol 2):

*2.2.1.1. Synthesis of tris[3-(acetylthio)propyl]isocyanurate (**TAMPTT**):*

1,3,5-Tris(3-mercaptopropyl)-1,3,5-triazine-2,4,6-trione (**Thiol 2**) was synthesized in a two-step synthesis in accordance with Reinet *et al.*.[248, 249]

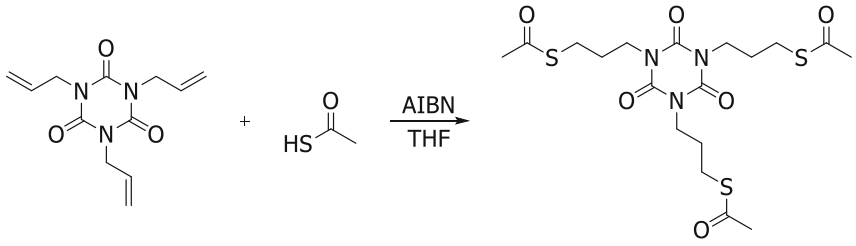

TAMPTT

Compound	eq.	n [mmol]	m [g]	V [mL]
1,3,5-Triallyl-1,3,5-triazine-2,4,6-trione	1	321	80	-
Thioacetic acid	3.6	1155	87.9	-
AIBN	0.15	48	7.9	
dry THF				500

First, the tris[3-(acetylthio)propyl]isocyanurate (**TAMPTT**) was synthesized, starting with 1,3,5-triallyl-1,3,5-triazine-2,4,6-trione, thioacetic acid and AIBN were added to a 1000 mL three-neck round-bottom flask and suspended in 500 mL dry THF. The reaction mixture was purged with argon for 30 min at room temperature and then heated to reflux. After 24 h, the reaction mixture was cooled with an ice bath and 200 mL 1N Na_2CO_3 solution was added. The mixture was extracted three times with DCM (600/200/200 mL) and the combined organic phase was washed with 160 mL aqueous 1N NaOH and 160 mL brine. Then, the organic phase was dried over Na_2SO_4, filtered and the solvent was removed under a high vacuum to obtain the crude product as a dark yellow solid. The crude product was recrystallized from ~200 mL MeOH three times to obtain **TAMPTT** with 110 g (72% calculated yield) as a white solid for purification.

m.p.: 65-68 °C (Lit.: 64-66 °C)[32],

^{1}H-NMR (400 MHz, $CDCl_3$, δ): 3.89 (t, J = 7.1 Hz, 6H, -N-CH_2-), 2.83 (t, J = 7.1 Hz, 6H, -CH_2S-), 2.26 (s, 9H, -CH_3), 1.87 (quin., J = 7.1 Hz, 6H, -CH_2-) ppm. ^{13}C-NMR (100 MHz, $CDCl_3$, δ): 195.45 (-S(C=O)CH_3), 149.03 (-C=O), 42.07 (-N-CH_2-), 30.68 (-CH_3), 28.03 (-CH_2-), 26.27 (-CH_2-S-) ppm.

*2.2.1.2. Synthesis of 1,3,5-tris(3-mercaptopropyl)-1,3,5-triazine-2,4,6-trione (**Thiol 2**):*

In the second step, **TAMPTT** was hydrolyzed to **Thiol 2**.

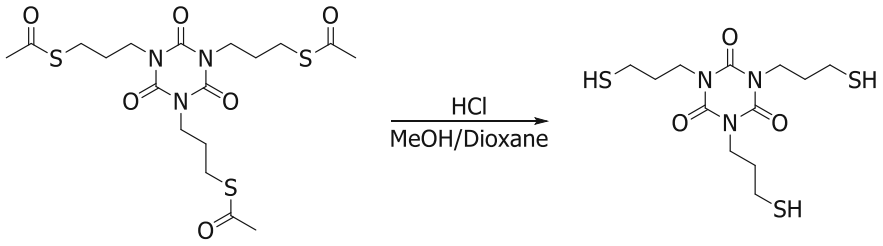

TAMPTT **Thiol 2**

Compound	eq.	n [mmol]	m [g]	V [mL]
TAMPTT	1	230	110	-
conc. HCl	3.2	735	-	86
MeOH	-	-	-	460
Dioxane	-	-	-	150

Therefore, **TAMPTT** was dissolved in a mixture of 460 mL MeOH and 150 mL dioxane and conc. HCl was added. The solution was purged with argon for 30 min. and heated to reflux for 24 h. 200 mL deion. water was added after cooling to ambient temperature and the reaction mixture was extracted four times (400/400/200/200 mL) with DCM, two times with 200 mL sat. $NaHCO_3$ solution and once with brine. Then, the organic phases were dried over Na_2SO_4, filtered and the solvent was removed under reduced pressure. The product was dried under high vacuum, isolated as colorless oil in 75.3 g (93% calculated yield), and used without further purification. n_D^{20}= 1.5678, ^{1}H-NMR (400 MHz, $CDCl_3$, δ): 4.01 (t, J = 7.0 Hz, 6H, -N-CH_2-), 2.56 (dt, J = 6.9 Hz, 8.0 Hz, 6H, -CH_2S-), 1.97 (quin., J = 7.0 Hz, 6H, -CH_2-), 1.54 (t, J = 8.0 Hz, 3H, -CH_2-SH) ppm. ^{13}C-NMR (100 MHz, $CDCl_3$, δ): 149.10 (-C=O), 41.91 (-N-CH_2-), 31.94 (-CH_2-), 22.03 (-CH_2-SH) ppm.

3. Characterization of PCL based toughness enhancers

3.1. Investigation of the chemical properties

3.1.1. Formulation preparation of functionalized PCLs

The impact of functionalized PCLs on mechanical properties should be thoroughly investigated. Two reference formulations (**Ref. Thiol 1** and **Ref. Thiol 2**) were prepared; one with the commercially available **Thiol 1** and one with the synthesized rigid **Thiol 2**. Therefore, divinyl adipate (DVA), 15db% of thiol (**Thiol 1** or **Thiol 2**) referenced to the sum of double bonds (here only DVA), 0.5wt% Ivocerin® as photoinitiator and 0.02wt% pyrogallol as inhibitor were mixed.

Then, 5-25wt% toughness enhancers (**ACxkPCL**) were added to the reference system. However, the thiol amount was adjusted (sum of DB from DVA and toughness enhancers). The formulations were heated up to ensure the melting of the PCL component and mixed with a vortex-speed mixer for about one minute until complete homogeneity was assured.

3.1.2. RT-FT-NIR-photorheology

RT-FT-NIR-Photorheology measurements were conducted on an *Anton Paar MCR 302 WESP*. As a measuring system, a PP25 plate-plate arrangement and a P-PTD 200/GL Peltier glass plate were used. Polyethylene tape (TESA 4668 MDPE) was used to cover the glass plate for wasy removal of the photopolymerized samples. The formulation was applied to the glass disk in 75 µL and the gap between the measuring system and the plate was set to 50 µm. A light-emitting diode light source (LED, λ = 460 nm, light intensity of 15 mW·cm^{-2} at the surface of the PE tape) was used for UV curing. The light intensity was measured by an *Ocean Optics* USB 2000+ spectrometer. An oscillatory sheer with an angular strain of 1% and a frequency of 1 Hz was applied to the sample. The formulation was cured for 300 s after an equilibration period of 60 s. For the guidance of the IR beam through the sample during the rheology measurements, an FTIR spectrometer (*Bruker Vertex 80*) with external mirrors was coupled with the rheometer and the reflected beam was detected by a mercury cadmium telluride (MCT)-detector. More details about the setup and the measurements can be found in the literature.[33] The measurements were performed in triplicates at room temperature (25 °C) with satisfactory reproducibility. The double bond conversions (DBC) can be calculated over time because of simultaneously measured NIR spectra. Hence, the reduction of the integrated peak area of the double bonds of vinyl esters at about 6194 cm^{-1} wavenumbers was integrated.

The photorheology measurements were analyzed with Rheoplus V3.62 from Anton Paar and the IR spectra with Opus 7.0 from *Bruker*.

Table 3: Photorheological measurement results of formulations containing DVA, 15 db% thiol (**Thiol 1**), 0.5 wt% Ivocerin and 0.02 wt% PYR. **Ref. Thiol 1** (without additive); containing additional 5-25 wt% YxkPCL.

additive	additive [wt%]	t_{gel} [s]	DBC_{gel} [%]	t_{95} [s]	DBC_{final} [%]	G'_{max} [kPa]	F_{Nmax} [N]
Ref. Thiol 1	0	4.5 ± 0.5	20 ± 1	81 ± 4	82 ± 0	143 ± 1	-10.9 ± 0.1
AC10kPCL	5	4.0 ± 0.9	20 ± 1	87 ± 0	82 ± 0	128 ± 3	-11.6 ± 0.8
	10	4.1 ± 0.2	20 ± 1	85 ± 3	83 ± 0	124 ± 3	-12.7 ± 0.3
	15	3.5 ± 0.5	19 ± 2	85 ± 2	84 ± 0	121 ± 2	-11.8 ± 0.3
	20	3.0 ± 0.4	21 ± 1	81 ± 2	86 ± 0	151 ± 1	-8.9 ± 0.6
	25	2.7 ± 0.4	20 ± 1	81 ± 2	86 ± 0	150 ± 2	-8.5 ± 0.9
AC45kPCL	5	3.7 ± 0.4	20 ± 1	89 ± 3	83 ± 0	137 ± 2	-10.1 ± 0.5
	10	3.7 ± 0.2	20 ± 1	89 ± 3	84 ± 1	134 ± 3	-10.4 ± 0.1
	15	3.2 ± 0.6	19 ± 1	90 ± 3	84 ± 0	163 ± 6	-11.1 ± 0.2
	20	2.6 ± 0.3	18 ± 1	83 ± 2	85 ± 0	129 ± 3	-0.4 ± 0.3
	25	2.9 ± 0.1	19 ± 1	84 ± 4	85 ± 0	130 ± 5	-10.9 ± 0.1

Table 4: Photorheological measurement results of formulations containing DVA, 15 db% thiol (**Thiol 2**), 0.5 wt% Ivocerin and 0.02 wt% PYR. **Ref. Thiol 2** (without additive); containing additional 5-25 wt% YxkPCL.

additive	additive [wt%]	t_{gel} [s]	DBC_{gel} [%]	t_{95} [s]	DBC_{final} [%]	G'_{max} [kPa]	F_{Nmax} [N]
Ref. Thiol 2	0	9.1 ± 0.3	20 ± 0	104 ± 6	74 ± 0	148 ± 1	-11.3 ± 0.9
AC10kPCL	5	4.8 ± 0.2	20 ± 1	77 ± 1	80 ± 0	118 ± 1	-11.6 ± 0.6
	10	4.6 ± 0.2	20 ± 1	79 ± 1	81 ± 0	113 ± 4	-120 ± 0.2
	15	4.6 ± 0.2	21 ± 1	85 ± 2	82 ± 0	109 ± 4	-11.9 ± 0.5
	20	5.9 ± 0.2	21 ± 0	88 ± 4	82 ± 0	144 ± 2	-10.0 ± 0.7
	25	4.6 ± 0.2	21 ± 1	72 ± 1	86 ± 0	145 ± 0	-9.0 ± 0.7
AC45kPCL	5	5.6 ± 0.0	21 ± 0	88 ± 4	80 ± 0	132 ± 3	-10.9 ± 0.6
	10	4.8 ± 0.3	20 ± 0	84 ± 2	81 ± 0	128 ± 2	-12.2 ± 0.5
	15	4.7 ± 0.5	19 ± 1	83 ± 3	81 ± 0	121 ± 2	-11.8 ± 0.7
	20	4.5 ± 0.9	19 ± 1	92 ± 3	81 ± 0	124 ± 3	-10.9 ± 0.4
	25	4.3 ± 0.3	19 ± 0	90 ± 2	82 ± 0	120 ± 2	-10.5 ± 0.1

3.2. Investigation of (thermo)mechanical properties

3.2.1. Sample preparation of functionalized PCLs

The freshly prepared formulations were kept at an evaluated temperature for easier handling for molding. Then, all formulations were poured into silicone molds of respective sizes and shapes for thermal and mechanical experiments. For DMTA, specimens (2 x 5 x 40 mm^3) and bone-shaped specimens (according to ISO527-2:2012 geometry 5B with a height of 2 mm) were prepared for tensile testing. Photopolymerization was carried out in the PrograPrint Cure from Ivoclar® with a wavelength of 460 nm (274 mW/cm^2)[253] and an exposure time of 10 min on each side. Before the measurements, all samples were ground and polished with sandpaper to remove artifacts from the surface and ensure uniform geometries.

3.2.2. DMTA

The final thermomechanical properties of the material are affected by the change in the network architecture, which needs to be characterized by dynamic mechanical thermal analysis (DMTA). DMTA provides the impact of the high molecular weight additives on the

thermomechanical properties of the polymer network. This method was used to obtain the storage modulus (G') at different temperatures and to determine the glass transition temperatures (T_g) from the maximum of the loss factor (tanδ). The storage modulus at the rubber plateau (G'_R) correlates with the degree of network cross-linking. A high G'_R is indicative of a highly cross-linked network. DMTA experiments were performed in torsion mode from -100 °C to 200 °C with a heating rate of 2 °C·min^{-1}. The torsion strain was set to 0.1% and a frequency of 1 Hz. The experiments were done as a single measurement due to the high reproducibility.

Table 5: Results of DMTA measurements of formulations containing DVA, 15 db% thiol (**Thiol 1**), 0.5 wt% Ivocerin and 0.02 wt% PYR. **Ref. Thiol 1** (without additive); containing additional 5-25 wt% YxkPCL.

additive	additive [wt%]	T_g [°C]	$G'_{25°C}$ [MPa]	$G'_{37°C}$ [MPa]	G'_R [MPa]
Ref. Thiol 1	0	78	899	718	157
AC10kPCL	5	70	1245	1050	254
	10	65	973	812	218
	15	63	882	717	184
	20	80	651	502	142
	25	75	507	391	111
AC45kPCL	5	65	674	490	107
	10	80	679	534	127
	15	72	718	551	141
	20	67	569	427	109
	25	65	648	474	127

Table 6: Results of DMTA measurements of formulations containing DVA, 15 db% thiol (**Thiol 2**), 0.5 wt% Ivocerin and 0.02 wt% PYR. **Ref. Thiol 2** (without additive); containing additional 5-25 wt% YxkPCL.

additive	additive [wt%]	T_g [°C]	$G'_{25°C}$ [MPa]	$G'_{37°C}$ [MPa]	G'_R [MPa]
Ref. Thiol 2	0	90	1340	1170	234
AC10kPCL	5	98	1180	1040	145
	10	94	1010	888	141
	15	91	864	737	125
	20	90	817	682	151
	25	89	722	610	134
AC45kPCL	5	104	1140	975	171
	10	102	937	796	150
	15	98	862	708	148
	20	96	728	587	132
	25	81	685	538	127

3.2.3. Tensile tests

Tensile tests were done on a Zwick Z050 tensile testing machine with a 1 kN load sensor. Crosshead speed was set for 5 mm·min^{-1}, and the strain was measured using a mechanical extensometer. Analysis was done with the testXpert II testing software and to ensure reproducibility, at least five replicates were measured.

Table 7: Results of tensile test measurements of formulations containing DVA, 15 db% thiol (**Thiol 1**), 0.5 wt% Ivocerin and 0.02 wt% PYR. **Ref. Thiol 1** (without additive); containing additional 5-25 wt% YxkPCL.

additive	additive [wt%]	σ [MPa]	ε_B [%]	U_T [MJ·m^{-3}]
Ref. Thiol 1	0	34.2 ± 3.1	4.8 ± 0.8	0.9 ± 0.3
AC10kPCL	5	32.6 ± 6.3	5.9 ± 2.9	1.3 ± 1.0
	10	32.1 ± 2.8	9.6 ± 2.0	2.1 ± 0.6
	15	33.4 ± 1.2	8.0 ± 0.8	1.7 ± 0.2
	20	26.2 ± 1.9	8.4 ± 1.6	1.5 ± 0.4
	25	25.9 ± 1.0	10.9 ± 0.9	1.9 ± 0.2
AC45kPCL	5	27.7 ± 1.5	9.3 ± 1.5	1.7 ± 0.4
	10	31.6 ± 2.3	10.8 ± 1.5	2.3 ± 0.5
	15	30.0 ± 3.0	13.1 ± 2.5	2.6 ± 0.8
	20	28.4 ± 2.6	14.8 ± 2.9	2.8 ± 0.8
	25	25.5 ± 1.8	15.1 ± 1.5	2.5 ± 0.4

Table 8: Results of tensile test measurements of formulations containing DVA, 15 db% thiol (**Thiol 2**), 0.5 wt% Ivocerin and 0.02 wt% PYR. **Ref. Thiol 2** (without additive); containing additional 5-25 wt% YxkPCL.

additive	additive [wt%]	σ [MPa]	ε_B [%]	U_T [MJ·m^{-3}]
Ref. Thiol 2	0	47.0 ± 1.3	4.7 ± 0.2	1.3 ± 0.1
AC10kPCL	5	40.6 ± 2.8	4.6 ± 0.7	1.1 ± 0.3
	10	42.8 ± 1.3	8.2 ± 0.9	2.4 ± 0.4
	15	37.3 ± 2.7	8.7 ± 1.7	2.2 ± 0.6
	20	33.6 ± 3.1	9.3 ± 2.3	2.1 ± 0.8
	25	32.9 ± 4.1	10.2 ± 3.1	2.3 ± 0.9
AC45kPCL	5	36.6 ± 4.7	9.3 ± 1.1	2.1 ± 0.7
	10	41.7 ± 3.7	7.5 ± 1.7	2.1 ± 0.7
	15	37.5 ± 1.9	11.8 ± 1.3	2.9 ± 0.5
	20	35.8 ± 3.0	14.4 ± 2.5	3.5 ± 0.9
	25	32.8 ± 0.8	15.1 ± 0.7	3.3 ± 0.2

4. Influence of sterilization methods on (thermo)mechanical properties

The influence of the sterilization methods was investigated on DMTA and tensile test measurements. Therefore, a formulation containing DVA as a main monomer, **Thiol 2** (15db% regarding DVA and **AC45kPCL**), 25wt% **AC45kPCL**, 0.02wt% pyrogallol as an inhibitor and 0.5wt% Ivocerin® was prepared and specimens (2 x DMTA and 6 x tensile test specimens) were cured according to Chapter 3.2. The samples were sterilized at KLS Martin. The samples should be sterilized with the ethylene oxide (EO) method and were conducted to DIN EN ISO 11135-1. Therefore, a CO_2 mixture with 6% EO was used and the temperature was held for 2h at 55 °C, followed by a 6h desorption phase. A ^{60}Co-radiation source was used for the γ-radiation method. Here, two different dosages (high dose = 30.5 kGy; low dose = 18.6 kGy) were applied according to DIN EN ISO 9001, DIN EN ISO 13485, and DIN EN ISO 11137-1.

DMTA measurements were performed as described in 3.2.2, and tensile tests were conducted as described in 3.2.3.

Table 9: Results of DMTA measurements of sterilized specimens containing DVA, 15 db% **Thiol 2**, 0.5 wt% Ivocerin and 0.02 wt% PYR and 25wt% **AC45kPCL**.

Sterilization method	**T_g [°C]**	**$G'_{25°C}$ [MPa]**	**$G'_{37°C}$ [MPa]**	**G'_R [MPa]**
γ-radiation (low dose)	90	778	595	134
γ-radiation (high dose)	85	744	624	142
Ethylene oxide (EO)	89	698	526	117

Table 10: Results of tensile test measurements of sterilized specimens containing DVA, 15 db% **Thiol 2**, 0.5 wt% Ivocerin and 0.02 wt% PYR and 25wt% **AC45kPCL**.

Sterilization method	**σ [MPa]**	**ε_B [%]**	**U_T [MJ·m^{-3}]**
γ-radiation (low dose)	36.1 ± 3.7	14.0 ± 3.1	2.8 ± 1.1
γ-radiation (high dose)	31.1 ± 2.3	7.4 ± 1.3	1.8 ± 0.4
Ethylene oxide (EO)	31.6 ± 2.8	8.2 ± 1.8	2.1 ± 0.6

5. 3D Fabrication of medical device

5.1. Rheology measurements of formulations containing functionalized PCLs

In order to investigate the increase of the viscosity by adding PCL in different amounts to the standard formulation, rheology measurements at 25 °C were conducted. Therefore, an Anton Paar MCR rheometer, a Peltier temperature control unit to keep the temperature stable and a CP25 (cone-plate system) was used. 80 µL of the freshly prepared formulations were used for the measurements. For one minute, the temperature was held constant. Then, the shear rate was increased to 100 s^{-1} and afterwards, the rheology measurements were performed at the mentioned shear rate for one minute. The last five measurement points were used to calculate the average viscosity for all formulations with an increasing amount of additive.

Table 11: Rheological measurement results of formulations containing DVA, 15 db% thiol (**Thiol 1**), 0.5 wt% Ivocerin and 0.02 wt% PYR. **Ref. Thiol 1** (without additive); containing additional 5-25 wt% YxkPCL.

additive	**additive [wt%]**	**η [mPa·s]**
Ref. Thiol 1	0	4.4
AC10kPCL	5	10.5
	10	20.9
	15	33.6
	20	63.2
	25	82.7
AC45kPCL	5	22.7
	10	57.4
	15	132.0
	20	223.4
	25	495.1

Table 12: Rheological measurement results of formulations containing DVA, 15 db% thiol (**Thiol 2**), 0.5 wt% Ivocerin and 0.02 wt% PYR. **Ref. Thiol 2** (without additive); containing additional 5-25 wt% YxkPCL.

additive	additive [wt%]	η [mPa·s]
Ref. Thiol 2	0	4.7
AC10kPCL	5	14.0
	10	26.6
	15	48.8
	20	62.4
	25	93.8
AC45kPCL	5	25.3
	10	74.3
	15	217.2
	20	492.7
	25	772.5

5.2. 3D Fabrication

For the fabrication of the 3D-parts a formulation of DVA as a main monomer, **Thiol 2** (15db% regarding DVA and **AC45kPCL**), 25wt% **AC45kPCL**, 0.02wt% pyrogallol as an inhibitor, 0.75wt% Ivocerin® and 0.06wt% QY was used. The 3D printing was done using a CeraFab7500 with a wavelength of 450 nm. 0.75wt% Ivocerin® was used as a photoinitiator and 0.06wt% Quinoline Yellow (QY) as an absorber. The CAD file of the surgical screws was sliced into 25 µm layers with the aid of Lithoz CeraFab Control Software. The screws were printed with a light intensity of 71.3 mW/cm^2, a light dose of 400 mJ/cm^2 (500 mJ/cm^2 for the first five layers) and an exposure time of ~5.6 s. The noncured resin was cleaned with Lithasol30 and compressed air.

5.3. Imaging

The detailed imaging of the printed structures was performed using a Keyence VHX 6000 optical microscope in panorama mode.

5.4. 3D scan

The 3D scan of the printed screw was made with an AutoScan Inspec stripe-light scanner from Shining3D. For comparison of the .stl file and the scan, the software GOM Inspect 2019 from the company GOM was used.

B. Interpenetrating polymer networks

2. Influence of radical system on cationic photopolymerization

2.1. Inhibition study of cationic polymerization due to thiol-ene chemistry

To test photoreactivity, ~10 mg of every formulation was weighed into 25 µL aluminum crucibles and closed with a glass lid. Photo-DSC measurements were performed in triplicates on a Netzsch DSC 204 F1 with autosampler at 25 °C under N_2 atmosphere. Monomer formulations were irradiated twice with filtered UV-light (300-500 nm) with an Exfo OmiCureTM series 2000 broadband Hg-lamp at 25 °C under constant N_2 flow (20 mL min^{-1}). The light intensity was set to 1.2 W cm^{-2} at the tip of the light guide corresponding ~30 mW cm^{-2} on the surface of the sample and the heat flow of the polymerization reaction was recorded as a function of time. All samples were irradiated twice for 300 s. The heat flow curve of the second irradiation period was subtracted from the first 300 s irradiation curve to receive the final curve. Every formulation was measured in triplicates. The times when the maximum heat evolution was reached (t_{max}) and 95% of the overall heat evolved (t_{95}) were determined.

Table 13: Results of Photo-DSC measurements for formulations with dioxane (**DOX** or **XDO**) with 0.5 mol% (cationic PI) (Form.1), additional DOD as thiol (Form.2) and additional **NB10kPCL** and radical PI (Form.3).

Formulation	**ΔH [mW·mg^{-1}]**	**t_{max} [s]**	**t_{95} [s]**
DOX Form.1	632 ± 11	12 ± 0	27 ± 1
DOX Form.2	608 ± 21	13 ± 1	29 ± 1
DOX Form.3	611 ± 3	10 ± 1	29 ± 1
XDO Form.1	192 ± 2	25 ± 2	204 ± 7
XDO Form.2	148 ± 1	25 ± 2	198 ± 4
XDO Form.3	245 ± 1	20 ± 1	180 ± 32

2.2. Investigation of thermomechanical properties of an IPN *via* DMTA

DMTA measurements were done to investigate the thermomechanical properties of the formed IPNs.

Therefore, formulations containing the oxetane monomer **DOX** and 1wt% Cyracure uvi 6976 (S-Sb) as a cationic system were prepared. As a radical system, 10wt% of **NB10kPCL** with **Thiol 1** in an equimolar ratio referred to the functionalities was used. 1wt% TPO-L was added as a radical photoinitiator. The compounds were heated to ensure the PCL-based monomer was melted and mixed until complete homogeneity was reached.

The prepared formulations were poured into silicone molds of respective sizes and shapes for DMTA experiments (2 x 5 x 40 mm^3). Then, the specimens were cured for 10 minutes in a PrograPrint Cure[253] from Ivoclar® with a wavelength of 405 nm and an intensity of 274 $mW \cdot cm^{-2}$ for free radical photopolymerization. Afterwards, the samples were rotated and cured on the other side for 10 minutes. Then, the cationic curing was done in the UV oven (50% intensity) with a broadband lamp (300-500 nm). Again, both surfaces were cured for 10 minutes. Before the measurements, the samples were ground and polished with sandpaper in multiple steps to ensure uniform geometries and to remove artifacts from the surface.

DMTA provides information about the storage modulus (G') at different temperatures and the glass transition temperatures (T_g) from the maximum of the loss factor (tanδ). The storage modulus at the rubber plateau (G'_R) correlates with the degree of network cross-linking. A high G'_R is indicative of a highly cross-linked network. DMTA experiments were performed in torsion mode from -100 °C to 200 °C with a heating rate of 2 $°C \cdot min^{-1}$. The torsion strain was set to 0.1% and a frequency of 1 Hz. The experiments were done as a single measurement due to the high reproducibility.

Table 14: Results of DMTA measurements for formulations containing **DOX** with 1wt% S-Sb (cationic PI) (**Ref.DOX**) respectively 10wt% **NB10kPCL** with **Thiol 1**.

Formulation	**T_g [°C]**	**$G'_{25°C}$ [MPa]**	**$G'_{37°C}$ [MPa]**	**G'_R [MPa]**
Ref. DOX	71	1160	1070	961
IPN	62	833	678	219
IPN 2nd cycle	90	960	845	220
IPN_pc90 °C	60	874	825	244
IPN_pc120 °C	67	878	751	215
IPN_pc180 °C	103	994	880	214

3. Synthesis of multifunctional and degradable oxetane monomers

3.1. Synthesis of 1,3,5-tris[(3-ethyl-3-oxetanyl)methoxyethyl]-1,3,5-benzenetricarboxylate (TOx):

1,3,5-Tris[(3-ethyl-3-oxetanyl)methoxyethyl]-1,3,5-benzenetricarboxylate (**TOx**) should be synthesized in a three-step synthesis according to literature.[297] In the first step, a better leaving group was introduced to EOM to synthesize **OLG**. **OLG** was etherified with an ethylene glycol spacer (**OEG**) in the following step. Finally, esterification of the trifunctional carbonyl chloride should lead to oxetane monomer 1,3,5-tris[(3-ethyl-3-oxetanyl)methoxyethyl]-1,3,5-benzenetricarboxylate (**TOx**). However, the last synthesis step was not performed due to insufficient purity and low yields of **OEG**.

3.1.1. Synthesis of 3-ethyl-3-methanesulfonyloxymethyloxetane (OLG):

The first step of the synthesis of **TOx** was the synthesis of 3-ethyl-3-methanesulfonyloxymethyloxetane (**OLG**) according to literature[297].

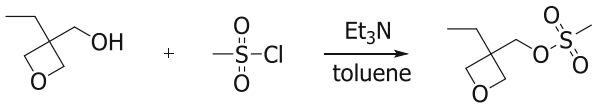

EOM **OLG**

Compound	eq.	n [mmol]	m [g]	V [mL]
3-Ethyl-3-hydroxymethyloxetane (EOM)	1.0	344	40.00	
Methane sulfonyl chloride (MsCl)	1.1	379	43.39	
Triethylamine	1.2	413	41.81	57.3
Toluene				160

Therefore, a three-necked round bottom flask was equipped with a thermometer, septum and dropping funnel. 3-Ethyl-3-hydroxymethyloxetane (EOM, 1 eq.) and triethylamine (1.2 eq.) were diluted in toluene (160 mL) and cooled down to -5 °C with an NaCl/ice bath. Methane sulfonyl chloride (MsCl) was weighed in, transferred into a dropping funnel and added dropwise (~1 h) to the reaction mixture without raising the temperature. The solution was stirred 3 h at -5 °C and then at room temperature for 16 h. Afterwards, sat. $NaHCO_3$ solution (80 mL) was added and the two formed phases were separated. The aqueous phase was extracted with 80 mL toluene once and then the combined organic phases with deionized water (4 x 80 mL). The toluene phase was dried over Na_2SO_4 and the solvent was evaporated. To completely remove the solvent, the product was dried in high-vacuum. **OLG** was isolated as a yellow oil in 81% calculated yield and was used without further purification for the next step.

n_D^{20}= 1.4603

^{1}H NMR (400 MHz, $CDCl_3$, δ): 4.42-4.45 (m, 4H, O-(CH_2)$_2$-C-), 4.36 (s, 2H, -S-O-CH_2-), 3.05 (s, 3H, -S-CH_3), 1.79 (q, J = 7.88 Hz, 2H, -C$\underline{H}_2$-CH_3), 0.93 (t, J = 7.50 Hz, 3H, -CH_3) ppm.

^{13}C NMR (100 MHz, $CDCl_3$, δ): 76.7, 70.9, 42.9, 37.4, 26.2, 7.9 ppm.

3.1.2. Synthesis of 3-ethyl-3-(4-hydroxyethyl)oxymethyloxetane (OEG):

The second step was synthesizing 3-ethyl-3-(4-hydroxyethyl)oxymethyloxetane (**OEG**) according to literature.[297]

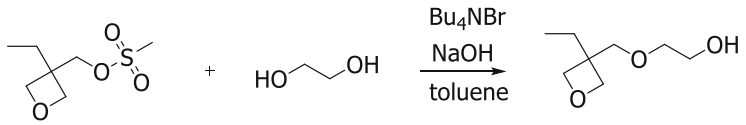

OLG **OEG**

Compound	**eq.**	**n [mmol]**	**m [g]**	**V [mL]**
OLG	1.0	140	30.00	
Ethylene glycol	2.1	293	18.22	
Tetrabutylammonium bromide	0.03	4	1.35	
NaOH	1.16	162	6.48	
Toluene				65

Therefore, ethylene glycol (2.1 eq.) was dissolved in 50 mL toluene and heated to 60 °C (oil bath 75 °C). Then, sodium hydroxide pellets (1.16 eq.) and tetrabutylammonium bromide (0.03 eq.) was added to the solution. After 1 h of stirring at elevated temperature (~80 °C reaction temperature), the pellets were still not dissolved completely. However, **OLG** (synthesized before) was slowly added to the reaction mixture *via* a dropping funnel within 15 minutes. Here, a jelly-like precipitate was formed and the reaction mixture was stirred for another 20 h at 80 °C. Then, the mixture was quenched with 240 mL deion. water, whereas the formed salt was dissolved. The organic phase was diluted with 160 mL toluene and the two phases were stirred vigorously while the pH was set to ~9 with diluted acetic acid. The two phases were separated and the aqueous phase was extracted with toluene (2 x 80 mL). Then, the combined organic phase was dried over Na_2SO_4, filtered and the solvent was removed. The crude product was obtained in 36% theoretical yield.

In literature, the crude product was purified by distillation (19 mbar, 157-159 °C) but with this method, no pure product was obtained (only mixed fractions of **OLG** (29%) and **OEG**). Purification by Kugelrohr distillation also did not yield a pure product.

^{1}H NMR (400 MHz, $CDCl_3$, δ): 4.45-4.42 (m, 4H, O-(CH_2)$_2$-C-), 4.35 (s, 2H, -C-CH_2-O-), 3.64 (s, 2H, -O-C$\underline{H}_2$-CH_2-O-), 3.59 (s, 2H, -O-CH_2-C$\underline{H}_2$-O-), 1.73 (q, *J* = 7.78 Hz, 2H, -C$\underline{H}_2$-CH_3), 0.87 (t, *J* = 7.60 Hz, 3H, -CH_3) ppm.

4. Influence of a chain transfer agent on the cationic photopolymerization of oxetanes

4.1. Synthesis of 3-[benzyloxy(methyl)]-3-ethyloxetane (BOX)

The monofunctional oxetane 3-[benzyloxy(methyl)]-3-ethyloxetane (**BOX**) was synthesized in a one-step synthesis, according to Kury *et al.*[293].

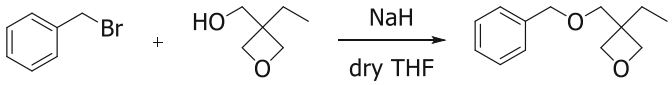

EOM **BOX**

Compound	eq.	n [mmol]	m [g]	V [mL]
Benzyl bromide	1.0	40	6.82	
3-Ethyl-3-hydroxymethyloxetane (EOM)	1.1	44	5.10	
NaH (60% in wax)	1.5	60	2.39	
dry THF				50

Therefore, 3-ethyl-3- hydroxymethyloxetane (EOM, 1.1 eq.) was diluted in dry THF and the flask was purged with argon. Afterwards, the solution was cooled to -5 °C and NaH (1.5 eq.) was added portion-wise. Then, benzyl bromide (1.0 eq.) was added dropwise, and the suspension was stirred for 16 h at room temperature. The excess NaH was quenched with water. THF was evaporated and the aqueous phase was diluted and extracted with diethyl ether. Afterwards, the organic phase was removed, and the residual oil was purified by column chromatography (8.6g crude product; 70/230 column; cond.: PE, sep.: 100%PE (35min), 20min 0% EE → 20% EE (30 min)). **BOX** was isolated as colorless oil in 52% calculated yield.

n_D^{20}= 1.5081

TLC (SiO_2, PE:EE = 4:2): R_f = 0.51

^{1}H NMR (400 MHz, $CDCl_3$, δ): 7.30-7.18 (m, 5H, Ar), 4.49 (s, 2H, Ar-CH_2-O), 4.35 (dd, 4H, -CH_2- (oxetane), J= 17.4, 11.7 Hz), 3.50 (s, 2H, -O-CH_2-), 1.69 (q, 2H, -$C\underline{H}_2$-CH_3, J= 11.7 Hz), 0.88 (t, 3H, -CH_2-$C\underline{H}_3$, J= 7.5 Hz) ppm.

^{13}C NMR (100 MHz, $CDCl_3$, δ): 138.4, 128.4, 127.7, 127.6, 78.6, 73.4, 72.8, 43.5 26.8, 8.2 ppm.

4.2. Study of adduct formation of BOX with chain transfer agents

^{1}H-NMR measurements followed photo-DSC experiments to evaluate the conversions of **BOX** and two varying alcohols as CTAs; 1-hexanol and 1,2-cyclohexanediol (**CHD**), respectively.

One formulation only containing **BOX** and 1wt% S-Sb as cationic photoinitiator was prepared. Then, two formulations containing **BOX**, S-Sb, and the CTAs in an equimolar ratio (referred to the functional groups) were mixed.

The freshly prepared formulations were irradiated by Photo-DSC at room temperature with a broadband lamp with a wavelength of 300-500 nm and 60 mW·cm^{-2} light intensity. The samples were irradiated for 300 s twice. Immediately after the irradiation, the samples were dissolved 0.5 mL $CDCl_3$ with pyridine to quench the dark reaction of the oxetane. Then, a ^{1}H-NMR was measured to determine the conversion.

Formulations containing the chain transfer agents showed no reaction (neither in the photo-DSC measurements nor the ^{1}H-NMR). Therefore, the light intensity was increased to 200 mW·cm$^{-2,}$ and the polymerization temperature was set to 100 °C. The evaluation *via* ^{1}H-HMR was performed as described above.

5. Synthesis of multifunctional degradable chain transfer agents

The synthesis of tris(2-hydroxyethyl)-1,3,5-benzenetricarboxylate (**THEB**) was a two-step synthesis and is described by Azumaya *et al.*.[301] Here, the acid chloride was first esterified with a one-side protected ethylene glycol (**pTHEB**) and then, the protecting group was cleaved off. This led to the trifunctional hydroxyl-terminated CTA.

5.1. Synthesis of 1,3,5-tris(2-hydroxyethyl)-1,3,5-benzenetricarboxylate (THEB)

5.1.1. Synthesis of tris[2-(tert-butyldimethylsilyloxy)ethyl]-1,3,5-benzene tricarboxylate (pTHEB):

The synthesis of tris(2-hydroxyethyl)-1,3,5-benzenetricarboxylate (**THEB**) is a two-step synthesis, according to Azumaya *et al.*.[301]

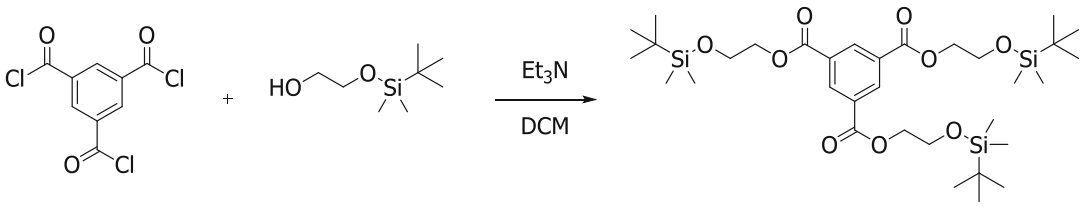

Compound	eq.	n [mmol]	m [g]	V [mL]
1,3,5-Benzenetricabonyl trichloride	1.0	38.0	10.00	
2-(tert-Butyldimethylsilyloxy)ethanol	3.6	136.0	23.91	26.8
Triethylamine	3.6	136.0	13.72	18.9
dry DCM				600

For the synthesis of tris[2-(tert-butyldimethylsilyloxy)ethyl]-1,3,5-benzene tricarboxylate (**pTHEB**), a 1 L three-necked round bottom flask was equipped with a condenser, dropping funnel and a septum. The apparatus was evacuated and flushed with argon three times. Then 2-(*tert*-butyldimethylsilyloxy)ethanol (3.6 eq.) and Et_3N as an acid scavenger (3.6 eq.) were mixed with dry DCM (400 mL) and stirred at room temperature. 1,3,5-Benzenetricabonyl trichloride (1 eq.) was dissolved in dry DCM (200 mL) in a round bottom flask and transferred with a transfer needle into the dropping funnel. The solution of the carbonyl chloride was added over a period of 3 h to the reaction mixture and after complete addition, the reaction mixture was stirred for 6 days (the conversion was followed by TLC). Deion. water (200 mL) was added to the solution and extracted with DCM (3 x 100 mL). The combined organic phases were then washed with 3 x 150 mL deion. water. The organic phases were dried over Na_2SO_4, filtered and then, the solvent was removed under reduced pressure. The obtained crude product was then purified by column chromatography (22g crude product; 100/460 column; cond.: 95:5% PE:EE, sep.: 20min 5% EE → 20% EE (60 min)). The product was isolated as a white solid in 24% calculated yield.

m.p.: 48.6-52.8 °C (Lit.: colorless oil[301])

^{1}H NMR (400 MHz, $CDCl_3$, δ): 8.89 (s, 3H, Ar-H), 4.45 (t, *J* = 5.20 Hz, 6H, -O-C<u>H$_2$</u>-CH$_2$-O-), 3.96 (t, *J* = 5.20 Hz, 6H, -O-CH$_2$-C<u>H$_2$</u>-O-), 0.89 (s, 27H, Si-C(CH$_3$)$_3$), 0.08 (s, 18H, Si-CH$_3$) ppm.
^{13}C NMR (100 MHz, $CDCl_3$, δ): 164.9, 134.8, 131.4, 66.8, 61.2, 25.9, 18.4 ppm.

5.1.2. Synthesis of tris(2-hydroxyethyl)-1,3,5-benzenetricarboxylate (THEB):

The protection groups will be cleaved off in the second step to obtain the product **THEB**.

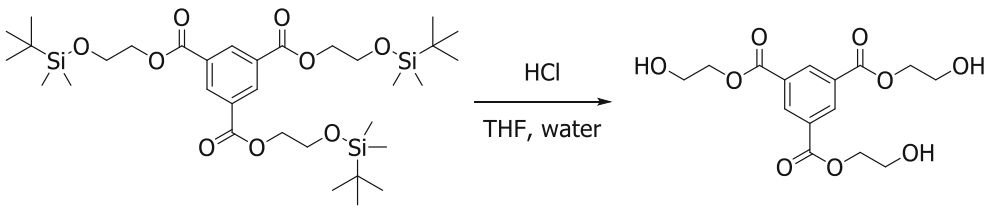

pTHEB **THEB**

Compound	eq.	n [mmol]	m [g]	V [mL]
pTHEB	1.0	8.0	5.80	
6M HCl				0.5
THF				80

In the second step, **pTHEB** (1 eq.) was dissolved in THF (80 mL) in a round bottom flask. Then, 0.5 mL 6M HCl was added slowly. After addition, the reaction mixture was stirred for 20 h and the product precipitated as a white solid. Afterwards, the solvent was removed under reduced pressure and the residual product was washed 4 times with petroleum ether. After drying, the pure product was isolated as a white powder with a theoretical yield of 81%.
m.p.: 147-150.6 °C (Lit.: 132-137 °C[304])
^{1}H NMR (400 MHz, DMSO, δ): 8.74 (s, 3H, Ar-H), 5.00 (t, *J* = 5.51 Hz, 3H, -OH), 4.38 (t, *J* = 4.49 Hz, 6H, HO-CH$_2$-CH$_2$-), 3.76-3.72 (m, 6H, HO-CH$_2$-CH$_2$-) ppm.
^{13}C NMR (100 MHz, DMSO, δ): 164.4, 133.7, 131.2, 67.4, 58.9 ppm.

5.2. Synthesis of (3,4-dihydroxycyclohexyl)methyl 3,4-dihydroxy cyclohexane carboxylate (CEOH)

3,4-Dihydroxycyclohexyl)methyl 3,4-dihydroxycyclohexanecarboxylate (**CEOH**) was synthesized in a one-step synthesis by a ring-opening of the difunctional epoxide 3,4-epoxycyclohexylmethyl 3,4-epoxycyclohexanecarboxylate (CE). The reaction was done according to Ratcliffe *et al.*.[302]

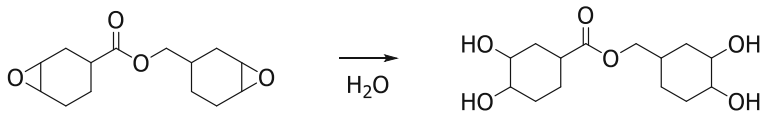

CE **CEOH**

Compound	eq.	n [mmol]	m [g]	V [mL]
3,4-Epoxycyclohexanecarboxylate (CE)	1.0	120	30.49	
Water	70			152

A 250 mL round bottom flask was charged with 3,4-epoxycyclohexylmethyl-3,4-epoxycyclohexanecarboxylate (CE) and mixed in water. The two-phased reaction mixture was heated to 80 °C for 16 h until a homogenous phase formed. The solvent was removed and the highly viscous oil was dried under reduced pressure. Then, the crude product was recrystallized in acetone, yielding a white precipitate. The precipitate was filtered and dried in a high vacuum. **CEOH** was obtained as a white powder in 82% calculated yield.

HRMS: calc.: 288.3363, found: 289.3436 (EM+H)
m.p.: 142.2-145.4 °C

^{1}H NMR (400 MHz, DMSO, δ): 5.08-5.06 (m, 1H, O=C-CH-CH$_2$-CH$_2$-CH-OH), 4.97-4.95 (m, 2H, O=C-CH-CH$_2$-CH-OH, -O-CH$_2$-CH-CH$_2$-CH-OH), 4.89-4.88 (m, 1H, -O-CH$_2$-CH-CH$_2$-CH$_2$-CH-OH), 4.28-4.19 (m, 2H, -O-CH$_2$-), 3.97-1.74 (m, 4H, 4x-CH-OH), 3.05-2.99 (m, 1H, O=C-CH-), 2.37-1.52 (m, 13H, -O-CH$_2$-CH-, and 6x-CH$_2$-(ring)) ppm.

^{13}C NMR (100 MHz, DMSO, δ): 175.1, 69.1, 68.83, 68.79, 68.4, 67.9, 37.2, 27.5, 26.9, 23.1, 22.9 ppm.

6. Selection of cationic photocurable system

6.1. Formulation preparation of the cationic photocurable formulation

The impact of chain transfer agents on the (thermos)mechanical properties should be thoroughly investigated. Therefore, the three different formulations with the monomers **DOX**, **XDO** and **S160** were mixed with 1wt% S-Sb (cationic photoinitiator). Then, another three formulations were prepared, where the chain transfer agent **CEOH** was added in an equimolar ratio referred to their functionalities. Again, 1wt% S-Sb was added as PI. The formulations were heated to 120 °C to ensure the melting of the **CEOH** and mixed with a vortex-speed mixer until complete homogeneity was assured.

6.2. Sample preparation of the cationic photocurable system for (thermo)mechanical testing

The freshly prepared formulations were kept at 120 °C temperature until use to avoid unintended recrystallization and to decrease the viscosity for easier handling. The formulations were transferred with a hot glass pipette into pre-heated silicon molds (120 °C) for DMTA- and tensile specimens. For DMTA, specimens (2 x 5 x 40 mm^3) and bone-shaped specimens (according to ISO527-2:2012 geometry 5B with a height of 2 mm) were prepared for tensile testing. Bubbles were removed, and the specimens were cured in a hot mold at 120 °C with a wavelength of 365 nm (630 mW/cm^2.) and an exposure time of 5 min on each side. Before the measurements, the samples were ground and polished with sandpaper in multiple steps to ensure uniform geometries and to remove artifacts from the surface.

6.3. Investigation of thermomechanical properties *via* DMTA

The DMTA measurements were conducted according to Experimental Part 3.2.2. The collected data are shown in Table 15.

Table 15: Results of DMTA measurements for formulations containing the oxetane monomer alone (**DOX**, **XDO** and **S160**) and formulations containing additional CEOH as CTA in an equimolar ratio. 1wt% S-Sb is added as a cationic photoinitiator.

Formulation	**T_g [°C]**	**G'_{25} [MPa]**	**G'_{37} [MPa]**	**G'_R [MPa]**
DOX	77	965	871	137
DOX:CEOH (1:1)	82	1640	1090	13
XDO	97	940	874	38
XDO:CEOH (1:1)	61	1380	856	11
S160	104	1150	961	56
S160:CEOH (1:1)	97	1160	864	17

6.4. Investigation of mechanical properties *via* tensile tests

Tensile tests were done on a Zwick Z050 tensile testing machine with a 1 kN load sensor. Crosshead speed was set for 5 mm·min^{-1}, and the strain was measured using a mechanical extensometer. Analysis was done with the testXpert II testing software and to ensure reproducibility, at least five replicates were measured. The collected data are shown in Table 16.

Table 16: Results of tensile tests for formulations containing the oxetane monomer alone (**DOX**, **XDO** and **S160**) and formulations containing additional **CEOH** as CTA in an equimolar ratio. 1wt% S-Sb is added as a cationic photoinitiator.

Formulation	**σ [MPa]**	**ε_B [%]**	**U_T [MJ·m^{-3}]**
DOX	36.2 ± 2.2	6.0 ± 0.4	1.3 ± 0.2
DOX:CEOH (1:1)	40.3 ± 7.0	4.4 ± 0.8	1.0 ± 0.4
XDO	44.7 ± 0.7	8.9 ± 2.1	2.8 ± 0.9
XDO:CEOH (1:1)	52.9 ± 2.4	11.9 ± 2.5	3.9 ± 1.2
S160	55.3 ± 1.4	8.1 ± 1.6	2.9 ± 0.8
S160:CEOH (1:1)	42.3 ± 2.3	10.2 ± 0.7	3.2 ± 0.2

7. Formation of interpenetrating polymer networks: screening of the radical system

7.1. Formulation preparation of IPNs

Two reference formulations were prepared; one with only **XDO** (**Ref. XDO**) and one with **XDO** and **CEOH** in equimolar ratio, referred to the functionalities (**Ref. XDO:CEOH**). As a cationic photoinitiator 1wt% S-Sb was added.

The high molecular weight PCL-based monomer (**AC45kPCL**) and the trifunctional thiol 1,3,5-tris(3-mercaptopropyl)-1,3,5-triazine-2,4,6-trione (**Thiol 2**) are compounds of the radical system. **Thiol 2** is used in an equimolar ratio to the functionalized PCL, referred to the functionalities. 1wt% TPO-L was added as a radical photoinitiator.

The radical system was then added in 5-25wt% to the cationic system. 1wt% of both photoinitiators are always referred to the entire formulation (cationic and radical system). The formulations were heated to 120 °C to ensure that **CEOH** and the PCL-compound were melted and mixed with a vortex-speed mixer until complete homogeneity was assured.

7.2. Sample preparation of IPNs for (thermo)mechanical testing

The freshly prepared formulations were kept at 120 °C to avoid unintended recrystallization and to decrease the viscosity for easier handling. The formulations were transferred with a hot glass pipette into pre-heated silicon molds (120 °C) for DMTA- and tensile specimens.

Bubbles were removed, and the specimens were cured in the hot mold at 120 °C. First, the radical curing with a wavelength of 405 nm and an intensity of 36 mW/cm^2, was conducted, followed by irradiation with λ = 365 nm and an intensity of 630 mW/cm^2. The exposure time was 5 minutes for each wavelength. Then, the mold was removed and cooled to room temperature. Then, the specimens were turned. The second irradiation cycle was again at 120°C for 5 minutes for each wavelength. Before the measurements, the samples were ground and polished with sandpaper in multiple steps to ensure uniform geometries and to remove artifacts from the surface.

7.3. Investigation of thermomechanical properties of IPNs *via* DMTA

The DMTA measurements were conducted according to Experimental Part 3.2.2. The collected data are shown in Table 17.

Table 17: Results of DMTA measurements for formulations containing the oxetane monomer **XDO** alone (radical system) combined with an increasing amount of soft content (5-25wt%); and for formulations containing **XDO** with additional **CEOH** as CTA in an equimolar ratio with an increasing amount of soft content (5-25wt%). 1wt% S-Sb is added as a cationic photoinitiator and 1wt% TPO-L as a radical photoinitiator. The soft content consists of **AC45kPCL** and **Thiol 2** in an equimolar ratio.

Cationic System	Soft network [wt%]	T_g [°C]	G'_{25} [MPa]	G'_{37} [MPa]	G'_R [MPa]
XDO	0 (Ref. XDO)	97	940	874	38
	5	75	888	763	35
	10	83	791	657	36
	15	81	678	536	29
	20	85	792	628	40
	25	88	525	412	27
XDO:CEOH (1:1)	0 (Ref. XDO:CEOH)	61	1380	856	11
	5	62	1050	560	9
	10	61	93	502	9
	15	65	911	478	8
	20	62	843	449	8
	25	61	662	380	5

7.4. Investigation of mechanical properties of IPNs *via* tensile tests

Tensile test experiments were conducted according to Experimental Part 3.2.3. The collected data are shown in Table 18.

Table 18: Results of tensile tests for formulations containing the oxetane monomer **XDO** alone (radical system) combined with an increasing amount of soft content (5-25wt%); and for formulations containing **XDO** with additional **CEOH** as CTA in an equimolar ratio with an increasing amount of soft content (5-25wt%). 1wt% S-Sb is added as a cationic photoinitiator and 1wt% TPO-L as a radical photoinitiator. The soft content consists of **AC45kPCL** and **Thiol 2** in an equimolar ratio.

Cationic System	Soft network [wt%]	σ [MPa]	ε_B [%]	U_T [MJ·m^{-3}]
XDO	0 (Ref. XDO)	44.7 ± 0.7	8.9 ± 2.1	2.8 ± 0.9
	5	37.8 ± 1.2	15.3 ± 1.4	4.8 ± 0.5
	10	35.3 ± 0.4	20.6 ± 1.1	6.1 ± 0.4
	15	32.6 ± 0.7	24.8 ± 1.6	6.5 ± 0.5
	20	28.3 ± 1.0	19.5 ± 2.0	4.3 ± 0.6
	25	28.1 ± 0.6	23.1 ± 1.5	5.0 ± 0.4
XDO:CEOH (1:1)	0 (Ref. XDO:CEOH)	52.9 ± 2.4	11.9 ± 2.5	3.9 ± 1.2
	5	42.4 ± 1.4	10.9 ± 2.7	3.4 ± 1.1
	10	33.2 ± 0.3	10.9 ± 3.1	2.7 ± 1.0
	15	33.6 ± 1.0	18.2 ± 4.1	4.9 ± 1.2
	20	31.2 ± 1.5	18.9 ± 3.2	4.9 ± 1.1
	25	26.4 ± 1.1	40.4 ± 4.9	9.0 ± 1.2

APPENDIX

A. Toughness enhancers for 3D printed Photopolymers

1. Synthesis of PCL based toughness enhancers

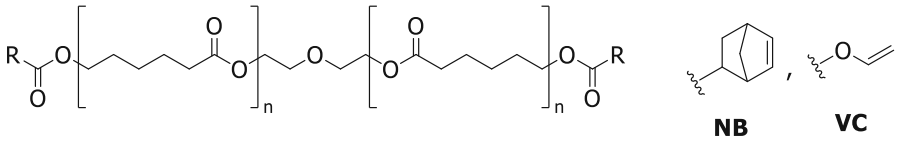

Figure 61: Chemical structures of the PCL-based toughness enhancers with norbornene (**NBxkPCL**) and vinyl carbonate functionality (**VCxkPCL**).

The commercially available PCL diol (xkPCL) in two different molecular weights (10kDa and 45kDa) were end-capped. The systematic names YxkPCL, where Y indicates the end modification (norbornene (NB), vinyl carbonate (VC)) and x the molecular weight (MW) in kDa (10 kDa or 45kDa) are henceforth used in the text.

1.1. Synthesis of norbornene-modified PCL (NBxkPCL)

NBxkPCL was synthesized in a two-step synthesis. In the first step, the 5-norbornene-2-carbonyl chloride (NBCl) was synthesized and then, converted with a PCL diol to obtain the product.

1.1.1. Synthesis of 5-norbornene-2-carbonyl chloride (NBCl)

In the first step NBCl was obtained by the conversion of norbornene carboxylic acid and oxalyl chloride in accordance to Chae *et al.*.[305]

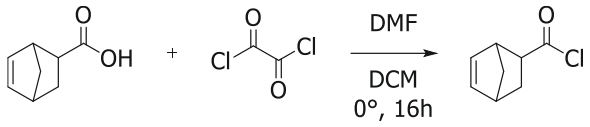

Compound	eq.	n [mmol]	m [g]	V [mL]
5-Norbornene-2-carboxylic acid	1	71	9.76	-
Oxalyl chloride	4	280	-	24
DMF	-	-	-	0.1
dry DCM				50

A three-neck round bottom flask was equipped with a dropping funnel, evacuated, and flushed with argon three times. The flask was charged with oxalyl chloride (4 eq.), DCM (50 mL) and DMF (0.1 mL). A solution of 5-norbornene-2-carboxylic acid (1 eq.) and dry DCM (50 mL) was filled into the dropping funnel and was added dropwise to the precooled oxalyl chloride solution. The ice bath was removed after complete addition and the reaction mixture was stirred for 24 h at room temperature. The residual oxalyl chloride and DCM was removed under reduced pressure. The crude product was distilled at 6 mbar and 47 °C to obtain 5-norbornene-2-carbonyl chloride (NBCl) as colorless liquid in 84% calculated yield.

^{1}H-NMR (400 MHz, $CDCl_3$, δ): 6.32-6.17 (m, 1H, CH=CH endo/exo), 6.17-5.99 (m, 1H, CH=CH exo/endo), 3.49-2.71 (m, 3H, CH), 2.07-1.87 (m, 1H, CH_2, CH_2 bridge), 1.57-1.38 (m, 2H, CH_2, CH_2 bridge), 1.37-1.28 (m, 1H, CH_2, CH_2 bridge) ppm.

^{13}C-NMR (100 MHz, $CDCl_3$, δ): 175.19 (s, C=O), 139.17 (s, CH=CH exo), 138.83 (s, CH=CH endo), 135.02 (s, CH=CH exo), 131.75 (s, CH=CH endo), 56.56 (s, CHC=O endo), 56.45 (s, CHC=O exo), 49.36 (s, CH_2 bridge), 47.29 (s, CH endo), 47.03 (s, CH exo), 46.43 (s, CH_2 bridge), 43.00 (s, CH endo), 42.00 (s, CH exo), 31.29 (s, CH_2 exo), 30.21 (s, CH_2 endo) ppm.

1.1.2. Synthesis of norbornene modified PCL (NBxkPCL)

In the second step, PCL diol was converted with NBCl to synthesize **NBxkPCL**.

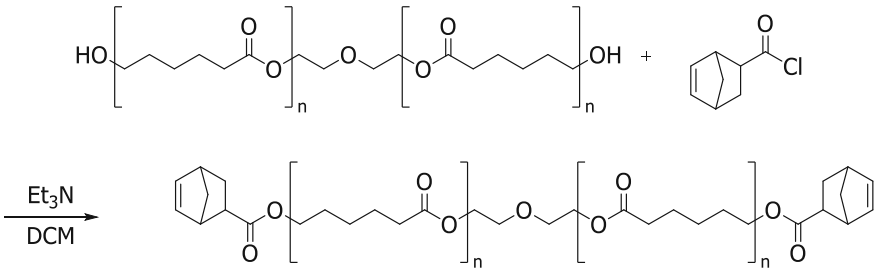

NBxkPCL

Compound	eq.	n [mmol]	m [g]	V [mL]
PCL diol (10kDa|45kDa)	1	5|1	50|50	-
dry Pyridine	4|12	20|13	-	1.6|1.1
Allyl chloroformate	4|12	20|13	-	1.8|1.5
dry DCM				200|400

The hydroxyl-terminated PCL is commercially available and was used as received. The hydroxyl terminated PCL diol in respective molecular weight (1 eq.) was added to a three-neck round bottom flask, was evacuated and flushed with argon. Then, dry DCM (200| 400 mL) to dissolve the PCL diol and Et_3N (10 eq.) as acid scavenger were added. The reaction mixture was cooled with an ice bath and NBCl (10 eq.) was added dropwise *via* a syringe. After complete addition, the ice bath was removed, and the reaction mixture was stirred for 24 h at room temperature. The solution was extracted with 1N HCl (3x500 mL), then sat. $NaHCO_3$ (2x500 mL) and last with 500 mL deion. water. The organic phase was precipitated twice in cold MeOH, filtered, and dried under reduced pressure at 50 °C to obtain the purified products in quantitative yields. After functionalization with norbornene, a conversion of 90% for **NB10kPCL** and for **NB45kPCL** 95% could be reached.

^{1}H NMR (600 MHz, $CDCl_3$,δ): 6.17-5.90 (ddd, , *J* = 163.7, 3.4, 2.7 Hz, 2H, CH=CH endo/exo), 6.13-6.12 (m, 2H, CH=CH endo/exo), 4.22 (t, *J* = 6.7 Hz, 4H, -O-C$\underline{H}_2$-CH_2-O-), 4.05 (t, *J* = 6.7 Hz, ~300 or 1800H, -CO-O-C$\underline{H}_2$-CH_2-CH_2-CH_2-CH_2-CO-O-), 3.68 (m, 4H, -O-CH_2-C$\underline{H}_2$-O-), 2.28 (t, *J* = 7.5 Hz, ~300 or 1800H, -CO-O-CH_2-CH_2-CH_2-CH_2-C$\underline{H}_2$-CO-O-), 1.92-1.86 (m, 1H, CH_2, CH_2 bridge)1.63 (ddt, *J* = 13.8, 11.6, 7.2 Hz, ~600 or 3600H, -CO-O-CH_2-C$\underline{H}_2$-CH_2-C$\underline{H}_2$-CH_2-CO-O-), 1.41 – 1.33 (m, ~300 or 1800H, -CO-O-CH_2-CH_2-C$\underline{H}_2$-CH_2-CH_2-CO-O-) ppm;

GPC (THF): $\overline{M_w}$ = 14 or 44 kDa.

DS calculated from ^{31}P(IG)-NMR = 90% or 95%.

1.2. Synthesis of vinyl carbonate modified PCL (VCxkPCL)

In a one-step synthesis, the PCL diol was converted with an excess of viyl chloroformate to obtain the product **VCxkPCL**. The synthesis was performed according to Orman *et al.*.[35]

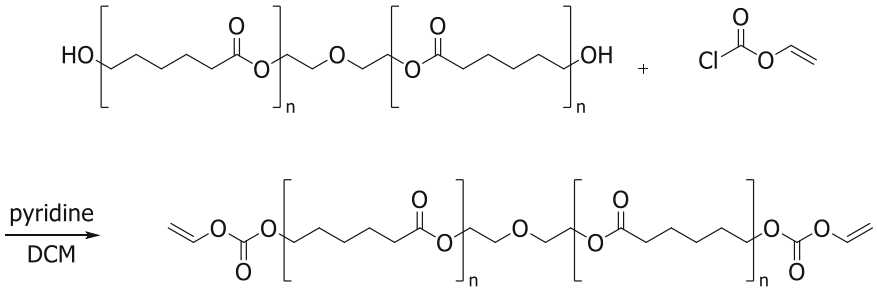

VCxkPCL

Compound	eq.	n [mmol]	m [g]	V [mL]
PCL diol (10kDa|45kDa)	1	5|1	50|50	-
dry Pyridine	12	60|13	-	4.8|1.1
Vinyl chloroformate	12	60|13	-	5.6|1.3
dry DCM				200|400

The hydroxyl terminated PCL diol (1 eq.) and dry pyridine (12 eq.) were dissolved in 200 | 400 mL of dry DCM under argon atmosphere. After cooling to -5 °C, vinyl chloroformate (12 eq.) was added dropwise *via* syringe to the stirred solution within 10 min and the temperature was kept at 0 °C for 30 min. The solution was stirred for 24 h at room temperature and was quenched afterwards with 5 mL deionized water. The reaction mixture was extracted with 3 x 500 mL 1N HCl, then two times with 500 mL sat. $NaHCO_3$ solution and once with 500 mL water. For purification of the product, the solution was precipitated twice in cold MeOH (1200 mL). The purified product was filtered and dried *in vacuum* at 40 °C. The vinyl carbonate modified products could be synthesized with a conversion of 98% (**VC10kPCL**) and 93% (**VC45kPCL**).

^{1}H NMR (600 MHz, $CDCl_3$, δ) 7.08 (dd, J = 6.05, 13.74 Hz, 2 H, CH_2=C<u>H</u>), 5.07 (dd, J = 2.70, 13.74 Hz, 2 H, trans-CH_2=), 4.77 (dd, J = 2.70, 6.05 Hz, 2 H, cis-CH_2=)., 4.22 (t, *J* = 6.7 Hz, 4H, -O-C<u>H</u>$_2$-CH_2-O-), 4.05 (t, *J* = 6.7 Hz, ~300 or 1800H, -CO-O-C<u>H</u>$_2$-CH_2-CH_2-CH_2-CH_2-CO-O-), 3.68 (m, 4H, -O-CH_2-C<u>H</u>$_2$-O-), 2.28 (t, *J* = 7.5 Hz, ~300 or 1800H, -CO-O-CH_2-CH_2-CH_2-CH_2-C<u>H</u>$_2$-CO-O-), 1.92-1.86 (m, 1H, CH_2, CH_2 bridge)1.63 (ddt, *J* = 13.8, 11.6, 7.2 Hz, ~600 or 3600H, -CO-O-CH_2-C<u>H</u>$_2$-CH_2-C<u>H</u>$_2$-CH_2-CO-O-), 1.41 – 1.33 (m, ~300 or 1800H, -CO-O-CH_2-CH_2-C<u>H</u>$_2$-CH_2-CH_2-CO-O-) ppm;

GPC (THF): $\overline{M_w}$ = 14 or 44 kDa.

DS calculated from ^{31}P(IG)-NMR = 98% or 93%.

2. Characterization of PCL based toughness enhancers

2.1. Investigation of the chemical properties *via* RT-FT-NIR-photorheology

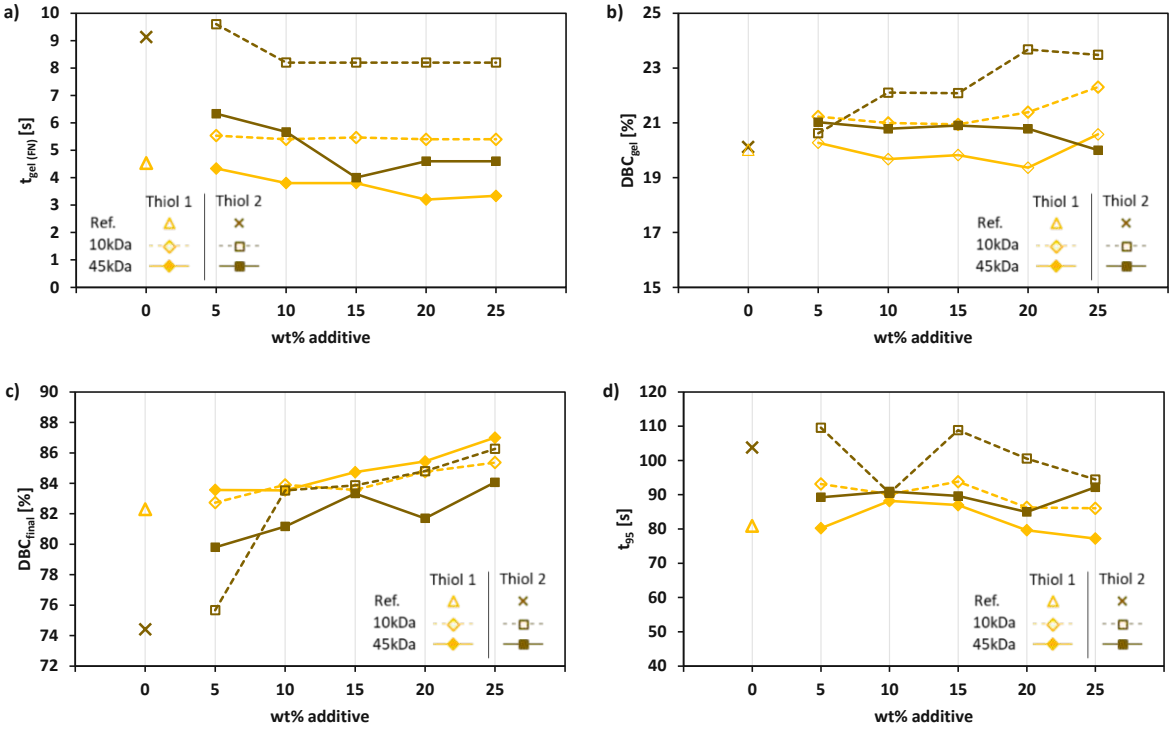

Figure 62: Photorheological measurement results of formulations containing DVA, 15 db% thiol, 0.5 wt% Ivocerin and 0.02 wt% PYR. **Ref. Thiol 1** (without additive): yellow triangle; containing additional 5-25 wt% **NBxkPCL** (yellow diamonds) or **Ref. Thiol 2** (without additive): ochre cross; containing additional 5-25 wt% **NBxkPCL** (ochre squares). Empty symbols with dashed lines indicate **NB10kPCL** and full symbols with solid lines indicate **NB45kPCL**. The straight lines are only for a better visibility. a) Obtained values for the gel point (t_{gel}); b) obtained values for the double bond conversion at t_{gel} (DBC_{gel}); c) obtained values for the final double bond conversion (DBC_{final}) and d) obtained values for the time to reach 95% of the final DBC (t_{95}).

Table 19: Photorheological measurement results of formulations containing DVA, 15 db% thiol (**Thiol 1**), 0.5 wt% Ivocerin and 0.02 wt% PYR. **Ref. Thiol 1** (without additive); containing additional 5-25 wt% **NBxkPCL**.

additive	additive [wt%]	t_{gel} [s]	DBC_{gel} [%]	t_{95} [s]	DBC_{final} [%]	G'_{max} [kPa]	F_{Nmax} [N]
Ref. Thiol 1	0	4.5 ± 0.5	20 ± 1	81 ± 4	82 ± 0	143 ± 1	-10.9 ± 0.1
NB10kPCL	5	5.5 ± 0.2	21 ± 1	93 ± 1	83 ± 0	143 ± 1	-10.9 ± 0.1
	10	5.4 ± 0.0	21 ± 0	90 ± 3	84 ± 0	142 ±1	-10.8 ± 0.3
	15	5.5 ± 0.1	21 ± 0	94 ± 3	84 ± 0	143 ± 6	-10.0 ± 0.6
	20	5.4 ± 0.0	21 ± 0	86 ± 4	84 ± 0	148 ± 6	-12.4 ± 1.6
	25	5.4 ± 0.0	22 ± 1	86 ± 2	85 ± 0	145 ± 4	-12.7 ± 0.6
NB45kPCL	5	4.3 ± 0.1	20 ± 1	80 ± 1	84 ± 0	112 ± 2	-15.0 ± 0.6
	10	3.8 ± 0.3	20 ± 1	88 ± 2	84 ± 0	103 ± 2	-15.5 ± 0.1
	15	3.8 ± 0.2	20 ± 0	87 ± 1	85 ± 0	98 ± 7	-15.1 ± 0.0
	20	3.2 ± 0.0	19 ± 0	80 ± 3	85 ± 0	139 ± 3	-9.9 ± 0.7
	25	3.3 ± 0.1	21 ± 0	77 ± 2	87 ± 0	143 ± 2	-10.8 ± 0.7

Table 20: Photorheological measurement results of formulations containing DVA, 15 db% thiol (**Thiol 2**), 0.5 wt% Ivocerin and 0.02 wt% PYR. **Ref. Thiol 2** (without additive); containing additional 5-25 wt% **NBxkPCL**.

additive	additive [wt%]	t_{gel} [s]	DBC_{gel} [%]	t_{95} [s]	DBC_{final} [%]	G'_{max} [kPa]	F_{Nmax} [N]
Ref. Thiol 2	0	9.1 ± 0.3	20 ± 0	104 ± 6	74 ± 0	148 ± 1	-11.3 ± 0.9
NB10kPCL	5	9.6 ± 0.0	21 ± 0	110 ± 3	76 ± 0	146 ± 5	-11.6 ± 0.7
	10	8.2 ± 0.0	22 ± 1	91 ± 5	84 ± 0	145 ± 0	-12.1 ± 0.2
	15	8.2 ± 0.0	22 ± 0	109 ± 5	84 ± 0	141 ± 1	-11.2 ± 0.1
	20	8.2 ± 0.0	24 ± 1	101 ± 3	85 ± 0	139 ± 2	-10.3 ± 0.4
	25	8.2 ± 0.0	23 ± 1	94 ± 7	86 ± 1	140 ± 6	-7.7 ± 2.1
NB45kPCL	5	6.3 ± 0.1	21 ± 0	89 ± 1	80 ± 0	119 ± 1	-10.8 ± 0.7
	10	5.7 ± 0.1	21 ± 1	91 ± 7	81 ± 0	119 ± 3	-10.5 ± 0.5
	15	4.0 ± 0.2	21 ± 1	90 ± 2	83 ± 0	110 ± 2	-9.6 ± 0.3
	20	4.6 ± 0.2	21 ± 0	85 ± 4	82 ± 1	110 ± 9	-9.2 ± 0.3
	25	4.6 ± 0.2	20 ± 1	92 ± 2	84 ± 0	125 ± 1	-11.4 ± 0.7

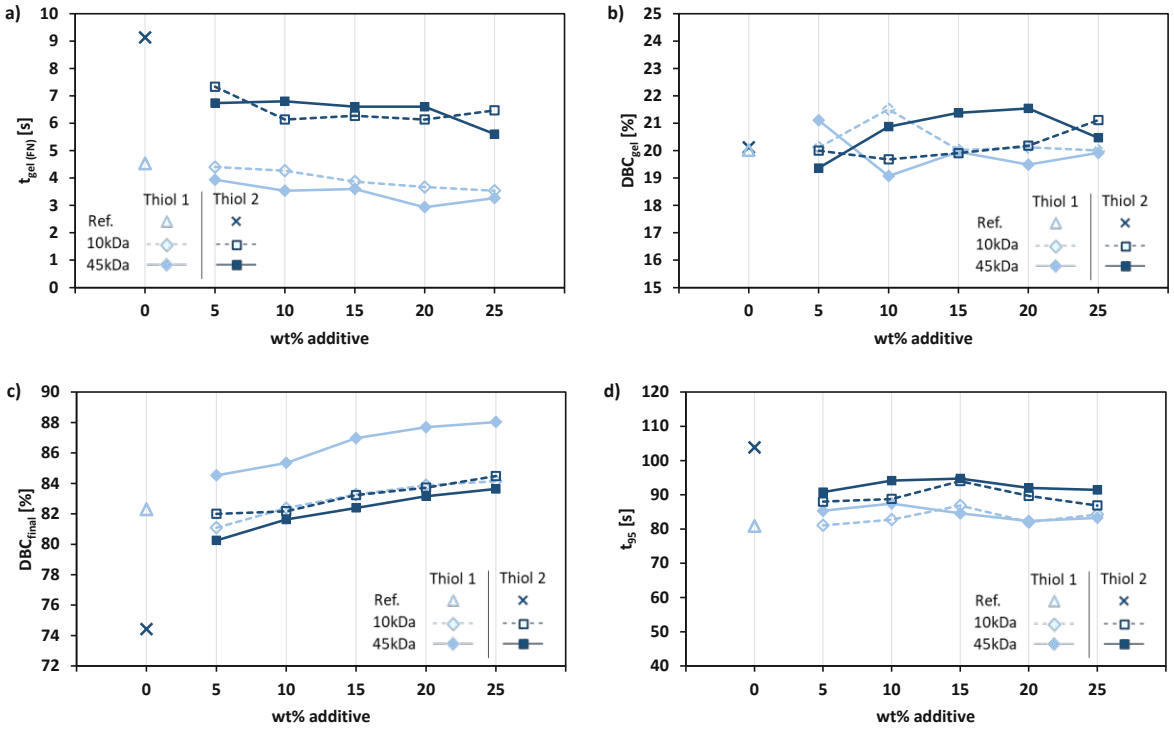

Figure 63: Photorheological measurement results of formulations containing DVA, 15 db% thiol, 0.5 wt% Ivocerin and 0.02 wt% PYR. **Ref. Thiol 1** (without additive): light blue triangle; containing additional 5-25 wt% **VCxkPCL** (light blue diamonds) or **Ref. Thiol 2** (without additive): dark blue cross; containing additional 5-25 wt% **VCxkPCL** (dark blue squares). Empty symbols with dashed lines indicate **VC10kPCL** and full symbols with solid lines indicate **VC45kPCL**. The straight lines are only for a better visibility. a) Obtained values for the gel point (t_{gel}); b) obtained values for the double bond conversion at t_{gel} (DBC_{gel}); c) obtained values for the final double bond conversion (DBC_{final}) and d) obtained values for the time to reach 95% of the final DBC (t_{95}).

Table 21: Photorheological measurement results of formulations containing DVA, 15 db% thiol (**Thiol 1**), 0.5 wt% Ivocerin and 0.02 wt% PYR. **Ref. Thiol 1** (without additive); containing additional 5-25 wt% **VCxkPCL**.

additive	additive [wt%]	t_{gel} [s]	DBC_{gel} [%]	t_{95} [s]	DBC_{final} [%]	G'_{max} [kPa]	F_{Nmax} [N]
Ref. Thiol 1	0	4.5 ± 0.5	20 ± 1	81 ± 4	82 ± 0	143 ± 1	-10.9 ± 0.1
VC10kPCL	5	4.4 ± 0.4	20 ± 0	81 ± 3	81 ± 0	130 ± 2	-14.5 ± 1.3
	10	4.3 ± 0.8	22 ± 1	83 ± 3	82 ± 0	133 ± 7	-11.8 ± 1.8
	15	3.9 ± 0.4	20 ± 1	87 ± 0	83 ± 0	133 ± 2	-10.8 ± 0.3
	20	3.7 ± 0.8	20 ± 2	82 ± 3	84 ± 0	129 ± 4	-11.4 ± 0.6
	25	3.5 ± 0.2	20 ± 1	84 ± 3	84 ± 0	126 ± 1	-11.4 ± 0.5
VC45kPCL	5	3.9 ± 0.1	21 ± 1	85 ± 2	85 ± 0	136 ± 2	-11.0 ± 1.4
	10	3.5 ± 0.8	19 ± 1	87 ± 2	85 ± 0	133 ± 0	-11.4 ± 0.5
	15	3.6 ± 0.4	20 ± 1	85 ± 3	87 ± 0	129 ± 4	-11.7 ± 0.5
	20	2.9 ± 0.4	19 ± 1	82 ± 1	88 ± 0	126 ± 0	-11.1 ± 0.2
	25	3.3 ± 0.3	20 ± 1	83 ± 1	88 ± 0	123 ± 2	-11.6 ± 0.5

Table 22: Photorheological measurement results of formulations containing DVA, 15 db% thiol (**Thiol 2**), 0.5 wt% Ivocerin and 0.02 wt% PYR. **Ref. Thiol 2** (without additive); containing additional 5-25 wt% **VCxkPCL**.

additive	**additive [wt%]**	**t_{gel} [s]**	**DBC_{gel}** [%]	**t_{95}** [s]	**DBC_{final}** [%]	**G'_{max}** [kPa]	**F_{Nmax}** [N]
Ref. Thiol 2	0	9.1 ± 0.3	20 ± 0	104 ± 6	74 ± 0	148 ± 1	-11.3 ± 0.9
VC10kPCL	5	7.3 ± 0.1	20 ± 1	88 ± 3	82 ± 1	146 ± 4	-13.8 ± 1.1
	10	6.1± 0.6	20 ± 2	89 ± 4	82 ± 0	142 ± 2	-13.6 ± 1.2
	15	6.3 ± 0.6	20 ± 1	94 ± 5	83 ± 0	139 ± 2	-13.7 ± 0.5
	20	6.1 ± 0.3	20 ± 0	90 ± 1	84 ± 0	136 ± 1	-12.9 ± 0.6
	25	6.5 ± 0.8	21 ± 2	87 ± 2	84 ± 0	133 ± 2	-13.4 ± 1.2
VC45kPCL	5	6.7 ± 0.3	19 ± 1	91 ± 1	80 ± 0	154 ± 2	-12.0 ± 1.4
	10	6.8 ± 0.4	21 ± 0	94 ± 4	82 ± 0	151 ± 2	-11.7 ± 0.8
	15	6.6 ± 0.0	21 ± 1	95 ± 3	82 ± 0	146 ± 3	-10.4 ± 0.1
	20	6.6 ± 0.4	22 ± 1	92 ± 0	83 ± 0	144 ± 1	-9.9 ± 0.2
	25	5.6 ± 0.0	20 ± 1	91 ± 1	84 ±	140 ± 4	-9.6 ± 0.3

2.2. Investigation of thermomechanical properties *via* DMTA

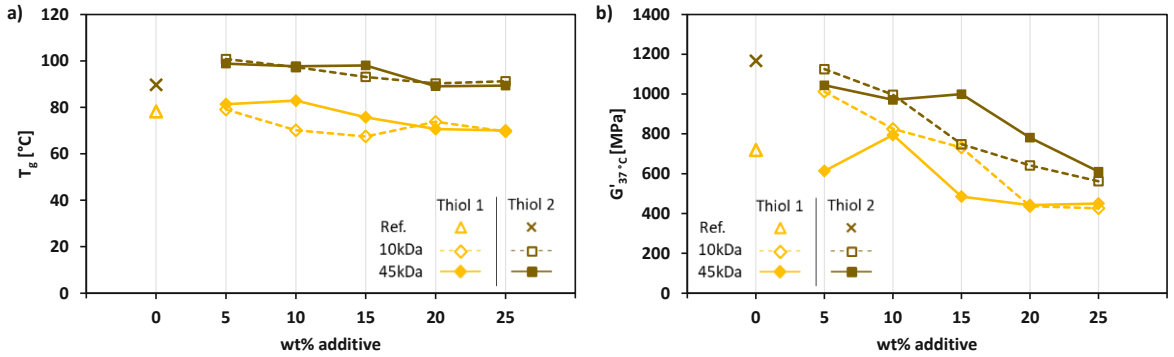

Figure 64: Results of DMTA measurements of formulations containing DVA, 15 db% thiol, 0.5 wt% Ivocerin and 0.02 wt% PYR. **Ref. Thiol 1** (without additive): yellow triangle; containing additional 5-25 wt% **NBxkPCL** (yellow diamonds) or **Ref. Thiol 2** (without additive): ochre cross; containing additional 5-25 wt% **NBxkPCL** (ochre squares). Empty symbols with dashed lines indicate **NB10kPCL** and full symbols with solid lines indicate **NB45kPCL**. The straight lines are only for a better visibility. a) Obtained values for the glass transition temperature (T_g); b) obtained values for the storage modulus at body temperature ($G'_{37\,°C}$).

Table 23: Results of DMTA measurements of formulations containing DVA, 15 db% thiol (**Thiol 1**), 0.5 wt% Ivocerin and 0.02 wt% PYR. **Ref. Thiol 1** (without additive); containing additional 5-25 wt% **NBxkPCL**.

additive	additive [wt%]	T_g [°C]	$G'_{25°C}$ [MPa]	$G'_{37°C}$ [MPa]	G'_R [MPa]
Ref. Thiol 1	0	78	899	718	157
NB10kPCL	5	79	1190	1010	236
	10	70	982	825	214
	15	67	892	731	191
	20	74	542	437	111
	25	70	536	426	117
NB45kPCL	5	81	757	613	115
	10	83	954	795	139
	15	76	636	485	107
	20	71	573	442	120
	25	70	589	450	126

Table 24: Results of DMTA measurements of formulations containing DVA, 15 db% thiol (**Thiol 2**), 0.5 wt% Ivocerin and 0.02 wt% PYR. **Ref. Thiol 2** (without additive); containing additional 5-25 wt% **NBxkPCL**.

additive	additive [wt%]	T_g [°C]	$G'_{25°C}$ [MPa]	$G'_{37°C}$ [MPa]	G'_R [MPa]
Ref. Thiol 2	0	90	1340	1170	234
NB10kPCL	5	101	1280	1130	157
	10	97	1150	997	148
	15	93	877	748	129
	20	90	751	642	141
	25	91	673	562	128
NB45kPCL	5	99	1210	1040	154
	10	98	1150	971	161
	15	98	1210	1000	177
	20	89	943	781	-
	25	89	752	610	135

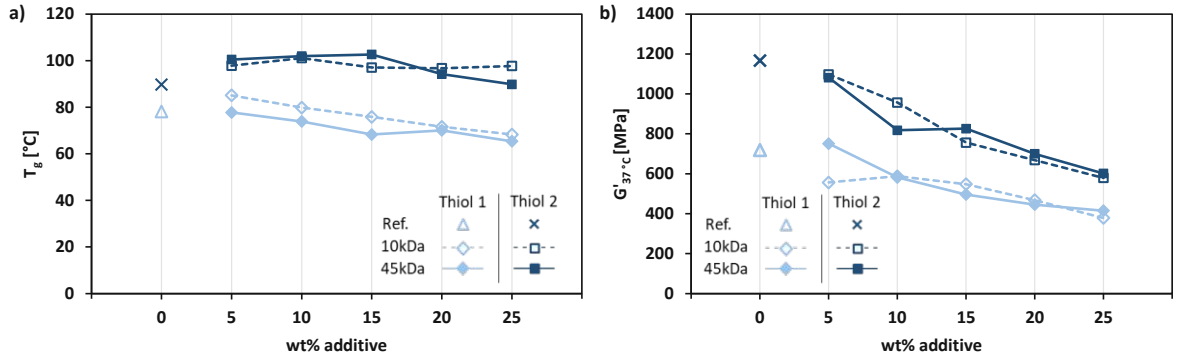

Figure 65: Results of DMTA measurements of formulations containing DVA, 15 db% thiol, 0.5 wt% Ivocerin and 0.02 wt% PYR. **Ref. Thiol 1** (without additive): light blue triangle; containing additional 5-25 wt% **VCxkPCL** (light blue diamonds) or **Ref. Thiol 2** (without additive): dark blue cross; containing additional 5-25 wt% **VCxkPCL** (dark blue squares). Empty symbols with dashed lines indicate **VC10kPCL** and full symbols with solid lines indicate **VC45kPCL**. The straight lines are only for a better visibility. a) Obtained values for the glass transition temperature (T_g); b) obtained values for the storage modulus at body temperature ($G'_{37\,°C}$).

Table 25: Results of DMTA measurements of formulations containing DVA, 15 db% thiol (**Thiol 1**), 0.5 wt% Ivocerin and 0.02 wt% PYR. **Ref. Thiol 1** (without additive); containing additional 5-25 wt% **ACxkPCL**.

additive	additive [wt%]	T_g [°C]	$G'_{25°C}$ [MPa]	$G'_{37°C}$ [MPa]	G'_R [MPa]
Ref. Thiol 1	0	78	899	718	157
VC10kPCL	5	85	674	556	106
	10	80	713	588	128
	15	76	686	548	131
	20	72	589	468	111
	25	68	488	379	101
VC45kPCL	5	78	934	751	157
	10	74	747	582	134
	15	68	664	496	124
	20	70	598	445	114
	25	65	564	415	108

Table 26: Results of DMTA measurements of formulations containing DVA, 15 db% thiol (**Thiol 2**), 0.5 wt% Ivocerin and 0.02 wt% PYR. **Ref. Thiol 2** (without additive); containing additional 5-25 wt% **VCxkPCL**.

additive	additive [wt%]	T_g [°C]	$G'_{25°C}$ [MPa]	$G'_{37°C}$ [MPa]	G'_R [MPa]
Ref. Thiol 2	0	90	1340	1170	234
VC10kPCL	5	98	1260	1100	191
	10	101	1100	957	171
	15	97	891	756	152
	20	97	794	669	139
	25	98	692	579	129
VC45kPCL	5	100	1240	1080	189
	10	102	968	818	147
	15	103	987	826	156
	20	94	860	700	155
	25	90	762	601	138

2.3. Investigation of mechanical properties *via* tensile tests

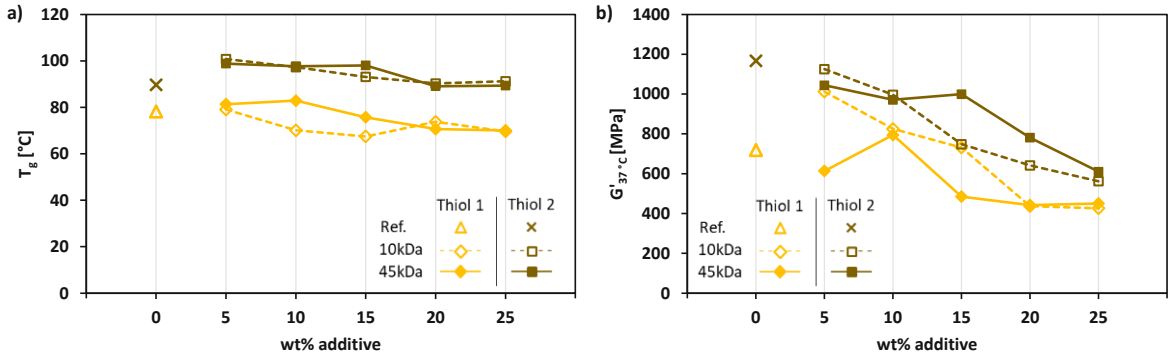

Figure 66: Results of tensile test measurements of formulations containing DVA, 15 db% thiol, 0.5 wt% Ivocerin and 0.02 wt% PYR. **Ref. Thiol 1** (without additive): yellow triangle; containing additional 5-25 wt% **NBxkPCL** (yellow diamonds) or **Ref. Thiol 2** (without additive): ochre cross; containing additional 5-25 wt% **NBxkPCL** (ochre squares). Empty symbols with dashed lines indicate NB10kPCL and full symbols with solid lines indicate **NB45kPCL**. The straight lines are only for a better visibility. a) Obtained values for the tensile strength σ; b) obtained values for the elongation at break ε_B.

Table 27: Results of tensile test measurements of formulations containing DVA, 15 db% thiol (**Thiol 1**), 0.5 wt% Ivocerin and 0.02 wt% PYR. **Ref. Thiol 1** (without additive); containing additional 5-25 wt% **NBxkPCL**.

additive	**additive [wt%]**	**σ [MPa]**	**ε_B [%]**	**U_T [MJ·m^{-3}]**
Ref. Thiol 1	0	34.2 ± 3.1	4.8 ± 0.8	0.9 ± 0.3
NB10kPCL	5	27.8 ± 1.2	4.4 ± 0.8	0.7 ± 0.1
	10	33.4 ± 1.9	7.6 ± 1.0	1.6 ± 0.3
	15	27.3 ± 3.2	5.4 ± 1.5	1.0 ± 0.2
	20	26.4 ± 3.8	9.2 ± 3.1	1.7 ± 0.8
	25	25.0 ± 3.1	9.6 ± 2.4	1.6 ± 0.6
NB45kPCL	5	32.6 ± 2.6	6.8 ± 1.1	1.5 ± 0.4
	10	32.4 ± 2.3	10.7 ± 2.1	2.4 ± 0.7
	15	31.3 ± 0.8	13.3 ± 0.8	2.8 ± 0.3
	20	29.4 ± 2.2	12.2 ± 2.0	2.4 ± 0.6
	25	28.7 ± 3.1	13.9 ± 2.6	2.7 ± 0.7

Table 28: Results of tensile test measurements of formulations containing DVA, 15 db% thiol (**Thiol 2**), 0.5 wt% Ivocerin and 0.02 wt% PYR. **Ref. Thiol 2** (without additive); containing additional 5-25 wt% **NBxkPCL**.

additive	additive [wt%]	σ [MPa]	ε_B [%]	U_T [MJ·m^{-3}]
Ref. Thiol 2	0	47.0 ± 1.3	4.7 ± 0.2	1.3 ± 0.1
NB10kPCL	5	42.7 ± 4.2	6.0 ± 2.0	1.7 ± 0.9
	10	40.9 ± 3.5	6.3 ± 1.3	1.7 ± 0.5
	15	39.0 ± 1.8	9.6 ± 1.3	2.6 ± 0.5
	20	31.5 ± 2.8	7.6 ± 1.7	1.6 ± 0.5
	25	31.9 ± 1.3	9.9 ± 1.1	2.2 ± 0.4
NB45kPCL	5	40.6 ± 1.7	7.0 ± 1.6	1.9 ± 0.5
	10	39.6 ± 3.5	10.0 ± 2.6	2.8 ± 1.1
	15	36.2 ± 1.0	9.7 ± 1.0	2.4 ± 0.3
	20	31.2 ± 2.1	10.5 ± 1.8	2.2 ± 0.6
	25	32.7 ± 2.0	14.7 ± 1.5	3.2 ± 0.5

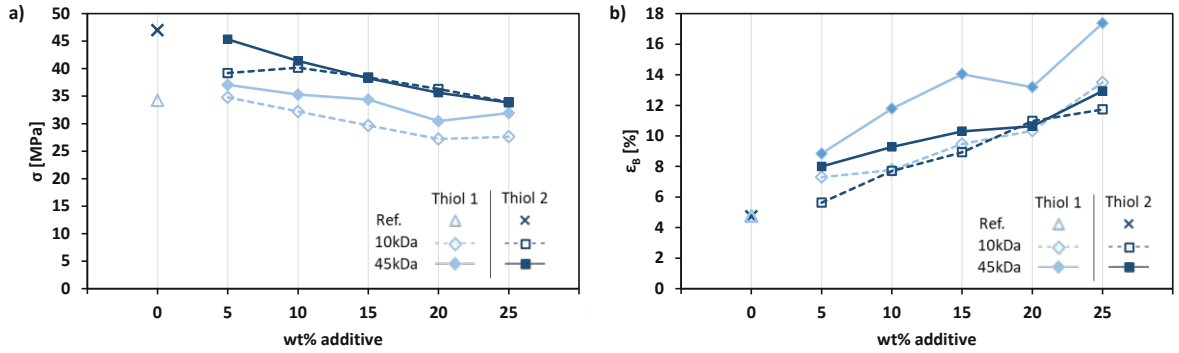

Figure 67: Results of tensile test measurements of formulations containing DVA, 15 db% thiol, 0.5 wt% Ivocerin and 0.02 wt% PYR. **Ref. Thiol 1** (without additive): light blue triangle; containing additional 5-25 wt% **VCxkPCL** (light blue diamonds) or **Ref. Thiol 2** (without additive): dark blue cross; containing additional 5-25 wt% **VCxkPCL** (dark blue squares). Empty symbols with dashed lines indicate **VC10kPCL** and full symbols with solid lines indicate **VC45kPCL**. The straight lines are only for a better visibility. a) Obtained values for the tensile strength σ; b) obtained values for the elongation at break ε_B.

Table 29: Results of tensile test measurements of formulations containing DVA, 15 db% thiol (**Thiol 1**), 0.5 wt% Ivocerin and 0.02 wt% PYR. **Ref. Thiol 1** (without additive); containing additional 5-25 wt% **VCxkPCL**.

additive	**additive [wt%]**	**σ [MPa]**	**ε_B [%]**	**U_T [MJ·m^{-3}]**
Ref. Thiol 1	0	34.2 ± 3.1	4.8 ± 0.8	0.9 ± 0.3
VC10kPCL	5	34.8 ± 2.3	7.3 ± 1.5	1.7 ± 0.5
	10	32.2 ± 2.4	7.8 ± 1.7	1.7 ± 0.5
	15	29.7 ± 3.9	9.5 ± 2.7	1.9 ± 0.8
	20	27.2 ± 2.9	10.3 ± 2.4	1.9 ± 0.7
	25	27.6 ± 2.0	13.5 ± 2.0	2.5 ± 0.6
VC45kPCL	5	37.1 ± 2.2	8.8 ± 1.5	2.2 ± 0.5
	10	35.3 ± 1.8	11.8 ± 2.2	2.9 ± 0.7
	15	34.4 ± 0.8	14.0 ± 0.8	3.3 ± 0.2
	20	30.5 ± 2.3	13.2 ± 2.4	2.7 ± 0.7
	25	31.9 ± 2.2	17.4 ± 2.1	3.7 ± 0.7

Table 30: Results of tensile test measurements of formulations containing DVA, 15 db% thiol (**Thiol 2**), 0.5 wt% Ivocerin and 0.02 wt% PYR. **Ref. Thiol 2** (without additive); containing additional 5-25 wt% **VCxkPCL**.

additive	additive [wt%]	σ [MPa]	ε_B [%]	U_T [MJ·m^{-3}]
Ref. Thiol 2	0	47.0 ± 1.3	4.7 ± 0.2	1.3 ± 0.1
VC10kPCL	5	39.2 ± 5.4	5.6 ± 1.8	1.6 ± 0.8
	10	40.2 ± 2.5	7.7 ± 1.3	2.1 ± 0.5
	15	38.4 ± 1.0	8.9 ± 0.7	2.3 ± 0.3
	20	36.3 ± 2.1	11.0 ± 1.9	2.8 ± 0.7
	25	33.9 ± 2.1	11.7 ± 1.8	2.7 ± 0.6
VC45kPCL	5	45.3 ± 2.2	8.0 ± 1.4	2.6 ± 0.6
	10	41.4 ± 1.5	9.3 ± 0.9	2.6 ± 0.4
	15	38.3 ± 3.5	10.3 ± 2.4	2.7 ± 0.9
	20	35.6 ± 3.5	10.6 ± 2.3	2.6 ± 0.9
	25	33.8 ± 1.8	12.9 ± 1.3	2.9 ± 0.5

2.4. 3-point bending tests

3-point bending tests from selected materials (references, 5 and 25wt% of **ACxkPCL**) were performed to further corroborate the results of the tensile tests (see chapter 3.2.3).

These experiments were done with rectangular shaped specimens (2x5x40 mm³) on a Zwick Z050 testing machine with a span length of 32 mm and a fin of 2.5 mm radius. The crosshead speed was set to 1 mm·min^{-1} and the standard strain σ_{fC} was set to 7%. Analysis was done with the testXpert II testing software.

As expected, these results show the same trend.

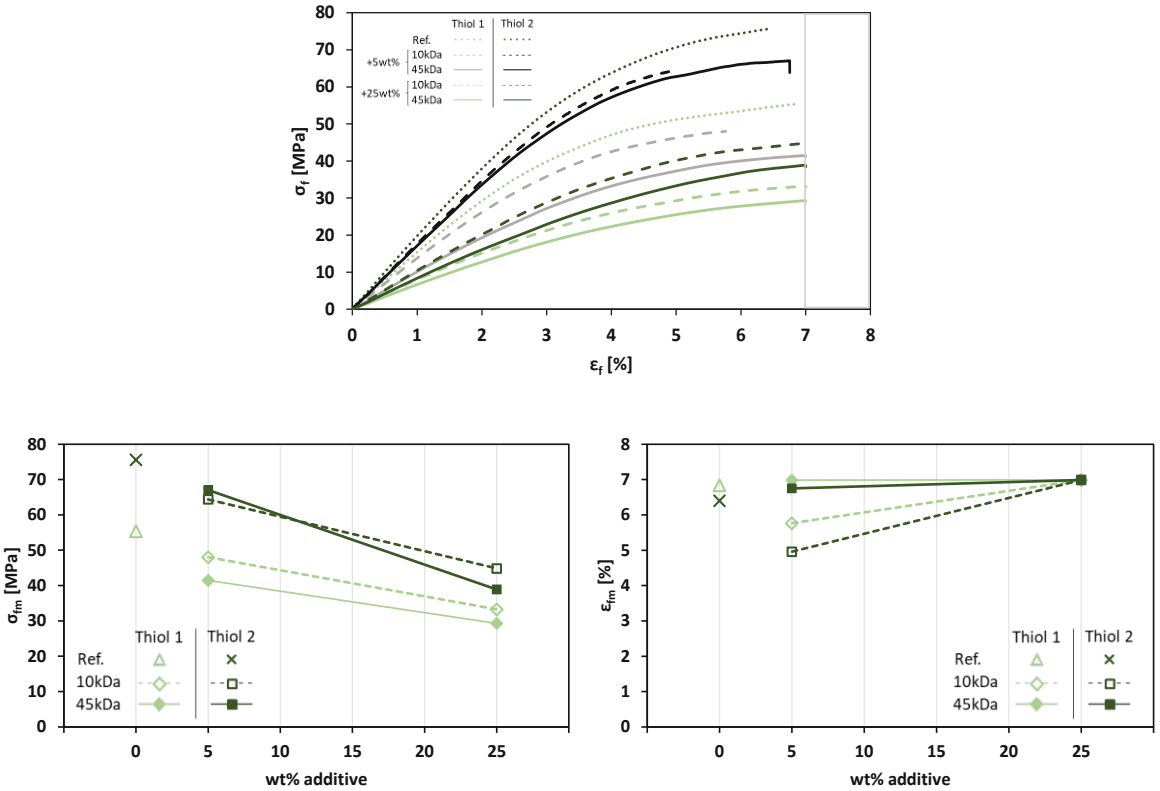

Figure 68: Results of 3-point bending experiments of formulations containing DVA, 15 db% thiol, 0.5 wt% Ivocerin and 0.02 wt% PYR. Empty symbols with dashed lines indicate **AC10kPCL** and full symbols with solid lines indicate AC45kPCL. Exemplary curves (above) and obtained values for the strength σ_{fm} and elongation ε_{fm} at room temperature.

Table 31: Results of 3-point bending experiments of formulations containing DVA, 15 db% thiol, 0.5 wt% Ivocerin and 0.02 wt% PYR. Ref. Thiol (without additive); containing additional 5 or 25 wt% **ACxkPCL**

Thiol	additive	additive [wt%]	σ_{fM} [MPa]	ε_{fm} [%]
Thiol 1	**Ref. Thiol 1**	0	55.4	6.8
	AC10kPCL	5	48.0	5.8
		25	33.3	6.9*
	AC45kPCL	5	41.5	6.9*
		25	29.3	6.9*
Thiol 2	**Ref. Thiol 2**	0	75.6	6.4
	AC10kPCL	5	64.4	5.0
		25	44.8	6.9*
	AC45kPCL	5	67.1	6.8
		25	38.9	6.9*

*Indicates no break (standard strain σ_{fC} was set to 7%).

2.5. Rheology measurements of formulations containing functionalized PCLs

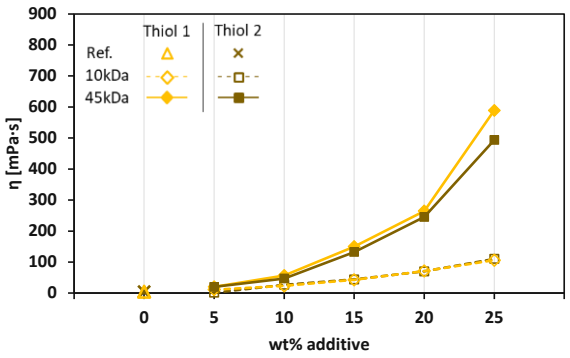

Figure 69: Rheological measurement results of formulations containing DVA, 15 db% thiol, 0.5 wt% Ivocerin and 0.02 wt% PYR. **Ref. Thiol 1** (without additive): yellow triangle; containing additional 5-25 wt% **NBxkPCL** (yellow diamonds) or **Ref. Thiol 2** (without additive): ochre cross; containing additional 5-25 wt% **NBxkPCL** (ochre squares). Empty symbols with dashed lines indicate NB10kPCL and full symbols with solid lines indicate **NB45kPCL**. The straight lines are only for a better visibility.

Table 32: Rheological measurement results of formulations containing DVA, 15 db% thiol (**Thiol 1**), 0.5 wt% Ivocerin and 0.02 wt% PYR. **Ref. Thiol 1** (without additive); containing additional 5-25 wt% **NBxkPCL**.

additive	**additive [wt%]**	**η [mPa·s]**
Ref. Thiol 1	0	4.4
NB10kPCL	5	11.4
	10	23.4
	15	42.7
	20	71.1
	25	106.0
NB45kPCL	5	20.4
	10	56.9
	15	150.0
	20	264.8
	25	589.0

Table 33: Rheological measurement results of formulations containing DVA, 15 db% thiol (**Thiol 2**), 0.5 wt% Ivocerin and 0.02 wt% PYR. **Ref. Thiol 2** (without additive); containing additional 5-25 wt% **NBxkPCL**.

additive	**additive [wt%]**	**η [mPa·s]**
Ref. Thiol 2	0	4.7
NB10kPCL	5	1.3
	10	26.9
	15	44.1
	20	70.0
	25	110.2
NB45kPCL	5	19.9
	10	47.1
	15	132.3
	20	245.6
	25	493.5

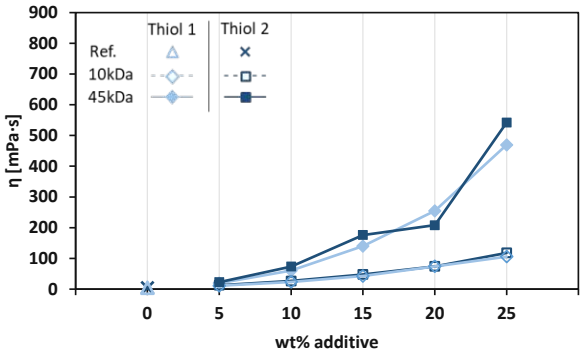

Figure 70: Rheological measurement results of formulations containing DVA, 15 db% thiol, 0.5 wt% Ivocerin and 0.02 wt% PYR. **Ref. Thiol 1** (without additive): light blue triangle; containing additional 5-25 wt% **VCxkPCL** (light blue diamonds) or **Ref. Thiol 2** (without additive): dark blue cross; containing additional 5-25 wt% **VCxkPCL** (dark blue squares). Empty symbols with dashed lines indicate **VC10kPCL** and full symbols with solid lines indicate **VC45kPCL**. The straight lines are only for a better visibility.

Table 34: Rheological measurement results of formulations containing DVA, 15 db% thiol (**Thiol 1**), 0.5 wt% Ivocerin and 0.02 wt% PYR. **Ref. Thiol 1** (without additive); containing additional 5-25 wt% **VCxkPCL**.

additive	**additive [wt%]**	**η [mPa·s]**
Ref. Thiol 1	0	4.4
VC10kPCL	5	11.1
	10	23.6
	15	42.7
	20	74.1
	25	106.0
VC45kPCL	5	19.4
	10	60.4
	15	140.0
	20	254.6
	25	469.4

Table 35: Rheological measurement results of formulations containing DVA, 15 db% thiol (**Thiol 2**), 0.5 wt% Ivocerin and 0.02 wt% PYR. **Ref. Thiol 2** (without additive); containing additional 5-25 wt% **VCxkPCL**.

additive	**additive [wt%]**	**η [mPa·s]**
Ref. Thiol 2	0	4.7
VC10kPCL	5	12.7
	10	26.6
	15	47.8
	20	74.4
	25	118.0
VC45kPCL	5	22.9
	10	73.4
	15	176.0
	20	208.0
	25	542.0

3. Influence of broad MW distribution

Another concept to further increase the toughness of materials is to broaden the polydispersity index (PDI) of the toughness enhancer. Therefore, different molecular weights (10kDa and 45kDa) of the norbornene functionalized PCL were mixed. The first trials were made with additional 10wt% toughness enhancer and these 10wt% were split into different ratios of **NB10kPCL** and **NB45kPCL**. Here, three different ratios were prepared (75%:25%, 50%:50% and 25%:75% of 10kDa:45kDa). The samples were named as **NB(x%10kPCL, y%45k)PCL**, where x indicates the percentage of **NB10kPCL** and y of **NB45kPCL**. The results of the tensile test for these mixtures and of formulations containing only 10wt% of one additive are shown in Figure 71.

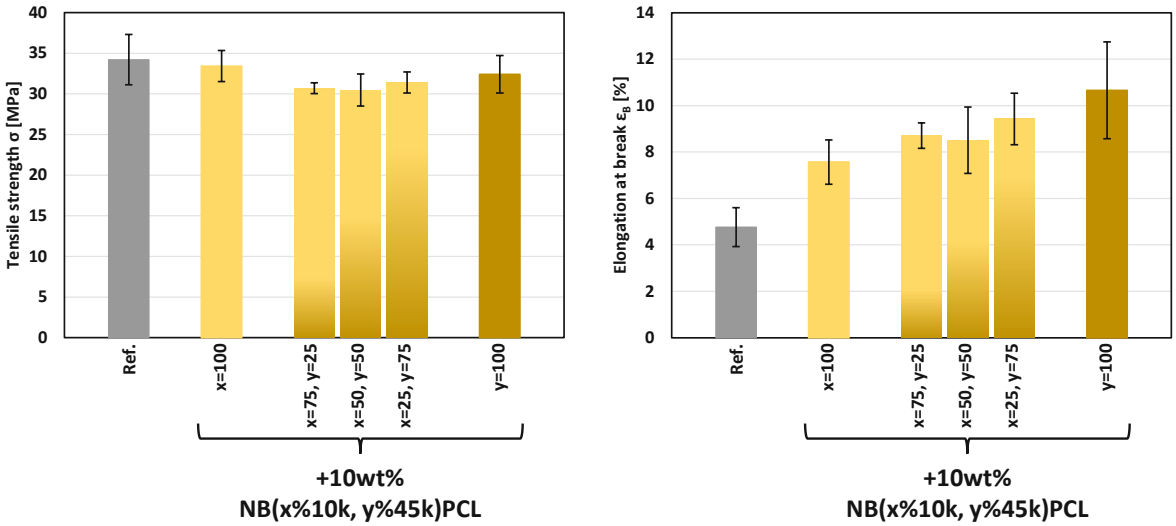

Figure 71: Collected data from tensile tests for tensile strength (σ) and elongation at break (ε_B) for the standard formulation containing the thiol **Thiol 1** (without additive (Ref.)) and additional 10wt% of the norbornene modified toughness enhancer (10kDa and 45kDa) and mixtures NB(x%10kPCL, y%45k)PCL of the different molecular weights.

The results showed that the mixture of different molecular weights does not influence the tensile strength. However, the elongation at break is in between the formulations containing only one MW. Nevertheless, the formulations with **NB45kPCL** showed the best results.

4. Comparison stress-relaxation tests

Stress relaxation tests can describe the long-time behavior of materials. Here, a defined strain at a constant temperature is applied to the polymer sample, and the stress is recorded as a function of time. Stress relaxation is only possible on a molecular level (molecular relaxation of viscous flow).

Stress relaxation experiments were conducted at 37 °C under ambient atmosphere as a three-point bending test and a strain of 2% was applied to the sample for 120 min. The different modifications (**NBxkPCL** and **ACxkPCL**) with varying molecular weights should be investigated. Additionally, formulations with **NB45kPCL** and different thiol were compared and depicted in Figure 72.

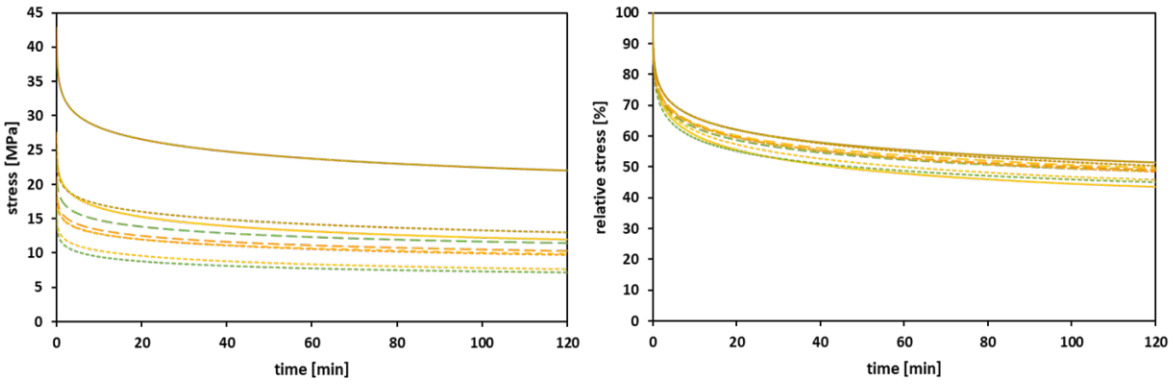

Figure 72: Stress relaxation of the photopolymer specimens of **Ref. Thiol 1** (—), +10wt% NB10kPCL (– –), +10wt% NB45kPCL (▪▪▪), +10wt% NB(75%10k+25%45k)PCL (▪▪▪), +10wt% NB(25%10k+75%45k)PCL (– –), +10wt% AC10kPCL (– –), +10wt% AC45kPCL (▪▪▪) and **Ref. Thiol 2** (—), and +10wt% NB45kPCL (▪▪▪) over time.

The reference **Ref.Thiol 1** exhibited maximum stress of 28 MPa and decreased to 12 MPa after two hours. After adding the toughness enhancer **NB10PCL** (10wt%) the stress dropped to 20 MPa and reached a level of 10 MPa at the end of the measurement. In comparison, the values for the specimen with 10wt% **NB45kPCL** are slightly lower, starting with 17 MPa and ending with 8 MPa. The specimens with mixtures of the two molecular weights showed values in between. Specimens with **ACxkPCL** showed the same values as the norbornene modified toughness enhancers with the same molecular weight. Moreover, specimens with **Thiol 2** were also measured. The reference (**Ref. Thiol 2**) showed significantly higher values with 43 MPa stress initially and dropped to 22 MPa. After the addition of 10wt% **NB45kPCL** the stress decreased to 26 MPa and further decreased to 13 MPa. Nevertheless, consideration of the relative remaining stress, all formulations dropped about 50-60%.

B. Storage stability studies of NB-thiol containing formulations

The interest in thiol-ene chemistry increased during the last decades, as it shows huge advantages for tailoring the physical and mechanical properties of the network structures. For example, higher network homogeneity can be reached with lower shrinkage and delayed gelation during polymerization. The thiol-ene step-growth radical polymerization leads, therefore, to reduced brittleness. The reactivity of monomers depends on the resonance stabilization of the formed radicals of the monomers. The reactivity of variable "ene" groups towards thiol-ene conjugation is shown in Figure 73. A low resonance stabilization leads to a high reactivity towards chain transfer reaction with thiols, which is favorable during polymerization.[296]

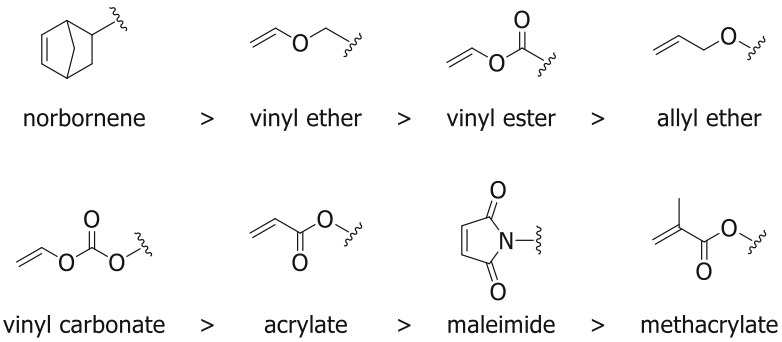

Figure 73: Reactivity sequence of variable "ene" groups towards thiol-ene conjugation.[296]

Unfortunately, a severe drawback is the limited shelf-life, ranging from seconds to a few weeks, but generally, they are quite low. Reasons for this low stability were proposed by Holy *et al.*, which are (1) initiation of a thermal free-radical reaction upon decomposition of peroxide impurities, (2) the initiated polymerization due to thiyl radical intermediates, which were formed by the reaction of hydroperoxide impurities, (3) nucleophilic addition of thiol to the "ene" functionality, which was catalyzed by a base or (4) the spontaneous polymerization due to the thiol-ene reaction of generated radicals upon a ground-state charge transfer complex.[306] The shelf life can be extended by adding a stabilizer to the thiol-ene mixtures, avoiding undesired premature polymerization at room temperature. Stabilizers described in the literature are, *e.g.,* phosphonic acid, triphenyl phosphite or aluminium cupferronate. Other thermal stabilizers like pyrogallol, hydroquinone and catechol were presented in the early 1990s by Klemm *et al.*[306], Moszner *et al.*[307] and others, whereas pyrogallol was proposed as the most successful.[308] But, too high stabilizer concentrations can slow down or inhibit the radical photopolymerization and therefore, acidic co-stabilizers were investigated as they are proposed to assist the stabilization effect. Esfandiari *et al.*[308] proved that combining the phosphonic acid MA154 with pyrogallol showed a significantly higher thermal stabilization of

thiol-ene systems than the single components. Unfortunately, pyrogallol is cancerogenic and may cause tumors.[309] For this reason, this study has aimed to investigate radical stabilizers, which will not harm the surrounding tissue and inhibit spontaneous gelation of the formulation.

A promising alternative to pyrogallol (**PYR**) is the stabilizer n-propyl gallat (**nPG**), as it showed the best results in studies of the antioxidation of fatty acids.[310, 311] Further, it is already used in the cosmetics and food industry. It is practically non-toxic when applied to the skin and nontumorigenic and -carcinogenic in *in vivo* animal studies when injected.[312] In addition, other stabilizers such as 5-tert-butylpyrogallol (**tBPYR**), 3,4,5-trihydroxybenzaldehyde (**3,4,5-THB**) and 2,3,4-trihydroxybenzalhdeyde (**2,3,4-THB**) will be tested. Co-stabilization is possible with the acidic co-additive MA154 (**MA**). All structures of the different radical stabilizers are depicted in Figure 74.

1. Assessing radical inhibitors

The different stabilizers should be tested for the storage stability study of formulations containing norbornene components in combination with thiols. Therefore, the monofunctional norbornene monomer 2-(hydroxymethyl)-5-norbornene (**NB-MeOH**) and the thiol **Thiol 1** were mixed in an equimolar ratio referenced to the functionalities. Samples were stored at 37°C in brown flasks to avoid photo-induced reactions. The reference (**Ref.**) is a formulation containing NB-MeOH and **Thiol 1** but without any stabilizer. Then, different formulations were prepared with varying stabilizers such as **PYR**, **nPG**, **tBPYR**, **3,4,5-THB** and **2,3,4-THB**.

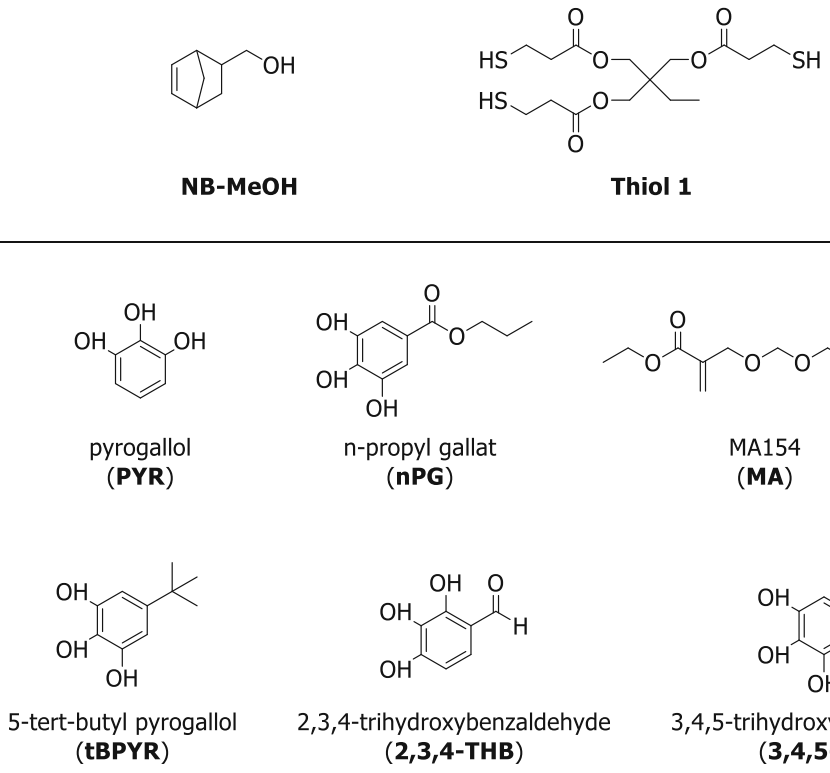

Figure 74: Components for the storage stability study of the monofunctional 5-norbornene-2-methanol (NB-MeOH) and **Thiol 1** as thiol.

The efficiency of the different radical stabilizers was evaluated by ^{1}H-NMR spectroscopy. For this purpose, the methyl group of **Thiol 1** was set to three protons (0.90 ppm) and used as an internal standard. The decrease in the proton signal of the norbornene double bond (6.16-5.59 ppm) was observed and thus the stabilization effect was evaluated. The formulations were measured in deuterated chloroform ($CDCl_3$) immediately after preparation. Afterwards, they were stored at elevated temperatures, and aliquots were taken and measured again after defined time frames. The decrease of the characteristic double bond signal was followed over time, and the norbornene concentration was plotted against the time (Figure 75).

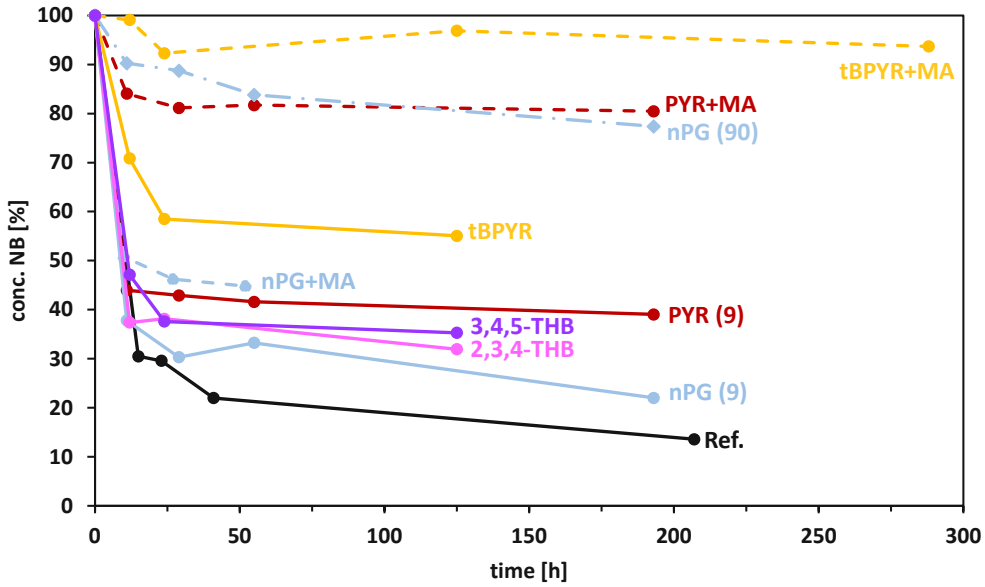

Figure 75: Storage stability of formulations without stabilizer (Ref.) in black ● with pyrogallol (**PYR**) in red ●, n-propylgallat (**nPG**) in light blue (● for 9mM and ◆ for 90mM), 5-tert-butylpyrogallol (**tBPYR**) in yellow ●, 2,3,4-trihydroxybenzaldehyde (**2,3,4-THB**) in pink ● and 3,4,5-trihydroxybenzaldehyde (**3,4,5-THB**) in purple ●. All stabilizers were added as 9mM concentration is otherwise noted in brackets. Dashed lines indicate the addition of 90mM of the phosphonic acid MA154 (MA) in the respective colors for the study of storage stability of norbornenes with thiol at 37°C. For a better visibility, the symbols were connected with straight lines.

Figure 75 shows that the norbornene concentration of a formulation without stabilizer decreased by 70% within the first 12 h. Unfortunately, formulations containing the stabilizers **PYR**, **nPG (9)**, **2,3,4-THB** and **3,4,5-THB** in a concentration of 9 mM show the same values and hence, did not significantly increase the stability. The formulation of **tBPYR** showed better stabilization than the others. Here, only 30% of the norbornene double bonds vanished. n-Propyl gallat is a nontoxic compound; therefore, the concentration was increased to 90 mM, and the stabilization effect was investigated again. Here, 70% of norbornene functionality is still present after the first 12 h, but the high concentration may lead to suppressed polymerization rates. The literature described a good stabilization effect of **PYR** in combination with MA154.[308] This NMR-experiment proved this statement again.

For this reason, the co-additive MA154 was added in a conc. of 90 mM to formulations containing **nPG** and **tBPYR** in low concentrations (9 mM). However, no stabilization was observed for the formulation containing **nPG(9)**. However, the norbornene-thiol formulation containing **tBPYR** showed excellent stability.

In order to investigate the influence of the stabilizers on the reactivity of the photopolymerization, photo-DSC measurements were conducted.

2. Photo reactivity of stabilized thiol-norbornene formulations

Adding a high stabilizer concentration may slow down or inhibit radical photopolymerization. For this reason, the best-performing stabilizers will be tested for their photoreactivity *via* photo-DSC. Freshly prepared formulations of NB-MeOH, **Thiol 1** (equimolar), 0.5wt% Ivocerin as photoinitiator and stabilizers were mixed and measured with a 400-500 nm wavelength and a light intensity of ~18 mW·cm^{-2}. Figure 76 shows a section of the photo-DSC curves.

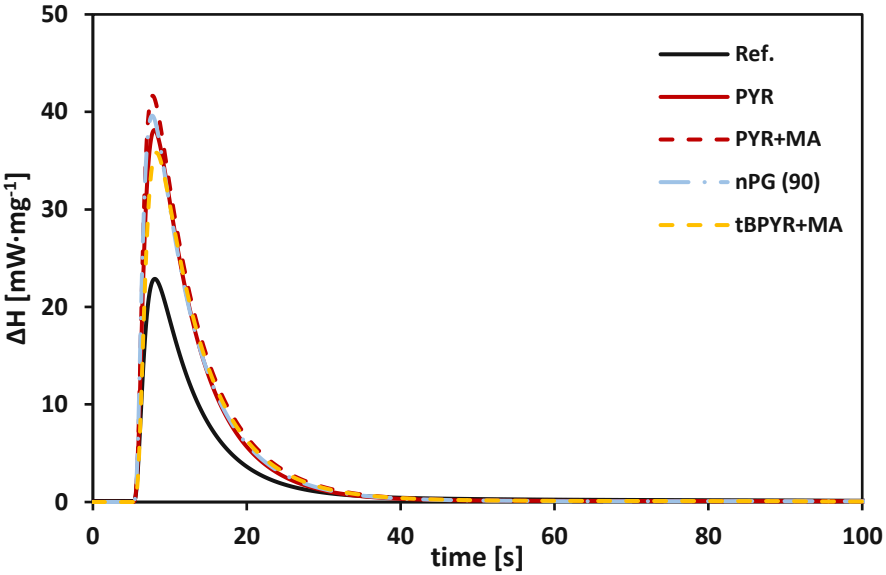

Figure 76: Exothermic photo-DSC curves of formulations containing NB-MeOH, **Thiol 1** (equimolar) and 0.5wt% Ivocerin without stabilizer (Ref., solid black), with 9 mM pyrogallol (**PYR**, solid red), 9mM **PYR** and 90 mM MA154 (**PYR+MA**, dashed red), 90 mM n-propylgallat (**nPG (90)**, dash-dotted blue), and 9 mM 5-tert-butylpyrogallol and 90 mM MA154 (**tBPYR+MA**, dashed yellow) at room temperature.

The three best stabilizer from the above described experiment (Figure 75) were chosen for the photo-reactivity study. For comparison, one formulation was measured without stabilizer (Ref.) and one with 9 mM pyrogallol (b).

The black curve shows the reactivity of a formulation without any stabilizer. The best curve is shown here, but the formulation is unstable, causing the other two measurements to show lower heat deflection ΔH. Besides the reference, formulations with 90 mM **nPG** (dash-dotted blue curve), 9 mM **PYR** (solid red curve), 9 mM **PYR** in combination with 90 mM MA154 (dashed red curve), and 9 mM **tBPYR** + 90 mM MA154 (dashed yellow curve) were investigated. All of them showed excellent reactivity. However, the best performances showed the formulation with **PYR** and MA154. 5-tert-Butylpyrogallol with MA154 showed the lowest heat deflection but still high reactivity. The exact values for the measurements are listed in Table 36.

Table 36: Results of photo-DSC measurements of formulations containing NB-MeOH, **Thiol 1** (equimolar) and 0.5wt% Ivocerin, without stabilizer (Ref.), with 9 mM pyrogallol (**PYR**), 9 mM **PYR** in combination with 90 mM MA154 (**PYR+MA**), 90 mM n-propylgallat (**nPG (90)**), and 9 mM 5-tert-butylpyrogallol in combination with 90 mM MA154 (**tBPYR+MA**).

Formulation	Area [J/g]	t_{max} [s]	Onset [s]	Height [mW/mg]	t_{95} [s]
Ref. (without stabilizer)*	158	9	6	12	106
PYR (9)	311 ± 10	8 ± 0	6 ± 0	35 ± 3	32 ± 2
PYR+MA	353 ± 7	8 ± 0	6 ± 0	41 ± 3	30 ± 1
nPG (90)	319 ± 19	8 ± 0	6 ± 0	38 ± 4	31 ± 1
tBPYR+MA	321 ± 1	8 ± 0	6 ± 0	35 ± 1	32 ± 0

*only the best measurement is shown, due to instability of the formulation.

3. Shelf life stability study of stabilized thiol-norbornene formulations

In order to investigate the shelf life stabilities of formulations containing norbornene monomers in combination with thiols, several stabilzers were added and the viscosities were measured. Therefore, a difunctionalized norbornene should be synthesized, first.

3.1. Synthesis of 2-(5-norbornen-2-yl-carbonyloxy)ethyl 5-norbornene-2-carboxylate (bisNB)

The difunctional norbornene monomer can be synthesized in a two-step synthesis. In the first step, the 5-norbornene-2-carbonyl chloride (**NBCl**) should be formed starting with the carboxylic acid and oxalyl chloride. Then, a esterification reaction with ethylene glycol will led to the desired product 2-(5-norbornen-2-yl-carbonyloxy)ethyl 5-norbornene-2-carboxylate (**bisNB**).

3.1.1. Synthesis of 5-norbornene-2-carbonyl chloride (NBCl)

In the first step NBCl was obtained by the conversion of norbornene carboxylic acid and oxalyl chloride according to Chae *et al.*.[305]

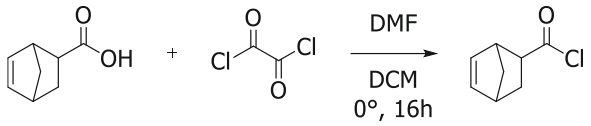

Compound	eq.	n [mmol]	m [g]	V [mL]
5-Norbornene-2-carboxylic acid	1	71	9.76	-
Oxalyl chloride	4	280	-	24
DMF	-	-	-	0.1
dry DCM				50

A three-neck round bottom flask was equipped with a dropping funnel, evacuated, and flushed with argon three times. The flask was charged with oxalyl chloride (4 eq.), DCM (50 mL) and DMF (0.1 mL). A solution of 5-norbornene-2-carboxylic acid (1 eq.) and dry DCM (50 mL) was filled into the dropping funnel and was added dropwise to the precooled oxalyl chloride solution. The ice bath was removed after complete addition and the reaction mixture was stirred for 24 h at room temperature. The residual oxalyl chloride and DCM was removed under reduced pressure. The crude product was distilled at 6 mbar and 47 °C to obtain 5-norbornene-2-carbonyl chloride (NBCl) as colorless liquid in 84% calculated yield.

^{1}H-NMR (400 MHz, $CDCl_3$, δ): 6.32-6.17 (m, 1H, CH=CH endo/exo), 6.17-5.99 (m, 1H, CH=CH exo/endo), 3.49-2.71 (m, 3H, CH), 2.07-1.87 (m, 1H, CH_2, CH_2 bridge), 1.57-1.38 (m, 2H, CH_2, CH_2 bridge), 1.37-1.28 (m, 1H, CH_2, CH_2 bridge) ppm.

^{13}C-NMR (100 MHz, $CDCl_3$, δ): 175.19 (s, C=O), 139.17 (s, CH=CH exo), 138.83 (s, CH=CH endo), 135.02 (s, CH=CH exo), 131.75 (s, CH=CH endo), 56.56 (s, CHC=O endo), 56.45 (s, CHC=O exo), 49.36 (s, CH_2 bridge), 47.29 (s, CH endo), 47.03 (s, CH exo), 46.43 (s, CH_2 bridge), 43.00 (s, CH endo), 42.00 (s, CH exo), 31.29 (s, CH_2 exo), 30.21 (s, CH_2 endo) ppm.

3.1.2. Synthesis of 2-(5-norbornen-2-ylcarbonyloxy)ethyl 5-norbornene-2-carboxylate (bisNB)

BisNB was synthesized using general esterification procedures, including acid chlorides with alcohol.[313]

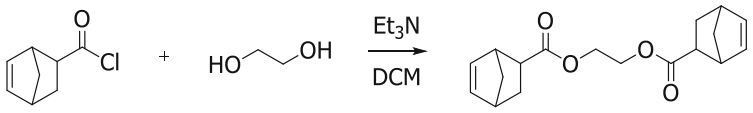

Compound	eq.	n [mmol]	m [g]	V [mL]
NBCl	2.5	249	39.0	-
Ethylene glycol	1	100	-	5.6
Et_3N	2.5	249	-	35
DMF				0.1
dry DCM				270

A 500 mL three-necked round bottom flask was equipped with a dropping funnel. The apparatus was evacuated and purged with argon three times. Afterwards, ethylene glycol (1 eq.), triethylamine (2.5 eq.) and a droplet of DMF were dissolved in 270 mL dry DCM. The dropping funnel was filled with NBCl (2.5 eq.) and was added to the reaction mixture, while cooling via an ice bath. The mixture was stirred at room temperature for 16. The formed salts were filtered and the solvent was removed under reduced pressure. The crude product was purified via silica column chromatography (PE:EE 10:1) to yield 62% of the calculated yield as a colorless viscous liquid.

TLC (PE:EE 10:1) R_f = 0.64

^{1}H-NMR (400 MHz, $CDCl_3$, δ): 6.29 – 5.77 (m, 2x 2H, CH=CH endo/exo), 4.47 – 3.91 (m, 4H, -OCH2CH2O-), 3.32 – 2.66 (m, 6H, 6x CH), 2.31 – 0.98 (m, 6H, 2x CH2, 2x CH2 bridge) ppm.

^{13}C-NMR (100 MHz, $CDCl_3$, δ): 174.52, 137.80, 132.40, 62.02, 49.62, 45.60, 43.42, 42.55, 29.27 ppm.

4. Investigation of preliminary polymerization of stabilized thiol-norbornene formulations

For the reference system (**Ref.**), the synthesized **bisNB** was mixed with the trifcuntional thiol **Thiol 1**. Unfortunately, this mixture was highly reactive and polymerized during the mixing process. Therefore, no measurements were possible. For the other formulations, **bisNB** was mixed with the different stabilizers and then, the thiol was added. Afterwards, the formulations were mixed for about one minute until the formulations were homogenous.

The viscosity of the freshly prepared formulations were measured immediately and the values of the first measurements were set as zero-point for each formulation. The prepared formulations were stored at 37 °C and measured after 4 h, 24 h, 2 d, 3 d, 5 d and 7 d.

Viscosity measurements were conducted by using a Physica MCR 300 Modular Compact Rheometer from Anton Paar. 75 µL of the freshly prepared sample was loaded on the plate and a Peltier temperature control unit to keep the temperature stable at 25 °C and a CP25 (cone-plate system) was used. For one minute, the temperature was held constant. Then, the shear rate was increased to 100 s^{-1} and afterwards, the rheology measurements were performed at the mentioned shear rate for one minute. The last five measurement points were used to calculate the average viscosity.

Figure 77 shows the increase of the viscosity in the time frame of one week. As stabilizers, 90 mM **nPG** (dash-dotted blue curve), 9 mM **PYR** (solid red curve), 9 mM **PYR** in combination with 90 mM MA154 (dashed red curve), and 9 mM **tBPYR** + 90 mM MA154 (dashed yellow curve) were added.

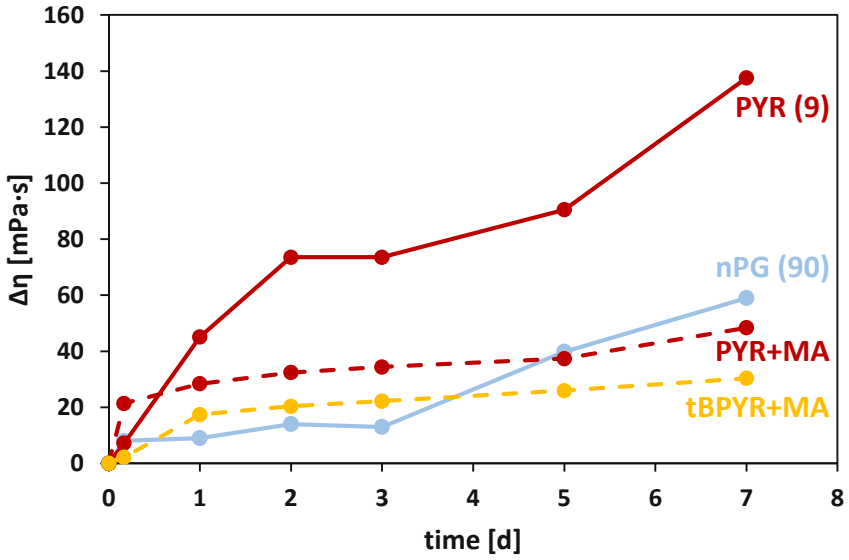

Figure 77: Increase of viscosity at 37 °C of formulations containing bisNB, **Thiol 1** (equimolar) with 9 mM pyrogallol (**PYR (9)**, solid red), 9 mM **PYR** and 90 mM MA154 (**PYR+MA**, dashed red), 90 mM n-propylgallat (**nPG (90)**, dash-dotted blue), and 9 mM 5-tert-butylpyrogallol and 90 mM MA154 (**tBPYR+MA**, dashed yellow).

This experiment showed that within the first three days, the formulation with high concentrations of **nPG (90)**, are the best stabilized ones. However, considering a period of one week, **tBPYR** in combination with MA154 showed the best performance. Here, the viscosity increased by 30 mPa·s. In comparison, after one week the formulations **PYR+MA** increased by 50 mPa·s, **nPG (90)** by 60 mPa·s and **PYR (9)** by 138 mPa·s.

The measured viscosity values are listed in Table 37.

Table 37: Results of viscosity measurements of formulations containing NB-MeOH, **Thiol 1** (equimolar) without stabilizer (Ref.), with 9 mM pyrogallol (**PYR**), 9 mM **PYR** in combination with 90 mM MA154 (**PYR+MA**), 90 mM n-propylgallat (**nPG (90)**), and 9 mM 5-tert-butylpyrogallol in combination with 90 mM MA154 (**tBPYR+MA**).

Formulation	$\eta_{t=0h}$ [mPa·s]	$\eta_{t=4h}$ [mPa·s]	$\eta_{t=1d}$ [mPa·s]	$\eta_{t=2d}$ [mPa·s]	$\eta_{t=3d}$ [mPa·s]	$\eta_{t=5d}$ [mPa·s]	$\eta_{t=7d}$ [mPa·s]
Ref. (without stabilizer)*	-	-	-	-	-	-	-
PYR (9)	89	97	135	163	163	180	227
PYR+MA	85	106	113	117	119	122	133
nPG (90)	114	122	123	128	127	154	173
tBPYR+MA	93	95	110	113	115	119	123

ABBREVIATIONS

abbreviation	meaning
2PP	two-photon induced polymerization
2,3,4-THB	2,3,4-trihydroxybenzaldehyde
3,4,5-THB	3,4,5-trihydroxybenzaldehyde
3D	3 dimensional
4D	4 dimensional
AC10kPCL	poly(caprolactone) diallylcarbonate, 10 kDa
AC45kPCL	poly(caprolactone) diallylcarbonate, 45 kDa
ACE	activated chain end mechanism
ACN	acetonitrile
AIBN	2,2′-azobis(2-methylpropionnitrile)
AM	activated monomer mechanism
AMT	additive manufacturing technology
BHET	bis(2-hydroxyethyl)terephthalate
bisNB	2-(5-norbornen-2-yl-carbonyloxy)ethyl 5-norbornene-2-carboxylate
BOX	3-[benzyloxy(methyl)]-3-ethyloxetane
BTE	bone tissue engineering
CAD	computer-aided-design
$CDCl_3$	deuterated chloroform
CE	3,4-epoxycyclohexylmethyl 3,4-epoxycyclohexanecarboxylate
CEOH	3,4-dihydroxycyclohexyl)methyl-3,4-dihydroxycyclohexanecarboxylate
CHD	1,2-cyclohexanediol
CTA	chain transfer agent
CQ	camphorquinone
DB/db%	double bond/double bond percent
DBC	double bond conversion
DBC_{final}	final double bond conversion
DBC_{gel}	double bond conversion at the gel point
DCM	dichloromethane
DLP	digital light processing
DLP-sla	digital light processing-based stereolithography
dmab	ethyl 4-(dimethylamino)benzoate
DMF	dimethylformamide
dmso	dimethyl sulfoxide
$DMSO\text{-}d_6$	deuterated dimethyl sulfoxide
DMTA	dynamic mechanical analysis
DOD	2,2'-[1,2-ethanediylbis(oxy)]bis-ethanethiol

DOX	3,3'-[oxybis(methylene)]bis[(3-ethyl)oxetane]
DSC	differential scanning calorimetry
DVA	divinyl adipate
DVC	divinyl carbonate
EE	ethylacetate
EO	ethylene oxide
EOM	3-ethyl-3-hydroxymethyloxetane
eq.	equivalent
Et_3N	triethyl amine
FDA	Federal Drug Administration
fdm	fused deposition modeling
$F_{N,max}$	maximum normal force
FT-IR	fourier transformed infrared
G'	storage modulus
G''	loss modulus
$G'_{25°C}$ and $G'_{37°C}$	storage modulus at 25 °C or 37 °C
G'_{final}	final storage modulus
G'_R	storage modulus at the rubber plateau
GPC	gel permeation chromatogaphy
HA	hyaluoronic acid
HAp	hydroxyapatite
HDD(M)A	1,6-hexanediol di(meth)acrylate
HIPS	high-impact polystyrene
homo	highest occupied molecular orbital
ib(m)a	isobornyl (meth)acrylate
IC	internal conversion
IC290	borate-based triarylsulfonium salt Irgacure® 290
isc	intersystem-crossing
IPN	interpenetrating polymer network
IR	infrared
IS	internal standard
ivocerin	bis(4-methoxybenzoyl)diethylgermanium
lumo	lowest unoccupied molecular orbital
kDa	kilo Dalton
L-AMT	lithography-based additive manufacturing technology
laser-sla	laser-based stereolithography
LD_{50}	lethal dose, which causes death of 50% of test subjects
LED	light emission diode
(M)A	(meth)acrylate
Ma154/ MA	(2-((2-(ethoxycarbonyl)allyl)oxy)ethyl)phosphonic acid
M_n	number average molecular weight

MOCl	3-chloromethyl-3-methyloxacyclobutane
M_w	molecular weight
NMR	nuclear magnetic resonance
NB10kPCL	poly(caprolactone) dinorbornene, 10 kDa
NB45kPCL	poly(caprolactone) dinorbornene, 45 kDa
NBCl	5-norbornene-2-carbonyl chloride
NB-MeOH	2-(hydroxymethyl)-5-norbornene
nPG	n-propyl gallat
OEG	3-ethyl-3-(4-hydroxyethyl)oxymethyloxetane
OLG	3-ethyl-3-methanesulfonyloxymethyloxetane
PAG	photoacid generator
pcl	poly(Ɛ-caprolactone)
$Pdac_2$	palladium(II) acetate
PDI	polydispersity index
pe	petroleum ether
peek	poly(etheretherketone)
peg	poly(ethylene glycol)
pga	poly(glycolic acid)
PI	photoinitiator
pla	poly(lactic acid)
P(M)AA	poly((meth)acrylic acid)
pu	poly(urethane)
pTHEB	1,3,5-tris[2-[[(1,1-dimethylethyl)dimethylsilyl]oxy]ethyl]ester-1,3,5-benzenetricarboxylic acid
pTMC-TMA	poly(trimethylene carbonate) with methacrylate endgroups
PVA	poly(vinyl alcohol)
pyr	benzene-1,2,3-triol, pyrogallol
QY	quinoline yellow
rt	room temperature
RT-NIR	real time near infrared
s	singlet state
S160	4,4’-bis[(3-ethyloxetan-3-yl)methoxymethyl]-1,1’-biphenyl
SEM	scanning electron microscopy
SINs	simultaneous interpenetrating networks
SLA	stereolithography
SLS	selective laser sintering
S-Sb	triarylsulfonium hexafluoroantimonate salts in propylene carbonate
t	triplet state
t_{95}	time when 95 % of DBC is reached
TAMPTT	tris[3-(acetylthio)propyl]isocyanurate
tanδ	loss factor

tBPYR	5-tert-butyl pyrogallol
te	tissue engineering
THEB	1,3,5-tris(2-hydroxyethyl)-1,3,5-benzenetricarboxylate
TEGDMA	triethyleneglycoldimethacrylate
T_g	glass transition temperature
t_{gel}	time until gelation
THF	tetrahydrofuran
Thiol 1	1,1,1-trimethylolpropane-tris(3-mercaptopropionate)
Thiol 2	1,3,5-triallyl-1,3,5-triazine-2,4,6-trione
TIPS	thermally-induced phase separation
TMDP	2-chloro-4,4,5,5-tetramethyl-1,3,2-dioxaphospholane
TOx	1,3,5-tris[(3-ethyl-3-oxetanyl)methoxyethyl]-1,3,5-benzenetricarboxylate
tt(M)A	trimethylolpropane tri(meth)acrylate
TPO-L	ethyl (2,4,6-trimethylbenzoyl) phenylphosphinate
UDT	polyesterurethane dithiol
U_T	tensile toughness
UV	ultraviolet
VC10kPCL	poly(caprolactone) divinylcarbonate, 10 kDa
VC45kPCL	poly(caprolactone) divinylcarbonate, 45 kDa
VIS	visible
XDO	1,4-bis(((3-ethyloxetane-3-yl)methoxy)methyl) benzene
ΔH_p	heat of polymerization
β-TCP	β-tricalcium phosphate
ε_B	elongation at break
σ	tensile stress
σ_M	maximum tensile strength

MATERIALS AND METHODS

All chemicals necessary for synthesizing the final products and commercially available are listed below, together with their commercial supplier. Unless otherwise noted, all chemicals were used without further treatment. Solvents and reagents were, unless otherwise noted, applied in a quality that is common for organic synthesis. Commercially grade dioxane (Donau Chemie), methanol (MeOH, Donau Chemie), methylene chloride (DCM, Donauchemie) and tetrahydrofuran (THF, Donau Chemie) were dried using a PureSolvsystem (Intert, Amesbury, MA). The photoinitiator bis(4-methoxybenzoyl) diethylgermanium (Ivocerin®) was kindly provided by Ivoclar Vivadent AG and used as received.

reagent	supplier
Allyl chloroformat (97%)	Sigma Aldrich
2,2′-Azobis(2-methylpropionitril) (98%), AIBN, recrystallized from dest. MeOH at room temperature;	Sigma Aldrich
Chloroform-d	Eurisotop
2-chloro-4,4,5,5-tetramethyl-1,3,2-dioxaphospholane	Sigma Aldrich
Cyclohexanol as internal standard	Sigma Aldrich
Diethylether	Donauchemie
Divinyl adipate	TCI Europe
DMSO-d_6	Eurisotop
Epichlorohydrin	Sigma Aldrich
Ethyl acetate	Donauchemie
HCl	VWR
molecular sieve (4 Å)	Sigma Aldrich
5-norbornene-2-carboxylic acid (endo/exo mixture)	TCI Chemicals
Oxalyl chloride (>98.0%)	Sigma Aldrich
PCL (hydroxyl terminated, $\overline{M_w}$ = 14kDa;$\overline{M_w}$ = 45kDa)	Sigma Aldrich
Petroleum ether	Donauchemie

Pyridine (anhydrous, 99.8%)	Sigma Aldirch
Quinoline Yellow	Sigma Aldrich
Sodium chloride	Carl Roth
Sodium hydride (60 wt% in paraffin oil)	TCI
Sodium hydrogen carbonate	Donau Chemie
Sodium hydroxide	Merck
Sodium sulfate	VWR
Speedcure TPO-L	Lambson
Tetrahydrofuran	Donauchemie
Thioacetic acid	TCI
1,3,5-Triallyl-1,3,5-triazine-2,4,6-trione	TCI
TRIARYLSULFONIUM HEXAFLUOROANTIMONATE SALTS IN PROPYLENE CARBONATE (S-Sb)	DOW
Triethylamine	Bartelt
1,1,1-Trimethylolpropane-tris(3-mercaptopropionate) (Thiol 1)	Sigma Aldrich
Vinyl chloroformate	Merck

3D Fabrication was done using a CeraFab7500 with a wavelength of 450 nm. The CAD file was sliced into 25 µm layers with the aid of Lithoz CeraFab Control Software.

3D scan of the printed screw was made with a AutoScan Inspec stripe-light scanner from Shining3D. For comparison of the .stl file and the scan the software GOM Inspect 2019 from the company GOM was used.

3-point bending test experiments were done with rectangular shaped specimens (2x5x40 mm³) on a Zwick Z050 testing machine with a span length of 32 mm and a fin of 2.5 mm radius. The crosshead speed was set to 1 mm·min^{-1} and the standard strain σ_{fC} was set to 7%. Analysis was done with the testXpert II testing software.

Column chromatography was performed on a Büchi Sepacore Flash System (Büchi pump module C-605, Büchi control unit C-620, Büchi UV-Photometer C-635, Büchi fraction collector C-660), using glass columns, packed with silica gel 60 (Merck, 0.040-0.063 mm).

Dynamic Mechanical Thermo Analysis (DMTA) experiments were performed with an Anton Paar MCR 301 device with a CTD 450 oven and an SRF 12 measuring system in torsion mode from -100 to 200 °C with a heating rate of 2 °C·min^{-1}. The torsion strain was set to 0.1 % and a frequency of 1 Hz. The experiments were done as a single measurement due to the high reproducibility. The glass transition temperatures (T_g) were defined from the maximum dissipation factor (tan δ).

Gel permeation analysis (GPC) was performed with a Waters GPC, with three columns connected in series (Styragel HR 0.5, Styragel HR 3 and Styragel HR4) and three attached detectors (Waters 2410 RI, UV Detector Module 2550 for TDA 305, VISCOTEK SEC-MALS 9 for light scattering). Molecular weight of the polymers was examined using conventional calibration with polystyrene standards of 375 – 177 000 Da. OmniSEC 5.12 from Malvern was used for data analysis.

HR-MS analysis was performed from acetonitrile solutions (concentration: 10 µM) by using an HTC PAL system autosampler (CTC Analytics AG, Zwingen, Switzerland), an Agilent 1100/1200 HPLC with binary pumps, degasser, and column thermostat (Agilent Technologies, Waldbronn, Germany), and an Agilent 6230 AJS ESI-TOF mass spectrometer (Agilent Technologies, Palo Alto, CA).

Imaging of the printed structures was performed using a Keyence VHX 6000 optical microscope in panorama mode.

Light sources-

- UV chamber: uvitron International INTELLI-RAY 600 with a Hg broad bond UV lamp (600 W, UV-A: 125 mW/cm², Vis: 125 mW/cm²)
- Omnicure-System: Omnicure Series 200 EXFO with a 200 W Hg lamp and an installed filter with 400-500 nm
- PrograPrint Cure^{253} from Ivoclar® (wavelength of 405 nm, intensity of 274 mW·cm^{-2})
- HÖNLE LED POWERDRIVE with LED Cube 100 (wavelength of 405±10 nm, intensity 36 mW·cm^{-2} (100%))
- Uvet UV LED flood curing system (UVSS-144A, wavelength of 365 nm, intensity of 630 mW·cm^{-2} (20%))

Melting points were determined with an Optimelt devise from SRS Stanford Research Systems.

NMR spectra were recorded at room temperature on a Bruker Avance at 400 MHz for ^{1}H (100 MHz for ^{13}C). ^{31}P-NMR spectra for quantitative spectroscopy were recorded on a Bruker Avance 600 MHz at room temperature.

The chemical shifts are in parts per million (ppm) and related to trimethylsilane (TMS, δ = 0 ppm). The signals are referenced to the solvent (^{1}H: $CDCl_3$ δ = 7.26 ppm, DMSO-d_6 δ = 2.50 ppm; ^{13}C: $CDCl_3$ δ = 77.16 ppm, DMSO-d_6 δ = 39.52 ppm).

Multiplicities are termed s (singlet), d (doublet), t (triplet), q (quartet), and m (multiplet), and coupling constants (*J* values) are given in hertz. The data were processed with the software TopSpin 3.5 pl 7 from Bruker.

Orange light lab: all weightings, reactions and measurements of light sensitive substances are carried out in an orange light lab. The windows are laminated with Asmetec metolight SF-UV- foils (type ASR-SF-LY5) and all lamps were type Osram lumix with chip controlled light color 62.

Photo-DSC measurements were conducted on a Photo-DSC 204 F1 from Netzsch, using 15 µL aluminum pans. An Omnicure 2000 from Lumen Dynamics with glass fiber light wave guides was used as light source, which was calibrated *via* an Omnicure R2000 radiometer. All measurements were conducted under N_2-atmosphere (flow rate: 20 mL min^{-1}). The data analysis was performed with the program Netzsch Proteus Thermal Analysis in version 8.0.1.

Rheology was measured on a Anton Paar MCR 300 rheometer with a Peltier PTD 150 system and a CP-25 measuring system. The software used for evaluation was RheoPlus v3.40.

The temperature was held for one minute, and the shear rate increased to 100 s^{-1}. Afterwards, the rheology measurements were performed at the mentioned shear rate for one minute. The average shear viscosity was calculated from these data for all formulations with an increasing amount of additive.

RT-FT-NIR-Photorheology measurements were conducted on an *Anton Paar MCR 302 WESP*. A PP25 plate-plate arrangement and a P-PTD 200/GL Peltier glass plate were used as a measuring system. The glass plate was covered with polyethylene tape (TESA 4668 MDPE). An FTIR spectrometer (*Bruker Vertex 80*) with external mirrors was coupled with the rheometer and the reflected beam was detected by a mercury cadmium telluride (MCT)-detector. The photorheology measurements were analyzed with the software Rheoplus V3.62 from *Anton Paar* and the IR spectra with the software Opus 7.0 from *Bruker*.

Tensile test measurements were done on a Zwick Z050 tensile testing machine equipped with a 1 kN load sensor. Analysis was done with the testXpert II testing software.

Thin layer chromatography (TLC) was performed on aluminum TLC-plates coated with silica gel 60 F245 (supplier: Merck).

REFERENCES

1. Clarke, B., Normal bone anatomy and physiology. *Clin. J. Am. Soc. Nephrol.* **2008,** *3* (Suppl. 3), S131-S139.

2. Currey, J. D., *Bones*. Princeton University Press: 2002.

3. Henkel, J.; Woodruff, M. A.; Epari, D. R.; Steck, R.; Glatt, V.; Dickinson, I. C.; Choong, P. F. M.; Schuetz, M. A.; Hutmacher, D. W., Bone Regeneration Based on Tissue Engineering Conceptions - A 21st Century Perspective. *Bone research* **2013,** *1* (3), 216-248.

4. Ethier, C. R.; Simmons, C. A., *Introductory Biomechanics: From Cells to Organisms*. Cambridge University Press: 2007.

5. Buckwalter, J. A.; Glimcher, M. J.; Cooper, R. R.; Recker, R., Bone biology. I: Structure, blood supply, cells, matrix, and mineralization. *Instr. Course Lect.* **1996,** *45*, 371-86.

6. SEER https://training.seer.cancer.gov/anatomy/skeletal/tissue.html.

7. Hadjidakis, D. J.; Androulakis, I. I., Bone remodeling. *Ann. N. Y. Acad. Sci.* **2006,** *1092* (Women's Health and Disease), 385-396.

8. Alghazali, K. M.; Nima, Z. A.; Hamzah, R. N.; Dhar, M. S.; Anderson, D. E.; Biris, A. S., Bone-tissue engineering: complex tunable structural and biological responses to injury, drug delivery, and cell-based therapies. *Drug Metab. Rev.* **2015,** *47* (4), 431-454.

9. Liu, Y.; Luo, D.; Wang, T., Hierarchical Structures of Bone and Bioinspired Bone Tissue Engineering. *Small* **2016,** *12* (34), 4611-4632.

10. Morgan, E. F.; Gerstenfeld, L. C., Chapter 2 - The bone organ system: form and function. In *Marcus and Feldman's Osteoporosis (Fifth Edition)*, Dempster, D. W.; Cauley, J. A.; Bouxsein, M. L.; Cosman, F., Eds. Academic Press: 2021; pp 15-35.

11. Vedi, S.; Compston, J., Bone Histomorphometry. In *Bone Research Protocols*, Helfrich, M. H.; Ralston, S. H., Eds. Humana Press: Totowa, NJ, 2003; pp 283-298.

12. Huch, R.; Jürgens, K. D., *Mensch Körper Krankheit*. 2015.

13. Silver, I. A.; Murrills, R. J.; Etherington, D. J., Microelectrode studies on the acid microenvironment beneath adherent macrophages and osteoclasts. *Exp. Cell Res.* **1988,** *175* (2), 266-276.

14. Eriksen, E. F., Normal and Pathological Remodeling of Human Trabecular Bone: Three Dimensional Reconstruction of the Remodeling Sequence in Normals and in Metabolic Bone Disease*. *Endocr. Rev.* **1986,** *7* (4), 379-408.

15. Schindeler, A.; McDonald, M. M.; Bokko, P.; Little, D. G., Bone remodeling during fracture repair: The cellular picture. *Semin. Cell Dev. Biol.* **2008,** *19* (5), 459-466.

16. Raggatt, L. J.; Partridge, N. C., Cellular and Molecular Mechanisms of Bone Remodeling. *J. Biol. Chem.* **2010,** *285* (33), 25103-25108.

17. Miller, S. C.; de Saint-Georges, L.; Bowman, B. M.; Jee, W. S., Bone lining cells: structure and function. *Scanning Microsc.* **1989,** *3* (3), 953-60; discussion 960-1.

18. Dobnig, H.; Turner, R. T., Evidence that intermittent treatment with parathyroid hormone increases bone formation in adult rats by activation of bone lining cells. *Endocrinology* **1995,** *136* (8), 3632-3638.

19. Servier, L. https://commons.wikimedia.org/wiki/File:Fracture_repair_--_Smart-Servier_%28cropped%29.jpg (accessed 16.03.2023).

20. https://my.clevelandclinic.org/health/diseases/15241-bone-fractures (accessed 10.01.2023).

21. Nauth, A.; Schemitsch, E.; Norris, B.; Nollin, Z.; Watson, J. T., Critical-Size Bone Defects: Is There a Consensus for Diagnosis and Treatment? *J. Orthop. Trauma* **2018,** *32 Suppl 1*, S7-s11.

22. Correlo, V. M.; Oliveira, J. M.; Mano, J. F.; Neves, N. M.; Reis, R. L., CHAPTER 32 - Natural Origin Materials for Bone Tissue Engineering – Properties, Processing, and Performance. In *Principles of Regenerative Medicine (Second Edition)*, Atala, A.; Lanza, R.; Thomson, J. A.; Nerem, R., Eds. Academic Press: San Diego, 2011; pp 557-586.

23. Hutmacher, D. W.; Schantz, J. T.; Lam, C. X. F.; Tan, K. C.; Lim, T. C., State of the art and future directions of scaffold-based bone engineering from a biomaterials perspective. *J. Tissue Eng. Regen. Med.* **2007,** *1* (4), 245-260.

24. Chan, G.; Mooney, D. J., New materials for tissue engineering: towards greater control over the biological response. *Trends Biotechnol.* **2008,** *26* (7), 382-392.

25. Tumedei, M.; Savadori, P.; Del Fabbro, M., Synthetic Blocks for Bone Regeneration: A Systematic Review and Meta-Analysis. *Int. J. Mol. Sci.* **2019,** *20* (17).

26. Pae, H.-C.; Kang, J.-H.; Cha, J.-K.; Lee, J.-S.; Paik, J.-W.; Jung, U.-W.; Kim, B.-H.; Choi, S.-H., 3D-printed polycaprolactone scaffold mixed with β-tricalcium phosphate as a bone regenerative material in rabbit calvarial defects. *Journal of Biomedical Materials Research Part B: Applied Biomaterials* **2019,** *107* (4), 1254-1263.

27. Chen, P. Y.; Yang, K. C.; Wu, C. C.; Yu, J. H.; Lin, F. H.; Sun, J. S., Fabrication of large perfusable macroporous cell-laden hydrogel scaffolds using microbial transglutaminase. *Acta Biomater.* **2014,** *10* (2), 912-20.

28. Frasca, P.; Harper, R.; Katz, J. L., Strain and frequency dependence of shear storage modulus for human single osteons and cortical bone microsamples—Size and hydration effects. *J. Biomech.* **1981,** *14* (10), 679-690.

29. Moore, W. R.; Graves, S. E.; Bain, G. I., Synthetic bone graft substitutes. *ANZ J. Surg.* **2001,** *71* (6), 354-361.

30. Kuehn, K.-D.; Berberich, C.; Bösebeck, H., *Knochenersatzwerkstoffe als lokale Wirkstoffträger: Aktueller Stand bei Ersatzstoffen verschiedenen Ursprungs*. 2017; Vol. 47.

31. Williams, D., Biomaterials Science: An Introduction to Materials in Medicine, Buddy D. Ratner, et al.(Eds.), Academic Press (2004),(864pp., $95/£ 49.99), ISBN: 0-12-582463-7. Elsevier: 2005.

32. Wang, Y.; Wang, K.; Li, X.; Wei, Q.; Chai, W.; Wang, S.; Che, Y.; Lu, T.; Zhang, B., 3D fabrication and characterization of phosphoric acid scaffold with a HA/β-TCP weight ratio of 60:40 for bone tissue engineering applications. *PLoS One* **2017,** *12* (4), e0174870-e0174870.

33. Hench, L. L.; Boccaccini, A. R.; Day, R. M.; Gabe, S. M., Third-Generation Gene-Activating Biomaterials. *Mater. Sci. Forum* **2003,** *426-432*, 179-184.

34. Heinemann, S.; Gelinsky, M.; Worch, H.; Hanke, T., Resorbierbare Knochenersatzmaterialien. *Der Orthopäde* **2011,** *40* (9), 761-773.

35. Orman, S. Toughening of Photopolymers for Additive Manufacturing of Bone Replacements. Dissertation, TU Wien, 2018.

36. Bose, S.; Roy, M.; Bandyopadhyay, A., Recent advances in bone tissue engineering scaffolds. *Trends Biotechnol.* **2012,** *30* (10), 546-554.

37. Rezwan, K.; Chen, Q. Z.; Blaker, J. J.; Boccaccini, A. R., Biodegradable and bioactive porous polymer/inorganic composite scaffolds for bone tissue engineering. *Biomaterials* **2006,** *27* (18), 3413-3431.

38. Ibrahim, M. Z.; Sarhan, A. A. D.; Yusuf, F.; Hamdi, M., Biomedical materials and techniques to improve the tribological, mechanical and biomedical properties of orthopedic implants – A review article. *J. Alloys Compd.* **2017,** *714*, 636-667.

39. Staiger, M. P.; Pietak, A. M.; Huadmai, J.; Dias, G., Magnesium and its alloys as orthopedic biomaterials: A review. *Biomaterials* **2006,** *27* (9), 1728-1734.

40. Hartwig, A., Role of magnesium in genomic stability. *Mutation Research/Fundamental and Molecular Mechanisms of Mutagenesis* **2001,** *475* (1), 113-121.

41. U.S. Titanium Industry Inc. (2020, S. https://www.azom.com/properties.aspx?ArticleID=1547 (accessed 01.02.2023).

42. Sedelnikova, M.; Komarova, E.; Sharkeev, Y.; V. Tolkacheva, T.; Khlusov, I.; Sheikin, V., *Bioactive calcium phosphate coatings on metallic implants*. 2017; Vol. 1882, p 020062.

43. Cai, S.; Liu, Y.; Zheng Shu, X.; Prestwich, G. D., Injectable glycosaminoglycan hydrogels for controlled release of human basic fibroblast growth factor. *Biomaterials* **2005,** *26* (30), 6054-6067.

44. S. Nair, L.; T. Laurencin, C., *Biodegradable Polymers as Biomaterials*. 2007; Vol. 32, p 762-798.

45. George, M.; Abraham, T. E., Polyionic hydrocolloids for the intestinal delivery of protein drugs: Alginate and chitosan — a review. *J. Controlled Release* **2006,** *114* (1), 1-14.

46. Changhong, Y.; Xiongwei, L.; Xiaoli, C.; Danqing, W.; Dachang, Z.; Tianzhi, T.; Kitano, H., Anticancer gelatin microspheres with multiple functions. *Biomaterials* **1991,** *12* (7), 640-644.

47. Horowitz, R.; Leventis, M.; D Rohrer, M.; S Prasad, H., *Bone grafting: History, rationale, and selection of materials and techniques*. 2014; Vol. 35, p 1-6;quiz7.

48. Lee, S.-H.; Shin, H., Matrices and scaffolds for delivery of bioactive molecules in bone and cartilage tissue engineering. *Adv. Drug Del. Rev.* **2007,** *59* (4), 339-359.

49. Matsumoto, Y.; Arai, K.; Momose, H.; Kuroyanagi, Y., Development of a Wound Dressing Composed of a Hyaluronic Acid Sponge Containing Arginine. *J. Biomater. Sci. Polym. Ed.* **2009,** *20* (7-8), 993-1004.

50. Salgado, A. J.; Coutinho, O. P.; Reis, R. L., Bone Tissue Engineering: State of the Art and Future Trends. *Macromol. Biosci.* **2004,** *4* (8), 743-765.

51. Katti, D. S.; Lakshmi, S.; Langer, R.; Laurencin, C. T., Toxicity, biodegradation and elimination of polyanhydrides. *Adv. Drug Del. Rev.* **2002,** *54* (7), 933-961.

52. Tangpasuthadol, V.; Pendharkar, S. M.; Kohn, J., Hydrolytic degradation of tyrosine-derived polycarbonates, a class of new biomaterials. Part I: Study of model compounds. *Biomaterials* **2000,** *21* (23), 2371-2378.

53. Rainbolt, E. A.; Washington, K. E.; Biewer, M. C.; Stefan, M. C., Recent developments in micellar drug carriers featuring substituted poly(ε-caprolactone)s. *Polymer Chemistry* **2015,** *6* (13), 2369-2381.

54. Xiao, Y.; Yuan, M.; Zhang, J.; Yan, J.; Lang, M., Functional Poly(ε-caprolactone) Based Materials: Preparation, Self-assembly and Application in Drug Delivery. *Curr. Top. Med. Chem.* **2014,** *14* (6), 781-818.

55. Yang, P.; Zhu, G.; Xu, S.; Zhang, X.; Shen, X.; Cui, X.; Gao, Y.; Nie, J., A novel shape memory poly(ε-caprolactone) network via UV-triggered thiol-ene reaction. *J. Polym. Sci., Part B: Polym. Phys.* **2017,** *55* (8), 692-701.

56. Siparsky, G. L.; Voorhees, K. J.; Miao, F., Hydrolysis of Polylactic Acid (PLA) and Polycaprolactone (PCL) in Aqueous Acetonitrile Solutions: Autocatalysis. *J. Environ. Polymer Degradation* **1998,** *6* (1), 31-41.

57. S, S.; YT, K.; T, S.; M, G.; E, P.; P, K.; P, R., Immune response to polyglycolic acid implants. *The Journal of Bone and Joint Surgery. British volume* **1990,** *72-B* (4), 597-600.

58. Jandt, K. D., Evolutions, Revolutions and Trends in Biomaterials Science – A Perspective. *Adv. Eng. Mater.* **2007,** *9* (12), 1035-1050.

59. Mautner, A.; Qin, X.; Kapeller, B.; Russmueller, G.; Koch, T.; Stampfl, J.; Liska, R., Efficient Curing of Vinyl Carbonates by Thiol-Ene Polymerization. *Macromol. Rapid Commun.* **2012,** *33* (23), 2046-2052.

60. Heller, C.; Schwentenwein, M.; Varga, F.; Stampfl, J.; Liska, R., Additive Manufacturing Technologies for the 3D Fabrication of Biocompatible and Biodegradable Photopolymers. *MRS Proceedings* **2009,** *1239*, 1239-VV08-05.

61. Anseth, K. S.; Shastri, V. R.; Langer, R., Photopolymerizable degradable polyanhydrides with osteocompatibility. *Nat. Biotechnol.* **1999,** *17*, 156.

62. Guo, B.; Ma, P. X., Synthetic biodegradable functional polymers for tissue engineering: a brief review. *Science China Chemistry* **2014,** *57* (4), 490-500.

63. Rho, J. Y.; Kuhn-Spearing, L.; Zioupos, P., Mechanical properties and the hierarchical structure of bone. *Med. Eng. Phys.* **1998,** *20* (2), 92-102.

64. Olszta, M. J.; Cheng, X.; Jee, S. S.; Kumar, R.; Kim, Y.-Y.; Kaufman, M. J.; Douglas, E. P.; Gower, L. B., Bone structure and formation: A new perspective. *Materials Science and Engineering: R: Reports* **2007,** *58* (3), 77-116.

65. Fan, Y.; Fan, Y.; Li, Z.; Loan, M.; Lv, C.; Bo, Z., Optimal Principle of Bone Structure. *PLoS One* **2011,** *6* (12), e28868.

66. Roseti, L.; Parisi, V.; Petretta, M.; Cavallo, C.; Desando, G.; Bartolotti, I.; Grigolo, B., Scaffolds for Bone Tissue Engineering: State of the art and new perspectives. *Mater. Sci. Eng. C Mater. Biol. Appl.* **2017,** *78*, 1246-1262.

67. Sumner, D. R.; Galante, J. O., Determinants of stress shielding: design versus materials versus interface. *Clin. Orthop. Relat. Res.* **1992,** (274), 202-12.

68. Pilliar, R. M.; Cameron, H. U.; Binnington, A. G.; Szivek, J.; Macnab, I., Bone ingrowth and stress shielding with a porous surface coated fracture fixation plate. *J. Biomed. Mater. Res.* **1979,** *13* (5), 799-810.

69. Mikos, A. G.; Temenoff, J. S., *Formation of highly porous biodegradable scaffolds for tissue engineering*. 2000.

70. Liao, C.-J.; Chen, C.-F.; Chen, J.-H.; Chiang, S.-F.; Lin, Y.-J.; Chang, K.-Y., Fabrication of porous biodegradable polymer scaffolds using a solvent merging/particulate leaching method. *J. Biomed. Mater. Res.* **2002,** *59* (4), 676-681.

71. Johnson, T.; Bahrampourian, R.; Patel, A.; Mequanint, K., Fabrication of highly porous tissue-engineering scaffolds using selective spherical porogens. *Bio-Med. Mater. Eng.* **2010,** *20*, 107-118.

72. Nam, Y. S.; Yoon, J. J.; Park, T. G., A novel fabrication method of macroporous biodegradable polymer scaffolds using gas foaming salt as a porogen additive. *J. Biomed. Mater. Res.* **2000,** *53* (1), 1-7.

73. Di Maio, E.; Mensitieri, G.; Iannace, S.; Nicolais, L.; Li, W.; Flumerfelt, R. W., Structure optimization of polycaprolactone foams by using mixtures of CO2 and N2 as blowing agents. *Polymer Engineering & Science* **2005,** *45* (3), 432-441.

74. Barbetta, A.; Rizzitelli, G.; Bedini, R.; Pecci, R.; Dentini, M., Porous gelatin hydrogels by gas-in-liquid foam templating. *Soft Matter* **2010,** *6* (8), 1785-1792.

75. Ning, Z.; Xiongbiao, C., Biofabrication of Tissue Scaffolds. In *Advances in Biomaterials Science and Biomedical Applications*, Rosario, P., Ed. IntechOpen: Rijeka, 2013; p Ch. 12.

76. Quirk, R. A.; France, R. M.; Shakesheff, K. M.; Howdle, S. M., Supercritical fluid technologies and tissue engineering scaffolds. *Curr. Opin. Solid State Mater. Sci.* **2004,** *8* (3), 313-321.

77. Liu, X.; Ma, P. X., Polymeric Scaffolds for Bone Tissue Engineering. *Ann. Biomed. Eng.* **2004,** *32* (3), 477-486.

78. G.V, Y. D.; Prabhu, A.; Anil, S.; Venkatesan, J., Preparation and characterization of dexamethasone loaded sodium alginate-graphene oxide microspheres for bone tissue engineering. *J. Drug Deliv. Sci. Technol.* **2021,** *64*, 102624.

79. Whang, K.; Thomas, C. H.; Healy, K. E.; Nuber, G., A novel method to fabricate bioabsorbable scaffolds. *Polymer* **1995,** *36* (4), 837-842.

80. Turnbull, G.; Clarke, J.; Picard, F.; Riches, P.; Jia, L.; Han, F.; Li, B.; Shu, W., 3D bioactive composite scaffolds for bone tissue engineering. *Bioactive Materials* **2018,** *3* (3), 278-314.

81. Bhushan, S.; Singh, S.; Maiti, T. K.; Sharma, C.; Dutt, D.; Sharma, S.; Li, C.; Tag Eldin, E. M., Scaffold Fabrication Techniques of Biomaterials for Bone Tissue Engineering: A Critical Review. *Bioengineering* **2022,** *9* (12), 728.

82. Shi, X.; Su, K.; Varshney, R. R.; Wang, Y.; Wang, D.-A., Sintered Microsphere Scaffolds for Controlled Release and Tissue Engineering. *Pharm. Res.* **2011,** *28* (5), 1224-1228.

83. Jeon, J. H.; Bhamidipati, M.; Sridharan, B.; Scurto, A. M.; Berkland, C. J.; Detamore, M. S., Tailoring of processing parameters for sintering microsphere-based scaffolds with dense-phase carbon dioxide. *Journal of Biomedical Materials Research Part B: Applied Biomaterials* **2013,** *101B* (2), 330-337.

84. Reneker, D. H.; Yarin, A. L., Electrospinning jets and polymer nanofibers. *Polymer* **2008,** *49* (10), 2387-2425.

85. Venugopal, J.; Vadgama, P.; Sampath Kumar, T. S.; Ramakrishna, S., Biocomposite nanofibres and osteoblasts for bone tissue engineering. *Nanotechnology* **2007,** *18* (5), 055101.

86. Agarwal, S.; Wendorff, J. H.; Greiner, A., Use of electrospinning technique for biomedical applications. *Polymer* **2008,** *49* (26), 5603-5621.

87. Chu, C. F. L.; Lu, A.; Liszkowski, M.; Sipehia, R., Enhanced growth of animal and human endothelial cells on biodegradable polymers. *Biochimica et Biophysica Acta (BBA) - General Subjects* **1999,** *1472* (3), 479-485.

88. Zhang, R.; Ma, P. X., Processing of polymer scaffolds: Phase separation. *Methods of Tissue Engineering* **2001**, 715-724.

89. Bolland, B. J. R. F.; Kanczler, J. M.; Ginty, P. J.; Howdle, S. M.; Shakesheff, K. M.; Dunlop, D. G.; Oreffo, R. O. C., The application of human bone marrow stromal cells and poly(dl-lactic acid) as a biological bone graft extender in impaction bone grafting. *Biomaterials* **2008,** *29* (22), 3221-3227.

90. Gunatillake, P. A.; Adhikari, R., Biodegradable synthetic polymers for tissue engineering. *European cells & materials* **2003,** *5*, 1-16; discussion 16.

91. Helminen, A. O.; Korhonen, H.; Seppälä, J. V., Crosslinked poly(ester anhydride)s based on poly(ε-caprolactone) and polylactide oligomers. *J. Polym. Sci., Part A: Polym. Chem.* **2003,** *41* (23), 3788-3797.

92. Elomaa, L.; Teixeira, S.; Hakala, R.; Korhonen, H.; Grijpma, D. W.; Seppälä, J. V., Preparation of poly(ε-caprolactone)-based tissue engineering scaffolds by stereolithography. *Acta Biomater.* **2011,** *7* (11), 3850-3856.

93. Abbasi, N.; Hamlet, S.; Love, R. M.; Nguyen, N.-T., Porous scaffolds for bone regeneration. *Journal of Science: Advanced Materials and Devices* **2020,** *5* (1), 1-9.

94. Jariwala, S. H.; Lewis, G. S.; Bushman, Z. J.; Adair, J. H.; Donahue, H. J., 3D Printing of Personalized Artificial Bone Scaffolds. *3D printing and additive manufacturing* **2015,** *2* (2), 56-64.

95. Bose, S.; Vahabzadeh, S.; Bandyopadhyay, A., Bone tissue engineering using 3D printing. *Mater. Today* **2013,** *16* (12), 496-504.

96. Yuan, B.; Zhou, S. Y.; Chen, X. S., Rapid prototyping technology and its application in bone tissue engineering. *J Zhejiang Univ Sci B* **2017,** *18* (4), 303-315.

97. Ligon, S. C.; Liska, R.; Stampfl, J.; Gurr, M.; Mülhaupt, R., Polymers for 3D Printing and Customized Additive Manufacturing. *Chem. Rev.* **2017,** *117* (15), 10212-10290.

98. Raos, P.; Klapan, I.; Galeta, T., Additive Manufacturing of Medical Models--Applications in Rhinology. *Coll. Antropol.* **2015,** *39* (3), 667-73.

99. Leong, K. F.; Cheah, C. M.; Chua, C. K., Solid freeform fabrication of three-dimensional scaffolds for engineering replacement tissues and organs. *Biomaterials* **2003,** *24* (13), 2363-2378.

100. Hutmacher, D. W.; Sittinger, M.; Risbud, M. V., Scaffold-based tissue engineering: rationale for computer-aided design and solid free-form fabrication systems. *Trends Biotechnol.* **2004,** *22* (7), 354-362.

101. Gibas, I.; Janik, H., *Review: Synthetic polymer hydrogels for biomedical applications*. 2010; Vol. 4, p 297-304.

102. Faber, J.; Berto, P. M.; Quaresma, M., Rapid prototyping as a tool for diagnosis and treatment planning for maxillary canine impaction. *Am. J. Orthod. Dentofacial Orthop.* **2006,** *129* (4), 583-589.

103. Kim, M.-J.; Lee, S.-R.; Lee, M.-Y.; Sohn, J. W.; Yun, H. G.; Choi, J. Y.; Jeon, S. W.; Suh, T. S., Characterization of 3D printing techniques: Toward patient specific quality assurance spine-shaped phantom for stereotactic body radiation therapy. *PLoS One* **2017,** *12* (5), e0176227-e0176227.

104. Xing, J.-F.; Zheng, M.-L.; Duan, X.-M., Two-photon polymerization microfabrication of hydrogels: an advanced 3D printing technology for tissue engineering and drug delivery. *Chem. Soc. Rev.* **2015,** *44* (15), 5031-5039.

105. Wang, W.-K.; Sun, Z.-B.; Zheng, M.-L.; Dong, X.-Z.; Zhao, Z.-S.; Duan, X.-M., Magnetic Nickel–Phosphorus/Polymer Composite and Remotely Driven Three-Dimensional Micromachine Fabricated by Nanoplating and Two-Photon Polymerization. *The Journal of Physical Chemistry C* **2011,** *115* (22), 11275-11281.

106. Kawata, S.; Sun, H.-B.; Tanaka, T.; Takada, K., Finer features for functional microdevices. *Nature* **2001,** *412* (6848), 697-698.

107. Liska, R.; Schuster, M.; Inführ, R.; Turecek, C.; Fritscher, C.; Seidl, B.; Schmidt, V.; Kuna, L.; Haase, A.; Varga, F.; Lichtenegger, H.; Stampfl, J., Photopolymers for rapid prototyping. *Journal of Coatings Technology and Research* **2007,** *4* (4), 505-510.

108. Göppert-Mayer, M., Elementary processes with two quantum transitions. *Annalen der Physik* **2009,** *18* (7-8), 466-479.

109. Wu, S.; Serbin, J.; Gu, M., Two-photon polymerisation for three-dimensional micro-fabrication. *J. Photochem. Photobiol. A: Chem.* **2006,** *181* (1), 1-11.

110. Billiet, T.; Vandenhaute, M.; Schelfhout, J.; Van Vlierberghe, S.; Dubruel, P., A review of trends and limitations in hydrogel-rapid prototyping for tissue engineering. *Biomaterials* **2012,** *33* (26), 6020-6041.

111. Formlabs Formlabs Ultimate guide to stereolithography (SLA) 3D prining. https://formlabs.com/blog/ultimate-guide-to-stereolithography-sla-3d-printing/#sla-systems (accessed 06.04.2019).

112. Formlabs SLA vs. DLP: 3D-Drucktechnologien für Kunstharze im Vergleich. https://formlabs.com/de/blog/vergleich-3d-druck-sla-dlp/ (accessed 20.2.2023).

113. Tesavibul, P.; Felzmann, R.; Gruber, S.; Liska, R.; Thompson, I.; Boccaccini, A. R.; Stampfl, J., Processing of 45S5 Bioglass (R) by lithography-based additive manufacturing. *Mater. Lett.* **2012,** *74*, 81-84.

114. Schwentenwein, M.; Schneider, P.; Homa, J., Lithography-Based Ceramic Manufacturing: A Novel Technique for Additive Manufacturing of High-Performance Ceramics. *Advances in Science and Technology* **2014,** *88*, 60-64.

115. Lithoz https://lithoz.com/en/technology/lcm-technology.

116. Bagheri, A.; Jin, J., Photopolymerization in 3D Printing. *ACS Applied Polymer Materials* **2019,** *1* (4), 593-611.

117. Fouassier, J.-P.; Rabek, J. F., *Radiation curing in polymer science and technology*. Elsevier Applied Science: London; New York, 1993.

118. Barner-Kowollik, C.; Vana, P.; Davis, T. P., The kinetics of free-radical polymerization. *Handbook of radical polymerization* **2002,** *4*, 187-261.

119. Dendukuri, D.; Panda, P.; Haghgooie, R.; Kim, J. M.; Hatton, T. A.; Doyle, P. S., Modeling of Oxygen-Inhibited Free Radical Photopolymerization in a PDMS Microfluidic Device. *Macromolecules* **2008,** *41* (22), 8547-8556.

120. Fouassier, J. P.; Allonas, X.; Burget, D., Photopolymerization reactions under visible lights: principle, mechanisms and examples of applications. *Prog. Org. Coat.* **2003,** *47* (1).

121. Crivello, J. V.; Reichmanis, E., Photopolymer Materials and Processes for Advanced Technologies. *Chem. Mater.* **2014,** *26* (1), 533-548.

122. Gorsche, C.; Koch, T.; Moszner, N.; Liska, R., Exploring the benefits of β-allyl sulfones for more homogeneous dimethacrylate photopolymer networks. *Polymer Chemistry* **2015,** *6* (11), 2038-2047.

123. Gorsche, C. Synthesis and characterization of monomers and additives for photopolymer-based dental restoratives. Dissertation, 2015.

124. Ligon-Auer, S. C.; Schwentenwein, M.; Gorsche, C.; Stampfl, J.; Liska, R., Toughening of photo-curable polymer networks: a review. *Polymer Chemistry* **2016,** *7* (2), 257-286.

125. Crivello, J. V.; Dietliker, K.; Bradley, G., *Photoinitiators for Free Radical Cationic & Anionic Photopolymerisation*. John Wiley and sons: 1998.

126. Perkampus, P. e. D. H.-H. In *UV-VIS Spectroscopy and Its Applications*, Springer Lab Manuals, 1992.

127. Gruber, H., Photoinitiators for free radical polymerization. *Prog. Polym. Sci.* **1992,** *17*, 953-1044.

128. National Center for Biotechnology Information (2023). PubChem Patent Summary for US-6027324-A. Retrieved February 1, f. h. p. n. n. n. g. p. U.-.-A.

129. Bayrakçeken, F., Triplet–triplet optical energy transfer from benzophenone to naphthalene in the vapor phase. *Spectrochimica Acta Part A: Molecular and Biomolecular Spectroscopy* **2008,** *71* (2), 603-608.

130. Green, W. A., Industrial Photoinitiators: A Technical Guide (1st ed.). **2010**.

131. J-P., F., *Photoinitiation Photopolymerization and Photocuring : Fundamentals and Applications.* Munich New York: Hanser ; : 1995.

132. Pawlizak, S. University of Leipzig, 2009.

133. K., D., *A Compilation of Photoinitiators : Commercially Available for Uv Today.* Edinbergh London: SITA Technology: 2002.

134. K., V. Research and Development Ivoclar Vivadent AG: 2015.

135. Moszner, N.; Fischer, U. K.; Ganster, B.; Liska, R.; Rheinberger, V., Benzoyl germanium derivatives as novel visible light photoinitiators for dental materials. *Dent. Mater.* **2008,** *24* (7), 901-907.

136. Neshchadin, D.; Rosspeintner, A.; Griesser, M.; Lang, B.; Mosquera-Vazquez, S.; Vauthey, E.; Gorelik, V.; Liska, R.; Hametner, C.; Ganster, B.; Saf, R.; Moszner, N.; Gescheidt, G., Acylgermanes: Photoinitiators and Sources for Ge-Centered Radicals. Insights into their Reactivity. *J. Am. Chem. Soc.* **2013,** *135* (46), 17314-17321.

137. Griffith, M. L.; Halloran, J. W., Freeform Fabrication of Ceramics via Stereolithography. *J. Am. Ceram. Soc.* **1996,** *79* (10), 2601-2608.

138. Baxter, J. E.; Stephen Davidson, R.; Hageman, H. J., Acylphosphine oxides as photoinitiators for acrylate and unsaturated polyester resins. *Eur. Polym. J.* **1988,** *24* (5), 419-424.

139. Voll, D.; Barner-Kowollik, C., Photoinitiators for Polymer Synthesis. Scope, Reactivity, and Efficiency. By Jean-Pierre Fouassier and Jacques Lalavée. *Angew. Chem. Int. Ed.* **2013,** *52* (12), 3312-3312.

140. Ullrich, G.; Burtscher, P.; Salz, U.; Moszner, N.; Liska, R., Phenylglycine derivatives as coinitiators for the radical photopolymerization of acidic aqueous formulations. *J. Polym. Sci., Part A: Polym. Chem.* **2006,** *44* (1), 115-125.

141. Andrews, L. S.; Clary, J. J., Review of the toxicity of multifunctional acrylates. *J. Toxicol. Environ. Health* **1986,** *19* (2), 149-164.

142. Calnan, C. D., Acrylates in industry. *Contact Dermatitis* **1980,** *6* (1), 53-54.

143. Ohara, T.; Sato, T.; Shimizu, N.; Prescher, G.; Schwind, H.; Weiberg, O.; Marten, K.; Greim, H.; Shaffer, T. D.; Nandi, P., Acrylic Acid and Derivatives. In *Ullmann's Encyclopedia of Industrial Chemistry*, pp 1-21.

144. Final report of the safety assessment of methacrylic acid. *Int. J. Toxicol.* **2005,** *24 Suppl 5*, 33-51.

145. Mautner, A.; Qin, X.; Wutzel, H.; Ligon, S. C.; Kapeller, B.; Moser, D.; Russmueller, G.; Stampfl, J.; Liska, R., Thiol-ene photopolymerization for efficient curing of vinyl esters. *J. Polym. Sci., Part A: Polym. Chem.* **2013,** *51* (1), 203-212.

146. Orman, S.; Hofstetter, C.; Aksu, A.; Reinauer, F.; Liska, R.; Baudis, S., Toughness enhancers for bone scaffold materials based on biocompatible photopolymers. *J. Polym. Sci., Part A: Polym. Chem.* **2019,** *57* (2), 110-119.

147. Husár, B.; Heller, C.; Schwentenwein, M.; Mautner, A.; Varga, F.; Koch, T.; Stampfl, J.; Liska, R., Biomaterials based on low cytotoxic vinyl esters for bone replacement application. *J. Polym. Sci., Part A: Polym. Chem.* **2011,** *49* (23), 4927-4934.

148. Husár, B.; Liska, R., Vinyl carbonates, vinyl carbamates, and related monomers: synthesis, polymerization, and application. *Chem. Soc. Rev.* **2012,** *41* (6), 2395-405.

149. Heller, C.; Schwentenwein, M.; Russmueller, G.; Varga, F.; Stampfl, J.; Liska, R., Vinyl esters: Low cytotoxicity monomers for the fabrication of biocompatible 3D scaffolds by lithography based additive manufacturing. *J. Polym. Sci., Part A: Polym. Chem.* **2009,** *47* (24), 6941-6954.

150. Kade, M. J.; Burke, D. J.; Hawker, C. J., The power of thiol-ene chemistry. *J. Polym. Sci., Part A: Polym. Chem.* **2010,** *48* (4), 743-750.

151. Hofecker, A.; Knaack, P.; Steinbauer, P.; Markovic, M.; Ovsianikov, A.; Liska, R., Novel synthesis routes for the preparation of low toxic vinyl ester and vinyl carbonate monomers. *Synth. Commun.* **2020,** *50* (23), 3629-3641.

152. Hoyle, C. E.; Lowe, A. B.; Bowman, C. N., Thiol-click chemistry: a multifaceted toolbox for small molecule and polymer synthesis. *Chem. Soc. Rev.* **2010,** *39* (4), 1355-1387.

153. Hoyle, C. E.; Lee, T. Y.; Roper, T., Thiol–enes: Chemistry of the past with promise for the future. *J. Polym. Sci., Part A: Polym. Chem.* **2004,** *42* (21), 5301-5338.

154. Northrop, B. H.; Coffey, R. N., Thiol–Ene Click Chemistry: Computational and Kinetic Analysis of the Influence of Alkene Functionality. *J. Am. Chem. Soc.* **2012,** *134* (33), 13804-13817.

155. Northrop, B. H.; Frayne, S. H.; Choudhary, U., Thiol–maleimide "click" chemistry: evaluating the influence of solvent, initiator, and thiol on the reaction mechanism, kinetics, and selectivity. *Polymer Chemistry* **2015,** *6*, 3415-3430.

156. Machado, T. O.; Sayer, C.; Araujo, P. H. H., Thiol-ene polymerisation: A promising technique to obtain novel biomaterials. *Eur. Polym. J.* **2017,** *86*, 200-215.

157. Carioscia, J. A.; Schneidewind, L.; O'Brien, C.; Ely, R.; Feeser, C.; Cramer, N.; Bowman, C. N., Thiol–norbornene materials: Approaches to develop high Tg thiol–ene polymers. *J. Polym. Sci., Part A: Polym. Chem.* **2007,** *45* (23), 5686-5696.

158. Dadashi-Silab, S.; Doran, S.; Yagci, Y., Photoinduced Electron Transfer Reactions for Macromolecular Syntheses. *Chem. Rev.* **2016,** *116* (17), 10212-10275.

159. Crivello, J. V.; Bulut, U., Photoactivated cationic ring-opening frontal polymerizations of oxetanes. *Designed Monomers and Polymers* **2005,** *8* (6), 517-531.

160. Cowie, J. M. G., & Arrighi, V., *Polymers: Chemistry and Physics of Modern Materials, Third Edition (3rd ed.)*. Boca Raton, (2007).

161. Bulut, U.; Crivello, J. V., Reactivity of oxetane monomers in photoinitiated cationic polymerization. *J. Polym. Sci., Part A: Polym. Chem.* **2005,** *43* (15), 3205-3220.

162. Bulut, U.; Crivello, J. V., Investigation of the Reactivity of Epoxide Monomers in Photoinitiated Cationic Polymerization. *Macromolecules* **2005,** *38*, 3584-3595.

163. Vitale, A.; Sangermano, M.; Bongiovanni, R.; Burtscher, P.; Moszner, N., Visible Light Curable Restorative Composites for Dental Applications Based on Epoxy Monomer. *Materials (Basel)* **2014,** *7* (1), 554-562.

164. Crivello, J. V., Effect of Temperature on the Cationic Photopolymerization of Epoxides. *Journal of Macromolecular Science, Part A* **2008,** *45* (8), 591-598.

165. Crivello, J. V., The discovery and development of onium salt cationic photoinitiators. *J. Polym. Sci., Part A: Polym. Chem.* **1999,** *37* (23), 4241-4254.

166. Klikovits, N.; Knaack, P.; Bomze, D.; Krossing, I.; Liska, R., Novel photoacid generators for cationic photopolymerization. *Polymer Chemistry* **2017,** *8* (30), 4414-4421.

167. Sangermano, M., Advances in cationic photopolymerization. *Pure Appl. Chem.* **2012,** *84*, 2089 - 2101.

168. Spurr, A. R., A low-viscosity epoxy resin embedding medium for electron microscopy. *J. Ultrastruct. Res.* **1969,** *26* (1), 31-43.

169. Liu, W.; Wang, Z.; Xiong, L.; Zhao, L., Phosphorus-containing liquid cycloaliphatic epoxy resins for reworkable environment-friendly electronic packaging materials. *Polymer* **2010,** *51* (21), 4776-4783.

170. Crivello, J. V., Vinyl epoxide accelerators for the photoinitiated cationic polymerization of oxetane monomers. *Polymer* **2015,** *64*, 227-233.

171. Rajaraman, S. K.; Mowers, W. A.; Crivello, J. V., Interaction of epoxy and vinyl ethers during photoinitiated cationic polymerization. *J. Polym. Sci., Part A: Polym. Chem.* **1999,** *37* (21), 4007-4018.

172. Dillman, B.; Jessop, J. L. P., Chain transfer agents in cationic photopolymerization of a bis-cycloaliphatic epoxide monomer: Kinetic and physical property effects. *J. Polym. Sci., Part A: Polym. Chem.* **2013,** *51* (9), 2058-2067.

173. Crivello, J. V., Cationic photopolymerization of alkyl glycidyl ethers. *J. Polym. Sci., Part A: Polym. Chem.* **2006,** *44* (9), 3036-3052.

174. Dorfinger, P.; Stampfl, J.; Liska, R., Toughening of Photopolymers for Stereolithography (SL). *Mater. Sci. Forum* **2015,** *825-826*, 53-59.

175. Nagarajan, V.; Mohanty, A. K.; Misra, M., Perspective on Polylactic Acid (PLA) based Sustainable Materials for Durable Applications: Focus on Toughness and Heat Resistance. *ACS Sustainable Chemistry & Engineering* **2016,** *4* (6), 2899-2916.

176. Hillmyer, M. A.; Lipic, P. M.; Hajduk, D. A.; Almdal, K.; Bates, F. S., Self-Assembly and Polymerization of Epoxy Resin-Amphiphilic Block Copolymer Nanocomposites. *J. Am. Chem. Soc.* **1997,** *119* (11), 2749-2750.

177. Chan, C.-M.; Wu, J.; Li, J.-X.; Cheung, Y.-K., Polypropylene/calcium carbonate nanocomposites. *Polymer* **2002,** *43* (10), 2981-2992.

178. Zheng, Y.; Song, P.; Liu, S.; Wu, M.; Xu, H.; Qiao, C.; Liu, J.; Gao, Z.; Ban, Q., Transparent and toughening epoxy thermosets modified by linear telechelic polymer containing rigid spiroacetal moieties: Uncovering the relationship between the heterogeneous crosslinked network and thermoset performances. *Journal of Polymer Science* **2021,** *59* (13), 1390-1398.

179. Michaudel, Q.; Kottisch, V.; Fors, B. P., Cationic Polymerization: From Photoinitiation to Photocontrol. *Angew. Chem. Int. Ed.* **2017,** *56* (33), 9670-9679.

180. Erhard, G., *Designing with plastics*. Carl Hanser Verlag: Munich: 2006; p p.34-38.

181. Pfaffinger, M., Hot Lithography – New Possibilities in Polymer 3D Printing. *Laser Technik Journal* **2018,** *15* (4), 45-47.

182. Pierau, L.; Elian, C.; Akimoto, J.; Ito, Y.; Caillol, S.; Versace, D.-L., Bio-sourced monomers and cationic photopolymerization–The green combination towards eco-friendly and non-toxic materials. *Prog. Polym. Sci.* **2022,** *127*, 101517.

183. Sangermano, M.; Razza, N.; Crivello, J. V., Cationic UV-Curing: Technology and Applications. *Macromolecular Materials and Engineering* **2014,** *299* (7), 775-793.

184. Karak, N., 1 - Fundamentals of polymers. In *Vegetable Oil-Based Polymers*, Karak, N., Ed. Woodhead Publishing: 2012; pp 1-30.

185. Sperling, L. H., Interpenetrating Polymer Networks: An Overview. In *Interpenetrating Polymer Networks*, American Chemical Society: 1994; Vol. 239, pp 3-38.

186. Fouassier, J. P. L., J., Photochemical Production of Interpenetrating Polymer Networks; Simultaneous Initiation of Radical and Cationic Polymerization Reactions. *Polym. Polym. Compos.* **2014,** *6*, 2588-2610.

187. Charnley, J., ANCHORAGE OF THE FEMORAL HEAD PROSTHESIS TO THE SHAFT OF THE FEMUR. *The Journal of Bone & Joint Surgery British Volume* **1960,** *42-B* (1), 28-30.

188. Malinauskas, M.; Baltriukiene, D.; Kraniauskas, A.; Danilevicius, P.; Jarasiene, R.; Sirmenis, R.; Zukauskas, A.; Balciunas, E.; Purlys, V.; Gadonas, R.; Bukelskiene, V.; Sirvydis, V.; Piskarskas, A., In vitro and in vivo biocompatibility study on laser 3D microstructurable polymers. *Appl. Phys. A* **2012,** *108* (3), 751-759.

189. Dellago, B.; Altun, A. A.; Liska, R.; Baudis, S., Exploring the limits of toughness enhancers for 3D printed photopolymers as bone replacement materials. *Journal of Polymer Science* **2023,** *61* (2), 143-154.

190. Mautner, A.; Steinbauer, B.; Orman, S.; Russmüller, G.; Macfelda, K.; Koch, T.; Stampfl, J.; Liska, R., Tough photopolymers based on vinyl esters for biomedical applications. *J. Polym. Sci., Part A: Polym. Chem.* **2016,** *54* (13), 1987-1997.

191. Russmueller, G.; Liska, R.; Stampfl, J.; Heller, C.; Mautner, A.; Macfelda, K.; Kapeller, B.; Lieber, R.; Haider, A.; Mika, K.; Schopper, C.; Perisanidis, C.; Seemann, R.; Moser, D., 3D Printable Biophotopolymers for in Vivo Bone Regeneration. *Materials* **2015,** *8* (6), 3685.

192. Cameron, J. F.; Willson, C. G.; Fréchet, J. M. J., Photogeneration of Amines from α-Keto Carbamates: Photochemical Studies. *J. Am. Chem. Soc.* **1996,** *118* (51), 12925-12937.

193. Arimitsu, K.; Takemori, Y.; Nakajima, A.; Oguri, A.; Furutani, M.; Gunji, T.; Abe, Y., Photobase generators derived from trans-o-coumaric acid for anionic UV curing systems without gas generation. *J. Polym. Sci., Part A: Polym. Chem.* **2015,** *53* (10), 1174-1177.

194. Chae, K. H.; Lee, C. S.; Kim, J. H., One component photo-curing agent for epoxy resins based on multifunctional photobase generators containing oxime–urethane groups. *Polym. Adv. Technol.* **2011,** *22* (10), 1427-1433.

195. Chan, J. W.; Shin, J.; Hoyle, C. E.; Bowman, C. N.; Lowe, A. B., Synthesis, Thiol−Yne "Click" Photopolymerization, and Physical Properties of Networks Derived from Novel Multifunctional Alkynes. *Macromolecules* **2010,** *43* (11), 4937-4942.

196. Oesterreicher, A.; Gorsche, C.; Ayalur-Karunakaran, S.; Moser, A.; Edler, M.; Pinter, G.; Schlögl, S.; Liska, R.; Griesser, T., Exploring Network Formation of Tough and Biocompatible Thiol-yne Based Photopolymers. *Macromol. Rapid Commun.* **2016,** *37* (20), 1701-1706.

197. Beigi, S.; Yeganeh, H.; Atai, M., Evaluation of fracture toughness and mechanical properties of ternary thiol–ene–methacrylate systems as resin matrix for dental restorative composites. *Dent. Mater.* **2013,** *29* (7), 777-787.

198. Senyurt, A. F.; Wei, H.; Phillips, B.; Cole, M.; Nazarenko, S.; Hoyle, C. E.; Piland, S. G.; Gould, T. E., Physical and Mechanical Properties of Photopolymerized Thiol−Ene/Acrylates. *Macromolecules* **2006,** *39* (19), 6315-6317.

199. Sycks, D. G.; Safranski, D. L.; Reddy, N. B.; Sun, E.; Gall, K., Tough Semicrystalline Thiol–Ene Photopolymers Incorporating Spiroacetal Alkenes. *Macromolecules* **2017,** *50* (11), 4281-4291.

200. Sycks, D. G.; Wu, T.; Park, H. S.; Gall, K., Tough, stable spiroacetal thiol-ene resin for 3D printing. *J. Appl. Polym. Sci.* **2018,** *135* (22), 46259.

201. Fairbanks, B. D.; Scott, T. F.; Kloxin, C. J.; Anseth, K. S.; Bowman, C. N., Thiol-Yne Photopolymerizations: Novel Mechanism, Kinetics, and Step-Growth Formation of Highly Cross-Linked Networks. *Macromolecules* **2009,** *42* (1), 211-217.

202. Oesterreicher, A.; Wiener, J.; Roth, M.; Moser, A.; Gmeiner, R.; Edler, M.; Pinter, G.; Griesser, T., Tough and degradable photopolymers derived from alkyne monomers for 3D printing of biomedical materials. *Polymer Chemistry* **2016,** *7* (32), 5169-5180.

203. McNair, O. D.; Brent, D. P.; Sparks, B. J.; Patton, D. L.; Savin, D. A., Sequential Thiol Click Reactions: Formation of Ternary Thiourethane/Thiol–Ene Networks with Enhanced Thermal and Mechanical Properties. *ACS Applied Materials & Interfaces* **2014,** *6* (9), 6088-6097.

204. Lowe, A. B., Thiol-yne 'click'/coupling chemistry and recent applications in polymer and materials synthesis and modification. *Polymer* **2014,** *55* (22), 5517-5549.

205. Gorsche, C.; Seidler, K.; Knaack, P.; Dorfinger, P.; Koch, T.; Stampfl, J.; Moszner, N.; Liska, R., Rapid formation of regulated methacrylate networks yielding tough materials for lithography-based 3D printing. *Polymer Chemistry* **2016,** *7* (11), 2009-2014.

206. Seidler, K.; Griesser, M.; Kury, M.; Harikrishna, R.; Dorfinger, P.; Koch, T.; Svirkova, A.; Marchetti-Deschmann, M.; Stampfl, J.; Moszner, N.; Gorsche, C.; Liska, R., Vinyl Sulfonate Esters: Efficient Chain Transfer Agents for the 3D Printing of Tough Photopolymers without Retardation. *Angew. Chem. Int. Ed. Engl.* **2018,** *57* (29), 9165-9169.

207. Moad, G.; Rizzardo, E.; Thang, S. H., Radical addition–fragmentation chemistry in polymer synthesis. *Polymer* **2008,** *49* (5), 1079-1131.

208. Yagci, Y.; Reetz, I., Addition–fragmentation reactions in polymer chemistry. *React. Funct. Polym.* **1999,** *42* (3), 255-264.

209. Gorsche, C.; Griesser, M.; Gescheidt, G.; Moszner, N.; Liska, R., β-Allyl Sulfones as Addition–Fragmentation Chain Transfer Reagents: A Tool for Adjusting Thermal and Mechanical Properties of Dimethacrylate Networks. *Macromolecules* **2014,** *47* (21), 7327-7336.

210. Sato, E.; Uehara, I.; Horibe, H.; Matsumoto, A., One-Step Synthesis of Thermally Curable Hyperbranched Polymers by Addition–Fragmentation Chain Transfer Using Divinyl Monomers. *Macromolecules* **2014,** *47* (3), 937-943.

211. Grunenberg, D.; Ehrmann, K.; Gorsche, C.; Steyrer, B.; Koch, T.; Stampfl, J.; Liska, R., Heterotelechelic poly(propylene oxide) as migration-inhibited toughening agent in hot lithography based additive manufacturing. *Polymer Chemistry* **2021,** *12* (9), 1260-1272.

212. Boyer, C.; Bulmus, V.; Davis, T. P.; Ladmiral, V.; Liu, J.; Perrier, S., Bioapplications of RAFT polymerization. *Chem. Rev.* **2009,** *109* (11), 5402-36.

213. Tornøe, C. W.; Christensen, C.; Meldal, M., Peptidotriazoles on solid phase: [1,2,3]-triazoles by regiospecific copper(i)-catalyzed 1,3-dipolar cycloadditions of terminal alkynes to azides. *J. Org. Chem.* **2002,** *67* (9), 3057-64.

214. Rostovtsev, V. V.; Green, L. G.; Fokin, V. V.; Sharpless, K. B., A stepwise huisgen cycloaddition process: copper(I)-catalyzed regioselective "ligation" of azides and terminal alkynes. *Angew. Chem. Int. Ed. Engl.* **2002,** *41* (14), 2596-9.

215. Adzima, B. J.; Tao, Y.; Kloxin, C. J.; DeForest, C. A.; Anseth, K. S.; Bowman, C. N., Spatial and temporal control of the alkyne-azide cycloaddition by photoinitiated Cu(II) reduction. *Nat. Chem.* **2011,** *3* (3), 256-59.

216. Yilmaz, G.; Yagci, Y., Light-induced step-growth polymerization. *Prog. Polym. Sci.* **2020,** *100*, 101178.

217. Song, H. B.; Sowan, N.; Baranek, A.; Sinha, J.; Cook, W. D.; Bowman, C. N., Effects of Network Structures on the Tensile Toughness of Copper-Catalyzed Azide–Alkyne Cycloaddition (CuAAC)-Based Photopolymers. *Macromolecules* **2021,** *54* (2), 747-756.

218. Song, H. B.; Baranek, A.; Worrell, B. T.; Bowman, C. N.; Cook, W. D., Photopolymerized Triazole-Based Glassy Polymer Networks with Superior Tensile Toughness. *Adv. Funct. Mater.* **2018,** *28* (22).

219. Ragosta, G.; Abbate, M.; Musto, P.; Scarinzi, G.; Mascia, L., Epoxy-silica particulate nanocomposites: Chemical interactions, reinforcement and fracture toughness. *Polymer* **2005,** *46* (23), 10506-10516.

220. Zhang, H.; Zhang, Z.; Friedrich, K.; Eger, C., Property improvements of in situ epoxy nanocomposites with reduced interparticle distance at high nanosilica content. *Acta Mater.* **2006,** *54* (7), 1833-1842.

221. Zhang, H.; Tang, L.-C.; Zhang, Z.; Friedrich, K.; Sprenger, S., Fracture behaviours of in situ silica nanoparticle-filled epoxy at different temperatures. *Polymer* **2008,** *49* (17), 3816-3825.

222. Sangermano, M.; Naguib, M.; Messori, M., Fracture Toughness Enhancement of UV-Cured Epoxy Coatings Containing Al2O3 Nanoparticles. *Macromolecular Materials and Engineering* **2013,** *298* (11), 1184-1189.

223. Guo, T.; Wang, L.; Zhang, A.; Cai, T., Effects of nano calcium carbonate modified by a lanthanum compound on the properties of polypropylene. *J. Appl. Polym. Sci.* **2005,** *97* (3), 1154-1160.

224. Liu, Z. H.; Kwok, K. W.; Li, R. K. Y.; Choy, C. L., Effects of coupling agent and morphology on the impact strength of high density polyethylene/CaCO3 composites. *Polymer* **2002,** *43* (8), 2501-2506.

225. Termonia, Y., Chain confinement in polymer nanocomposites and its effect on polymer bulk properties. *J. Polym. Sci., Part B: Polym. Phys.* **2010,** *48* (6), 687-692.

226. Jordan, J., Jacob, Karl I., Tannenbaum, Rina, Sharaf, Mohammed A., Jasiuk, Iwona, Experimental trends in polymer nanocomposites - A review. **2005**.

227. Maalihan, R. D.; Chen, Q.; Agueda, J. R. H. S.; Pajarito, B. B.; Tamura, H.; Advincula, R. C., On the Use of Surfactant-Complexed Chitosan for Toughening 3D Printed Polymethacrylate Composites. *Macromolecular Materials and Engineering* **2021,** *306* (1), 2000448.

228. Pearson, R. A.; Yee, A. F., Influence of particle size and particle size distribution on toughening mechanisms in rubber-modified epoxies. *Journal of Materials Science* **1991,** *26* (14), 3828-3844.

229. Ullett, J. S.; Chartoff, R. P., Toughening of unsaturated polyester and vinyl ester resins with liquid rubbers. *Polymer Engineering & Science* **1995,** *35* (13), 1086-1097.

230. Azimi, H. R.; Pearson, R. A.; Hertzberg, R. W., Fatigue of rubber-modified epoxies: effect of particle size and volume fraction. *Journal of Materials Science* **1996,** *31* (14), 3777-3789.

231. Maazouz, A.; Sautereau, H.; Gérard, J. F., Toughening of epoxy networks using pre-formed core-shell particles or reactive rubbers. *Polym. Bull.* **1994,** *33* (1), 67-74.

232. Xia, J.; Luo, X.; Huang, J.; Ma, J.; Yang, J., Preparation of core/shell organic–inorganic hybrid polymer nanoparticles and their application to toughening poly(methyl methacrylate). *RSC Advances* **2021,** *11* (54), 34036-34047.

233. Luo, F.; Sun, T. L.; Nakajima, T.; Kurokawa, T.; Zhao, Y.; Sato, K.; Ihsan, A. B.; Li, X.; Guo, H.; Gong, J. P., Oppositely Charged Polyelectrolytes Form Tough, Self-Healing, and Rebuildable Hydrogels. *Adv. Mater.* **2015,** *27* (17), 2722-2727.

234. Neal, J. A.; Mozhdehi, D.; Guan, Z., Enhancing Mechanical Performance of a Covalent Self-Healing Material by Sacrificial Noncovalent Bonds. *J. Am. Chem. Soc.* **2015,** *137* (14), 4846-4850.

235. Yoshida, S.; Ejima, H.; Yoshie, N., Tough Elastomers with Superior Self-Recoverability Induced by Bioinspired Multiphase Design. *Adv. Funct. Mater.* **2017,** *27* (30), 1701670.

236. Salminen, L.; Karjalainen, E.; Aseyev, V.; Tenhu, H., Tough Materials Through Ionic Interactions. *Frontiers in Chemistry* **2021,** *9*.

237. Smith, K. E.; Temenoff, J. S.; Gall, K., On the toughness of photopolymerizable (meth)acrylate networks for biomedical applications. *J. Appl. Polym. Sci.* **2009,** *114* (5), 2711-2722.

238. Rebizant, V.; Venet, A.-S.; Tournilhac, F.; Girard-Reydet, E.; Navarro, C.; Pascault, J.-P.; Leibler, L., Chemistry and Mechanical Properties of Epoxy-Based Thermosets Reinforced by Reactive and Nonreactive SBMX Block Copolymers. *Macromolecules* **2004,** *37* (21), 8017-8027.

239. Nguyen, T. K. L.; Livi, S.; Soares, B. G.; Benes, H.; Gérard, J.-F.; Duchet-Rumeau, J., Toughening of Epoxy/Ionic Liquid Networks with Thermoplastics Based on Poly(2,6-dimethyl-1,4-phenylene ether) (PPE). *ACS Sustainable Chemistry & Engineering* **2017,** *5* (1), 1153-1164.

240. Chikhi, N.; Fellahi, S.; Bakar, M., Modification of epoxy resin using reactive liquid (ATBN) rubber. *Eur. Polym. J.* **2002,** *38* (2), 251-264.

241. Inoue, T., Reaction-induced phase decomposition in polymer blends. *Prog. Polym. Sci.* **1995,** *20* (1), 119-153.

242. Ruiz-Pérez, L.; Royston, G. J.; Fairclough, J. P. A.; Ryan, A. J., Toughening by nanostructure. *Polymer* **2008,** *49* (21), 4475-4488.

243. Liu, Y., Polymerization-induced phase separation and resulting thermomechanical properties of thermosetting/reactive nonlinear polymer blends: A review. *J. Appl. Polym. Sci.* **2013,** *127* (5), 3279-3292.

244. Szczepanski, C. R.; Pfeifer, C. S.; Stansbury, J. W., A new approach to network heterogeneity: Polymerization induced phase separation in photo-initiated, free-radical methacrylic systems. *Polymer* **2012,** *53* (21), 4694-4701.

245. Szczepanski, C. R.; Stansbury, J. W., Modification of linear prepolymers to tailor heterogeneous network formation through photo-initiated Polymerization-Induced Phase Separation. *Polymer (Guildf)* **2015,** *70*, 8-18.

246. Schüller-Ravoo, S.; Feijen, J.; Grijpma, D. W., Flexible, elastic and tear-resistant networks prepared by photo-crosslinking poly(trimethylene carbonate) macromers. *Acta Biomater.* **2012,** *8* (10), 3576-3585.

247. Pu, Y.; Cao, S.; Ragauskas, A. J., Application of quantitative 31P NMR in biomass lignin and biofuel precursors characterization. *Energy Environ. Sci.* **2011,** *4* (9), 3154-3166.

248. Reinelt, S.; Tabatabai, M.; Fischer, U. K.; Moszner, N.; Utterodt, A.; Ritter, H., Investigations of thiol-modified phenol derivatives for the use in thiol-ene photopolymerizations. *Beilstein J. Org. Chem.* **2014,** *10*, 1733-1740.

249. Reinelt, S.; Tabatabai, M.; Moszner, N.; Fischer, U. K.; Utterodt, A.; Ritter, H., Synthesis and Photopolymerization of Thiol-Modified Triazine-Based Monomers and Oligomers for the Use in Thiol-Ene-Based Dental Composites. *Macromol. Chem. Phys.* **2014,** *215* (14), 1415-1425.

250. Gorsche, C.; Harikrishna, R.; Baudis, S.; Knaack, P.; Husar, B.; Laeuger, J.; Hoffmann, H.; Liska, R., Real Time-NIR/MIR-Photorheology: A Versatile Tool for the in Situ Characterization of Photopolymerization Reactions. *Anal. Chem.* **2017,** *89* (9), 4958-4968.

251. Karalekas, D.; Aggelopoulos, A., Study of shrinkage strains in a stereolithography cured acrylic photopolymer resin. *J. Mater. Process. Technol.* **2003,** *136* (1), 146-150.

252. Schoerpf, S.; Catel, Y.; Moszner, N.; Gorsche, C.; Liska, R., Enhanced reduction of polymerization-induced shrinkage stress via combination of radical ring opening and addition fragmentation chain transfer. *Polymer Chemistry* **2019,** *10* (11), 1357-1366.

253. digital, i., PrograPrint Cure Bedienungsanleitung.

254. Mezger, T., *Applied Rheology: With Joe Flow on Rheology Road*. Paar: 2015.

255. Mittal, V.; Akhtar, T.; Matsko, N., Mechanical, Thermal, Rheological and Morphological Properties of Binary and Ternary Blends of PLA, TPS and PCL. *Macromolecular Materials and Engineering* **2015,** *300* (4), 423-435.

256. Ye, D.; Chang, C.; Zhang, L., High-Strength and Tough Cellulose Hydrogels Chemically Dual Cross-Linked by Using Low- and High-Molecular-Weight Cross-Linkers. *Biomacromolecules* **2019,** *20* (5), 1989-1995.

257. Wagoner Johnson, A. J.; Herschler, B. A., A review of the mechanical behavior of CaP and CaP/polymer composites for applications in bone replacement and repair. *Acta Biomater.* **2011,** *7* (1), 16-30.

258. Brostow, W.; Hagg Lobland, H. E.; Khoja, S., Brittleness and toughness of polymers and other materials. *Mater. Lett.* **2015,** *159*, 478-480.

259. Govindaraj, S., & Muthuraman, M. S., Systematic review on sterilization methods of implants and medical devices. *Int J ChemTech Res* **2015,** *8(2)*, 897-911.

260. https://www.sterixpert.de/en/irradiation-service.html#validation (accessed 06.02.2023).

261. Normungen, D. I. f., Sterilisation von Produkten für die Gesundheitsfürsorge. . **2015,** *Vol. 11137*.

262. Rogers, W. J., 4 - The effects of sterilization on medical materials and welded devices. In *Joining and Assembly of Medical Materials and Devices*, Zhou, Y.; Breyen, M. D., Eds. Woodhead Publishing: 2013; pp 79-130.

263. Altun, A. A.; Ertl, F.; Marechal, M.; Makaya, A.; Sgambati, A.; Schwentenwein, M., Additive manufacturing of lunar regolith structures. *Open Ceramics* **2021,** *5*, 100058.

264. Guo, Z.; Poot, A. A.; Grijpma, D. W., Advanced polymer-based composites and structures for biomedical applications. *Eur. Polym. J.* **2021,** *149*, 110388.

265. Sperling, L. H., *Interpenetrating polymer networks and related materials*. Springer Science & Business Media: 2012.

266. Widmaier, J. M.; Sperling, L. H., Phase continuity in sequential poly(n-butyl acrylate)/polystyrene interpenetrating polymer networks. *Macromolecules* **1982,** *15* (2), 625-631.

267. Klempner, D.; Sperling, L. H.; Utracki, L. A. *Interpenetrating polymer networks*; American Chemical Society, Washington, DC (United States): 1994.

268. Burillo, G.; Bucio, E.; Garcia-Uriostegui, L., The Synthesis and the Applications of IPNs based on Smart Polymers. In *Micro- and Nano-structured Interpenetrating Polymer Networks*, 2016; pp 179-198.

269. Arya Soman, F. M., A.J.Chacko, Mini Alias, G.Vinoda; Poosan, Interpenetrating polymer network (Ipn) – hydrogels. *The Pharma Innovation Journal* **2014,** *3* (8), 59-66.

270. Millar, J. R., 263. Interpenetrating polymer networks. Styrene–divinylbenzene copolymers with two and three interpenetrating networks, and their sulphonates. *Journal of the Chemical Society (Resumed)* **1960,** (0), 1311-1317.

271. Klempner, D.; Frisch, H. L.; Frisch, K. C., Topologically interpenetrating elastomeric networks. *Journal of Polymer Science Part A-2: Polymer Physics* **1969,** *8*, 921-935.

272. Shibayama, K.; Suzuki, Y., Viscoelastic Properties of Multiple Network Polymers. IV. Copolymers of Styrene and Divinylbenzene. *Rubber Chem. Technol.* **1967,** *40* (2), 476-483.

273. Curtius, A. J.; Covitch, M. J.; Thomas, D. A.; Sperling, L. H., Polybutadiene/polystyrene interpenetrating polymer networks. *Polymer Engineering & Science* **1972,** *12* (2), 101-108.

274. Sperling, L. H.; Arnts, R. R., Simultaneous interpenetrating networks. *J. Appl. Polym. Sci.* **1971,** *15* (9), 2317-2319.

275. Kim, S. C.; Klempner, D.; Frisch, K. C.; Frisch, H. L.; Ghiradella, H., Polyurethane—polystyrene interpenetrating polymer networks. *Polymer Engineering & Science* **1975,** *15* (5), 339-342.

276. Lecamp, L.; Pavillon, C.; Lebaudy, P.; Bunel, C., Influence of temperature and nature of photoinitiator on the formation kinetics of an interpenetrating network photocured from an epoxide/methacrylate system. *Eur. Polym. J.* **2005,** *41* (1), 169-176.

277. Hsieh, K. H.; Chou, L. M.; Wong, S. S., Effect of charge groups in polyurethane and polystyrene interpenetrating polymer networks. *Die Angewandte Makromolekulare Chemie* **1989,** *168* (1), 145-155.

278. Ilmain, F.; Tanaka, T.; Kokufuta, E., Volume transition in a gel driven by hydrogen bonding. *Nature* **1991,** *349* (6308), 400-401.

279. Gudeman, L. F.; Peppas, N. A., Preparation and characterization of pH-sensitive, interpenetrating networks of poly(vinyl alcohol) and poly(acrylic acid). *J. Appl. Polym. Sci.* **1995,** *55* (6), 919-928.

280. Zhang, J.-T.; Cheng, S.-X.; Zhuo, R.-X., Poly(vinyl alcohol)/poly(N-isopropylacrylamide) semi-interpenetrating polymer network hydrogels with rapid response to temperature changes. *Colloid. Polym. Sci.* **2003,** *281* (6), 580-583.

281. Decker, C.; Decker, D., Photoinitiated Polymerization of Vinyl Ether and Acrylate Monomer Mixtures. *Journal of Macromolecular Science, Part A* **1997,** *34* (4), 605-625.

282. Decker, C.; Nguyen Thi Viet, T.; Decker, D.; Weber-Koehl, E., UV-radiation curing of acrylate/epoxide systems. *Polymer* **2001,** *42* (13), 5531-5541.

283. Decker, C., UV-radiation curing chemistry. *Pigment & Resin Technology - PIGM RESIN TECHNOL* **2001,** *30*, 278-286.

284. Sangermano, M.; Malucelli, G.; Bongiovanni, R.; Priola, A., Photopolymerization of oxetane based systems. *Eur. Polym. J.* **2004,** *40* (2), 353-358.

285. Sangermano, M.; Carbonaro, W.; Malucelli, G.; Priola, A., UV-Cured Interpenetrating Acrylic-Epoxy Polymer Networks: Preparation and Characterization. *Macromolecular Materials and Engineering* **2008,** *293* (6), 515-520.

286. Crivello, J. V., Hybrid acrylate-oxetane photopolymerizable systems. *J. Polym. Sci., Part A: Polym. Chem.* **2015,** *53* (4), 594-601.

287. Hasa, E.; Scholte, J. P.; Jessop, J. L. P.; Stansbury, J. W.; Guymon, C. A., Kinetically Controlled Photoinduced Phase Separation for Hybrid Radical/Cationic Systems. *Macromolecules* **2019,** *52* (8), 2975-2986.

288. Zhang, X.; Kim, G. J.; Kang, M. G.; Lee, J. K.; Seo, J. W.; Do, J. T.; Hong, K.; Cha, J. M.; Shin, S. R.; Bae, H., Marine Biomaterial-Based Bioinks for Generating 3D Printed Tissue Constructs. *Mar. Drugs* **2018,** *16* (12).

289. Chen, C.-S.; Zeng, F.; Xiao, X.; Wang, Z.; Li, X.-L.; Tan, R.-W.; Liu, W.-Q.; Zhang, Y.-S.; She, Z.-D.; Li, S.-J., Three-Dimensionally Printed Silk-Sericin-Based Hydrogel Scaffold:

A Promising Visualized Dressing Material for Real-Time Monitoring of Wounds. *ACS Applied Materials & Interfaces* **2018,** *10* (40), 33879-33890.

290. Zhao, T.; Li, X.; Yu, R.; Zhang, Y.; Yang, X.; Zhao, X.; Wang, L.; Huang, W., Silicone–Epoxy-Based Hybrid Photopolymers for 3D Printing. *Macromol. Chem. Phys.* **2018,** *219* (10), 1700530.

291. Yu, R.; Yang, X.; Zhang, Y.; Zhao, X.; Wu, X.; Zhao, T.; Zhao, Y.; Huang, W., Three-Dimensional Printing of Shape Memory Composites with Epoxy-Acrylate Hybrid Photopolymer. *ACS Applied Materials & Interfaces* **2017,** *9* (2), 1820-1829.

292. Hoekstra, D. C.; van der Lubbe, B. P. A. C.; Bus, T.; Yang, L.; Grossiord, N.; Debije, M. G.; Schenning, A. P. H. J., Wavelength-Selective Photopolymerization of Hybrid Acrylate-Oxetane Liquid Crystals. *Angew. Chem. Int. Ed.* **2021,** *60* (19), 10935-10941.

293. Kury, M. Tough photopolymers for 3D printing. TU Wien, 2020.

294. F., M. Interpenetrating polymer networks for 3D printing. Diploma Thesis, 2021.

295. Shimomura, O.; Tomita, I.; Endo, T., Application of S-alkylsulfonium salts of aromatic sulfides as new thermal latent cationic initiators. *Journal of Polymer Science, Part A: Polymer Chemistry* **2000,** *38* (1), 18-27.

296. Qin, X.-H.; Ovsianikov, A.; Stampfl, J.; Liska, R., Additive manufacturing of photosensitive hydrogels for tissue engineering applications. *BioNanoMaterials* **2014,** *15* (3-4), 49-70.

297. Ito, T. H., Tsuneo; Hirotsu, Kenji; Murakami, Tadashi RESIN COMPOSITION FOR STEREOLITHOGRAPHY. 2007.

298. Castaldi, M. P.; Gibson, S. E.; Rudd, M.; White, A. J., A new approach to enantiopure C3-symmetric molecules. *Chemistry (Easton)* **2005,** *12* (1), 138-48.

299. Noordzij, G. J.; Dietz, C. H. J. T.; Leoné, N.; Wilsens, C. H. R. M.; Rastogi, S., Small-scale screening of novel biobased monomers: the curious case of 1,3-cyclopentanediol. *RSC Advances* **2018,** *8* (70), 39818-39828.

300. Wang, J.-S.; Zhao, H.-B.; Ge, X.-G.; Liu, Y.; Chen, L.; Wang, D.-Y.; Wang, Y.-Z., Novel Flame-Retardant and Antidripping Branched Polyesters Prepared via Phosphorus-Containing Ionic Monomer as End-Capping Agent. *Ind. Eng. Chem. Res.* **2010,** *49* (9), 4190-4196.

301. Azumaya, I.; Uchida, D.; Kato, T.; Yokoyama, A.; Tanatani, A.; Takayanagi, H.; Yokozawa, T., Absolute helical arrangement of stacked benzene rings: heterogeneous double-helical interaction comprising a hydrogen-bonding belt and an offset parallel aromatic-aromatic-interaction array. *Angew. Chem. Int. Ed. Engl.* **2004,** *43* (11), 1360-3.

302. Ratcliffe, L. P. D.; Ryan, A. J.; Armes, S. P., From a Water-Immiscible Monomer to Block Copolymer Nano-Objects via a One-Pot RAFT Aqueous Dispersion Polymerization Formulation. *Macromolecules* **2013,** *46* (3), 769-777.

303. Dall'Argine, C.; Hochwallner, A.; Klikovits, N.; Liska, R.; Stampf, J.; Sangermano, M., Hot-Lithography SLA-3D Printing of Epoxy Resin. *Macromolecular Materials and Engineering* **2020,** *305* (10), 2000325.

304. 1967.

305. Chae, C.-G.; Yu, Y.-G.; Seo, H.-B.; Kim, M.-J.; Grubbs, R. H.; Lee, J.-S., Experimental Formulation of Photonic Crystal Properties for Hierarchically Self-Assembled POSS–Bottlebrush Block Copolymers. *Macromolecules* **2018,** *51* (9), 3458-3466.

306. Klemm, E.; Sensfuß, S.; Holfter, U.; Flammersheim, H. J., Free-Radical stabilizers for the thiol/ene-systems. *Die Angewandte Makromolekulare Chemie* **1993,** *212* (1), 121-127.

307. Moszner, N.; Schöb, W.; Rheinberger, V., Synthesis, characterization and thiol-ene polymerization of hydrolyzed/condensed norbornenyl silic acid ester. *Polym. Bull.* **1996,** *37* (3), 289-295.

308. Esfandiari, P.; Ligon, S. C.; Lagref, J. J.; Frantz, R.; Cherkaoui, Z.; Liska, R., Efficient stabilization of thiol-ene formulations in radical photopolymerization. *J. Polym. Sci., Part A: Polym. Chem.* **2013,** *51* (20), 4261-4266.

309. Mercado-Feliciano, M.; Herbert, R. A.; Wyde, M. E.; Gerken, D. K.; Hejtmancik, M. R.; Hooth, M. J., Pyrogallol-associated dermal toxicity and carcinogenicity in F344/N rats and B6C3F1/N mice. *Cutan. Ocul. Toxicol.* **2013,** *32* (3), 234-240.

310. Dunn, R. O., Effect of antioxidants on the oxidative stability of methyl soyate (biodiesel). *Fuel Process. Technol.* **2005,** *86* (10), 1071-1085.

311. Mittelbach, M.; Schober, S., The influence of antioxidants on the oxidation stability of biodiesel. *J. Am. Oil Chem. Soc.* **2003,** *80* (8), 817-823.

312. Liebert, M. A., 2 Final Report on the Safety Assessment of Propyl Gallate. *J. Am. Coll. Toxicol.* **1985,** *4* (3), 23-64.

313. Steinbauer, P. Photopolymerizable adhesives for bone headling. TU Wien, 2021.